Fundamental Links Between Cellular Stress and Neurodegeneration in a Parkinson's Disease Model

Laura Elizabeth Shippey

A thesis jointly submitted in partial fulfilment of the requirements of Sheffield Hallam University for the degree of Doctor of Philosophy

August 2025

Fundamental Links Between Cellular Stress and Neurodegeneration in a Parkinson's Disease Model

Submitted By

Laura Elizabeth Shippey

Bachelor of Science (BSc), University of Leicester (2018)

Master of Science (MSc), King's College London (2020)

A thesis jointly submitted in total fulfilment of the requirements

for the degree of

Doctor of Philosophy

School of Biosciences and Chemistry

Sheffield Hallam University

Sheffield, United Kingdom

School of Agriculture, Biomedicine and Environment

La Trobe University

Victoria, Australia

August 2025

Candidate Declaration (Sheffield Hallam University)

I hereby declare that:

1. I have not been enrolled for another award of the University, or other academic or professional organisation, whilst undertaking my research degree.
2. None of the material contained in the thesis has been used in any other submission for an academic award.
3. I certify that this thesis is my own work. The use of all published or other sources of material consulted have been properly and fully acknowledged.
4. The work undertaken towards the thesis has been conducted in accordance with the SHU Principles of Integrity in Research and the SHU Research Ethics Policy, and ethics approval has been granted for all research studies in the thesis.
5. The word count of the thesis is: 52,579

Name	Laura Elizabeth Shippey
Date of Submission	22nd August 2025
Award	Doctor of Philosophy (PhD)
Research Institute	Health and Wellbeing
Director of Studies	Professor David P. Smith

Statement of Authorship (La Trobe University)

Except where reference is made in the text of the thesis, this thesis contains no material published elsewhere or extracted in whole or in part from a thesis accepted for the award of any other degree or diploma. No other person's work has been used without due acknowledgement in the main text of the thesis. This thesis has not been submitted for the award of any degree or diploma in any other tertiary institution.

The details of contribution by co-authors are specified in the section titled 'Research dissemination', thesis methodology sections and figure captions.

Laura E. Shippey

22nd August 2025

Acknowledgement of Financial Support (La Trobe University)

This work was supported by a La Trobe University Full Fee Research Scholarship.

Additional (primary) funding for this work was provided by Sheffield Hallam University.

Acknowledgements

To my Director of Studies, Professor David Smith, you have provided an endless amount of support and care that has allowed me to grow as a scientist and as a person. Thank you for giving me a chance to have a life changing experience that I'll never forget! Dr Sue Campbell, I will always be grateful for your guidance throughout this process and the time you have taken to listen and support me in every area of my life. Professor Andy Hill and Professor Yuning Hong, you have introduced me to your great labs and made sure I was accommodated and comfortable. Thank you so much for allowing me to fall in love with Australia!

Dr Celine Souilhol and Dr Jef (Jennifer) Clark, I can't thank you enough for the training and support you have given me from day 1 of this experience. I couldn't have made it through my PhD without you both.

Dan English, you've been beyond kind and friendly throughout my time at Hallam, I really appreciate the conversations and help you've provided.

To the loves of my life, Madalena and Muna, there aren't enough pages in the world that would allow me to express how special you've made this experience. You both have given me beautiful memories, loads of laughs and supported me through ups and a lot of downs. I look forward to making more memories with you girlies.

Lucy and Josh, my partners in crime, you've made every day at the BMRC feel fun and light especially on days where I really needed it. You have brightened up really tough days, I appreciate you both so much.

Hannah, Veronika, Olivia and Chloe, my office sisters, I'll miss the daily entertainment! You guys are the best comedians; I'll always be grateful for the funniest conversations we've had.

Hector, Sarah, Sophie, Charlie and Marta thank you for the great conversations and making the office an enjoyable place to be!

Meg, Grace, Jerome and Thashani, you've been amazing, I'll miss the lab and corridor catch-ups!

To my big brother, Deron, thank you for making the long, long, long trips to Sheffield! You've helped me move out countless times and I'm really thankful for the support.

Nathan, my twin and my little brother, you are really the best. The cinema trips and the matcha outings were a pleasant distraction which I'm beyond grateful for.

To Mum and Dad, I love you both. I could not ask for better parents You've never stopped holding my hands throughout every life experience. The care, the love and the support has been overwhelming, and I'll always be grateful.

Thank you to everyone both in and out of the BMRC, that has shown kindness and made the last few years absolutely amazing!

Abstract

Parkinson's disease (PD) is a neurodegenerative disorder that affects millions of individuals globally. The condition arises through the loss of dopaminergic neurons caused by various cellular stresses. In the surviving neurons of patients diagnosed with PD, there are presence of Lewy bodies comprised of aggregated proteins particularly α-synuclein. It is believed that the aggregated forms of α-synuclein induces cellular stress causing progressive cell death. However, it is not completely understood what stress pathways are activated by α-synuclein aggregates that results in PD-associated cellular death. This study aims to link α-synuclein oligomers and preformed fibrils (PFFs) to the integrated stress response (ISR) pathway. The ISR is involved in the reprogramming of cellular translation to determine the cell's engagement in homeostatic or apoptotic downstream processes during various stress conditions including but not limited to oxidative and endoplasmic reticulum stress. We show that SH-SY5Y neuroblastoma cells will express ISR markers in response to toxic compounds such as sodium arsenite, thapsigargin and MPP+ iodide. Further, it was also demonstrated that oligomers and PFFs will activate the ISR which coincides with intracellular α-synuclein aggregation and oxidative stress. Additionally, this research aims to explore the manner in which small extracellular vesicles (sEVs) mediate pathological cell-to-cell transmission linked to PD. The data presented shows that upon cellular exposure to oligomers and PFFs, sEVs derived from these cells are positive for α-synuclein and various stress-associated proteins. Overall, the results show that α-synuclein aggregate-induced stress activates the ISR pathway and alters the proteome of sEVs.

Research Dissemination

Publications

- Owyong, Tze C., Shippey, Laura E., Ding, Siyang., Owen, David., Zhang, Shouxiang., White, Jonathan. M., Wallace, W H., Smith, David P., and Hong, Yuning. Development of NIAD-4 derivatives for fluorescence-based detection of protein aggregates. Sens. Diagn., 2024,4: 55- 62.
- Shippey, Laura E., Campbell, Susan M., Hill, Andrew F. and Smith, David P. Propagation of Parkinson's disease by extracellular vesicle production and secretion. Biochem Soc Trans 2022, 5: 1303-1314.

Conferences

- Translation UK 2024. Surrey, United Kingdom. (Poster Presentation)
- Gordon Research Conference, Protein Dynamics 2024. Galveston, Texas. (Poster Presentation)
- La Trobe Institute for Molecular Sciences Symposium, 2023. Melbourne, Australia. (Poster Presentation)
- Translation UK 2023. Cambridge, United Kingdom. (Poster Presentation)
- White Rose RNA Research Symposium 2023. Leeds, United Kingdom. (Poster Presentation)

Contents

Candidate Declaration (Sheffield Hallam University) i
Statement of Authorship (La Trobe University) ii
Acknowledgement of Financial Support (La Trobe University) iii
Acknowledgements iv
Abstract vi
Research Dissemination vii
Contents viii
List of tables xiv
List of figures xv
List of Abbreviations xx
1 Chapter One: General Introduction 1
1.1 Clinical overview of Parkinson's disease 1
1.2 Monomeric α-synuclein 2
1.3 Genetic risk factors of PD 4
1.4 Environmental risk factors of PD 9
1.5 Oligomers 11
1.6 Fibrils and preformed fibrils (PFFs) 14
1.7 Prion-like activities of α-synuclein 16
1.8 Molecular events implicated in PD 18
1.9 Stress responsive pathways and the impact protein synthesis 19
1.9.1 The molecular pathway of the integrated stress response, ISR 19
1.9.2 The ISR, neurodegeneration and disease 21
1.9.3 Unfolded protein response pathway 22
1.9.4 The mechanistic target of rapamycin (mTOR) signalling pathway 24
1.10 Stress granules 26
1.10.1 The structure of stress granules 26
1.10.2 Assembly and disassembly of SGs 26
1.10.3 The function of stress granules 27
1.10.4 Stress granules and neurodegeneration 30
1.11 Extracellular vesicles, neurodegeneration and Parkinson's disease 32
1.11.1 Physiological role of extracellular vesicles 32
1.11.2 Extracellular vesicles in disease and neurodegeneration 32
1.12 Research overview and aims 34
2 Chapter Two: Materials and methods 35

2.1 Reagents and materials 35
2.2 Cell culture 39
2.2.1 Culturing of SH-SY5Y cells 39
2.2.2 Cryopreservation of SH-SY5Y neuroblastoma cells 39
2.2.3 Thawing SH-SY5Y neuroblastoma cells 39
2.2.4 Differentiation of SH-SY5Y neuroblastoma cells 40
2.3 Production of monomeric α-synuclein 41
2.3.1 Transformation of BL21 (DE3) competent *Escherichia coli* (*E.coli*) cells 41
2.3.2 Growth of BL21 (DE3) competent cells 41
2.3.3 Crude purification 42
2.3.4 Purification by fast protein liquid chromatography (FPLC) 42
2.3.5 Sodium dodecyl-sulphate polyacrylamide gel electrophoresis (SDS-PAGE) for α-synuclein purity. 42
2.4 Production of aggregated α-synuclein 44
2.4.1 Determining the concentration of monomeric α-synuclein 44
2.4.2 Production of seedings oligomers (type C) 44
2.4.3 Production of fibrils and preformed fibrils 44
2.4.4 Characterising fibrils using AFM (outsourced technique). 44
2.5 Fluorescent dyes for amyloid detection 45
2.5.1 Continuous ThT assay 45
2.5.2 Discontinuous ThT assay 45
2.5.3 Fluorometric spectrophotometry for amyloid detection 45
2.6 Cellular treatments 46
2.7 Fluorescent images of cells 47
2.7.1 Immunocytochemistry (ICC) 47
2.7.2 Fluorescent imaging acquisition and analysis 47
2.8 Lactate dehydrogenase (LDH) cytotoxicity assay 49
2.8.1 Optimal seeding density 49
2.8.2 Measuring treatment LDH activity 50
2.9 Flow cytometry 51
2.9.1 Flow cytometry dyes 51
2.9.2 NIAD-4 and NIAD-CNEOT fluorescent dyes used for amyloid detection 51
2.9.3 CellROX Assay for oxidative stress detection 51
2.9.4 FlowJo analysis 52
2.10 Western blot 54

2.10.1 Protein extraction 54
2.10.2 BCA assay 54
2.10.3 Sample preparation 54
2.10.4 SDS-page 55
2.10.5 Semi-dry transfer 55
2.10.6 Western blotting 55
2.10.7 Puromycin incorporation assay 55
2.10.8 ImageJ densitometry analysis 56
2.11 Human ATF4 enzyme-linked immunosorbent assay (ELISA) 57
2.12 Quantitative real time polymerase chain reaction (qRT-PCR) 58
2.12.1 RNA extraction 58
2.12.2 cDNA synthesis 58
2.12.3 TaqMan gene expression assay 59
2.13 Extracellular vesicle isolation, characterisation and proteomics 60
2.13.1 Cell culture for EV isolation 60
2.13.2 Differential ultracentrifugation for EV isolation 60
2.13.3 Nanoparticle tracking analysis (NTA) 60
2.13.4 Electron microscopy (outsourced technique) 61
2.13.5 Mass spectrometry (outsourced technique) 61
2.14 General statistical analysis 64
3 Chapter Three: Validating ISR activation using stress-inducing compounds 65
3.1 Introduction 65
3.1.1 The ISR's role in stress and disease 65
3.1.2 Stress-inducing compounds in the investigation of the ISR 65
3.1.3 Stress response pathways in PD neurotoxin models 66
3.1.4 Objectives 67
3.2 Results 68
3.2.1 Oxidative and ER stress increases phosphorylation of eIF2α. 68
3.2.2 MPP+ induces phosphorylation of eIF2α 72
3.2.3 ATF4 is expressed in response to oxidative and ER stress 74
3.2.4 MPP+ increases in ATF4 expression 76
3.2.5 CHOP is expressed in response oxidative and ER stress 78
3.2.6 LDH indicates cytotoxicity overtime in response to oxidative and ER stress 79
3.2.7 Oxidative and ER stress induces GADD34 expression 81

3.2.8 Global protein synthesis is inhibited following MPP+ treatment 82
3.2.9 Chronic stress and the formation of SGs 84
3.2.10 SG formation in response to acute stress 90
3.2.11 MPP+ induces SG formation..... 95
3.3 Discussion..... 105
3.3.1 Oxidative and ER stress activates the ISR 105
3.3.2 High-dose MPP+ activates the ISR but does not enhance ATF4 expression. 107
3.3.3 Stress granules dynamics differ depending on stress conditions 108
3.4 Summary..... 111
4 Chapter Four: The production and characterisation of α-synuclein aggregates..... 113
4.1 Introduction 113
4.2 Objectives 113
4.3 Results 114
4.3.1 The production and characterisation of monomeric α-synuclein 114
4.3.2 Using ThT to report presence of amyloid conformations 117
4.3.3 ThT detects α-synuclein amyloid formation occurs overtime..... 119
4.3.4 Using NIAD-4 derivatives to assess presence of amyloid fibrils..... 121
4.3.5 NIAD-4 and NIAD CNEOT detected α-synuclein PFFs 123
4.3.6 Structural and size characterisation of α-synuclein fibrils..... 124
4.3.7 Detecting intracellular aggregation using NIAD-4 and NIAD CNEOT fluorescent dyes 125
4.4 Discussion..... 128
4.5 Summary..... 130
5 Chapter Five: α-Synuclein oligomers and preformed fibrils activate the ISR 131
5.1 Introduction 131
5.1.1 Oligomers and PFFs induce cellular stress..... 131
5.1.2 Objectives 132
5.2 Results 133
5.2.1 Oligomers and PFFs induces intracellular aggregation..... 133
5.2.2 α-Synuclein aggregates increase oxidative stress 137
5.2.3 α-Synuclein oligomers and PFFs aggregates are cytotoxic..... 140
5.2.4 EIF2α phosphorylation upon exposure to oligomers and PFFs..... 142
5.2.5 Oligomers and PFFs moderately increases ATF4 expression..... 143

5.2.6 ATF5 is not expressed in response to ER stress and moderately expressed upon treatment with PFFs 145
5.2.7 CHOP expression was not induced by oligomers and PFFs 147
5.2.8 GADD34 is expressed in response to ER stress and moderately in response to α-synuclein aggregates 149
5.2.9 PFFs inhibit cellular translation 151
5.2.10 Stress granules form in response to oligomers and PFF treatment 153
5.2.11 SGs co-localisation with intracellular α-synuclein aggregates increases in response to oligomer and PFF treatment 158
5.3 Discussion 161
5.3.1 Oligomers and PFFs induce intracellular α-synuclein aggregation that induces cellular stress 161
5.3.2 Oligomers and PFFs induces expression of specific ISR markers 161
5.3.3 Oligomers and PFFs triggers SG formation that co-localise with α-synuclein 165
5.4 Summary 167
6 Chapter Six: The effect of α-synuclein aggregates on the extracellular vesicle proteome 169
6.1 Introduction 169
6.1.1 The structure and function of extracellular vesicles 169
6.1.2 EVs role in neurodegenerative disease 170
6.1.3 Objectives 171
6.2 Results 172
6.2.1 Characterising the morphology of undifferentiated and differentiated SH-SY5Y neuroblastoma cells 172
6.2.2 α-Synuclein aggregation in differentiated cells 176
6.2.3 ROS increases in cells exposed to oligomers and PFFs 179
6.2.4 Characterising the size of sEVs isolated from SH-SY5Y cells 181
6.2.5 Validation of isolated SH-SY5Y derived sEVs 186
6.2.6 Detecting sEV markers 187
6.2.7 Protein expression is altered in response to oxidative stress 188
6.2.8 Oligomer and PFF treatment of undifferentiated SH-SY5Y cells are positive for α-synuclein as well as proteins indicatory of stress induction 209
6.2.9 Mitochondrial and PD associated proteins and α-synuclein are present in sEVs in response to oligomer and PFF treatment of differentiated SH-SY5Y cells 227
6.3 Discussion 242
6.3.1 Differentiated SY5Y cells experience intracellular aggregation upon exposure to α-synuclein oligomers and PFFs 242

6.3.2 The characterisation of sEVs derived from SH-SY5Y cells 242
6.3.3 Oxidative stress impacts the proteins expressed in sEVs 243
6.3.4 Oligomers and PFFs results in increased α-Synuclein sEV loading plus alterations in sEVs proteomics in undifferentiated and differentiated SH-SY5Y cells. 244
6.4 Summary 247
7 Chapter Seven: Discussion, conclusion and future work 249
7.1 Introduction 249
7.2 Discussion 250
7.2.1 Cellular adaptation occurs in conditions of chronic chemically induced stress. 250
7.2.2 High dose MPP+ activates the ISR but does not enhance ATF4 expression. 251
7.2.3 MPP+ SG dynamics differs to that of SA and Tg. 251
7.2.4 Oligomers and PFFs activates the eIF2α/ATF4 pathway 252
7.2.5 Small EVs carry proteins associated with the imposing cell stress.... 254
7.3 Concluding Remarks 256
7.4 Future work 258
8 Chapter Eight: References 261
9 Chapter Nine: Ethics approval 326

List of tables

Table 1.1 Genes that have been reported have mutations implicated in PD. 4
Table 1.2 Environmental risk factors involved in the pathogenesis and prognosis of PD. 10
Table 1.3 Types of α-synuclein oligomeric aggregates reported within literature. 12
Table 2.1 Reagents and materials used throughout the study. 35
Table 2.2 Primary and secondary antibodies used in immunocytochemistry (ICC) and western blot experiments. 37
Table 2.3 Cell treatments. 46
Table 2.4 Confocal image acquisition setting details.. 47
Table 2.5 Flow cytometry dyes.. 51
Table 2.6 Gene expression cycle stages. 59
Table 2.7 Genes investigated and corresponding IDs. 59
Table 6.1 Decreased expression of sEV proteins.). 194
Table 6.2 Increased expression of sEV proteins.. 197
Table 6.3 Decreased expression of oligomer treated cellular sEV proteins. 213
Table 6.4 Increased expression of oligomer treated cellular sEV proteins.. 214
Table 6.5 Decreased expression of PFF treated cellular sEV proteins.. 218
Table 6.6 Increased expression of PFF treated cellular sEV proteins..220
Table 6.7 Decreased expression of oligomer treated cellular sEV proteins. 233
Table 6.8 Increased expression of oligomer treated cellular sEV proteins 234
Table 6.9 Decreased expression of PFF treated cellular sEV proteins. 237
Table 6.10 Increased expression of PFF treated cellular sEV proteins. 238

List of figures

Figure 1.1 The structure of monomeric α-synuclein..... 3
Figure 1.2 The aggregation pathway of α-synuclein..... 13
Figure 1.3 The ISR pathway. 21
Figure 1.4 The UPR pathway during ER stress.. 24
Figure 1.5 The pathways that lead to formation of canonical and non-canonical SGs..... 29
Figure 2.1 Image analysis methodology. 48
Figure 2.2 Optimal number LDH assay experiment. 49
Figure 2.3 FlowJo gating for analysis. 53
Figure 3.1 Low-dose SA induces phosphorylation of eIF2α. 69
Figure 3.2 Low-dose SA induces phosphorylation of eIF2α. 70
Figure 3.3 Low-dose Tg induces phosphorylation of eIF2α..... 71
Figure 3.4 10 mM MPP+ increases eIF2α phosphorylation.. 73
Figure 3.5 Low dose SA and Tg initially increases ATF4 expression but decreases in conditions of chronic stress..... 75
Figure 3.6 MPP+ results in moderate increases in ATF4 expression. ... 77
Figure 3.7 30 μM SA and 0.15 μM Tg induces CHOP expression, but other investigated conditions do not..... 78
Figure 3.8 Long-term stress increases cytotoxicity..... 80
Figure 3.9 SA, Tg, MPP+ induces GADD34 expression. 81
Figure 3.10 Tg and MPP+ at 6 hr attenuates translation..... 83
Figure 3.11 Low-dose SA and Tg-induced SGs but the number of SGs reduce in response to long-term treatment.. 87
Figure 3.12 Quantification of SG parameters in response to low dose SA and Tg..... 89
Figure 3.13 SA and Tg induces SG formation during short and longer duration exposure. 93
Figure 3.14 SA and Tg acute/short-term treatment also forms SGs positive for TIA-1 94
Figure 3.15 5 mM MPP+ induces SGs in both short and long-term stress..... 98

Figure 3.16 5 mM MPP+ induces TIA-1 positive SGs during long-term stress. 100
Figure 3.17 Chronic treatment of cells with 10 mM MPP+ induces. 102
Figure 3.18 10 mM MPP+ induces TIA-1 positive SGs during long-term stress. 104
Figure 3.19 A summary of data exploring SA and Tg of ISR marker expression. 112
Figure 3.20 MPP+ timeline of ISR marker expression. 112
Figure 4.1 α-Synuclein positive SEC samples. 115
Figure 4.2 ESI-MS analysis of intact monomeric α-synuclein. 116
Figure 4.3 ThT indicates highest fluorescent intensity in response to α-synuclein fibrils.. 118
Figure 4.4 ThT fluorescence increases overtime when α-synuclein is agitated to induce aggregation. 120
Figure 4.5 NIAD-4 and NIAD CNEOT dyes are able to detect aggregation overtime of α-synuclein.). 122
Figure 4.6 NIAD-4 and NIAD CNEOT dyes are able to detect aggregation overtime of α-synuclein. 123
Figure 4.7 AFM images of day 4 fibrils. 124
Figure 4.8 Flow cytometry gating strategy for NIAD-4 and NIAD CNEOT experiment. 126
Figure 4.9 NIAD-4 and NIAD CNEOT detects intracellular aggregation in response to PFFs.. 127
Figure 5.1 Intracellular α-synuclein aggregation takes place in response to cellular exposure to oligomers and PFFs. 135
Figure 5.2 Quantification of intracellular α-synuclein aggregation in response to cellular exposure to oligomers and PFFs. 136
Figure 5.3 Oligomers and PFFs induces ROS formation.. 139
Figure 5.4 Oligomers and PFFs are cytotoxic.. 141
Figure 5.5 EIF2α phosphorylation in response to oligomers and PFFs. 142
Figure 5.6 ATF4 RNA expression is enhanced in response to oligomers and PFFs.. 144
Figure 5.7 ATF5 expression is not enhanced in response to PFFs.. 146

Figure 5.8 Enhancement of CHOP expression does not occur in response to oligomers and PFFs. 148
Figure 5.9 GADD34 expression increased in response to oligomers and PFFs..... 150
Figure 5.10 Oligomers and PFFs attenuate cellular translation..... 152
Figure 5.11 Oligomers and PFFs trigger SG formation..... 155
Figure 5.12 Oligomers and PFFs trigger SG formation.. 157
Figure 5.13 Oligomers and PFFs increases SG co-localisation to α-synuclein intracellular aggregates.. 160
Figure 5.14 Timeline of ISR marker expression in response to oligomer and PFF treatment. 168
Figure 6.1 Morphology changes upon prolonged exposure to RA.. ... 173
Figure 6.2 Ki67 expressed reduces during prolonged exposure to RA.. 175
Figure 6.3 α-Synuclein aggregation in undifferentiated cells when treated with oligomers and PFFs. 178
Figure 6.4 Oligomers and PFFs increases ROS positive cells..... 180
Figure 6.5 NTA of EV samples derived the conditioned medium from undifferentiated cells treated with SA and Tg. 183
Figure 6.6 NTA of EV samples derived from undifferentiated cells treated with α-synuclein aggregates.. 184
Figure 6.7 NTA of EV samples derived from differentiated cells treated with α-synuclein aggregates 185
Figure 6.8 TEM of EV samples derived from undifferentiated and differentiated cells subjected to stress treatments. 186
Figure 6.9 ALIX and CD9 but not β-actin is expressed in sEV sample.187
Figure 6.10 Experimental workflow of EV isolation and proteomic analysis.. 192
Figure 6.11 LC-MS analysis of sEV proteins derived from cells treated with SA 24 hr.. 193
Figure 6.12 STRING analysis of sEV proteins found to have reduced expression in response to SA 24 hr treatment. 202
Figure 6.13 Gene ontology analysis of sEV proteins with reduced expression in response to SA 24 hr treatment. 203

Figure 6.14 STRING analysis of sEV proteins with increased expression in response to SA 24 hr treatment. 204
Figure 6.15 Gene ontology analysis of sEV proteins with increased expression in response to SA 24 hr treatment. 205
Figure 6.16 LC-MS analysis of sEV proteins derived from cells treated with Tg 24 hr. 206
Figure 6.17 Log_2 centred intensity of sEV proteins derived from cells treated with undifferentiated SA and Tg. 207
Figure 6.18 sEV protein expression in response to SA and Tg treatment of undifferentiated SH-SY5Y cells. 208
Figure 6.19 LC-MS analysis of sEV proteins in response to cell treatment with oligomer 48 hr. 212
Figure 6.20 STRING analysis of sEV proteins found to have decreased expression in response to oligomer 48 hr treatment.. 216
Figure 6.21 LC-MS analysis of sEV proteins isolated from cells treated with PFF 48 hr. 217
Figure 6.22 STRING analysis of sEV proteins with decreased expression derived from cells treated with PFF 48 hr. 222
Figure 6.23 Gene ontology analysis of sEV proteins found to have reduced expression isolated from cells subjected to PFF 48 hr treatment.. 223
Figure 6.24 STRING analysis of sEV proteins identified to have increased expression isolated from cells treated with PFF 48 hr. other databases; black line – proteins found to be co-expressed. 224
Figure 6.25 Log_2 centred intensity of sEV proteins derived from undifferentiated cells treated with oligomers and PFFs. 225
Figure 6.26 sEV protein expression in response to oligomer and PFF treatment of undifferentiated cells. 226
Figure 6.27 LC-MS analysis of sEV proteins from cells treated with oligomers 48 hr. 231
Figure 6.28 String analysis of sEV proteins with increased expression derived from cells treated with oligomers 48 hr. 232
Figure 6.29 Gene ontology analysis of sEV proteins found to have increased expression in response to oligomer 48 hr treatment.. . 235

Figure 6.30 LC-MS analysis of sEV proteins isolated from cells treated with PFF 48 hr.. 236
Figure 6.31 LC-MS analysis of sEV proteins.. 239
Figure 6.32 Log_2 centred intensity of sEV proteins derived from differentiated cells treated with oligomers and PFFs..... 240
Figure 6.33 sEV protein expression in response to oligomers and PFFs treatment of differentiated cells. 241
Figure 6.34 α-Synuclein-positive sEVs are released from cells treated oligomers and PFFs.. 248
Figure 7.1 A summary of the proposed sequence of events during stress caused by oligomers and PFFs. 257

List of Abbreviations

4E-BP1 – EIF4E binding protein 1

6-OHDA - 6-hydroxydopamine

ACO1 - Aconitase 1

AD – Alzheimer's disease

ADAMTS4 - Aggrecanase-1

ADH1C - Alcohol dehydrogenase 1C

AFM – Atomic force microscopy

AKR1B1 - Aldo-keto reductase family 1 member B1

ALCAM - Activated leukocyte cell adhesion molecule

ALP – Autophagy-lysosomal pathway

ALS – Amyotrophic lateral sclerosis

AP2B1 - Adaptor Protein Complex 1

APOA1 - Apolipoprotein A1

APP – Amyloid precursor protein

APS – Autophagy lysosomal system

ATF3 - Activating transcription factor 3

ATF4 - Activating transcription factor 4

ATF5 – Activating transcription factor 5

ATF6 – Activating transcription factor 6

ATP - Adenosine triphosphate

ATRA – all-trans-retinoic acid

BACE1 - β-site APP cleaving enzyme-1

BCA - Bicinchoninic Assay

BiP - binding immunoglobulin protein

BLMH - Bleomycin Hydrolase

BME - β-mercaptoethanol

BPGM - 2,3-bisphosphoglycerate mutase

bZIP - Basic leucine zipper

CARE - C/EBP-ATF response element

CD82 - CD82 antigen

cDNA – Complementary DNA

CFB - Complement Factor B

CHD3 - Chromodomain Helicase DNA Binding Protein 3

CHMP4B - Charged multivesicular body protein 4b

CHOP - C/EBP homologous protein

CHST14 - Carbohydrate Sulfotransferase 14

CLDN12 - Claudin-12

CNS – Central nervous system

COLEC11 - Collectin subfamily member 11

COTL1 - Coactosin Lie F-Actin Binding Protein 1

CPXM1 - Carboxypeptidase X, M14 Family Member 1

CXADR - Coxsackievirus and adenovirus receptor

DA – Dopamine

DAT – Dopamine transporter

DDIT3 – DNA damage-inducible transcript 3

DIRAS2 - DIRAS family GTPase 2

DLB – Dementia with Lewy bodies

DMEM - Dulbecco's Modified Eagle Medium

DMSO – Dimethyl Sulfoxide

DNA – Deoxyribonucleic acid

DPBS - Dulbecco’s Phosphate-Buffered saline

DSG1 – Desmoglein 1

ECPAS - Ecm29 Proteasome Adaptor

EHD4 - Eps15 homology domain

EIF2S3 - eukaryotic translation initiation factor 2 subunit 3

EIF3 – Eukaryotic initiation factor 3

EIF4A – eukaryotic initiation factor A

EIF4E – eukaryotic initiation factor E

EIF4F - eukaryotic initiation factor F

EIF4G - eukaryotic initiation factor G

ELISA – Enzyme-linked immunosorbent assay

EM – Electron microscopy

EML2 - Echinoderm microtubule-associated protein-like 2

ENAH - Enabled homolog

EPHB4 - ephrin B4

EPRS1 - Glutamyl-prolyl-tRNA synthetase 1

ER – Endoplasmic reticulum

ERBIN - Erbin

EV – Extracellular vesicle

EVA1A - Protein eva-1 homolog A

FBS - Foetal Bovine Serum

FDR – False discovery rate

FEN1 - Flap endonuclease 1

FLG2 - Filaggrin 2

FPLC – Fast protein liquid chromatography

FTD – Frontotemporal Dementia

FTLD - Frontotemporal Lobar Dementia

FUS - Fused in sarcoma

FXR1 - FMR1 Autosomal Homolog 1

G3BP - GTPase-activating protein SH3 domain-binding protein

GADD34 - Growth arrest and DNA damage-inducible protein

GBA1 - Glucosylceramidase Beta 1

GCN2 - General control nonderepressible 2

GNA11 - G protein subunits 11

GNG12 - Guanine nucleotide-binding protein G(I)/G(S)/G(O) subunit gamma 12

GPS1- G Protein Pathway Suppressor 1

GRP78 - 78 kDa glucose-regulated protein

GSK3A - Glycogen Synthase Kinase 3 Alpha (GSK3A)

H1-0 - Histone 1.0

H1-10 - Histones 1-10

H1-3 - Histones 1.3

H1-5 - Histone 1.5

H2BC18 - Histone H2B type 2-F

H2BC21 - Histone H2B type 2-E

H3-3B - Histone H3.3

H4 – Human neuroglioma

HD - Huntington’s disease

HNRNPA3 - Heterogeneous nuclear ribonucleoprotein A3

HNRNPL - Heterogenous Nuclear Ribonucleoprotein L

HRI - Heme-regulated inhibitor

HRP – Horse radish peroxidase

HSPD1 - 60 kDa heat shock protein D (HSPD1)

ICAM1 - Intercellular adhesion molecule 1

IDR – Intrinsically disorder region

ILV – Intraluminal vesicle

iPSCs - Induced pluripotent stem cells

ISR – Integrated stress response

ITM2B - Integral membrane protein 2B

KIF5B - Kinesin Family Member 5B

LAG3 - Lymphocyte-activation gene 3

LAMB1 - Laminin subunit beta-1

LAMC1- Laminin subunit gamma-1

LB – Lewy body

LC-MS – Liquid chromatography mass spectrometry

LDH – Lactate dehydrogenase

LLPS - Liquid-liquid phase separation

LMAN1 - Lectin, Mannose Binding 1

LPS – Lipopolysaccharide

MACROH2A1 - Core histone macro-H2A.1

MACROH2A2 - Core histone macro-H2A.2

MAO – Monoamine oxidase

MCM4 - Minichromosome Maintenance Complex Component 4

MPP^+ - 1-methyl-4-phenylpyridinium

MPTP - 1-methyl-4-phenyl-1,2,3,6-tetrahydropyridine

mRNA – Messenger RNA

mRNPs – Messenger ribonucleoproteins

MS – Multiple sclerosis

MSA – Multiple system atrophy

mTOR – Mechanistic target of rapamycin

MVBs – Multivesicular bodies

MW – Molecular Weight

NAC – non-amyloid component

NDUFB9- NADH dehydrogenase [ubiquinone] 1 beta subcomplex subunit 9

NDUFS7 - NADH dehydrogenase [ubiquinone] iron-sulfur protein 7, mitochondrial

NFT – Neurofibrillary tangles

NIAD-4 – [5'-(4-Hydroxyphenyl) [2,2'-bithiophen]-5-yl] methylene] propanedinitrile

NTA – Nanotracking analysis

P70S6K1 – p70 ribosomal S6 kinase 1

PABPC4 - poly(A) binding protein cytoplasmic 4

PAFAH1B12 - Platelet-activating factor acetyl hydrolase 1B1

PARK7 - Protein/nucleic acid deglycase DJ-1

PCR – Polymerase chain reaction

PD - Parkinson’s disease

PDD – Parkinson’s disease dementia

PERK - Protein kinase R-like endoplasmic reticulum kinase

PFAS - Phosphoribosylformylglycinamidine synthase

PFF – Preformed fibril

PGLYRP1- Peptidoglycan Recognition Protein 1

PI15 - Peptidase inhibitor 15

PIC - Pre-initiation complexes

PKR - Protein kinase R

PMPCA - Peptidase Mitochondrial Processing Subunit Alpha

POSTN - Periostin

PPP1R15A - Protein phosphatase 1 regulatory subunit 15A

PRG4 - Proteoglycan 4

PrP^{c} – Cellular prion protein

PrP^{Sc} – Abnormal PrP

PSM – Peptide spectrum matches

PSME1- Proteasome activator complex subunit 1

PSP – Progressive nuclear palsy

PTK7 - Inactive tyrosine-protein kinase 7

PYGB - Glycogen phosphorylase B

qRT-PCR – Quantitative real time polymerase chain reaction

RAB21 - Ras-related protein Rab-21

RAB3A - Ras-related protein Rab-3A

RAB5A - Ras-related protein Rab-5A

RALY - RBP associated with lethal yellow mutation

RAP1A Ras family GTPase 1

RBP – Ribonucleoprotein

RHOC - Rho-related GTP-binding protein RhoC

RIDD - Regulated IRE1-dependent decay

RNA – Ribonucleic acid

ROI – Region of interest

ROS – Reactive oxygen species

RPL7A - Ribosomal protein L7a

RPS6KA3 - Ribosomal Protein S6 Kinase A3

RRAS - Ras-related protein R-Ras

RTN4 - reticulon 4

SA – Sodium arsenite

SCRIB - Protein scribble homolog

SCRN1 - Secernin-1

SEC – Size exclusion chromatography

SELENBP1 - Selenium Binding Protein 1

Ser129 – Serine 129

SERCA - Sarco/ER Ca^{2+}-ATPase

SERPINB12 - Serpin Family B Member 12

sEVs – Small extracellular vesicles

SG – Stress granules

SLC12A2 - Solute Carrier Family 12 Member 12

SN – Substantia nigra

SNCA – α-Synuclein

SNpc – Substantia nigra pars compacta

SPCS2 - Signal peptidase complex subunit 2

SPP2 - Secreted Phosphoprotein 2

STMN1 - Stathmin

TARS1 - Threonine--tRNA ligase 1, cytoplasmic

TBHP - *tert*-Butyl hydrogen peroxide

TBI – Traumatic brain injury

TBRG4 - Transforming growth factor beta regulator 4

TDP-43 - TAR DNA-binding protein 43

TEM – Transmission electron microscopy

Tg – Thapsigargin

TH – Tyrosine hydroxylase

THSD4 - Thrombospondin type 1 domain containing 4

ThT – Thioflavin T

TIA-1 - T-cell intracytoplasmic antigen 1

TIAR - TIA1-related protein

TJP1 - Tight junction protein 1

TMB – 3,3', 5,5'-Tetramethylbenzidine

TNC - tenascin-C

tRNA – Transfer RNA

TSPAN18 - Tetraspanin 18

uORFs – Upstream open reading frames

UPR – Unfolded protein response

UPS – Ubiquitin proteosome system

USO1- USO1 Vesicle Transport Factor

UV – Ultraviolet light

UXS1 - UDP-Glucuronate Decarboxylase 1

VARS1 - Valine aminoacyl-tRNA synthetase

WT – Wild-type

XPO7 - Exportin 7

1 Chapter One: General Introduction

1.1 Clinical overview of Parkinson's disease

In 2020, 9 million individuals worldwide were reported to be diagnosed with Parkinson's disease (PD) (Pauwels and Boer, 2023). PD is the second most common neurodegenerative disorder behind Alzheimer's disease (AD) (Tolosa et al, 2021). PD arises due to the degeneration of dopaminergic neurons in the substantia nigra pars compacta (SNpc) (Sveinbjorndottir, 2016). However, cholinergic (Pasquini et al, 2021), GABAergic, glutamatergic, noradrenergic, adrenergic (Sveinbjorndottir, 2016; Braak and Braak, 2000) and serotonergic systems (Politis and Niccolini, 2015) have also been implicated. Symptoms associated with PD are often categorised into motor and non-motor symptoms. Motor symptoms often involve aberrant gait, issues with speech production, bradykinesia, akinesia, rigidity and tremor (Moustafa et al, 2016). There are also frequent reports of cases where patients will experience non-motor symptoms of a neuropsychiatric nature such as depression, anxiety, hallucinations, dementia, and attention deficits. Non-motor symptoms may also involve sleep disorders, gastrointestinal and autonomic dysfunction (Chaudhuri et al, 2006).

Currently, there is no cure for PD, but the reported main and most beneficial pharmacological treatment is carbidopa-levodopa (Armstrong and Okun, 2020). This combinational intervention consists of levodopa which allows for the production of dopamine, whereas carbidopa blocks L-dopa decarboxylase activity (Zhu et al, 2017). This serves to prevent conversion of levodopa to dopamine outside of the central nervous system (CNS) reducing the presentation of adverse effects (Zhu et al, 2017). Despite the benefits of this treatment, there are numerous complications such as dyskinesia and psychiatric issues (Salat and Tolosa, 2013). Altogether indicating a need for alternative treatments for PD with less debilitating side effects and further understanding of the condition itself.

1.2 Monomeric α-synuclein

α-Synuclein has been implicated in PD-associated neurodegeneration (Calabresi et al, 2023). The α-synuclein protein is comprised of 140 amino acids and encoded by the gene *SNCA*. There are three distinct regions of this protein consisting of the N-terminal, non-amyloid component (NAC) and C-terminal domains (Siddiqui et al, 2016). Protein residues 1-60 account for the N-terminal domain (Doherty et al, 2020), which interacts with lipidic membranes and is important for vesicle exocytosis (McGlinchey et al, 2021). Residues 61-95 represents the NAC region (Doherty et al, 2020) and amino acids 71-82 has been associated with α-synuclein axonal entry and transport (Anderson et al, 2020). Lastly, the C-terminal region consists of amino acids 96-140 which has both acidic and flexible characteristics (Doherty et al, 2020) **(Figure 1.1)**. Physiological and pathophysiological information pertaining to α-synuclein is discussed in **Table 1.1**. Monomeric α-synuclein has the propensity to aggregate into amyloid neurotoxic structures **(Figure 1.2)**. The N-terminal has been found to be integral to the self-assembly of α-synuclein into amyloid structures (Srinivasan et al, 2021). Additionally, metals such as copper and iron ions which bind to the N-terminal have been found to exacerbate aggregation of α-synuclein into insoluble structures (Srinivasan et al, 2021). Truncation of the C-terminal region of α-synuclein results in the formation of a β-sheet rich conformation and subsequent amyloid formation (Farzadfard et al, 2022, Srinivasan et al, 2021).

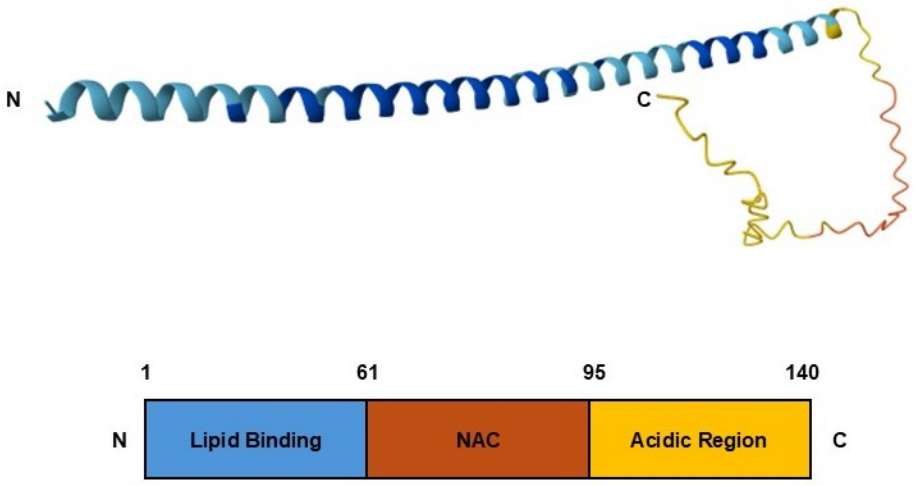

Figure 1.1 The structure of monomeric α-synuclein. **(A)** α-Synuclein chemical structure. Adapted from AlphaFold. **(B)** Schematic breakdown of the three regions of the α-synuclein monomeric protein. N: N-terminal domain, C: C-terminal domain, NAC: non amyloid component.

1.3 Genetic risk factors of PD

90% of PD cases are considered to be sporadic whilst 10% are reported to have a familial/genetic component (Schulze et al, 2018; Sandor et al, 2017) with the common mutations listed in **Table 1.1**. Notably the protein α-synuclein has several point mutations and triplications leading to increased aggregation of the protein triggering early onset disease, as discussed in **Table 1.1**.

Table 1.1 Genes that have been reported have mutations implicated in PD.

Gene/Protein	Physiological Role	Association with PD
APOE: **Apolipoprotein E**	*APOE* is involved in the maintenance of the blood brain barrier integrity; cerebral blood flow (Tai et al, 2016); synaptic plasticity (Liao et al, 2018); lipid and glucose metabolism (Huang and Mahley, 2014) and transcriptional regulation (Liao et al, 2018; Kim et al, 2014). *APOE* is considered a cholesterol carrier/involved in lipid transport as well as pivotal brain injury repair (Li et al, 2018).	Mutations may impair its ability to allow for neuronal repair contributing to neurodegeneration. Mutations are linked to cognitive decline observed in PD specifically PD dementia (PDD) (Szwedo et al, 2022).
ATP13A2: **Lysosomal type 5 P-type ATPase**	*ATP13A2* plays roles in the transportation of heavy metals and has the highest expression in the SNpc. It has been determined that *ATP13A2* is a lysosomal polyamine exporter and protects against polyamine toxicity. Examples of polyamines include spermine and spermidine which are organic polycations important for cell function (Veen et al, 2020). Specific processes that these polyamines are involved in, includes cell proliferation and differentiation; gene transcription and translation	Mutations in *ATP13A2* has been linked to α-synuclein aggregation. Reduction in *ATP13A2* expression was linked to intracellular accumulation of α-synuclein. Additionally, overexpression of wild-type (WT) *ATP13A2* has been found to prevent the aggregation of α-synuclein induced by oxidative stress (Si et al, 2021).

	(Igarashi and Kashiwagi, 2009). However, high concentrations of these polycations are toxic to cells (Veen et al, 2020).	
***GAK:* Cyclin G associated kinase**	*GAK* regulates the initiation of autophagy in neuronal and glial cells (Zhang et al, 2023). Autophagy is integral in the prevention of protein accumulation (Zhang et al, 2023). *GAK* acts as a co-chaperone with auxillin for heat shock proteins as well as playing roles in clathrin-mediated endocytosis (Baltussen et al, 2018).	Mutations in *GAK* leads to reduced *GAK* expression which has been connected to an increase in α-synuclein toxicity particularly when α-synuclein was overexpressed (Dumitriu et al, 2011). The reduction of *GAK* is accompanied by an increase in α-synuclein levels when α-synuclein was overexpressed in cells (Dumitriu et al, 2011).
***GBA:* Lysosomal hydrolase enzyme glucocerebrosidase (GCase)**	*GBA* is responsible for the cleavage of glycosphingolipids (GSLs), glucosylceramide (GlcCer) and glucosylsphingosine (GlcSph) into glucose and ceramide (Boer et al, 2020). GCase functions as a lysosomal hydrolase (Boer et al, 2020). GCase deficiency/dysfunction results in lysosomal accumulation as seen in Gaucher's disease or a build-up of cholesterol in lysosomes as observed Niemann-Pick disease type C (Boer et al, 2020).	*GBA1* is associated with early onset motor symptoms as well as impaired cognition and hallucinations (Brooker and Krainc, 2021; Neumann et al, 2009).
***LRRK2:* Leucine rich repeat kinase 2 (LRRK2) protein**	*LRRK2* has reported roles in the ubiquitin-proteasome system (UPS); autophagy-lysosomal system (APS); intracellular trafficking, and mitochondrial function (Esteves et al, 2014).	Mutations in *LRRK2* has been linked to both familial and sporadic PD. Mutated *LRRK2* has been linked to the MAPK-associated signal transduction pathway which is activated upon exposure endoplasmic reticulum (ER) stress (Rui et al, 2018). *LRRK2* has been found to co-localise with

		aggregated α-synuclein and thought to exacerbate α-synuclein cytotoxicity (Rui et al, 2018).
MAPT: **Microtubule-associated protein tau.**	*MAPT* (tau) allows for the assembly of tubulin monomers into microtubules, which are necessary for maintenance of cell shape and establishment of axonal transport tracks (Buée et al, 2000). Tau also helps microtubules stabilise and enables microtubules to connect with other components of the cytoskeleton (Guo et al, 2017).	Tau is a component of Lewy bodies (LBs) (Chin et al, 2020). Tau takes on a form described to be both filamentous, insoluble and phosphorylated in neurodegenerative pathological conditions (Brion et al, 2001). Mature fibrillar tau are called neurofibrillary tangles (NFTs) which spreads in a prion-like manner (Zhang et al, 2018). NFTs accumulate in cells and have been demonstrated to inhibit nucleocytoplasmic transport and induce dysfunctional axonal transport (Pan et al, 2023).
PARK7: **Parkinsonism associated deglycase (DJ-1)**	The DJ-1 protein has many functions including apoptosis regulation; autophagy; chaperone activity; mitochondrial homeostasis, and anti-oxidative cellular protection/reactive oxygen species (ROS) regulation (Mencke et al, 2021).	DJ-1 is a key biomarker in the familial forms of PD. There are considerable levels of oxidised DJ-1 in the medulla oblongata, striatum, and substantia nigra (SN) of the midbrain of patients (Saito, 2017). Furthermore, oxidised DJ-1 has been found to be a component of LBs (Saito, 2017).
PINK1: **PTEN induces putative kinase 1**	PINK1 is a mitochondrial-associated proteins that is believed to have connections to fission and fusion of the mitochondria.	The PINK1 protein has an integral role in mitochondrial function, it has been found that mutations in PINK1 leads to the selective loss of dopaminergic neurons (Ge et

		al, 2020). Its loss has been demonstrated to result in increased fission/fragmented mitochondria (Deas et al, 2009).
***PRKN:* Parkin**	Parkin is a member of the ubiquitin ligase family which will ubiquitinate proteins associated with the mitochondria and the cytosol (Seirafi et al, 2015). It functions specifically as a E3 ligase which is a contributor to the machinery responsible for tagging proteins with ubiquitin. This forms the foundation of the UPS which regulates protein levels and is involved in protein quality-control (Coelln et al, 2004).	Parkin is a causative gene in the autosomal recessive form of PD (Mizuno et al, 2001). α-Synuclein, specifically the O-glycosylated form, has been found to be a substrate of Parkin (Coelln et al, 2004). WT Parkin has been found to exude protective effects in the event of proteasome inhibition preventing α-synuclein related toxicity (Coelln et al, 2004).
***SNCA:* α-Synuclein**	Despite α-synuclein's association with PD pathophysiology, it has critical roles in normal cellular function. It is an intrinsically disordered protein (IDP) which is soluble and has been demonstrated to interact with the nucleus, ER, mitochondria, kinases, and other proteins (Bernal-Conde et al, 2020). α-Synuclein is located in the presynaptic terminals and has been found to interact and attach to high-curvature membranes (Sulzer and Edwards, 2019). It binds to synaptobrevin-2/VAMP2 of SNARE complexes which are essential in neurotransmitter release (Burré et al, 2010). α-Synuclein has been reported to have roles in maintenance of immunological host defences including the	Numerous *SNCA* mutations have been found to affect the rate of aggregation. Mutations A30P, E46K, A53T, G51D have been associated with early-onset PD (Flagmeier et al, 2016) and are associated with an alteration in the rate of formation and aggregate conformation (Alam et al, 2019). The A30P mutation has been shown to induce increased rates aggregation when compared to WT α-synuclein and produce oligomeric aggregates (Flagmeier et al, 2016). The A53T and E46K brings about accelerated rates of aggregation (Ohgita et al, 2022; Flagmeier et al, 2016). Aggregates of α-synuclein has

	inflammatory response (Alam et al, 2022).	been implicated in cell stress and apoptosis (Du et al, 2020).
***UCHL1:* Ubiquitin carboxyl-terminal esterase L1**	Found in high levels in neuronal cells. UCHL1 belongs to a group of deubiquitinating enzymes called ubiquitin C-terminal hydrolases essential in maintaining the balance of ubiquitination (a process in tagging proteins for degradation) and de-ubiquitination (removal ubiquitin from proteins) (Sharma et al, 2020).	Evidence demonstrates that in *Drosophila*, knock-down (KO) of UCHL1 enhances mitophagy which in turn rescues phenotypes associated with PD caused by PINK1 or Parkin mutations (Ham et al, 2021).

1.4 Environmental risk factors of PD

PD is an age-related neurological disorder. Studies focusing on global trends in 204 countries and territories show that patients diagnosed with PD tend to be over 65 years old (Ou et al, 2020). There are reported sex differences with twice as many males than females being diagnosed. Cases where women have been diagnosed with PD have yielded observations where progression is faster and mortality rates are higher (Cerri et al, 2019; Haaxma et al, 2007). Female patients with PD have been found to experience gastrointestinal dysfunction, pain and dysphagia (issues with swallowing) plus depressive symptoms (Cerri et al, 2019; Pavon et al, 2010). Whereas, males are more likely to experience cognitive impairment, freezing of gait and camptocormia (bending of the spine) (Cerri et al, 2019). It is reported that these differences are attributed to variations in genes likely to occur in one sex rather than the other. For example, mutations in GAPDH have been associated with mitochondrial damage and autophagy, which are seen more frequently in older males as opposed to females (Cerri et al, 2019; Ping et al, 2018). Additionally, the variations in symptoms and risks when comparing male and female patients were linked to job roles and stress levels (Cerri et al, 2019; Sieurin et al, 2018). Evidence suggests that elements of the individual's environment, noted in **Table 1.2**, contributes to the onset of sporadic PD cases.

Table 1.2 Environmental risk factors involved in the pathogenesis and prognosis of PD.

Environmental Risk	Pathophysiological Mechanisms
Cigarette Smoking	Individuals who had been reported to smoke had a lower risk of having PD compared to non-smokers (Mappin-Kasirer et al, 2020). It has been proposed that cigarettes act to inhibit monoamine oxidase (MAO) preventing the breakdown of dopamine. Further, cigarettes may act as a stimulant restricting the activity of the dopamine transporter (DAT) increasing dopamine at the synapse (Wang et al, 2022).
Metals/Heavy Metals	Exposure to metals such as thallium, chromium, mercury, nickel, and cobalt has been linked to neurotoxicity. Due to the reduced ability of neuronal cells to regenerate, the exposure to these metals in the environment or ingestion has been found to be problematic to health and function of these cells (Vellingiri et al, 2022). Cobalt, nickel, and mercury has been associated with aggregation of α-synuclein as well as disruption to other cellular mechanisms (Vellingiri et al, 2022). Chromium has been implicated in raised ROS levels and thallium has been found to result in the dysfunction of the mitochondria (Vellingiri et al, 2022).
MPTP/MPP^+	1-methyl-4-phenyl-1,2,3,6-tetrahydropyridine (MPTP), structurally similar to the herbicide Paraquat, generates the active metabolite 1-methyl-4-phenylpyridinium (MPP^+). MPP^+ is taken up by DAT, where it accumulates at the mitochondria of dopaminergic neurons blocking NADH-ubiquinone oxidoreductase (complex I) resulting in reduction in adenosine triphosphate (ATP) and increased ROS (Risiglione et al, 2020).
Pesticides/Herbicides	As reported in a cohort study of 140,000 participants, those who have been exposure to pesticides/herbicides before 1982 had a 70% higher incidence of PD 10 to 20 years later than those who were not exposed (Ascherio et al, 2006).

1.5 Oligomers

During the process of α-synuclein aggregation, the monomeric protein will aggregate into an intermediary oligomeric structure made up of approximately 11 monomers (Du et al, 2020). Other studies using baicalein-stabilized oligomers have recorded measurements up to 22 nm in width using electron microscopy (EM) imaging (Hong et al, 2008). The oligomeric structure consists of multiple α-synuclein monomers and are considered to be morphologically heterogenous plus unstable (Du et al, 2020; Ghosh et al, 2015). Aggregation into oligomers can be induced by the presence of metal ions, alcohol, lipids and lipid peroxidation products (Alam et al, 2019). Oligomers have been implicated as one of the primary toxic species associated with PD resulting in: impairment of the complex I machinery of the mitochondria; mitochondrial swelling; lipid peroxidation; ATP synthase oxidation (Du et al, 2020; Ludtmann et al, 2018); ER stress (Du et al, 2020; Pailusson et al, 2017); disrupted proteostasis (Du et al, 2020; Wilkaniec et al, 2019); inflammation; synaptic impairment and cellular apoptosis (Du et al, 2020). The phrase oligomers is an umbrella term relating to a broad range of self-assembling soluble complexes; the structure and biological function of which are highly dependent on the conditions in which assembly takes place. Due to variations in materials and experimental preparations, there are reports of different oligomers with differing characteristics which falls into various categories (**Table 1.3**) (Alam et al, 2019).

Table 1.3 Types of α-synuclein oligomeric aggregates reported in literature.

Oligomer Type	Description	Citations
Off-pathway oligomers	Off-pathway oligomers are reported to be dead end aggregates that do not form fibrillar structures and have been found to be comparatively stable resulting in the fibrils not forming (**see Figure 1.2**).	Alam et al (2019)
On-pathway oligomers	The term "on-pathway" refers to oligomers that are prerequisite structures formed prior to fibril formation. With further recruitment of monomeric α-synuclein they will eventually stabilise into amyloid fibrils (see **Figure 1.2**). These oligomers often have cytotoxic effects and have been linked with Ca^{2+} influx.	Alam et al (2019)
Type 1 Oligomers	The presence of these forms of oligomers arises due to the process of monomers undergoing primary nucleation. They will exist in equilibrium with monomers and form fibrils with a long and straight structure which relies on prolonged incubation.	Alam et al (2019) Ashe (2019)
Type 2 Oligomers	Type 2 oligomers are formed in a secondary nucleation process where fibrils are added to monomers increasing the propensity for oligomers to form through templated aggregation. This process is considered to be a more favourable reaction. These oligomers will also form worm-like fibrils. A process which also requires incubation.	Alam et al (2019) Ashe (2020)
Type A oligomers	Heterogenous small (40 – 45 nm in diameter), globular and protofibrillar structures with observed spherical or annular (ring-shaped) structures. There are variations in structure depending on preparation.	Danzer et al (2007)
Type B oligomers	Heterogenous population, with a large monomer to oligomer conversation rate than type A. Depending on lab preparations, oligomeric morphology takes on a compact spherical shape or amorphous (no definitive	Danzer et al (2007)

	shape) structure. There are variations in structure depending on preparation.	
Type C oligomers	When compared to type A and B oligomers, the oligomer particles were larger in size, observed to be primarily spherical in shape. These oligomers have the ability to induce intracellular aggregation, and oxidative stress.	Danzer et al (2007)

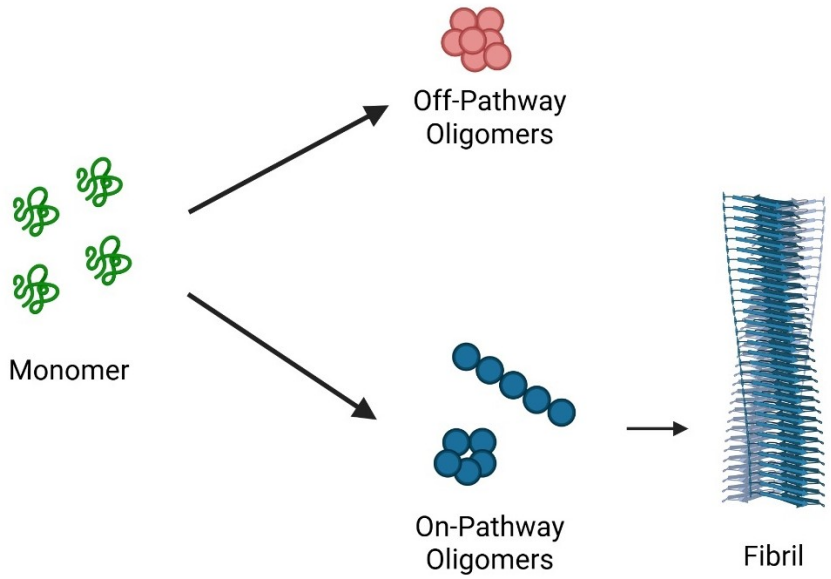

Figure 1.2 The aggregation pathway of α-synuclein. A summary of the aggregation pathway from monomeric α-synuclein oligomers (referred to as on-pathway oligomers, **Table 1.3**). These oligomers will then stabilise and further aggregate into higher-order structures such as full-length fibrils which are integral parts of LBs.

1.6 Fibrils and preformed fibrils (PFFs)

Some oligomers will aggregate further into fibrils (**Table 1.3, Figure 1.2**), which coincides with a conformational change from an α-helical to a β-sheet rich structure (Du et al, 2020; Ghosh et al, 2015). β-pleated sheets stack perpendicular to the fibril axis (Greenwald and Riek, 2010). They are able to undergo elongation through recruitment of monomers as well as fragmentation which allows for its successful replication (Sanchez et al, 2021). Fibrillar α-synuclein is evidenced by cryo-EM to have a diameter of 5 -10 nm (Guerrero-Ferreira et al, 2018). Fibrils can comprise of over 70 monomers (Sanchez et al, 2021). These aggregates can consist of α-synuclein that has been phosphorylated at serine-129, acetylated N-terminal or truncation of the C-terminal (Guerrero-Ferreira et al, 2018). α-Synuclein fibrils form a major component of highly organised cytoplasmic filamentous inclusions called Lewy bodies (LB) (Lashuel, 2020) (**Figure 1.2**) which are found in surviving dopaminergic neurons of the brains of patients diagnosed with PD (Parkkinen et al, 2011). LBs are features of numerous diseases such as PD, Parkinson's disease dementia (PDD), dementia with Lewy bodies, multiple system atrophy (MSA), frontotemporal lobar degeneration (FTLD) and corticobasal degeneration (Menšíková et al, 2022). There are a range of proteins additional to α-synuclein found to be enriched within LBs including but not limited to chaperones (e.g. heat shock proteins), oxidative stress related proteins (e.g. carbonyl reductase 1), kinases (e.g. protein kinase c, beta 1) and proteins associated with ubiquitination (Xia et al, 2008). Moreover, there is conflicting evidence regarding LBs themselves being primary contributors to neurodegeneration (Parkkinen et al, 2011). Instead, aggregates of α-synuclein have been linked to decreased cellular function, neuronal death and PD pathology (Cascella et al, 2021). Fibrils have been found to be both structurally long (mature) and short, with shorter forms being comparatively more toxic due to the presence of more fibrillar ends resulting in the release of oligomeric species (Cascella et al, 2021). Experimental findings show that longer fibrillar structures rescue oligomer-associated toxicity (Lam et al, 2016). Numerous studies that aim to model PD have reported the use of preformed fibrils (PFFs) which are full-length fibrils that have been subjected to sonication (Chmielrez

and Domanskyi, 2021; Patterson et al, 2019; Volpicelli-Daley, 2014; Wu et al, 2019). These PFFs model the mechanism in which long fibrils fragment due to a variety of reasons such as catalysis by chaperones forming shorter structures (Xue et al, 2009) also known as “seeds” (Wu et al, 2019). These seeds have a higher capability of inducing cytotoxicity when compared to other α-synuclein conformations (Xue et al, 2009). Treatment with PFFs have been shown to reduce the activity of neuronal synapses; inhibit synaptic formation (Wu et al, 2019); impair axonal transport; induce mitochondrial dysfunction; trigger inflammatory responses (Tapias et al, 2017) and upregulate the expression of senescence markers (Verma et al, 2022).

1.7 Prion-like activities of α-synuclein

Prion is a shortened term for proteinaceous infectious particles which encompasses a collection of neurodegenerative diseases found to be both fatal and transmissible (Zhu and Aguzzi, 2021). Well known examples include Creutzfeldt-Jakob disease, Gerstmann-Sträussler – Scheinker disease, fatal familial insomnia and bovine spongiform encephalopathy (Baiardi et al, 2023). These disorders particularly Creutzfeldt-Jakob disease and fatal familial insomnia consist of spongiform changes to multiple brain regions, where these spongiform changes are characterised by small round empty spaces (Baiardi et al, 2023; Liberski, 2004). Alternatively, there is a second class of prion disorders including that of Gerstmann-Sträussler – Scheinker disease known as prion protein (PrP) amyloidoses (Baiardi et al, 2023). The foundational occurrence of these amyloid prion conditions is the conversion of cellular prion protein (PrP^{C}) to abnormal PrP (PrP^{Sc}) (Baiardi et al, 2023). It is not well understood why PrP^{Sc} is formed but mutations in the *PRNP* gene, age, inflammation, oxidative stress and the failure of the ubiquitin-proteasomal system (UPS) can all influence this conversion (Baiardi et al, 2023). The failure of the UPS allows PrP^{Sc} to aggregate and stabilise into oligomers increasing the propensity to form amyloid fibrils (Baiardi et al, 2023). An intrinsic element of prion diseases is aggregates of PrP^{Sc} propagating and spreading from cell to cell (Baiardi et al, 2023). These abnormal prions can activate cellular stress responses such as the unfolded protein response (UPR) associated with ER stress (Baiardi et al, 2023).

There have been discussions surrounding α-synuclein being either a prion or prion-like protein (Leak et al, 2019). There is evidence in PD and MSA that α-synuclein has the ability to form aggregated and phosphorylated deposits in various regions of the mice CNS (Prusiner et al, 2015). Further, α-synuclein was also shown to be transmissible in cultured HEK cells (Prusiner et al, 2015). Additionally, when α-synuclein fibrils were taken from brains of MSA patients and added to SH-SY5Y cells, there were observations of an increase in phosphorylated insoluble α-synuclein aggregates (Tarutani et al, 2018). This provides some explanation for why PD has been characterised as a proteinopathy, a specific category of neurodegenerative disorders where there

are observed accumulation of specific proteins in neuronal cells causing cell death (Bayer et al, 2015).

1.8 Molecular events implicated in PD

The loss of dopaminergic neurons in the SNpc not only has underlying environmental and genetic causes but this cellular loss is associated with the dysfunction/failure of cellular systems and pathways. The signalling from the gut microbiota to the CNS has been linked to several neurodegenerative conditions including PD (Dong-Chen et al, 2023). It is believed that part of the importance of the gut-brain axis revolves around altered immune and endocrinologic activity in response to dysbiosis of the gut microbiota (Gallop et al, 2021). The bacterial endotoxin, lipopolysaccharide (LPS) is known to activate glial cells and result in elevated ROS levels in PD (Gallop et al, 2021).

Additionally, role of oxidative stress in PD has been highlighted in various studies (Dong-Chen et al, 2023; Dorszewska et al, 2021; Fujita et al, 2014; Gallop et al, 2021). Oxidative stress has been implicated in the misfolding of proteins which forms the foundation for pathological aggregation to occur (Chen et al, 2012). ROS is produced through various cellular processes including the metabolism of dopamine (DA) and the mitochondrial electron transport chain (Dorszewska et al, 2021). Dopaminergic neurons typically contain high levels of DA, therefore due to the constant metabolism of DA there are constantly high levels of ROS in these neurons causing these cells to be vulnerable (Dorszewska et al, 2021). Although ROS are physiologically necessary for processes such as supporting cell proliferation and host immune system defence (as phagocytes release ROS to kill pathogens) (Chen et al, 2012), there are consequences of elevated cellular ROS levels. ROS have been linked to impaired proteasomal function - normally required for the degradation of ubiquitinated proteins (Dorszewska et al, 2021) as well as lipid, protein and DNA oxidation (Chen et al, 2012). Altogether, literature points to oxidative stress as a key hallmark of PD pathophysiology.

1.9 Stress responsive pathways and the impact protein synthesis

1.9.1 The molecular pathway of the integrated stress response, ISR

It is well documented that α-synuclein aggregates results in cellular stresses such as ER stress and production of superoxides (Du et al, 2020; Pailusson et al, 2017). Further, oxidative stress has also been demonstrated to contribute to the aggregation of α-synuclein in rodent models (Scudamore et al, 2018).

The integrated stress response (ISR) (**Figure 1.3**) is an intrinsic mechanism within the cell's arsenal to respond to imposing stresses efficiently and appropriately for the purpose of promoting cell survival. The ISR modulates protein synthesis in a manner which allows attenuation of global translation and upregulation of specific messenger RNAs (mRNAs) (Costa-Mattioli and Walter, 2020). The initiation of such a molecular pathway can begin with stress events such as oxidative stress which is sensed by the eukaryotic initiation factor (eIF2) kinase stress sensor, heme-regulated inhibitor (HRI) (Suragani et al, 2012). Alternatively, viral infection activates protein kinase R (PKR) (Derisbourg et al, 2021). Accumulated misfolded proteins in the ER triggers protein kinase R-like endoplasmic reticulum kinase (PERK) and finally deprivation of amino acids induces general control nonderepressible 2 (GCN2) expression (Derisbourg et al, 2021). The activation of these kinases results in the subsequent phosphorylation of the α-subunit of eIF2 (Donnelly et al, 2013), at serine-51 (Humeau et al, 2020). This results in the inhibition of cap-dependent translation (Humeau et al, 2020) due to impeding the formation of the ternary complex, $tRNA^{Met}$-GTP-eIF2 (Liu et al, 2020). This process is contingent on the activity of EIF2B. EIF2B has five subunits – α, β, γ, δ and ε, which exists in various complexes, with each subunit having demonstrated or assumed specialised roles (Bogorad et al, 2018). The eIF2B complex is the guanine nucleotide exchange factor of the GTPase eIF2. EIF2B acts to destabilise the GDP-eIF2 structure allowing GTP to bind to eIF2 (Bogorad et al, 2018). Therefore, under normal conditions, the ternary complex allows the delivery of the initiating methionyl tRNA ($tRNA^{Met}$) to the 40S ribosome (Girardin et al, 2021). As a consequence of stress, the phosphorylation of

eIF2α alters eIF2B binding to eIF2, causing negative regulation of cap-dependent translation (Ito et al, 2023; Licari et al, 2021). This is physiologically beneficial because the ISR reprogrammes and rewires translation for the purpose of resolving imposing stresses (Zhang et al, 2021). Downstream of eIF2α phosphorylation, is the selective translation of mRNAs with short upstream open reading frames (uORFs) such as activating transcription factor 4 (ATF4), C/EBP homologous protein (CHOP) plus protein phosphatase 1 regulatory subunit 15A (PPP1R15A)/growth arrest and DNA damage-inducible protein (GADD34) (Derisbourg et al, 2021). GADD34 acts as a ISR antagonist through promotion of dephosphorylation of phosphorylated eIF2α (Derisbourg et al, 2021). ATF4 is a member of the ATF subfamily – a member of the basic leucine zipper (bZIP) transcription factor superfamily. It is integral to the regulation of transcription of various genes (B'chir et al, 2013). It can execute its role through binding to the C/EBP-ATF response element (CARE) sequences present on specific targeted genes (B'chir et al, 2013). There are approximately 234 known ATF4 target genes (Neill et al, 2023). Some of these genes that interact with the ATF4 protein include but are not limited to: CHOP, activating transcription factor 3 (ATF3) and Tribbles Homolog 3 (TRIB3) (Neill et al, 2023). DDIT3 known as the DNA damage-inducible transcript 3 also known as CHOP/GADD153 is expressed as a result of ER stress, DNA damage and starvation. This results in cell cycle arrest, apoptosis or differentiation depending on the cell type (Jauhiainen et al, 2012). ATF3 plays roles in regulating the inflammatory response (Hai et al, 2018) plus it has the ability to regulate the cell cycle and act as a pro-apoptotic agent (Lu et al, 2006). TRIB3 belongs to the pseudokinase gene family which are proteins that lack kinase activity but are able to regulate other kinases by competing for the same peptide substrate of target kinases (Arif et al, 2023). Therefore, ATF4 through its interactions, influences various cellular processes and potentially cell survival. When considering the ISR, the intensity and duration of the stress pose as a key factor when influencing downstream processes of the ISR (Derisbourg et al, 2021). Molecular events that result in extended/constant ISR activation/eIF2α phosphorylation may lead to ATP depletion and apoptosis (Derisbourg et al, 2021). Additionally, in response to ER stress, phosphorylation of eIF2α and ATF4 expression can lead to enhanced

expression of CHOP, that modulates death receptor 5 (DR5), BIM and PUMA which mediates ER stress related apoptosis (Hetz et al, 2020).

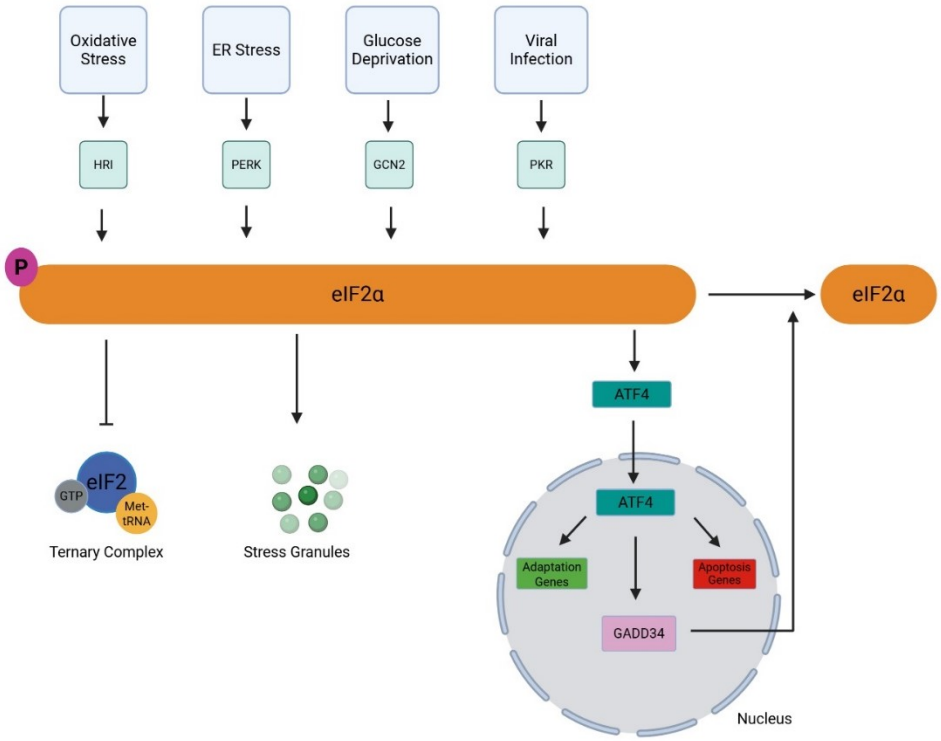

Figure 1.3 The ISR pathway. A summary of the ISR pathway showing various imposing cell stresses and the resulting consequences that occurs due to phosphorylation of eIF2α including the inhibition of the ternary complex resulting in inhibition of translation, formation of SGs and the activity of increased ATF4 expression.

1.9.2 The ISR, neurodegeneration and disease

The ISR has been implicated in numerous conditions such as cancer (Ghaddar et al, 2021; Licari et al, 2021; Tian et al, 2021) as well as neurological disorders (Costa-Mattioli and Walter, 2020) such as AD (Hu et al, 2021); amyotrophic lateral sclerosis (ALS) (Marlin et al, 2022); Huntington's disease (HD) (Paul, 2021); traumatic brain injury (TBI) (Chou et al, 2017); PD (Demmings et al, 2021) and Down's syndrome (Rosi and Frias, 2020). Studies have explored the concept that activation of the ISR, in pathological conditions, could become desensitised to imposing stresses altering the homeostatic balance necessary for cellular function and health (Costa-Mattioli and Walter, 2020). Evidence has shown that inhibition of PKR and/or inhibited eIF2α phosphorylation led to

increased tumour formation in mouse fibroblasts (Costa-Mattioli and Walter, 2020). This indicates that ISR desensitisation may be a contributor to cancer pathology. On the other hand, there are instances of hypersensitisation of the ISR in disease conditions (Costa-Mattioli and Walter, 2020) particularly when stress is sustained in a chronic manner resulting in ISR overactivation (Bond et al, 2020). This occurrence is believed to be synonymous with the presence of neurotoxic proteins that induce neurodegeneration (Bond et al, 2020). This can be observed when eIF2α phosphorylation was found to lead to the upregulation of the β-site amyloid precursor protein (APP) cleaving enzyme-1 (BACE1) in primary neurons, which suggests that the ISR may play roles in amyloid beta (Aβ) peptide production contributing to AD pathology (Bond et al, 2020). To expand, BACE1 mediates Aβ deposition which is heightened in clinical AD *in vivo* and is connected to the loss of neuronal cells (Bond et al, 2020). Aβ exists as a monomeric unstructured protein but undergoes a conversion from an α-helical to β-sheet rich structure, causing fibril formation (Chen et al, 2017). Studies have shown that the activation of the ISR in neurons has a connection to PD. This is due to correlating observations of α-synuclein aggregation, ER stress/PERK activation and caspase-3 expression (Jiang et al, 2010) providing an explanation for the cellular apoptosis underpinning neurodegeneration in PD. The link between PD and the ISR has also yielded experimental findings showing that α-synuclein aggregates such as PFFs induces the expression of protein markers associated with the ISR such as ATF4 in mesencephalic neuronal cultures (Demmings et al, 2021).

1.9.3 Unfolded protein response pathway

The UPR (**Figure 1.4**) is another stress specific pathway activated when there is an accumulation of unfolded and/or misfolded proteins in the ER (Hetz et al, 2020), a site for protein folding and maturation (Adams et al, 2019). There are three major branches of the UPR which can lead to adaptive and pro-apoptotic downstream processes (Hetz et al, 2020). For instance, the UPR mechanism supports cellular adaptation to ER stress, through the phosphorylation of eIF2α (Hetz et al, 2020). This allows the selective translation and reduction of global translation supporting ER protein folding, autophagy plus other beneficial cellular mechanisms (Hetz et al, 2020). Additionally, the IRE1α

RNase can cleave ER mRNAs leading to their degradation, through a mechanism called regulated IRE1-dependent decay (RIDD), necessary for reducing protein load and improving metabolism (Hetz et al, 2020). When RIDD is sustained, it results in the degradation of microRNAs (miRNAs) important in the negative control of caspase-2 resulting in inflammation and cellular death (Hetz et al, 2020). ATF6 cleavage is another event in the cell's efforts to adapt to ER stress, where the fragment ATF6p50, migrates to the nuclei activating transcription of UPR specific target genes contributing to protein folding and secretion plus ER and Golgi biogenesis (Hetz et al, 2020). In the absence of cellular stress, IRE1, PERK and ATF6 are inactive predominantly due to their association with the chaperone binding immunoglobulin protein (BiP) also known as 78 kDa glucose-regulated protein (GRP78) (Costa et al, 2020). When there are increases of unfolded or misfolded proteins in the ER, BiP/GRP78 will have a stronger and preferential association with the incorrectly folded proteins, resulting in dissociation from IRE1, PERK and ATF6 triggering UPR activation (Costa et al, 2020).

Phosphorylated PERK has been observed in post-mortem samples of PD and DLB patients. Additionally, regions of the brain such as the cingulate gyrus, has been shown to have elevated BiP mRNA levels (Costa et al, 2020). Overexpressed α-synuclein has been demonstrated to increase phosphorylation of eIF2α and BiP/GRP78 levels (Costa et al, 2020). Oligomeric α-synuclein has been shown to activate IRE1α in SH-SY5Y cells (Costa et al, 2020). The drug tunicamycin, a known ER-stress inducer, was shown to increase oligomer levels (Costa et al, 2020). All these findings show that ER stress is linked to α-synuclein and has the capacity to exacerbate α-synuclein aggregation and toxicity.

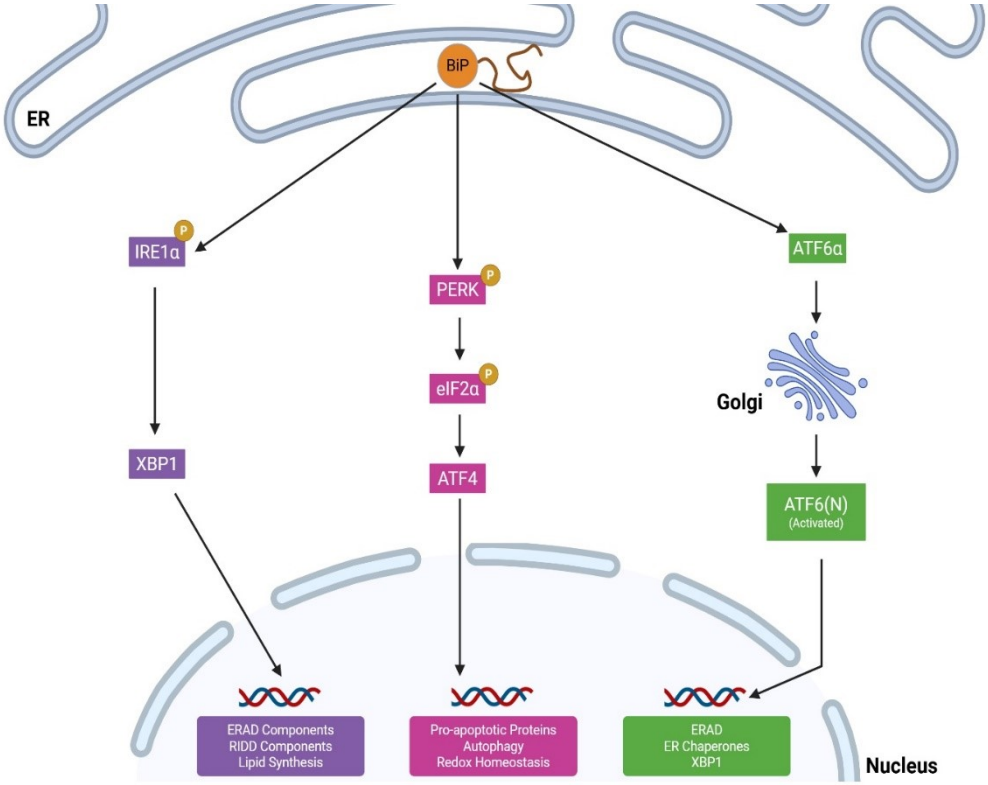

Figure 1.4 The UPR pathway during ER stress. A summary of the UPR pathway showing the activation of BiP upon interaction with unfolded proteins when there is an accumulation of unfolded/misfolded proteins. The activation of BiP is shown to cause phosphorylation of IRE1α and PERK leading to various downstream consequences due to the reprogramming of translation. Additionally, ATF6α localises to the Golgi apparatus where it is activated leading to numerous downstream events. RIDD - regulated IRE1-dependent decay (RIDD). ERAD – endoplasmic reticulum-associated degradation.

1.9.4 The mechanistic target of rapamycin (mTOR) signalling pathway

The mTOR pathway involves two protein complexes mTORC1 and mTORC2, which are involved in the cell's nutrient sensing pathway and is linked to aging, regulation of growth, metabolism (Querfurth and Lee, 2021) plus synaptic plasticity (Hoeffer and Klann, 2010). mTORC1 regulates with cell metabolism and growth, whilst mTORC2 is associated with cell proliferation and survival (Zou et al, 2020). mTOR specifically mTORC1 influences protein synthesis through the regulation cap-dependent translation by phosphorylating both p70 ribosomal S6 kinase 1 (p70S6K1) and eukaryotic initiation factor 4E (eIF4E)-binding protein 1 (4E-BP1) (Querfurth and Lee, 2021; Zou et al, 2020). When

4E-BP1 is phosphorylated, this prevents it binding to eIF4E. This allows eIF4E to promote cap-dependent translation (Laplante and Sabatini, 2009).

The translation of *PARK7*/DJ-1 (refer to **Table 1.1**) can depend on mTORC1 where inhibition of mTORC1 reduces the antioxidative and neuroprotective properties associates with DJ-1 (Querfurth and Lee, 2021). Indicating a potential link between the mTOR pathway and PD. Furthermore, REDD1 is a stress-responsive protein, involved in the inhibition of the mTOR pathway. It is overexpressed in response to ER stress, ROS, LPS, amyloid proteins, aging, alcohol and smoking (Kim et al, 2023). It has been shown that REDD1 is upregulated in response to PD neurotoxins like 1-methyl-4-phenylpyridnium (MPP+), 6-hydroxydopamine (6-OHDA) and rotenone (Querfurth and Lee, 2021). Additionally, mTOR activation has been shown to protective in PD neurotoxin models (Querfurth and Lee, 2021).

1.10 Stress granules

1.10.1 The structure of stress granules

Stress granules (SGs) are membraneless, cytoplasmic cellular foci which form in response to various stress-associated mechanisms including phosphorylation of eIF2α and inhibition of mTOR (Hofman et al, 2020; Protter and Parker, 2016; Kedersha et al, 2002; Sfakianos et al, 2018). Mammalian SGs typically range in the size of 100-1000 nm (Wolozin and Ivanov, 2019). They consist of a stable core and a dynamic shell (Hofmann et al, 2021). DNA-binding proteins and RNA-binding proteins such as GTPase-activating protein SH3 domain-binding protein (G3BP) SG assembly factor; TAR DNA-binding protein 43 (TDP-43), fused in sarcoma (FUS); T-cell intracytoplasmic antigen 1 (TIA1); cytotoxic granule associated RNA binding protein/TIA1-related protein (TIAR) and many others have been found to be contributors to SG formation during stress (Wang et al, 2022).

1.10.2 Assembly and disassembly of SGs

SGs exist in equilibrium with polysomes where conditions of stress results in the disassembly of polysomes resulting in an increased pool of untranslated mRNPs present in pre-initiation complexes (PIC) which provides an environment favouring SG formation (Wolozin and Ivanov, 2020). There are two prominent models that recapitulate the assembly of SGs. The first proposed model suggests an event of untranslated mRNAs that are attached to proteins with regions that are intrinsically disordered resulting in liquid-liquid phase separation (LLPS) synonymous with IDR-IDR (intrinsically disordered region) interactions forming a stable core (Wheeler et al, 2016). Alternatively, the second model suggests that there is aggregation of mRNAs and proteins that form stable cores allowing for formation of nucleation sites for LLPS due to the concentrating of proteins containing IDRs. Also, this model proposes that within the single SG there are potentially multiple cores (Wheeler et al, 2016). SGs exist in an equilibrium of fusion and fission, reflective of its dynamic nature (Protter and Parker, 2016).

There are numerous processes involved in the assembly and disassembly of SGs. Assembly of SGs can be regulated by post translational modifications

such as the addition of O-linked N-acetylglucosamine (O-GlcNAc) to serine and threonine residues (an event increased in oxidative stress). SG formation can also be promoted by G3BP and UBAP2L demethylation, ribosylation and SUMOylation (Hofmann et al, 2021). Chaperones and disaggregases (e.g. HSP70) have been implicated in the disassembly of SGs. In addition to this, decreased multivalency; arginine methylation; cold-shock and the degradation of abnormal SGs by autophagy has been shown to participate in the process of SG disassembly (Hofman et al, 2020)

1.10.3 The function of stress granules

SGs function to sequester translationally silent mRNAs for storage, degradation, and later translation for the purpose of cell recovery and homeostasis (Campos-Melo et al, 2021). SGs are essential in the reduction of energy consumption to allow for the resolution of cell stress (Sandoval et al, 2021).

There are three subtypes of SGs that has been identified (Advani and Ivanov, 2020; Hofmann et al, 2021; Ivanov et al, 2019; Riggs et al, 2020; Martin et al, 2022;) (**Figure 1.4**). Type I canonical SGs form in response to oxidative, ER and viral infection which induces eIF2α phosphorylation. These SGs require G3BP for assembly and contains 48S PICs but they lack eIF2 and eIF5 (Hofmann et al, 2021). Type II SGs form as a result of attenuated translation caused by eIF4A helicase inactivation that occurs due to eIF4A inhibitors. These SGs also require G3BP but will contain eIF2 and eIF5 (Hofmann et al, 2021). Examples of eIF4A inhibitors include: silvestrol (Zhen et al, 2022) and pateamine A (Bordeleau et al, 2006). Type I and II SGs are considered to be canonical SGs (Advani and Ivanov, 2020). Type III SGs, unlike Type I and II, lacks eIF3. Type III SGs, also considered to be non-canonical, form in response to ultraviolet (UV) light, selenite, nitric oxide and glucose starvation (Advani and Ivanov, 2020; Hofmann et al, 2021). Selenite for example inhibits mTORC1 activity preventing 4E-BP1 phosphorylation which allows for the binding of 4E-BP1 to eIF4E. This results in the displacement of eukaryotic initiation factors G/A (eIF4G/eIF4A) from the eIF4F complex causing cap-dependent translation to be inhibited (Advani and Ivanov, 2020). This promotes SG formation independent of eIF2α phosphorylation (Advani and

Ivanov, 2020). Further, non-canonical SGs in some cases will lack canonical SG components such as RACK1 and HDAC6 (Fujimara et al, 2012). These non-canonical SGs are considerably less dynamic compared to their canonical counterparts and have been shown to induce cytotoxicity (Advani and Ivanov, 2020).

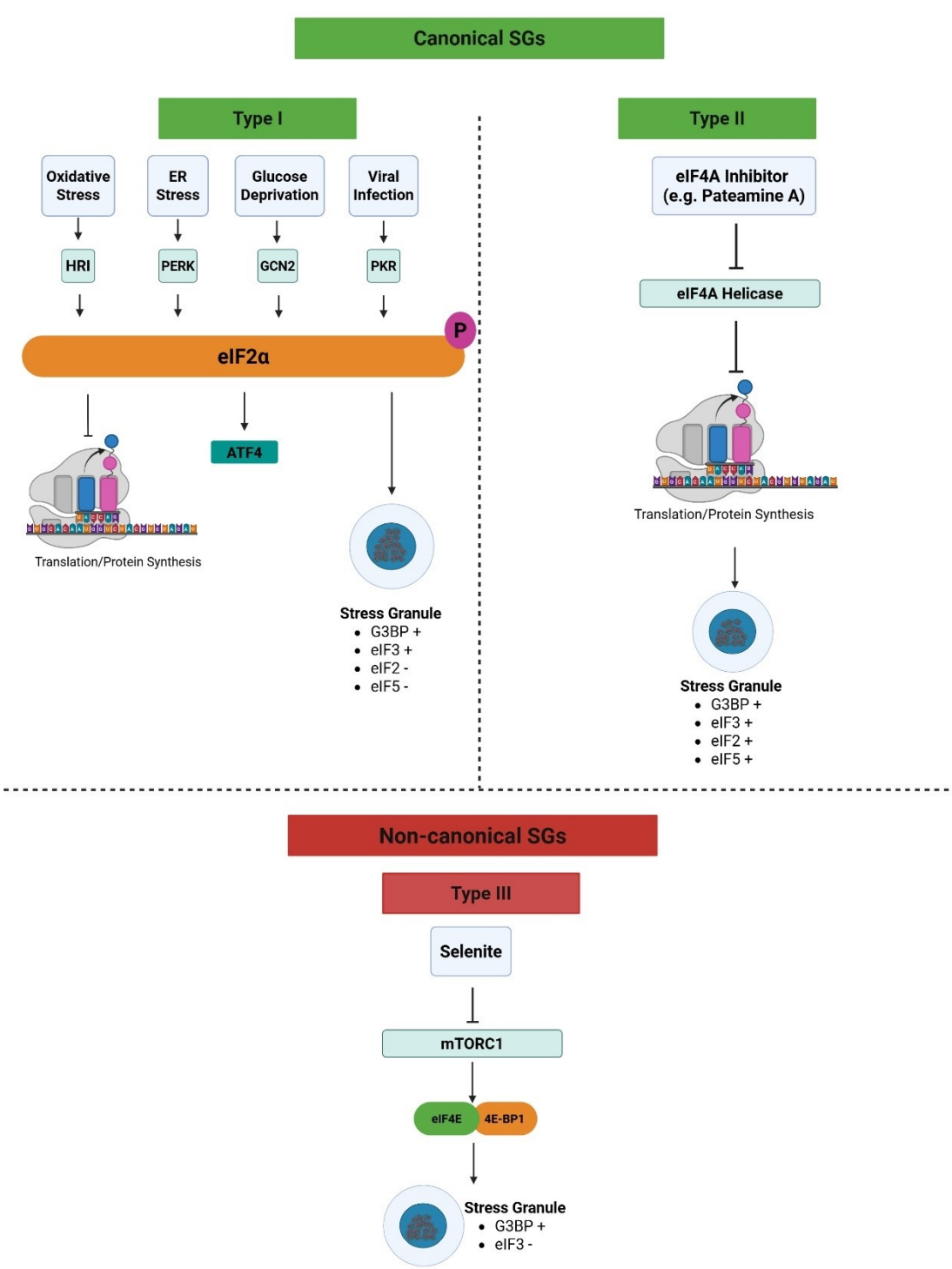

Figure 1.5 The pathways that lead to formation of canonical and non-canonical SGs. A summary of how the phosphorylation of eIF2α and eIF4A inhibitors lead to formation of canonical SGs containing eIF3. Whereas non-canonical SGs lack eIF3 and form in response to various stresses including selenite which inhibits mTORC1.

1.10.4 Stress granules and neurodegeneration

SGs are associated with the neuronal degeneration in diseases such as ALS, AD (Asadi et al, 2021; Wolozin and Ivanov, 2020), HD and multiple sclerosis (MS) (Martin et al, 2022). These conditions are examples of proteinopathy disorders where the pathological conditions are dependent or at least partially dependent on the presence of aggregated proteins that induce cytotoxicity. Aβ and tau has been associated with AD (Ganguly et al, 2017) and TDP-43 with ALS (Scotter et al, 2015). TDP-43 and tau which has been implicated in neurodegeneration, are also associated with SGs (Martin et al, 2022). Which is suggestive of a connection between SGs and neurodegenerative disorders. A key element of these conditions is the persistence of stress within the cell resulting in SGs taking on what is known as a "pro-death" phenotype (Martin et al, 2022). SGs can result from acute stress lasting for two hours or less, (Reineke and Neilson, 2019). Whereas chronic stress results in the inhibition of SG formation through overcoming phosphorylation of eIF2α (Reineke and Neilson, 2019). Chronic stress may also promote the assembly of SGs due to increased eIF2α phosphorylation which has been demonstrated in ALS and frontotemporal dementia (FTD) (Reineke and Neilson, 2019). There are observations of co-localisation of SGs with FUS and TDP-43 in FTD-ALS. These interactions can cause the usually dynamic and reversible SGs to become insoluble aggregates that are unlikely to undergo the typical process of disassembly even when the stress dissipates. This gives rise to impaired proteostasis, dysfunctional RNA homeostasis and alterations in protein synthesis resulting in serious neuronal impairment (Baradaran-Heravi et al, 2020). When exploring the effect of ALS-associated mutant *HNRNPA2B1* and *C9orf72* iPSc-derived motor neurons, it was found that there was increased formation of SGs as well as impaired clearance of SGs induced by puromycin treatment (Markmiller et al, 2018). It was also found that SGs in these mutant cells rather than localising in the neuronal soma (typically seen in WT cells), SGs were found to form in neurites. The neurite-localised SGs in the mutant cells were rich in proteins involved in RNA transport and translation inhibition which suggests SGs may exhibit aberrant assembly/disassembly dynamics and may alter contribute to dysfunction of neuronal function e.g. axonal transport potentially underpinning neurodegeneration in ALS (Markmiller et al,

2018). The connection between PD and SGs has yet to be explored in depth. However, the protein DJ-1 implicated in PD was found to associate with SGs during oxidative stress in mammalian cells (Repici et al, 2019).

1.11 Extracellular vesicles, neurodegeneration and Parkinson's disease

1.11.1 Physiological role of extracellular vesicles

Extracellular vesicles (EVs) have been a fundamental aspect of pathological propagation in neurodegenerative diseases (Ananbeh et al, 2021; Ferrara et al, 2023; Garcia-Contreras and Thakor, 2022; Upadhya and Shetty, 2021) and the cell-to-cell transference of prions (Soukup et al, 2023). EVs are important to cellular function due to its role in tissue maintenance and repair; inflammation regulation; stimulation of cell differentiation; waste removal and neurotransmission (Rashed et al, 2017).

1.11.2 Extracellular vesicles in disease and neurodegeneration

Despite the clear physiological importance of EVs, their ability to be released and taken up by cells have implications in the progression of cancer (Chang et al, 2021), cardiovascular (Fu et al, 2020), psychological (Kong et al, 2023) and neurodegenerative conditions (Raghav et al, 2022). There has been evidence of increases in the size of EVs in disorders such as ALS (Sproviero et al, 2018). EVs have been found to be enriched with proteins such as SOD1, TDP-43 and FUS which play a role in ALS pathology (Sproviero et al, 2018). Similar observations have been found in PD; when there is an accumulation of α-synuclein within the cell, the cell will engage in cellular mechanisms to remove α-synuclein which can occur by diffusion or exocytosis (Neupane et al, 2023). The presence of α-synuclein in EVs can be a result of dysfunction in specific cellular systems such as the autophagy-lysosome pathway (ALP) responsible for intracellular protein homeostasis (Minakaki et al, 2018). In human neuroglioma (H4) cells, ALP was inhibited by treatment with the lysosomal inhibitor bafilomycin A_1 or chloroquine diphosphate salt (a lysosomotropic drug) (Minakaki et al, 2018). EVs contained more α-synuclein when ALP inhibition occurred when treating cells with both compounds (Minakaki et al, 2018). Given that ALP is key in the regulation of α-synuclein levels, it shows that the cell will use the waste removal capabilities of EVs to regulate intracellular α-synuclein levels.

α-Synuclein internalization can occur by clathrin-mediated endocytosis; diffusion as well as the utilisation of the lymphocyte-activation gene-3 (LAG3); tunnelling nanotubules and heparan sulfate proteoglycans (Smith et al, 2023). The neuronal receptor, LRP1, that regulates endocytosis has also been found regulate the uptake of α-synuclein in human induced pluripotent stem cells (iPSCs) – derived neurons (iPSNs) (Chen et al, 2022). Furthermore, mutated genes associated with PD (e.g. *LRRK2*, *ATP13A2*, refer to **Table 1.1**) have also been found to play roles in cell-to-cell transmission of α-synuclein (Smith et al, 2023). It has been demonstrated that there was an increase in the cellular uptake of tagged α-synuclein associated with EVs in SH-SY5Y cells (Gustafsson et al, 2018) where α-synuclein was primarily present on the outside of EVs with some on the inside (Gustafsson et al, 2018). A53T α-synuclein was also found to reside on the EVs membrane. Additionally, the mutations, H50Q and G51D, coincided with increased levels of EV-associated α-synuclein (Gustafsson et al, 2018). Altogether, these reports show that EVs mediates α-synuclein cell-to-cell transmission.

1.12 Research overview and aims.

There are links in literature between α-synuclein and cell stress plus α-synuclein and EVs within PD pathophysiology. However, there is a lack of robust evidence on how specific stress pathways such as the ISR plays a role in aggregated α-synuclein-associated cellular toxicity. Furthermore, there is a lack of existing evidence exploring how α-synuclein aggregates alters the proteomic cargo of EVs.

Therefore, the aims of this thesis are as follows:

- to validate ISR activation and SG formation in response to various well-known compounds such as sodium arsenite (SA), thapsigargin (Tg) and MPP+ to provide a baseline of expectation in SH-SY5Y cells for later comparisons when investigating α-synuclein-induced stress.
- to demonstrate the ability of synthesised oligomers and PFFs to activate the ISR and induce SG formation.
- to begin to connect α-synuclein-induced stress to EV-mediated cell-to-cell transmission, the proteomics of sEVs derived from α-synuclein aggregate treated cells will be explored to determine presence of α-synuclein and stress-associated proteins.

2 Chapter Two: Materials and methods

2.1 Reagents and materials

Table 2.1 Reagents and materials used throughout the study.

Reagents and Materials	**Supplier**	**Catalogue Number**
4x Laemmli buffer	BioRad, UK	1610747
Ampicillin	VWR International, UK	A051-B
Bicinchoninic Assay (BCA)	ThermoFisher Scientific, UK	C23227
BL21 *E.coli* (DE3) Competent Cells	Thermo Scientific™, UK	EC0114
Bovine Serum Albumin (BSA)	Sigma-Aldrich, UK,	A7030
CellROX Green	ThermoFisher Scientific, UK	C10444
cOmplete Protease Inhibitor Cocktail	Sigma Aldrich, UK	11697498001
ProLong Diamond Antifade Mountant	ThermoFisher, UK	P36962
Countess™ Cell Counting Chamber slides	Invitrogen™, UK	C10228
CyQUANT™ LDH kit	ThermoFisher, UK	C7026
Dimethyl sulfoxide (DMSO)	Sigma-Adlrich, UK	D8418
Emetine	Sigma-Aldrich, UK	E2375
Gibco™ Dulbecco's Phosphate-Buffered saline (DPBS)	Gibco™, UK	14040182
Gibco™ Dulbecco's Modified Eagle Medium (DMEM), high glucose, GlutaMAX™	Gibco™, UK	10569010
Gibco™ Foetal Bovine Serum (FBS)	Gibco™, UK	10082147
Gibco™, Penicillin-Streptomycin (Pen-Strep)	Gibco™, UK	15140122
Hi-Load 26/200 Superdex 200 pg column	GE healthcare	28989336
Human ATF4 ELISA Kit	Proteintech, UK	KE00147

Imperial Gel Stain	Fisher Scientific, UK	24615
Molecular weight marker	LICORbio, UK	928-40000
MPP+ Iodide (in water)	Sigma-Aldrich, UK	D048
Mr Frosty™ Freezing Containers	ThermoFisher, UK	5100-0001
NIAD Dyes	La-Trobe University (Hong Lab)	N/A
Oligomers	BMRC (Laura Shippey)	-
PFFs	BMRC (Laura Shippey)	-
PhosSTOP™	Sigma Aldrich, UK	4906845001
Ponceau S staining solution	ThermoFisher Scientific, UK,	A40000279
Puromycin dihydrchloride	Gibco, UK	A1113803
RNA-to-cDNA™	ThermoFisher Scientific, UK	4387406
Sodium arsenite solution	ThermoFisher, UK	7784-46-5
SyTOX blue	Invitrogen, UK	S34857
Taqman Gene Expression Assay	Life Technologies, UK	4331182
tert-Butyl Hydrogen Peroxide (TBHP) solution	Sigma-Aldrich, UK	458139
Thapsigargin (in DMSO)	Sigma-Aldrich, UK	T9033
The ReliaPrep™ RNA Cell MiniPrep system	Promega, UK	Z6011
Thioflavin T (ThT)	Sigma Aldrich, UK	T3516-25G
Trypan Blue Solution	Gibco™, UK	15250061
VivaSpin 500 30000 MWCO	Scientific Laboratory Supplies, UK	FIL8560
β-mercaptoethanol (BME)	G Bioscience	BC98
10-well comb Mini-PROTEAN TGX™ Precast Gels (4-20%)	BioRad, UK	4561093
Gibco™ Trypsin-EDTA (0.25%)	Gibco™, UK	25200072

Table 2.2 Primary and secondary antibodies used in immunocytochemistry (ICC) and western blot experiments.

Primary Antibody/Host/Reactivity/ Clonality	**Supplier/Catalogue Number**	**Dilution**
Alix, Human, Rabbit, Polyclonal	Proteintech, UK, Cat No. 12422-1-AP	1:500
Beta-Actin, Mouse, Human, Monoclonal	Proteintech, Cat No. 66009-1-Ig	1:10000
Beta-Tubulin, Rabbit, Human, Polyclonal	Abcam, Cat No. ab6046	1:1000
CD9, Human, Rabbit, Polyclonal	Proteintech, UK, Cat No. 20597-1-AP	1:250
CHOP, Rabbit, Human, Polyclonal	Proteintech, Cat No. 15204-1-AP	1:500
EIF2S1, Mouse, Human, Monoclonal	Abcam, Cat No. ab5369	1:1000
GADD34, Rabbit, Human, Polyclonal	Proteintech, UK, Cat No. 10449-1-AP	1:250
Mouse anti-Alpha-Synuclein, Monoclonal	ThermoFisher Scientific, UK, 32-8100	1:500
Phospho-EIF2S1, Rabbit, Human, Monoclonal	Abcam, Cat No. ab32157	1:1000
Puromycin, Mouse, Human, Monoclonal	Sigma-Aldrich, Cat No. MABE343	1:500
Rabbit anti-Alpha-Synuclein, Monoclonal	Abcam, UK, ab209420	1:1000
Rabbit anti-G3BP1 (Conjugated to AlexaFluor 488), Monoclonal	Abcam, UK, ab214946	1:1000
Rabbit anti-Ki67, Monoclonal	Abcam, UK, ab16667	1:100
Rabbit anti-TIA1, Monoclonal	Abcam, UK, ab140595	1:150
Secondary Antibody/Reactivity/ Clonality	**Supplier**	**Dilution**
Goat Anti-Rabbit IgG (H+L) Texas Red, Polyclonal	ThermoFisher, UK, T-2767	1:1000
Goat Anti-Mouse IgG H&L AlexaFluor 594, Polyclonal	Abcam, UK, ab150116	1:1000

IRDye 680RD Goat anti-Rabbit IgG (H+L), Polyclonal	LiCOR, UK, Cat No. 926-68071	1:15000
IRDye 800CW Goat anti-Mouse IgG (H+L), Polyclonal	LiCOR, UK, Cat No. 926-32210	1:15000

2.2 Cell culture

2.2.1 Culturing of SH-SY5Y cells

Human SH-SY5Y neuroblastoma cells derived from the thrice-cloned sub-line of the bone marrow biopsy derived line SK-N-SH (European Collection of Authenticated Cell Cultures, UK) were maintained and cultured at 37 °C and 5 % CO_2 in DMEM in 175 cm^2 flasks. The medium was supplemented with 10 % (v/v) Foetal Bovine Serum (FBS) and 1 % (v/v) Penicillin-Streptomycin (Pen-Strep). The sub-culturing of SH-SY5Y cells involved cells being washed in Gibco™ Dulbecco's Phosphate-Buffered saline (DPBS) Subsequently, SH-SY5Y cells were detached from the surface of culture flasks using (0.25%) Trypsin-EDTA and inactivated using DMEM GlutaMAX™ (supplemented with 10 % (v/v) FBS, 1 % (v/v) Pen-Strep). Cells were centrifuged using the Mega Star 1.6R centrifuge at 500 x *g* for 5 mins and the remaining supernatant was removed, and the cell pellet was resuspended in DMEM GlutaMAX™ (supplemented with 10 %(v/v) FBS, 1 % (v/v) Pen-Strep) and introduced into a new 175 cm^2 flask and maintained at 37 °C and 5 % CO_2. Cells are sub-cultured every 3-4 days at 70 – 80 % confluency. Cells were not used over passage 25.

2.2.2 Cryopreservation of SH-SY5Y neuroblastoma cells

SH-SY5Y neuroblastoma cells were grown to a confluency of 70 % in 175 cm^2 flasks and sub-cultured. Cells were counted using Trypan Blue Solution (0.4 % (w/v)) and Countess™ Cell Counting Chamber slides. Cells were counted using the Countess™ 3 Automated Cell Counter. Cells (2 x 10^6) were suspended in 90 % (v/v) FBS and 10 % (v/v) dimethyl sulfoxide (DMSO) and stored in cryovials. Cryovials were stored in Mr Frosty™ Freezing Containers at -80 °C for 24 hrs. Cryovials were then moved to a dewar container containing liquid nitrogen to be frozen for long-term storage.

2.2.3 Thawing SH-SY5Y neuroblastoma cells

Cryovials containing frozen cells was taken from the liquid nitrogen dewar container and placed in a water bath set at 37 °C. Cells were thawed and placed in falcon tubes containing 5 mL DMEM (10 % FBS, 1 % Pen-Strep). Cells were centrifuged for 5 mins at 500 x *g*. Supernatant was removed, and

cells were resuspended in DMEM (10 % FBS, 1 % Pen-Strep) and placed in 25 cm^2 flasks. Cells were maintained in incubators at 37 °C and 5 % CO_2.

2.2.4 Differentiation of SH-SY5Y neuroblastoma cells

Cells were grown in 6-well plates or 24-well plates containing coverslips in DMEM (10 % FBS, 1 % Pen-Strep). The next day cell medium was replaced with DMEM (1% FBS, 1% Pen-Strep) containing all-trans-retinoic acid (ATRA) (Sigma-Aldrich, UK, R2625) at 10 µM for 4 days to induce differentiation. ATRA supplemented DMEM medium was replaced after 2 days. DMEM supplemented with 1 % (v/v) FBS and 1 % (v/v) Pen-Strep was replaced with DMEM (10 % FBS, 1 % Pen-Strep) for one day prior to further experimentation. Brightfield images were taken on different days of differentiation using the Olympus IX81 motorized inverted microscope using the 10x objective.

2.3 Production of monomeric α-synuclein

2.3.1 Transformation of BL21 (DE3) competent *Escherichia coli* (*E.coli*) cells

BL21 *E.coli* (DE3) Competent Cells were thawed on ice and subsequently incubated with a pET 23a^{+} vector containing the WT α-synuclein sequence on ice with periodic agitation for 20 min. Subsequently cells were then exposed to heat shock for 45 secs and then returned to ice for 1 min. Cells were then added to 500 µL of Luria-Bertani (LB) broth comprising of 10g tryptone, 10g sodium chloride and 5g yeast extract per Liter. Ampicillin was dissolved at a concentration 100 mg/mL in ultrapure water and filter sterilised through a 0.2 mm syringe filter. Ampicillin was added to LB media at a concentration of 1 µL/mL. Cells were incubated for 1 hr at 37 °C, 200 rpm using the Eppendorf ThermoMixer. Cells were centrifuged for 1 min at 2500 x *g* using the VWR Micro Star 21R microcentrifuge, some of the supernatant was removed and the remaining reaction was added to a LB agar plate containing the 1 µL/mL ampicillin. Agar plates were incubated at 37 °C for 24 hrs and colonies were observed.

2.3.2 Growth of BL21 (DE3) competent cells

Starter cultures were set up from single colonies of freshly transformed E-coli inoculated into flasks containing LB media and ampicillin. Liquid starter cultures were left shaking overnight in a New Brunswick Incubator Shaker Series at 200 rpm, 37 °C. Subsequently, 10 mL of the overnight culture was introduced into 1 L auto-induction media (Formedium, UK) (in 2 L conical flasks). These were incubated at 200 rpm and 37 °C for 24 hrs in the New Brunswick Incubator Shaker Series. Cells were pelleted by centrifugation at 17,700 x *g*, 4 °C for 20 mins in a Sorvall RC 6 Plus Superspeed Centrifuge. Lysis buffer was prepared fresh and comprised of 25 mM Tris-HCl (pH 8.0), lysozyme (100µg/mL), 2 mM phenylmethylsulfonyl fluoride (PMSF) (in isopropanol), DNase (20 µg/mL) and RNase (20 µg/mL). Bacterial cell pellets were resuspended in lysis buffer for 30 mins (40 g bacterial pellet in 50 mL lysis buffer)., EDTA was added to a final concentration of 1 mM. Lysate was then probe sonicated 10 sec x 10. Lysates were stored on ice between periods of sonication.

2.3.3 Crude purification

Following the preparation of overnight cultures, bacteria containing the a-synuclein expressing plasmid were centrifuged at 14,000 *x g* for 30 mins using the Eppendorf 5804 R centrifuge. The supernatant was collected and acidified to pH 4.5 using 1 M hydrochloric acid (HCl) then centrifuged for 30 min, at 14,000 *x g*. The supernatant was collected, and the pH was re-adjusted to pH 8.0 using (liquid) 1 M sodium hydroxide (NaOH).

2.3.4 Purification by fast protein liquid chromatography (FPLC)

The resulting supernatant left after the crude purification step was subjected to anion exchange chromatography and size exclusion chromatography (SEC) using the BioRad Next Generation Chromatography (NGC) Fast Protein Liquid Chromatography (FPLC) system. At both stages of purification, fractions corresponding with software graphical peaks were collected and tested for presence of protein by sodium dodecyl-sulfate polyacrylamide gel electrophoresis (SDS-PAGE) and gel staining using the Imperial Gel Stain. For anion exchange, a 50 mL Q-Sepharose column (Q1126; Q-Sepharose Fast Flow, Sigma-Aldrich) was equilibrated with two column volumes of buffer A (25 mM Tris-HCl, pH 8.0) followed by loading of the column with crude lysate. Bound protein was eluted with a 0-100% linear gradient of buffer B (25 mM Tris-HCL, 1 M NaCl, pH 8) in 5 mL fractions. After elution, protein was dialysed at 4^{o}C with at least six changes of water (over two days) prior to freeze drying. The lyophilised protein was subject to SEC. For SEC, a Hi-Load 26/200 Superdex 200 pg column was equilibrated with three column volumes of buffer A (25 mM Tris-HCl, pH 8.0, 25 mM NaCl). Lyophilised protein was dissolved in 3 mL buffer A before injection. Protein was eluted in 5 mL fractions before being subjected to dialysis and freeze drying. Lyophilised purified α-synuclein was stored at -20^{o}C.

2.3.5 Sodium dodecyl-sulphate polyacrylamide gel electrophoresis (SDS-PAGE) for α-synuclein purity.

To verify the purity of lyophilised α-synuclein, samples were collected at various steps of the protein production process including supernatant samples from crude purification steps and fractions that were collected in accordance with FPLC peaks. Supernatant or fraction samples were resuspended in 4x

Laemmli buffer and β-mercaptoethanol (BME) at a recommended ratio of 9:1 (Laemmli buffer: BME) and heated at 100 °C for 5 mins. Samples were then loaded onto 10-well comb BioRad Mini-PROTEAN TGX™ Precast Gels along with the molecular weight marker. Samples were resolved at 115 V for 1 hr. Following SDS-PAGE separation, the precast gel was washed with 100 mL double distilled water for 5 mins. The gel was then submerged in 25 mL of Imperial Protein for 2 hr and then washed 30 mins x 4. Electrospray ionisation (ESI) was used to determine the molecular weight of the sample.

2.4 Production of aggregated α-synuclein

2.4.1 Determining the concentration of monomeric α-synuclein

1 mg of α-synuclein was dissolved in 1 mL of 50 mM sodium phosphate buffer. 90 µL of 50 mM sodium phosphate is placed in UVettes cuvettes and 10 µL of the dissolved α-synuclein is added, and the absorbance was measured at 280 nm. The concentration of α-synuclein was calculated using Beer's Law; α-synuclein has an extinction coefficient of 5690 $M^{-1}cm^{-1}$.

2.4.2 Production of seedings oligomers (type C)

To produce seeding oligomers of α-synuclein, the Type C protocol (Danzer et al, 2007) was followed. Monomeric α-synuclein was dissolved at 1 mg/mL in 50 mM sodium phosphate, 20 % (v/v) molecular grade ethanol and was left shaking at 300 rpm, 28 °C for 24 hrs. Protein aggregates were concentrated using VivaSpin 500 30000 MWCO.

2.4.3 Production of fibrils and preformed fibrils

Monomeric α-synuclein was dissolved at a concentration of 1mg/mL (as previously described). To produce fibrils of α-synuclein, monomeric α-synuclein was dissolved in 50 mM sodium phosphate containing 150 mM NaCl and was left shaking at 1000 rpm, 37 °C for 7 days in a ThermoMixer. To produce PFFs, 500 µL the fibrillar α-synuclein solution was probe sonicated for 60 seconds (1 second on/off) in 1.5 mL Eppendorf tubes.

2.4.4 Characterising fibrils using AFM (outsourced technique).

Full length fibril samples were deposited on freshly cleaved mica and air dried for 1 hr, followed by gentle rinsing with 100 µL CHROMASOLV™ water (Honeywell) and brief drying under N2. A MultiMode 8 AFM, software v. 9.0, (Bruker) was operated in intermittent contact mode or ScanAsyst™ mode using TESPA-V2 probes (Bruker). Scans were collected at a line rate of 0.75–1.95 Hz with amplitude setpoints between 250–400 mV and pixel densities of 128, 256 or 512. All samples were scanned in air and images analysed using NanoScope Analysis v. 1.50 (Bruker). Images were first-order plane fitted in XY to remove tilt.

2.5 Fluorescent dyes for amyloid detection

2.5.1 Continuous ThT assay

200 µL of 50 µM ThT was used as a control. 20 µL of monomeric α-synuclein solution at a final concentration of 1 mg/mL and 2 mg/mL was mixed with 180 µL 50 µM ThT. The ThT/α-synuclein solution was incubated in black clear bottom 96-well plates. Plates were incubated at 37 °C in a CLARIOStar Microplate Reader with agitation at 200 rpm. Plates were subjected to 5 min intervals of shaking with intermittent fluorescence measurements over 5 days. Readings were taken at an excitation wavelength of 440 nm and an emission wavelength of 486 nm.

2.5.2 Discontinuous ThT assay

200 µL of 50 µM ThT was used as a control. 20 µL of oligomer, fibril or PFFs samples were collected at the same time daily during agitation (the process of stimulating aggregation in Eppendorf tubes as described in **Section 2.4**) and were added to 180 µL ThT 50 µM in black clear bottom 96-well plates and read at excitation wavelength of 440 nm and emission wavelength of 486 nm using the CLARIOStar Microplate Reader.

2.5.3 Fluorometric spectrophotometry for amyloid detection.

NIAD fluorescent dyes were synthesised by the author and done according to the method disclosed in Owyong et al (2024). 5 mM stocks diluted in DMSO. Dyes were diluted in PBS to a concentration of 50 µM. 100 µL of the diluted dye was added to black cuvettes and the Agilent Cary Eclipse Fluorescent Spectrophotometer was subsequently used to measure the emission of each dye. Monomeric α-synuclein and PFFs were added to each diluted dye in PBS for a concentration of 10 % (v/v). 100 µL of each protein-dye mixture was placed in black cuvettes, where the emission readings were calculated using a fluorescent spectrophotometer.

2.6 Cellular treatments

The following cellular treatments were used prior to biological assays detailed in the following sections.

Table 2.3 Cell treatments. The details of cell treatments employed throughout a variety of experimentation.

Cell Treatment	Concentrations	Incubation duration
Sodium Arsenite solution	10 µM	1, 6, 24 hr
	30 µM	1, 6, 24 hr
	250 µM	1 hr
Thapsigargin (in DMSO)	0.15 µM	1, 6, 24 hr
	1.5 µM	1 hr
tert-Butyl hydrogen peroxide (TBHP)	40 mM	30 min
MPP+ Iodide (in water)	0.1 mM	1, 6, 24 hr
	5 mM	1, 6, 24 hr
	10 mM	1, 6, 24 hr
Oligomers	10 % (v/v), 0.1 mg/mL (Monomeric equivalent)	1, 6, 24, 48 hr
PFFs	10 % (v/v), 0.1 mg/mL (Monomeric equivalent)	1, 6, 24, 48 hr

2.7 Fluorescent images of cells

2.7.1 Immunocytochemistry (ICC)

Cells grown on coverslips in 24-well plate were fixed in ice-cold 100 % (v/v) methanol for 15 mins at -20 °C. Subsequently, cells were washed in 1 X DPBS supplemented with 0.5% (v/v) Tween-20 for 3 min x 3. Cells were left in 1 X DPBS supplemented with 1% (w/v) Bovine Serum Albumin (BSA) for 1 hr on a plate shaker. Cells were then washed for 3 mins x 3 in 1 X PBS supplemented with 0.5% (v/v). Tween-20. The desired primary antibody was then added and incubated overnight at 4 °C, gently shaking. If not conjugated to a secondary antibody, the primary antibody was removed, and the cells were washed in 1 X DPBS supplemented with 0.5% (v/v) Tween-20 for 3 mins x 3 and then left in secondary antibody at the recommended dilution for 1 hr protected from the light. Finally, the secondary antibody solution was removed, and cells were washed in 1 X PBS supplemented with 0.5% (v/v) Tween-20 for 3 mins x 3. The coverslips were then transferred to microscopic slides containing ProLong Diamond Antifade Mountant and left to cure for 24hr. Cells were visualised using the Zeiss LSM 800 Confocal Laser Scanning Microscope.

2.7.2 Fluorescent imaging acquisition and analysis

The confocal ZEN blue system was used for analysis of fluorescent images acquired through imaging using the confocal LSM 800 microscope. The 63x oil objective was used in the acquisition of all Z-stack images with 1 µm (automatic optimal setting) slices. Acquisition settings are shown in **Table 2.4**.

Table 2.4 Confocal image acquisition setting details. Lasers and laser transmission/power used, corresponding with fluorophores available on the Zen Blue imaging system to image ICC microscopic slides.

Selected Fluorophore	Laser	Laser Power
DAPI	405 nm	2.0 %
Alexa Fluor 488	488 nm	0.2 %
Alexa Fluor 564	561 nm	2.0 %
Texas Red	561 nm	2.0 %

Images were exported from the ZEN blue imaging system (**Figure 2.1**) and opened on the ZEN blue analysis system (in .czi format). Fluorophores were automatically detected within the regions of interest (ROI) which were selected by using the drawing tool around the cell/region of interest. Parameters such as fluorescence intensity and area (μm^2) were selected and measurements were automatically generated specifically pertaining to data within the ROI.

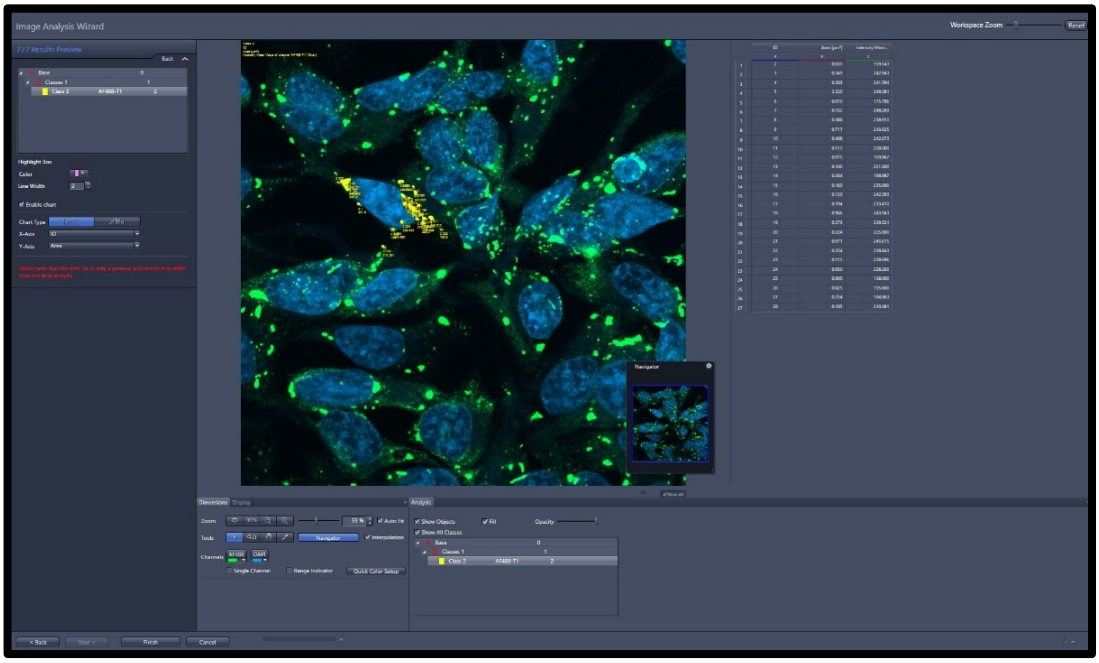

Figure 2.1 Image analysis methodology. Zen blue confocal analysis system was used to select puncta within ROIs which is highlighted in yellow. To the right of the image is the data acquired indicating area and fluorescence intensity of individual puncta present in the selected ROI.

2.8 Lactate dehydrogenase (LDH) cytotoxicity assay

2.8.1 Optimal seeding density

Cells were seeded in 96-well plates from 0-12,000 cells per well for undifferentiated cells. Cells were left overnight at 37 °C, 5 % CO_2 to adhere in 100 µL of DMEM (10 % FBS, 1 % Pen-Strep). To assess the optimal seeding density with the SH-SY5Y cell line, triplicates of various seeding densities were assayed for spontaneous and maximum LDH activity (**Figure 2.2**). To observe the spontaneous LDH activity, 10 µL of ultrapure water was added to each well overnight and incubated at 37°C, 5 % CO_2. 10 µL of lysis buffer supplied in the CyQUANT™ LDH kit was added to each well to assess maximum LDH activity and left for 45 mins in 37°C, 5 % CO_2. In accordance with the provided supplier protocol, 50 µL of medium was transferred to 96-well flat bottom plates and then incubated with the provided reaction mixture for 30 mins and protected from light. 50 µL stop solution provided was then added to the incubated medium/reaction mixture. As advised by the provided protocol, the absorbance was read using the ClARIOStar Microplate Reader at 490 nm and 680 nm (background signal) within 1-2 hrs of stop solution addition.

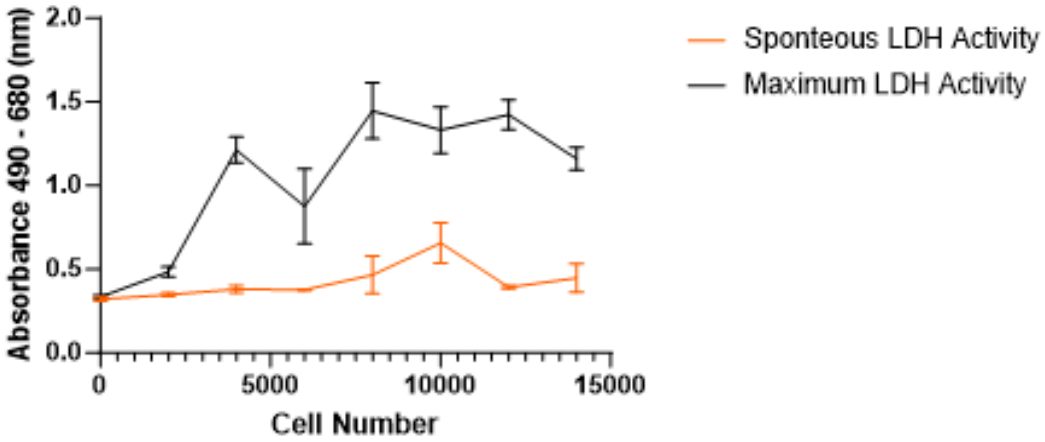

Figure 2.2 Optimal number LDH assay experiment. Cells were subjected to spontaneous and maximum conditions and the LDH activity was measured. Error bars: ± SEM (technical repeats, *n=3*).

2.8.2 Measuring treatment LDH activity

Cells were seeded in 96-well plates at a density of 10,000 cells per well. Cells were left to adhere overnight 37 °C, 5 % CO_2. Cells were treated with the desired concentration and duration of the treatment the day after seeding. In conjunction, separate wells were also treated with ultrapure and lysis buffer to measure spontaneous and maximum LDH activity. The CyQUANT™ LDH Assay kit protocol was followed (refer to **Section 2.8.1**). As advised, by the provided protocol the absorbance was read at 490 nm and 680 nm (background signal) within 1-2 hr of stop solution addition using the ClARIOStar Microplate Reader. LDH absorbance activity was calculated by performing 490 nm – 680 nm readings.

2.9 Flow cytometry

2.9.1 Flow cytometry dyes

Table 2.5 Flow cytometry dyes. The dyes (and associated details of cytometer settings) used to stain cells prior to feeding cells into the cytoFLEX for fluorescence intensity readings.

Fluorescent Dye/Compound	Laser	Band Pass Filter	Channel
CellROX Green	Blue (488 nm)	525/40	FITC
NIAD CNEOT	Blue (488 nm)	525/40	FITC
NIAD-4	Blue (488 nm)	525/40	FITC
SyTOX Blue	Violet (405 nm)	450/45	PB450

2.9.2 NIAD-4 and NIAD-CNEOT fluorescent dyes used for amyloid detection

Cells were grown in 12-well plates containing DMEM (10 % FBS, 1 % Pen-Strep). 24 hr after seeding cells, monomeric α-synuclein or PFFs at 10% v/v were added to the cells and left to incubate for 24 hr at 37 °C, 5 % CO_2. Cell media was removed, and cells were washed in 1X DPBS. Gibco™ DMEM GlutaMAX™ (10 % FBS, 1 % Pen-Strep) was added to cells, along with either NIAD-4 and NIAD CNEOT at a final concentration of 10 μM. Cells were incubated for 30 mins at 37 °C, 5 % CO_2. Cells were then washed in 1 X PBS three times (30 secs each). Cells were detached using Trypsin-EDTA (0.25%) for 5 mins at 37 °C, 5 % CO_2. DMEM (10 % FBS, 1 % Pen-Strep) was used to inactivate Trypsin-EDTA (0.25%). Cells were centrifuged for 5 mins; 1000 rpm and the pellet was resuspended in 500 μL of 1 X DPBS. SyTOX blue was then added to the cells in suspension at 1:500 for 5 mins as recommended by the supplier and protected from the light. Cells were transferred to round based tubes and analysed using the CytoFLEX S and 10,000 events were recorded.

2.9.3 CellROX Assay for oxidative stress detection

Undifferentiated and differentiated SH-SY5Y cells were maintained in 6-well plates at 37 °C, 5 % CO_2 in cell culture medium. Cells were then treated with oligomers and PFFs at the various concentrations and durations. 40 mM

TBHP was added for 30 mins (positive control). The CellROX green reagent was added to the untreated and treated wells at a concentration of 5 µM for 30 mins at 37 °C. Cell medium was removed, and cells were washed in in 1 X DPBS for 3 mins x 3. Adhered cells were detached from culture dish using Trypsin-EDTA and inactivated using DMEM cell culture medium. Cells were centrifuged and the remaining supernatant was removed, and the cell pellet were resuspended in 1 mL of 1 X DPBS supplemented with FBS (1 %). 2 µL of the SyTOX blue dead cell stain was added to 1 mL of cell suspension. Cells were transferred to round base tubes and ROS was measured using the CytoFLEX S and 10,000 events were recorded.

2.9.4 FlowJo analysis

Experimental files (.fcs format) were uploaded onto the FlowJo system. The unstained condition was used to establish gating. Gating applied to the unstained condition was applied to all conditions (**Figure 2.3**)

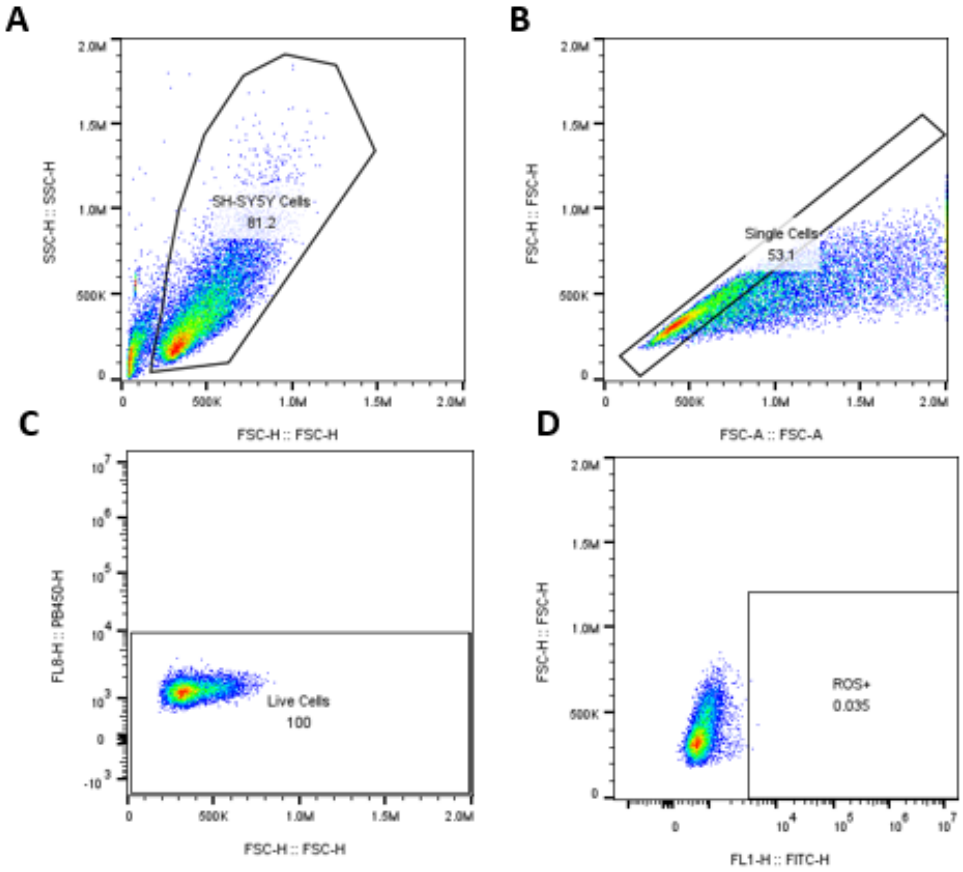

Figure 2.3 FlowJo gating for analysis. The sequential steps employed to analyse data acquired from the cytoFLEX. The unstained condition was used to establish gating for all other experimental conditions. **(A)** SH-SY5Y cells were selected using the available drawing tool to prevent the inclusion of debris. **(B)** Single cells were selected by using the drawing tool subsequent to setting the graph to have FSC.H x FSC.A axes. **(C)** The region that will contain live cells only to remove the dead cells from analysis was selected, by setting the axis to PB450.H x FSC.H. **(D)** To detect ROS positive cells, the unstained condition was used to gate the region free from unstained cells which will indicate the region of cells positive for ROS due to an increase in fluorescence

2.10 Western blot

2.10.1 Protein extraction

Following cell treatments, cells were washed with 1 X DPBS, then trypsinised at 37 °C for 2 min. Trypsin-EDTA was inactivated with the addition of DMEM (supplemented with 10 % FBS and 1 % Pen-Strep) and centrifuged at 450 x *g*, 5 min. Pellets were then washed with 1 X DPBS, then centrifuged again at 450 x *g*, 5 min. Pellets were resuspended with ice-cold CelLytic™ M supplemented with 10 % (v/v) cOmplete Protease Inhibitor Cocktail and 10 % (v/v) PhosSTOP™ for 20 mins. Lysed cells were centrifuged at 12,000 *x g* for 15 min using the MicroStar 21R centrifuge set to 4 °C. Lysates were either stored at - 20 °C for short-term storage or long-term storage at - 80 °C.

2.10.2 BCA assay

Standards were made according to the supplier's protocol. The BCA assay was preformed according to the microplate procedure. 12.5 µL of standard or protein sample was pipetted into each well in triplicate. 100 µL of the working reagent (made in accordance with supplier's instructions) was added to each well and mixed by placing plate on shaker for 30 sec. The plate was incubated at 37 °C for 30 min. Prior to measurement, the plate was allowed to cool to room temperature. The absorbance was read at 562 nm using the CLARIOStar Microplate Reader. The average 562 nm blank measurement was subtracted from the standard and unknown sample replicates. A blank-for corrected standard curve was prepared and the protein samples absorbances were interpolated against the standard curve to establish protein concentration in µg/mL.

2.10.3 Sample preparation

4x Laemmli buffer (LB), was supplemented with β-mercaptoethanol (BME) at a ratio of 9:1 (e.g. 900 µL 4x LB was mixed with 100 µL BME). One-part diluted LB was mixed with three-part protein sample in accordance with the supplier's protocol. Protein samples containing LB/BME was heated at 100 °C for 5 mins and stored at – 20 °C short-term and – 80°C for long-term storage.

2.10.4 SDS-page

Precast mini gels were placed in Bio-Rad Mini-PROTEAN Tetra Vertical Electrophoresis Cell cassettes which were then placed in the respective chamber. Running buffer comprising of 25 M Tris base, 1.92 M Glycine and 0.03M SDS was then placed in the chamber. Protein bands were resolved at 115 V for 60 min.

2.10.5 Semi-dry transfer

Transfer buffer was prepared using 600 mL double-distilled water, 200 mL 100 % (v/v) ethanol and 200 mL Bio-Rad premade 5x transfer buffer solution. Using the Trans-Blot Turbo ready-to-assemble transfer kit, 0.2 µm nitrocellulose membrane and filter paper was equilibrated in transfer buffer for 3 min. The gel and membrane are assembled between two ion reservoir stacks in the cassette of the Trans-Blot Turbo semi dry transfer instrument, and the transfer took place using the following conditions 1.3 A, 25 V for 7 min. Following transfer, to determine the integrity of the transfer the membrane was placed in double-distilled water and then submerged in the 0.1 % (w/v) Ponceau S in 5% acetic acid staining solution for 5 min. The membrane was washed in double-distilled water to clarify protein staining. Ponceau S stain was removed by washing membrane multiple times with TBS-T for 5 mins.

2.10.6 Western blotting

Membrane was blocked using 1 X TBS-T supplement with 5 % (w/v) non-fat milk for 1 hr at RT. Primary antibodies at various concentrations (**Table 2.2**) were added to 5 % (w/v) milk TBS-T overnight at 4 °C, with gently shaking using a plate shaker. The membrane was washed with TBS-T for 5 min x 3. Fluorescent secondary antibodies (**Table 2.2**) were diluted in TBS-T containing milk 5 % (w/v) which were subsequently added to the membranes and incubated with shaking for 1 hr at room temperature. The membrane was gently washed with TBS-T for 5 min x 3. Membranes were visualised using the LiCOR Odyssey.

2.10.7 Puromycin incorporation assay

Cells were treated with the various treatments outlined in **Table 2.3**. In the last 5 mins of the treatment, cells were treated with 91 µM puromycin

dihydrchloride and 208 µM emetine at 37 °C, 5 % CO_2. Cells were then subject to protein extraction methods outlined in **Section 2.10.1**. SDS-page and western blot of puromycin incorporation samples were carried out as described in **Sections 2.10.3 – 6**.

2.10.8 ImageJ densitometry analysis

Image J was used preform densitometry analysis of protein bands present on western blots acquired by the LiCOR Odyssey 9210 instrument. The image was converted to an 8-bit image. Measurements were acquired through selection of the ROI using the rectangle tool and the parameter “mean grey value” was selected to generate values within the ROI. The values were acquired for the bands of the protein of interest (plus the background) and housekeeping proteins (plus the background). The background values were subtracted from the protein of interest and housekeeping protein values. The net protein value was divided by the net housekeeping protein to normalise values. Net fold change values were calculated by dividing the normalised valued of the treated conditions by the normalised value of the ‘untreated condition’ to establish fold change of protein expression relative to the ‘untreated’ condition.

2.11 Human ATF4 enzyme-linked immunosorbent assay (ELISA)

The reagents provided with the Human ATF4 ELISA Kit were prepared according to the supplier's instructions. 100 µL of standards, controls and sample groups was added to each well and sealed using the cover seal. The plate was incubated for 2 hrs, at 37 °C. The plate was then washed with 400 µL of 1X wash buffer x 4. Subsequently, 100 µL of 1X Detection Antibody solution was added and the wells were re-sealed and incubated for 1 hr at 37 °C. The wash step was repeated. 100 µL of 1X horse radish peroxidase (HRP)-conjugated antibody solution was used, sealed and incubated for 40 mins at 37 °C. The wash step was repeated. 100 µL of 3,3', 5,5'-Tetramethylbenzidine (TMB) substrate was used and incubated for 20 mins. 100 µL of stop solution was added to each well for quenching colour development. The absorbance was read at 450 nm and 630 nm (background signal) using the CLARIOstar plate reader. A standard curve was plotted allowing for interpolation of the sample group to establish pg/mL concentration of ATF4.

2.12 Quantitative real time polymerase chain reaction (qRT-PCR)

2.12.1 RNA extraction

Cells were maintained and treated (**Table 2.3**) in 25 cm^2 flasks. Cells were trypsinised and trypsin-EDTA was inactivated using DMEM (10 % FBS, 1 % Pen-Strep). Further, cells were centrifuged at 300 x *g* for 5 min. Cell pellets for RNA extraction were washed with ice-cold PBS and centrifuged at 300 x *g* for 5 min. The ReliaPrep™ RNA Cell MiniPrep system was used according to supplier's instructions. Cell pellets were resuspended using BL (supplemented with 1-Thioglycerol) and TG buffer. 100% (v/v) RNase-free isopropanol was added to lysate extract and vortexed. The lysate was transferred to a mini column before centrifugation for 30 sec at 12,000 *x g* (room temperature) using the MicroStar 21R centrifuge. 500 µL RNA Wash Solution was added to the contents of the mini column and centrifuged 30 seconds at 12,000 *x g*. The DNase I incubation mix (24 µL Yellow Core Buffer, 3 µL 0.09M $MnCl_2$ and 3 µL DNase I enzyme) was prepared and added to the membrane inside the mini column. The membrane containing samples were incubated for 15 mins at room temperature. 200 µL of column wash solution was added, and the columns were centrifuged for 15 sec at 12,000 *x g.* 500 µL RNA Wash Solution was added to the mini column and centrifuged for 30 secs at 12,000 *x g*. A second wash using 300 µL RNA wash was carried out and the columns centrifuged for 2 min 12,000 *x g*. The mini column was transferred from the collection tube to the Elution Tube, where Nuclease-Free Water was added to the mini column membrane before centrifugation for 1 min at 12,000 *x g*. The eluted RNA was stored at -80 °C. RNA yield was determined spectrophotometrically at 260 nm using the Nanodrop instrument.

2.12.2 cDNA synthesis

The High-Capacity RNA-to-cDNA™ was used synthesise complementary (cDNA) from RNA sample extracts. For each reaction, 2 µg of RNA was used. The components for the reverse transcription reaction were prepared according to supplier instructions. The RT reaction mix was then incubated in a thermal cycler at 37°C for 60 mins, 95°C for 5 mins, then held at 4°C. Samples were then stored at -20°C.

2.12.3 TaqMan gene expression assay

All solutions were prepared, and the assay was performed as per the supplier's protocol. cDNA samples were thawed on ice and gently vortexed. cDNA samples were diluted to a concentration of 10 ng (RNA equivalent). The 18 µL of PCR Reaction Mix (Master Mix, Gene Expression Assay and Nuclease Free Water) was prepared as instructed and transferred to each well of the optical reaction plate. Subsequently, 2 µL of each cDNA samples (in nuclease-free water) were added to each well containing the Reaction Mix. The plate was then loaded into the thermal cycler and the cycling conditions outlined in **Table 2.6** were used.

Table 2.6 Gene expression cycle stages.

Step	Temperature (°C)	Time	Number of Cycles
UNG Incubation	50	2 min	1
Enzyme Activation	95	20 sec	1
Denature	95	1 sec	40
Anneal/Extend	60	20 sec	

Table 2.7 Genes investigated and corresponding IDs.

Gene	Gene ID	Supplier/Cat No.
ATF4	Hs00909569_g1	4331182
ATF5	Hs01119208_m1	4331182
DDIT3 (CHOP)	Hs00358796_g1	4331182
PPP1R15A (GADD34)	Hs00169585_m1	4331182
GAPDH	Hs02758991_g1	4331182

2.13 Extracellular vesicle isolation, characterisation and proteomics

2.13.1 Cell culture for EV isolation

SH-SY5Y cells were grown in DMEM supplemented with 10 % FBS and 1 % Pen-Strep in 175 cm^2 flasks. Cell nutrient medium was removed and replaced with in DMEM supplemented with 10 % (v/v) exosome-depleted FBS and 1 % (v/v) Pen-Strep, 48 hrs before EV collection.

2.13.2 Differential ultracentrifugation for EV isolation

24/48 hrs after treatment (**Table 2.3**), the cell medium was collected in 50 mL falcon tubes. Falcon tubes were centrifuged and spun in 2000 *x g* for 10 mins. The supernatant was transferred to a fresh 50 mL falcon tube and placed on ice. The supernatant was then transferred to 70 mL polycarbonate ultracentrifuge bottles (Beckman Coulter, AUS) and centrifuged in a T45i rotor in the Beckman Coulter Optima XPN-100 ultracentrifuge. An initial centrifugation at 10,000 x *g* for 30 mins was performed before transferring supernatants to clean ultracentrifuge tubes and was centrifuged at 100,000 x *g* for 70 mins. The supernatant was then removed carefully as to not disturb the pellet. The pellet was washed in 1X DPBS, and the sample was re-centrifuged at 100,000 x *g* for 70 mins. The DPBS was then removed, and the pellet was resuspended in100 µL of PBS.

2.13.3 Nanoparticle tracking analysis (NTA)

Recommended procedures by the supplier pertaining to cleaning and calibration of the ZetaView instrument were followed. Particles/sEVs isolated through methods such as ultracentrifugation and/or SEC were resuspended in 1 mL DPBS and subsequently vortexed. The dilution factor used was inputted into the ZetaView software. Using a 1 mL syringe, diluted sample containing sEVs, was inputted into the ZetaView machine via the inlet valve. Using the designated standard operating procedures (SOP), parameters such as particles/mL and particle diameter were acquired along with video acquisition of diluted sample. Reports were provided containing the peak, mean average analysis of particles/mL and particle diameter.

2.13.4 Electron microscopy (outsourced technique)

EM images were acquired at the La Trobe University, Melbourne Electron Microscopy platform. Copper TEM with a formvar-carbon support film (GSCU300CC-50, ProSciTech, Qld, Australia) were glow discharged for 60 sec using the Emitech k950x (k350 attachment. 5 µL (x 2) suspension of sEV samples and allowed to adsorb for 30 sec. Two drops of 2% uranyl acetate were used to negatively stain the particle sample and then left to dry prior to imaging. Imaging of grids were carried out using the Joel JEM-2100 TEM (with a Gatan Orius SC 200 CCD camera.

2.13.5 Mass spectrometry (outsourced technique)

The mass spectrometry experiment was carried out and EV data was acquired by the La Trobe University (Bundoora campus) mass spectrometry platform department.

2.13.5.1 Sample preparation

Isolated EVs and cell lysates were dried under vacuum, resuspended in 2 % (w/v) SDS 20 mM Ammonium bicarbonate, and sonicated for 15 minutes to disrupt EV particles. 20 µg of EV lysate was reduced by adding 2-carboxyethyl Tris phosphine to a final concentration of 5 mM and incubating at 60 ºC for 20 min. The reduced disulphide bonds were alkylated by adding iodoacetamide to a final concentration of 20 mM and incubating for 10 min in the dark at room temperature. The single pot, solid phase, sample preparation strategy (Hughes, et al. 2019) was used to clean up solubilised and alkylated protein for trypsin digestion. Proteins were captured onto carboxylate-modified magnetic SpeedBeads (Cytiva 65152105050250 and 45152105050250) in a 50 % (v/v) ethanol environment by incubating at 24°C for 5 min with shaking (900 rpm). Using a magnetic rack for separations, the beads were isolated, and the supernatant discarded. The beads were washed 3 times with 80 % (v/v) ethanol, discarding the supernatant each time. Trypsin protease at a ratio of 1:20 (w/w enzyme:protein) was added in 20 mM ammonium bicarbonate and incubated at 37 ºC overnight on a shaker. Peptide solution was separated from the beads and collected into fresh tubes. Digested samples were acidified by addition of trifluoroacetic acid to 0.5 % (v/v). The tryptic peptides were then

desalted using the StageTip method (Rappsilber et al, 2007) and dried in a speedvac.

2.13.5.2 LC-MS analysis of peptides

LC-MS was performed on a Thermo Ultimate 3000 RSLCnano UHPLC system and a Thermo Orbitrap LTQ Elite mass spectrometer (Thermo-Fisher Scientific, Waltham, MA, USA). Dried peptides were reconstituted in 0.1% (v/v) trifluoroacetic acid (TFA) and 2% (v/v) acetonitrile (ACN), and 500 ng of peptides were loaded onto PepMap C18 5 µm 1 cm trapping cartridge (Thermo-Fisher Scientific, Waltham, MA, USA) at 12 µL/min for 6 min before switching the trap in-line with the analytical column (Thermo Acclaim PepMap100 RSLC 75um x 50 cm, C18 2 um particle 100A). The column compartment was held at 55°C for the entire analysis. The separation of peptides was performed at 250 nL/min using a linear ACN gradient of buffer A (0.1% (v/v) formic acid, 2% (v/v) ACN) and buffer B (0.1% (v/v) formic acid, 80% (v/v) ACN), starting at 14% buffer B to 35% over 90 min, then rising to 50% B over 15 min followed by 95% B in 5 min. The column was then cleaned for 5 min at 95% B and afterward a ramped down to 1% B over 2 minutes and then held at 1% B for a final 3 min. Mass-spectra were collected in Data Dependent Acquisition (DDA) mode. MS1 spectra were collected in the Orbitrap while CID35 MS2 spectra were collected in the ion trap. MS1 scan parameters were scan range of 350-1500 m/z, 120,000 resolution, Polysiloxane lock mass (445.120028 m/z). was used. MS2 spectra were collected with rapid mode, top 15 peptides.

2.13.5.3 Database search

Raw files obtained from mass spectrometry analysis were searched against the Human reference proteome retrieved from Uniprot in February 2024 (UP000005640_9606), using Sequest HT through Proteome Discoverer (Version 2.4) (Thermo Scientific, Bremen, Germany). Precursor and fragment mass tolerance were set to 20 ppm and 0.5 Da, respectively. Carbamidomethylation of cysteine was set as fixed modification, while oxidation of methionine, acetylation of the protein N-terminus, met-loss at protein N-terminus and met-loss+acetyl at protein N-terminus were set as dynamic modifications. DIgest was set to Trypsin (Semi), A false discovery rate

(FDR) threshold of 1% was used to filter peptide spectrum matches (PSMs). FDR was calculated using a concatenated target/decoy strategy in Percolator. For label-free quantification, precursor peaks were detected using the Minora Feature Detector and quantified using Precursor Ions Quantifier on area and normalised to total peptideamoutn in Proteome Discoverer.

2.13.5.4 Data analysis

Multivariate statistics were performed using R, RStudio and the DEP package for statistical analysis of proteomics data (Zhang et al 2018). Additional packages included: readr, Hmisc, calibrate, edgeR, dplyr, tidyr, stringr, extrafont, Complex Heatmap and heatmap. A Summarized Experiment object was generated from Proteome Discoverer Proteins output using the experimental design information and protein abundance columns. The data was filtered to remove missing values, with only proteins identified in all three replicates of one condition retained. Normalization was performed using the normalize_vsn function, and the distributions of samples before and after normalization were inspected through boxplots. Missing values were imputed using the MinProb method to allow for descriptive statistics like PCA. The intensity distributions before and after imputation were also plotted to check for problems in data distributions. Differential enrichment analysis was conducted with DEP using linear models and empirical Bayes statistics via limma (Ritchie et al 2015). Significant proteins were identified based on user-defined cutoffs for alpha (0.5) and log fold change (0.5).

2.14 General statistical analysis

GraphPad Prism 8 was used to prepare data graphs and used to statistically analyse data. All data was subjected to the Shapiro-Wilk test to establish normality. Instances where the P value was <0.05, data was subjected to non-parametric tests and in the case where the P value was not <0.05, parametric tests were applied to the data. Where there were comparisons between two groups, the student t-test (one-tailed) was applied. When data with two groups were classed as non-parametric, the Mann Whitney test was performed. Cases where there were three or more conditions/group compared, the ordinary one-way ANOVA test was applied. When data was classed as parametric the post-hoc Tukey's multiple comparison test or Dunnett's multiple comparison test was carried out. Instances where data was non-parametric, the Kruskal-Wallis test (with Dunn's post hoc test) was used. Levels of significance are provided by assigning asterisk which indicates the following: P ≤0.05 (*), P ≤0.01 (**), P ≤ 0.001 (***), P≤0.0001 (****).

3 Chapter Three: Validating ISR activation using stress-inducing compounds

3.1 Introduction

3.1.1 The ISR's role in stress and disease

The ISR under normal conditions is crucial to the maintenance of function and health in various organisms (Costa-Mattioli and Walter, 2020), ranging from reproductive system regulation (Grmai et al, 2024) to memory (Rosi and Frias, 2020). Despite the ISR's importance in maintaining normal physiology, dysregulation of the ISR has been associated with various conditions such as cancer and neurodegeneration (Santos-Ribeiro et al, 2018; Licari et al, 2021; Lockshin and Calakos, 2024). Cases where the ISR exhibits dysfunction tends to occur where response to stresses is inappropriate or inefficient (Licari et al, 2021; Lockshin and Calakos, 2024; Santos-Ribeiro et al, 2018). This is particularly the case with neurodegenerative diseases where sustained and progressive stress has been implicated in conditions such as AD (Flury et al, 2025) and PD (Dias et al, 2013).

Stresses can be distinguished by duration and intensity (Schoof et al, 2021; Bond et al, 2020). Acute stress is described to be transient in nature (Guan et al, 2017) and chronic (sustained) stress which is defined by long-term stress sensing (Guan et al, 2017). It is important to consider that the use of "acute" and "chronic" is in a non-clinical context. Consequences of lasting activation of the ISR may lead to neurological dysfunction including axonal and myelin sheath loss (Chen et al, 2019) plus cell death (Bond et al, 2020).

3.1.2 Stress-inducing compounds in the investigation of the ISR

There are numerous factors that contribute to PD pathology including oxidative (Dias et al, 2013) and ER stress (Mou et al, 2020). Both stresses are found to activate the ISR (Bravo-Jimenez et al, 2025). There are a plethora of drugs and compounds that have been used in the study of the ISR such as SA and Tg (Rabouw et al, 2019). SA generates ROS - an indicator of oxidative stress (Ruiz-Ramos et al, 2009). SA works to inhibit phosphate-using enzymes resulting in dysfunctional cell metabolism (Rainey et al, 2024). Tg induces ER

stress by the blocking the sarco/ER Ca^{2+}-ATPase (SERCA) resulting in aberrant Ca^{2+} levels (Lindner et al, 2020).

3.1.3 Stress response pathways in PD neurotoxin models

The ISR has been linked to PD (Bravo-Jimenez et al, 2025). Toxin models have been useful in understanding the processes involved in neurodegeneration. Neurotoxins such as 6-OHDA, rotenone or paraquat have been used to treat cells and animals to formulate these models (Bové et al, 2005). 1-methy-4-pheyl-1,2,3,6-tetrahydropyridine (MPTP) is another neurotoxin known to cause parkinsonism in humans and monkeys due to dopaminergic neuronal cell death (Bové et al, 2005). 1-methyl-4-phenylpyridinium (MPP+), a metabolite of MPTP (Sallinen et al, 2009), has been implicated in the selective elimination of dopaminergic neurons causing PD-associated symptoms in mammals (Mapa et al, 2018). MPP+ has been shown to localise in the mitochondria where it binds to complex I of the electron transport chain leading to increased release of ROS (Risiglione et al, 2020). The phosphorylation of eIF2α has been implicated in neurodegeneration (Bravo-Jimenez et al, 2025) and investigated in PD neurotoxin models where cells have been treated with MPP+ iodide and 6-OHDA (Demmings et al, 2021). MPP+ and 6-OHDA has been shown to induce eIF2α phosphorylation and enhance ATF4 expression (Demmings et al, 2021). Further, pro-death genetic markers such as CHOP, PUMA and TRIB3 have also been expressed as a result of MPP+ and 6-OHDA exposure (Demmings et al, 2021). MPP+ has been demonstrated to increase mRNA levels of genes associated with ER (e.g. DDIT3), mitochondria (e.g. NOXA) and oxidative stress (e.g. NQO1). Other studies have demonstrated MPP+ treatment inducing the expression of ATF6 (Ghribi et al, 2003; Wang et al, 2023), PERK and IRE1-α (Holtz and O'Malley, 2003; Ryu et al, 2002; Wang et al, 2023) - all markers of the UPR.

3.1.4 Objectives

Chapter three aims to validate the activation of the ISR in known PD-related stress conditions such as oxidative and ER stress. This information will act as a foundation to understand the ISR in conditions of various stresses for later comparison with α-synuclein-induced stress. To achieve this, chapter three will explore:

- treatment of undifferentiated SH-SY5Y cells with SA and Tg at different time points to assess expression of ISR markers including: eIF2α phosphorylation, ATF4, CHOP and GADD34 expression plus attenuated protein synthesis.
- how MPP+-induced stress activates the ISR and how this compares to SA and Tg.
- the effect of SA, Tg and MPP+ on SG dynamics to determine how different stresses impact SG formation.

3.2 Results

3.2.1 Oxidative and ER stress increases phosphorylation of eIF2α.

SA and Tg are known to induce phosphorylation of eIF2α (Palangi et al, 2017), a core event of the ISR (Humeau et al, 2020). SA and Tg were used to assess ISR activation in SH-SY5Y cells by determining the presence of eIF2α phosphorylation. Cells were treated with SA and Tg for 1, 6 and 24 hr. Western blot analysis was performed to quantify eIF2α phosphorylation in comparison to total eIF2α. 10 μM SA increased phosphorylation of eIF2α at 6 and 24 hr by 1.4 and 1.6-fold compared to the untreated condition but was not significant (**Figure 3.1**). 30 μM SA treatment for 1 hr and 6 hr treatment were able to induce a 2.07 and 1.77-fold increase in eIF2α phosphorylation compared to the untreated condition (**Figure 3.2**). 30 μM SA induced significant cell death at 24 hr preventing measurable protein expression by western blot. Treatment with 0.15 μM Tg at 1, 6 and 24 hr yielded a 1.77, 2.62 and 2.06-fold increase in eIF2α phosphorylation respectively, when normalised to total eIF2α (**Figure 3.3**). Data points in the SA 30 μM and Tg 0.15 μM despite showing increases at certain timepoints were not significant. The data presented demonstrates that both SA and Tg induces eIF2α phosphorylation in SH-SY5Y cells in alignment with findings presented in existing literature.

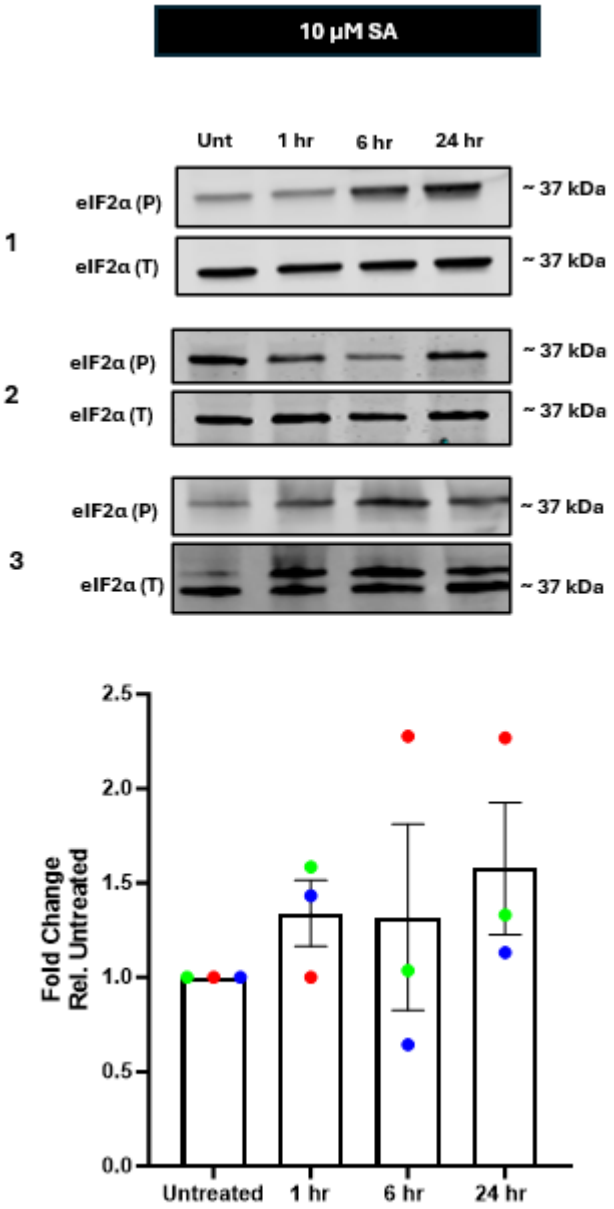

Figure 3.1 Low-dose SA induces phosphorylation of eIF2α. 10 μM SA was used to treat cells for 1, 6, 24 hr. ImageJ densitometry analysis was used to process immuno-stained blots. Data was analysed by one-way ANOVA followed by Tukey's post-hoc test for multiple comparisons. Data without asterisk have been deemed as not significant. Colours indicate individual biological replicates: **(1)** red, **(2)** green, **(3)** blue. Error bars: ± SEM (*n=3*).

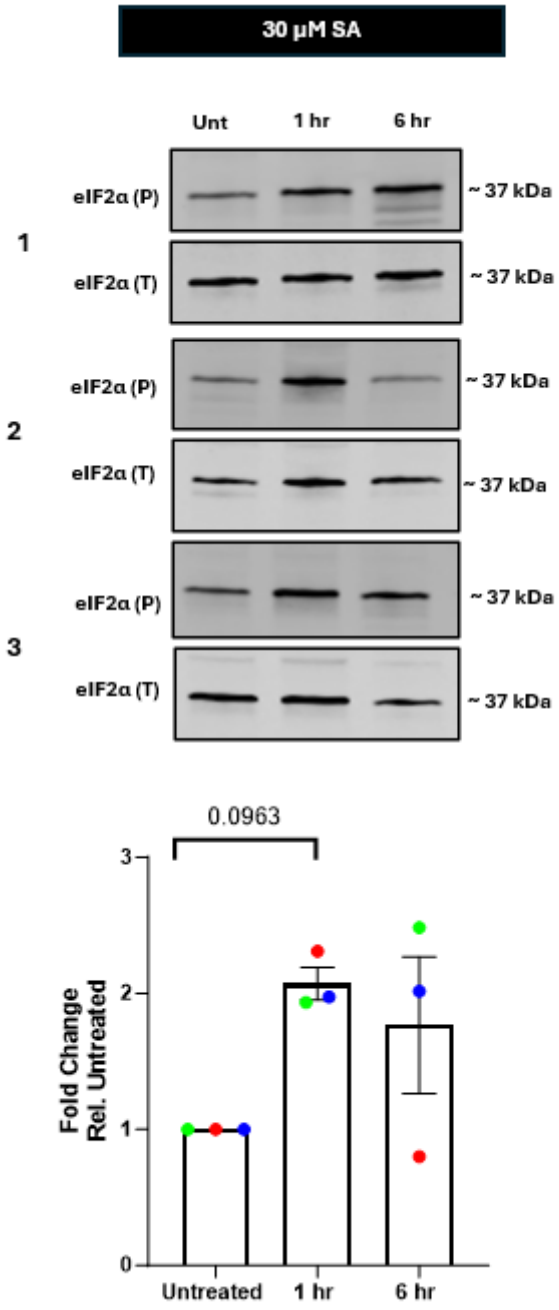

Figure 3.2 Low-dose SA induces phosphorylation of eIF2α. 30 µM SA was used to treat cells for 1, 6, 24 hr. ImageJ densitometry analysis was used to process immuno-stained blots. Data was analysed by one-way ANOVA followed by Tukey's post-hoc test for multiple comparisons. Levels of significance close to P ≤0.05 (*) was reported. Data without asterisk have been deemed as not significant. Colours indicate individual biological replicates: **(1)** red, **(2)** green, **(3)** blue. Error bars: ± SEM (*n=3*).

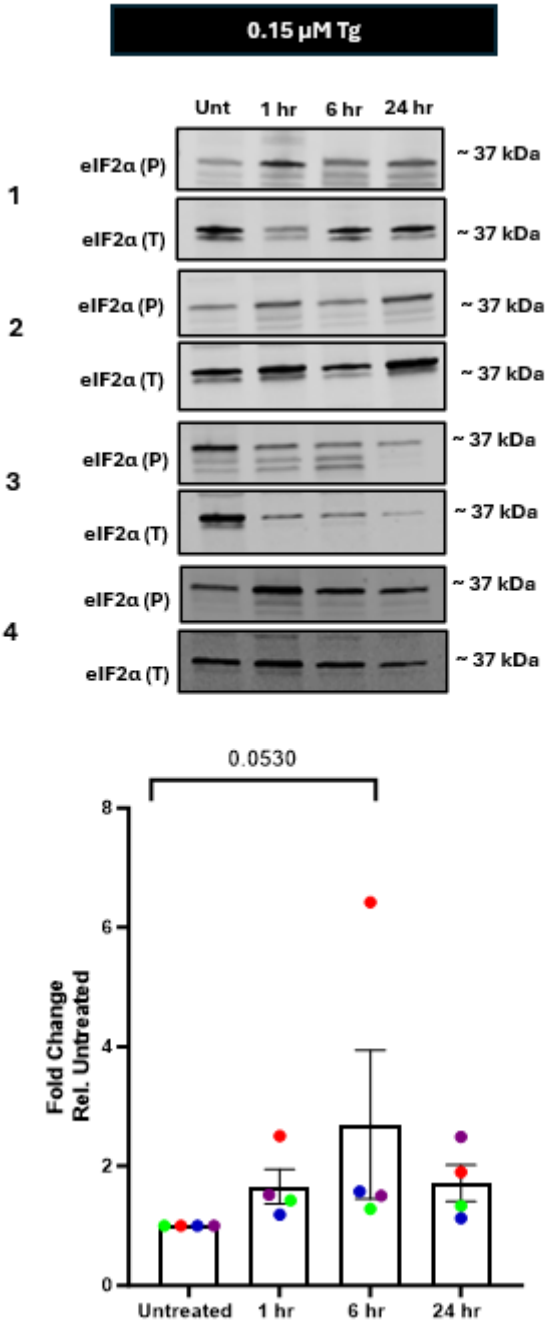

Figure 3.3 Low-dose Tg induces phosphorylation of eIF2α. 0.15 µM Tg was used to treat cells for 1, 6, 24 hr. ImageJ densitometry analysis was used to process immuno-stained blots. Data was analysed by one-way ANOVA followed by Tukey's post-hoc test for multiple comparisons. Levels of significance close to P ≤0.05 (*) was reported. Data without asterisk have been deemed as not significant. Colours indicate individual biological replicates: Colours indicate individual biological replicates: **(1)** red, **(2)** green, **(3)** blue **(4)** purple. Error bars: ± SEM (*n=4*)

3.2.2 MPP+ induces phosphorylation of eIF2α

10 μM to 5 mM MPP+ treatment for 24 - 72 hr has been shown to induce DNA fragmentation in SH-SY5Y cells (Pettifer et al, 2007). 500 μM MPP+ was also shown to increase caspase-3 activity (Pettifer et al, 2007). This shows that MPP+ has the ability to induce cellular stress and dysfunction. Further, it has been demonstrated that incubating cells such as mouse N2A, rat PC12 and SH-SY5Y with 10 mM MPP+ for 24 hr showed significant reduction in cell viability and mitochondrial oxygen consumption (Mazzio et al, 2010). Additionally, MPP+-associated stress has been shown to trigger the phosphorylation of eIF2α (Demmings et al, 2021).

To validate if MPP+ treatment activates the ISR in SH-SY5Y cells, eIF2α phosphorylation was assessed. Cells were treated with 10 mM MPP+ for 1, 6 and 24 hr. Western blotting analysis was used to assess eIF2α phosphorylation in comparison to total eIF2α. EIF2α phosphorylation was found to increase at 6 hr and 24 hr (1.62 and 1.64-fold increase) when compared to the untreated condition (**Figure 3.4**). Data was not significant when compared to the untreated condition but the significant when compared to the 1 hr timepoint. The data presented shows that high dose MPP+ is able to increase eIF2α phosphorylation indicating ISR activation.

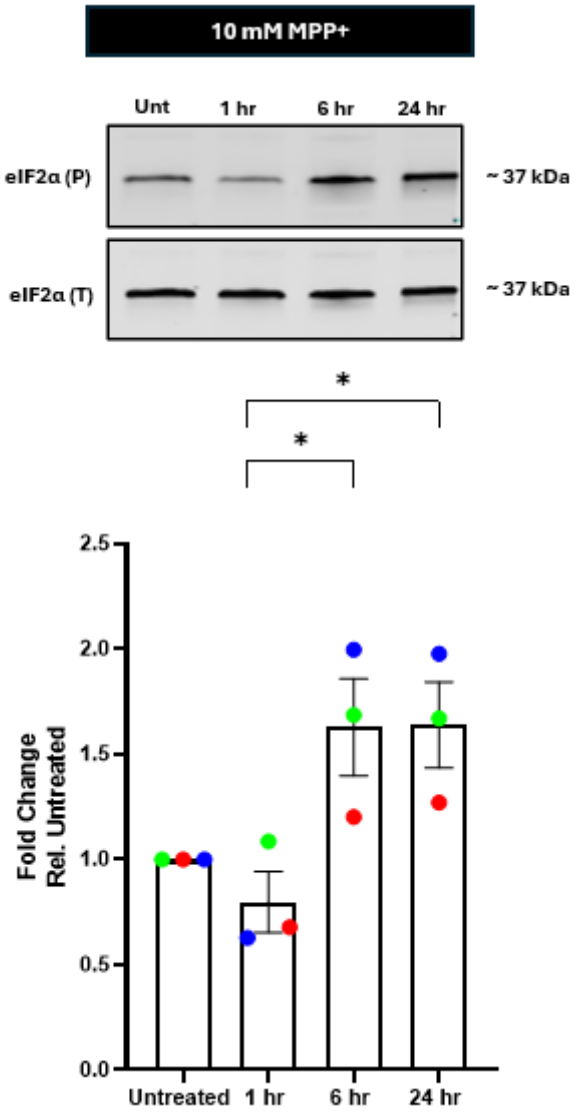

Figure 3.4 10 mM MPP+ increases eIF2α phosphorylation. 10 mM MPP+ was used to treat cells for 1, 6, 24 hr. ImageJ densitometry analysis was used to process immuno-stained blots. Data was analysed by one-way ANOVA followed by Tukey's post-hoc test for multiple comparisons. Levels of significance was indicated by the following: P ≤0.05 (*). Data without asterisk have been deemed as not significant. Colours indicate individual biological replicates: **(1)** red, **(2)** green, **(3)** blue. Error bars: ± SEM (*n*=*3*)**.**

3.2.3 ATF4 is expressed in response to oxidative and ER stress

ISR activation enhances expression of ATF4; a transcription factor which coordinates the expression of genes either supporting cellular survival and apoptosis, which is dependent on the conditions of the imposing stress (Wek et al, 2023; Wortel et al, 2017). To further corroborate findings that SA and Tg activates the ISR, SA and Tg was used to treat cells and ATF4 protein expression was examined using the enzyme-linked immunosorbent assay (ELISA). 30 μM SA was used to treat cells for 6 and 24 hr, ATF4 expression was primarily found to increase at 6 hr (2.64-fold increase when compared to the untreated condition) (**Figure 3.5**). SA 30 μM showed increases particularly at 6 hr but data was not shown to be significant at any explored timepoint. At 24 hr, ATF4 expression reduced and was found to have minimal difference compared to the untreated condition. ATF4 expression increased when cells were treated with 0.15 μM Tg for 6 hr (2.96-fold increase). Additionally, Tg treatment for 24 hr also showed a reduction in ATF4 expression compared to the Tg 6 hr condition but was still higher than that of the untreated condition (1.82-fold increase). With the consideration that SA and Tg at these concentrations increases eIF2α phosphorylation and ATF4 expression, the data presented supports SA and Tg's ability to activate the ISR. Additionally, the reduction of ATF4 expression is due to eventual inactivation of the ISR (Oliveira et al, 2024) and adaptation to stress.

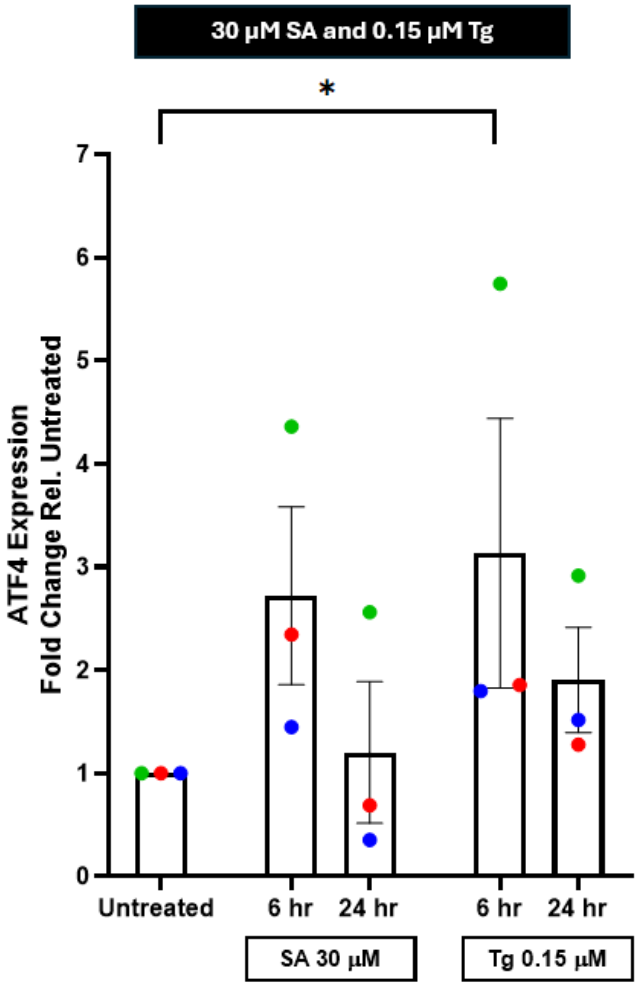

Figure 3.5 Low dose SA and Tg initially increases ATF4 expression but decreases in conditions of chronic stress. 30 µM SA and 0.15 µM Tg was used to treat undifferentiated SH-SY5Y cells for 6 and 24 hr. The ATF4 ELISA assay kit was used to establish pg/mL concentrations of ATF4 from cell lysates. Data was analysed by one-way ANOVA followed by Tukey's post-hoc test for multiple comparisons. Data without asterisk have been deemed as not significant. Colours indicate individual biological replicates: **(1)** red, **(2)** green, **(3)** blue. Error bars: ± SEM (*n*=*3*).

3.2.4 MPP+ increases in ATF4 expression

With the observation that MPP+ increases eIF2α phosphorylation, ATF4 expression was also quantified in response MPP+ treatment. Previous reports in the literature have used mild concentrations of MPP+ for treatment of SH-SY5Y cells, such as 10 and 200 μM (Sakamoto et al, 2017). ATF4 expression was also found to increase in cortical neurons in response to 50 μM MPP+ (Demmings et al, 2021).

To establish a comparison between the effect of low and higher concentrations of MPP+ on ATF4 expression in SH-SY5Y cells, 0.1 mM MPP+ was used to treat cells along with 5 and 10 mM MPP+ for 6 and 24 hr (**Figure 3.6**). 6 hr treatment with 0.1 and 5 mM MPP+ induced the most ATF4 expression (1.50 ± 0.94 and 1.85 ± 0.23) compared to the untreated condition. However, despite overall increases in ATF4 expression, data was not deemed to be significant. 10 mM MPP+ was not able to enhance ATF4 expression compared to the untreated condition at 6 and 24 hr. The findings presented indicate that expression of ATF4 reduces overtime which can be explained by cellular adaptation to stress. Additionally, MPP+ at high doses as shown with the 10 mM treatment condition does not appear to enhance ATF4 expression at the explored timepoints.

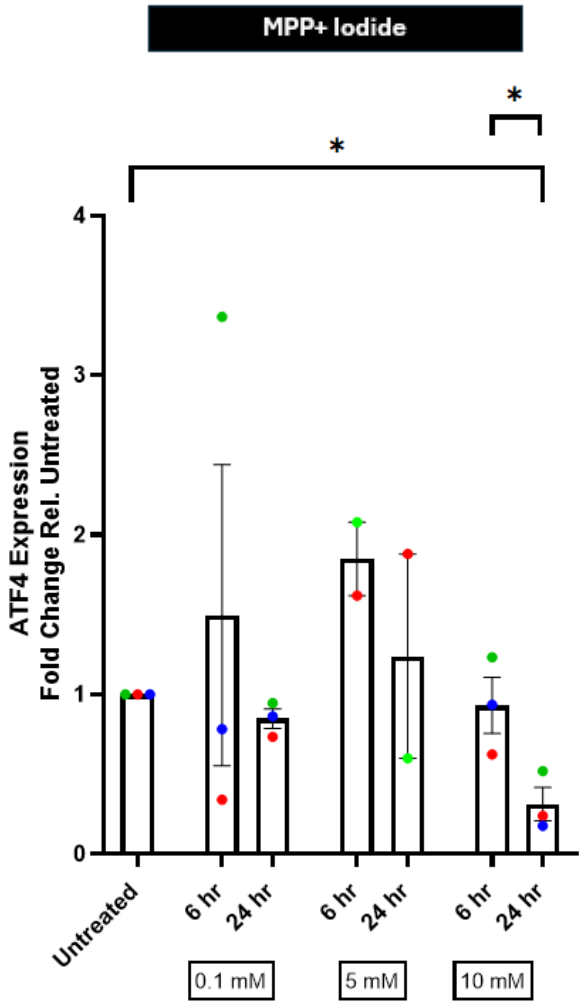

Figure 3.6 MPP+ results in moderate increases in ATF4 expression. 0.1 mM, 5 mM and 10 mM MPP+ was used to treat undifferentiated SH-SY5Y cells for 6 and 24 hr. The ATF4 ELISA kit was used to establish pg/mL concentrations of ATF4 from cell lysates. Data was analysed by one-way ANOVA followed by Tukey's post-hoc test for multiple comparisons. Levels of significance was indicated by the following: P ≤0.05 (*). Colours indicate individual biological replicates: **(1)** red, **(2)** green, **(3)** blue. Error bars: ± SEM (*n=2*, *n=3).*

3.2.5 CHOP is expressed in response oxidative and ER stress

Occasions where there is sustained and unresolved stress, apoptosis may occur (English et al, 2017). CHOP has been described as an effector of the ISR and in certain cases can be a pro-apoptotic marker (English et al, 2017; Zappa et al, 2025). But there are cases where CHOP is also involved in adaptation and recovery (Liu et al, 2023).

The expression of CHOP was explored in response to cell conditions used to previously investigate eIF2α phosphorylation. Cells were treated with 10 µM SA, 30 µM SA, 0.15 µM Tg and 10 mM MPP+ for 1, 6 and 24 hr. It was shown that 6 hr treatment of cells with 30 µM SA and 0.15 µM Tg induced CHOP expression (**Figure 3.7 B, 3.7 C**). 10 µM SA (**Figure 3.7 A**) and 10 mM MPP+ (**Figure 3.7 D**) did not induce expression of CHOP. Here, the data suggests that CHOP expression is concentration-dependent due to expression in response to 30 µM SA rather than 10 µM and stress-type specific as it was not seen to be expressed in the 10 mM MPP+ condition.

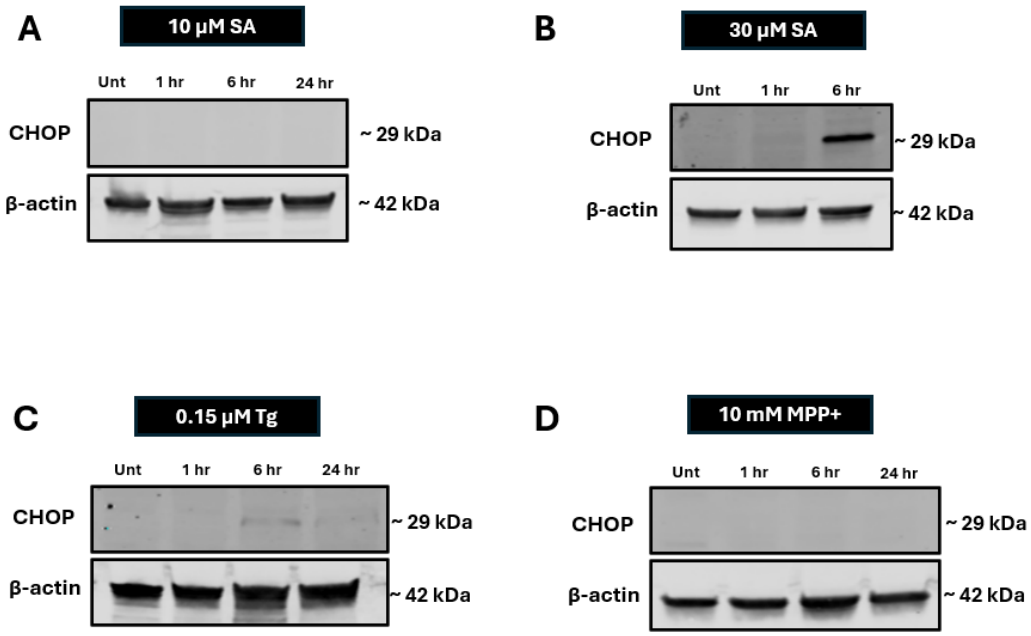

Figure 3.7 30 µM SA and 0.15 µM Tg induces CHOP expression, but other investigated conditions do not. (A) 10 µM SA, **(B)** 30 µM SA, **(C)** 0.15 µM Tg and **(D)** 10 mM MPP+ was used to treat cells for 1, 6, 24 hr. ImageJ densitometry analysis was used to process immuno-stained blots. Treatment of cells with 30 µM SA and 0.15 µM Tg for 6 hr resulted in CHOP expression. (*n=3*).

3.2.6 LDH indicates cytotoxicity overtime in response to oxidative and ER stress

CHOP expression was explored in response to SA, Tg and MPP+ (**Figure 3.7**). SA and Tg induced CHOP expression but expression was not observed in the MPP+ condition at the concentration explored. CHOP has been found to have downstream pro-death effects and the LDH assay was preformed to assess cell viability/cytotoxicity to indicate if CHOP expression coincided with reduced cell viability. LDH is released when cells are compromised which has been described as an indicator of cell death specifically late-stage apoptosis and early-stage necrosis (Parhamifar et al, 2013). Apoptosis is defined by programmed/controlled cell death often indicated by changes in biochemical processes or morphology. Whereas necrosis is characterised as be uncontrolled cell death often associated with cell fragments in culture medium (D'Arcy, 2019).

Cells were treated with SA, Tg and MPP+ for 1, 6 and 24 hr (**Figure 3.8**). Overall, all treatment conditions resulted in an increase in LDH activity overtime. Maximal increases were seen at 24 hr compared to previous respective treatment durations (10 µM SA, 24 hr: 0.79 ± 0.042; 30 µM SA, 24 hr: 0.96 ± 0.066; 0.15 µM Tg, 24 hr: 0.43 ± 0.0093; 5 mM MPP+: 0.58 ± 0.061 10 mM MPP+: 0.87 ± 0.055) and higher than the spontaneous condition (functions as a control condition for this assay, where water is added overnight, see **Section 2.8**) as well as higher than the untreated condition (0.39 ± 0.019 and 0.42 ± 0.023). Overall, the various compounds assessed using the LDH assay, increased LDH activity in cells particularly at the 24 hr timepoint which suggests that sustained exposure to SA, Tg and MPP+ increases cellular toxicity.

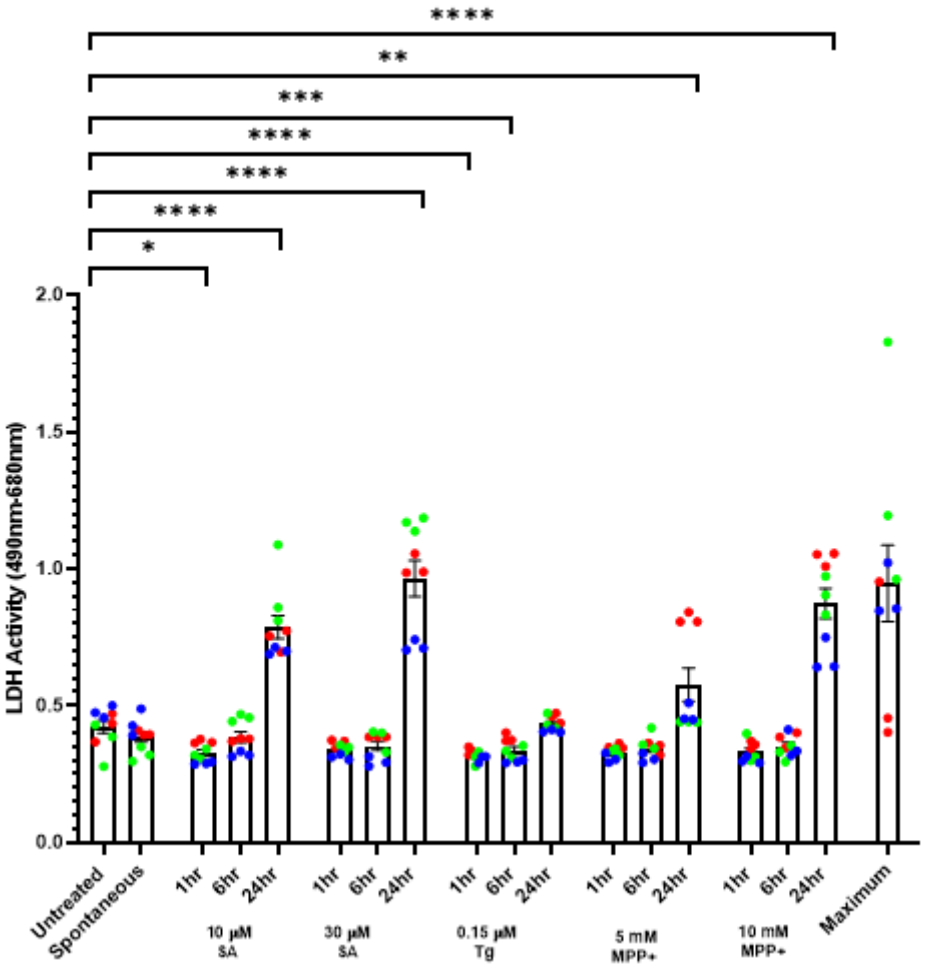

Figure 3.8 Long-term stress increases cytotoxicity. 10 µM SA, 30 µM SA, 0.15 µM Tg, 5 mM MPP+ and 10 mM MPP+ was used to treat cells for 1, 6, 24 hr. The LDH activity, indicatory of compromised cells and cytotoxicity, was measured from cell culture medium collected from the various conditions reported. Absorbance was measured from the colorimetric assay to establish LDH activity/levels. Data was analysed by one-way ANOVA followed by Dunnett's post-hoc test for multiple comparisons (comparing the treatment conditions to the untreated condition). Levels of significance was indicated by the following: P ≤ 0.001 (***) and P ≤ 0.0001 (****). Data without asterisk have been deemed as not significant. Colours indicate individual biological replicates **(1)** red, **(2)** green, **(3)** blue. Error bars: ± SEM (Biological replicates, *n=3* and technical replicates, *n=3*).

3.2.7 Oxidative and ER stress induces GADD34 expression

GADD34 is a protein phosphatase that promotes the dephosphorylation of eIF2α allowing protein synthesis to be appropriately restored (Oliveira et al, 2024). GADD34 is a target of ATF4 (Márton et al, 2022) and also activated by CHOP (Hu et al, 2019). GADD34 was assessed in response to SA, Tg and MPP+. 10 μM SA, 30 μM SA, 0.15 μM Tg and 10 mM MPP+ were used to treat cells for 1, 6 and 24 hr. Western blotting analysis indicated GADD34 expression was not seen with 10 μM SA treatment at any of the timepoints explored (**Figure 3.9 A**). However, expression of GADD34 in response to 30 μM SA for 6 hr and 0.15 μM Tg for 24 hr was observed (**Figure 3.9 B, C**). 10 mM MPP+ was also found to induce expression of GADD34 at 1, 6 and 24 hr (**Figure 3.9 D**). The stress conditions explored (except 10 μM SA) induces GADD34 expression which coincides with data previously presented showing reduced eIF2α phosphorylation and ATF4 expression.

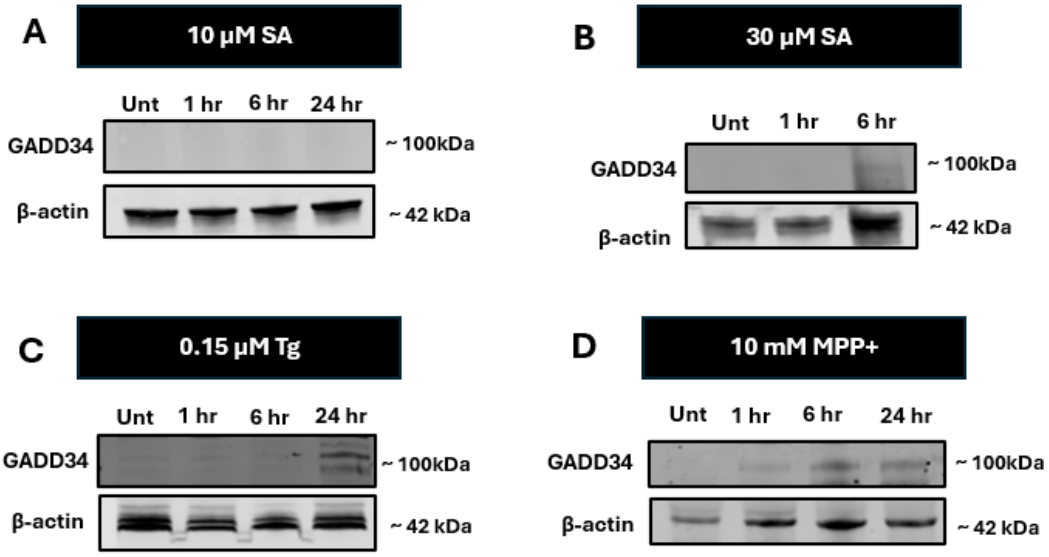

Figure 3.9 SA, Tg, MPP+ induces GADD34 expression. SA 10 μM, SA 30 μM, Tg 0.15 μM and MPP+ 10 mM was used to treat cells for 1, 6, 24 hr. Treatment of cells with Tg 0.15 μM for 24 hr resulted in GADD34 expression. (*n=1*).

3.2.8 Global protein synthesis is inhibited following MPP+ treatment

Activation of the ISR results in the reduction of global cellular translation (Ryoo and Vasudevan, 2017) to promote cell survival (Pakos-Zebrucka et al, 2016). To assess global translation, cells were treated with 30 μM SA, 0.15 μM Tg and 10 mM MPP+ for 6 hr. 6 hr was used as the treatment duration for this experiment as this timepoint induced the highest expression of ATF4 when compared to 24 hr (**Figure 3.5, 3.6**). The puromycin incorporation assay, used to assess cellular protein synthesis, involves cells being treated with puromycin and emetine towards the end of the stress/drug treatment as described in (**Section 2.10**). Puromycin is an aminonucleoside antibiotic that acts as a protein synthesis inhibitor. It is structurally similar to 3' end of aminoacylated tyrosyl tRNA (Enam et al, 2020). Puromycin is incorporated into elongating nascent C-terminus chains which prevents further extension and terminates translation by dissociating nascent peptides from their RNA in a process called puromycylation (Aviner, 2020; Enam et al, 2020). It results in the 80S ribosomes disassembling (Aviner, 2020). Emetine functions as a translation elongation inhibitor (Rosa-Mercado et al, 2024). Using an anti-puromycin antibody with subsequent immunoblotting as described in (**Section 2.10**) puromycylated proteins can be detected which indicates the successful incorporation of puromycin which acts as an indicator of newly synthesised proteins (Aviner, 2020). By comparing puromycin incorporation in stress conditions to the untreated condition; changes in translation can be quantified to investigate ISR activation.

30 μM SA, 0.15 μM Tg and 10 mM MPP+ were used to treat cells for 6 hr. 30 μM SA did not result in a reduction in puromycin incorporation. 0.15 μM Tg and 10 mM MPP+ induced a significant reduction in puromycin incorporation by 1.51 and 2.94-fold respectively (**Figure 3.10**). Considering the increased eIF2α phosphorylation and ATF4 expression in response to 30 μM SA treatment, the data showing puromycin incorporation similar to that of the untreated condition despite evidence of stress induction was unexpected. Regarding, 0.15 μM Tg and 10 mM MPP+, both treatments were able to

reduce puromycin incorporation which was in line with previous indicators of ISR activation (e.g. eIF2α phosphorylation).

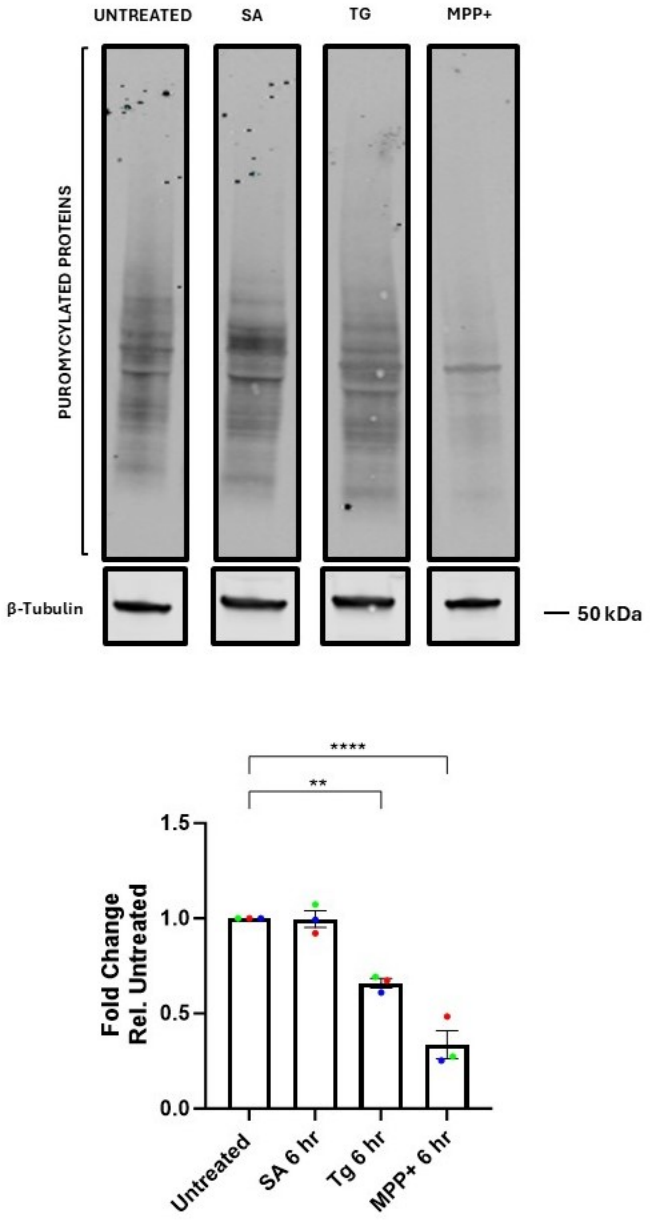

Figure 3.10 Tg and MPP+ at 6 hr attenuates translation. 30 μM SA, 0.15 μM Tg, and 10 mM MPP+ was used to treat cells for 6 hr. The puromycin incorporation assay was performed and subsequent ImageJ densitometry analysis was used to process resulting immuno-stained blots. Data was analysed by one-way ANOVA followed by Tukey's post-hoc test for multiple comparisons. Levels of significance was indicated by the following: P ≤0.01 (**), P ≤ 0.001 (***). Data without asterisk have been deemed as not significant. Colours indicate individual biological replicates: **(1)** red, **(2)** green, **(3)** blue. Error bars: ± SEM (*n=3*).

3.2.9 Chronic stress and the formation of SGs

SGs are known to form in response to SA and Tg (Wheeler et al, 2016; Zhang et al, 2019). There are various SG markers used in the assessment of SGs including G3BP and TIA-1 (Vanderweyde et al, 2012). G3BP is a stress-assembly marker that promotes the formation of SGs and the inhibition of G3BP has been shown to prevent the formation of SGs (Freibaum et al, 2023). It has been demonstrated that 30 μM SA and 0.15 μM Tg at low concentrations are able to activate the ISR. As such, 0.15 μM Tg, 10 μM SA and 30 μM SA was used to treat cells for 1, 6 and 24 hr to assess presence of SGs. Using immunocytochemistry, cells were stained for G3BP puncta (**Figure 3.11 A, B, C**). The area, percentage of SG-positive cells, the number of SGs per cell and the total number of SGs (across the total number of cells counted) were quantified.

The percentage of cells positive for G3BP-positive SGs increased in response to 0.15 μM Tg, 10 μM and 30 μM SA at 1 hr (74, 58, and 64 % on average) compared to the untreated condition (6.7 %) (**Figure 3.11 D**). Within each condition, the percentage of G3BP-positive cells reduced at the 6 and 24 hr timepoint (**Figure 3.12 A**). This was seen across all parameters where it was found that the total number of SGs and the number of SGs per cell in response to 0.15 μM Tg, 10 μM and 30 μM SA reduced at 6 and 24 hr compared to 1 hr timepoint (**Figure 3.12 B, C**). Additionally, SGs were larger at 1 hr compared to the 6 and 24 hr timepoints in response to SA and Tg (**Figure 3.12 D**). Data shows that low-dose SA and Tg-induced stress is capable of inducing SGs. SA and Tg are able to induce SGs at 1 hr but will disassemble overtime indicatory of adaptive mechanisms taking place during chronic stress (e.g. GADD34 expression). Similar patterns of SG dynamics have been seen in other literature.

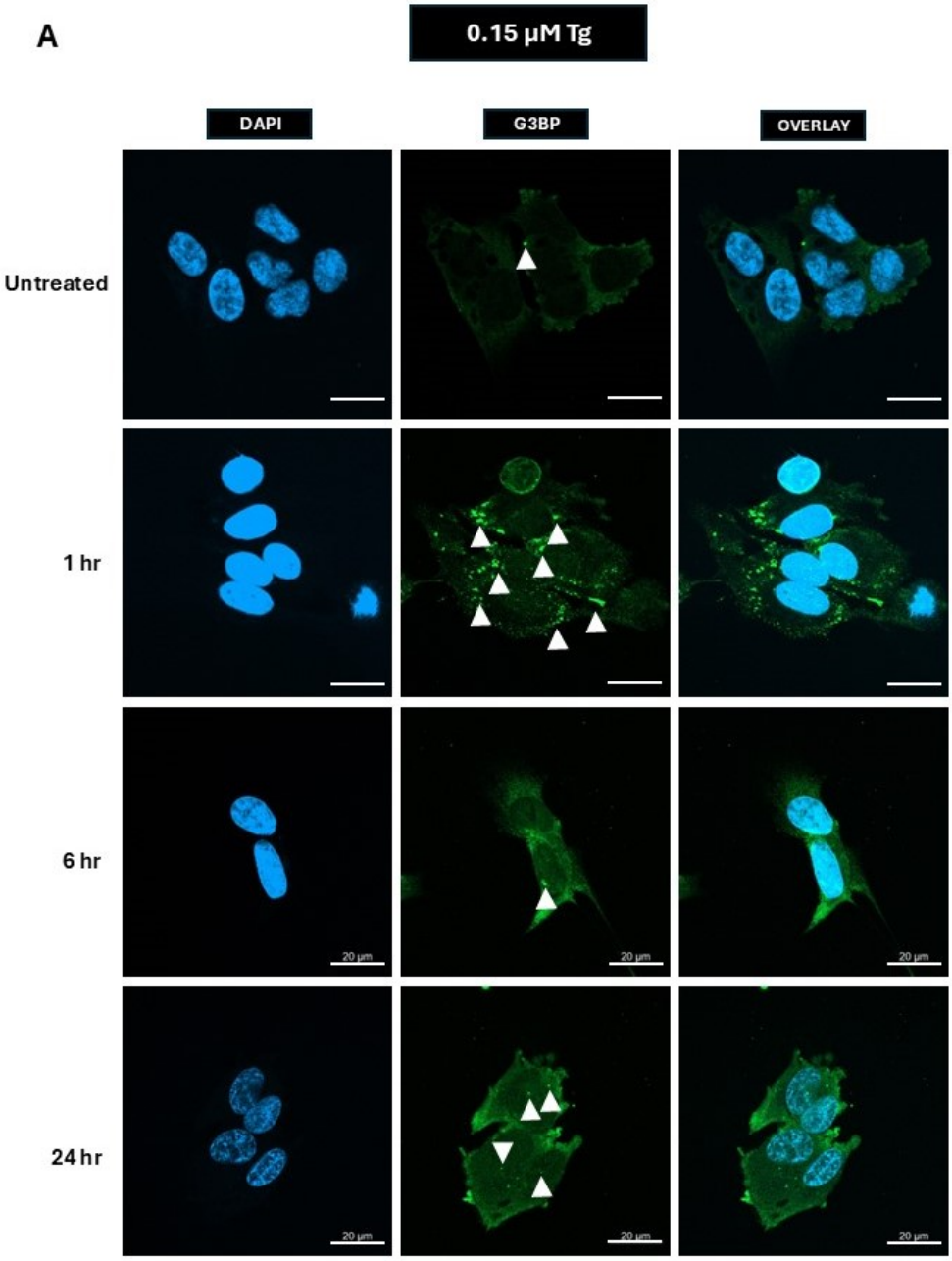
A
0.15 µM Tg
DAPI
G3BP
OVERLAY
Untreated
1 hr
6 hr
24 hr
20 µm

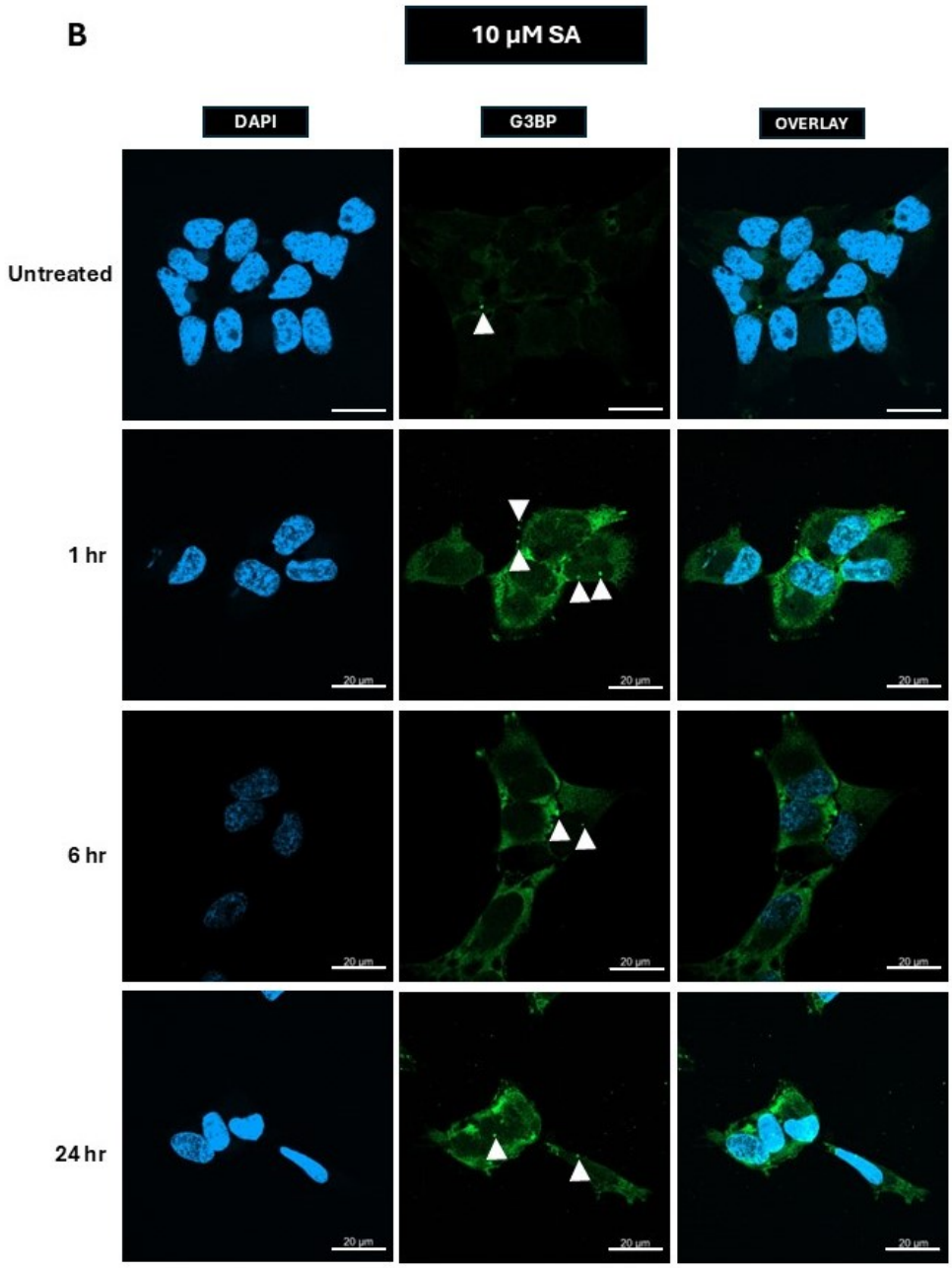
B
10 µM SA
DAPI
G3BP
OVERLAY
Untreated
1 hr
6 hr
24 hr
20 µm

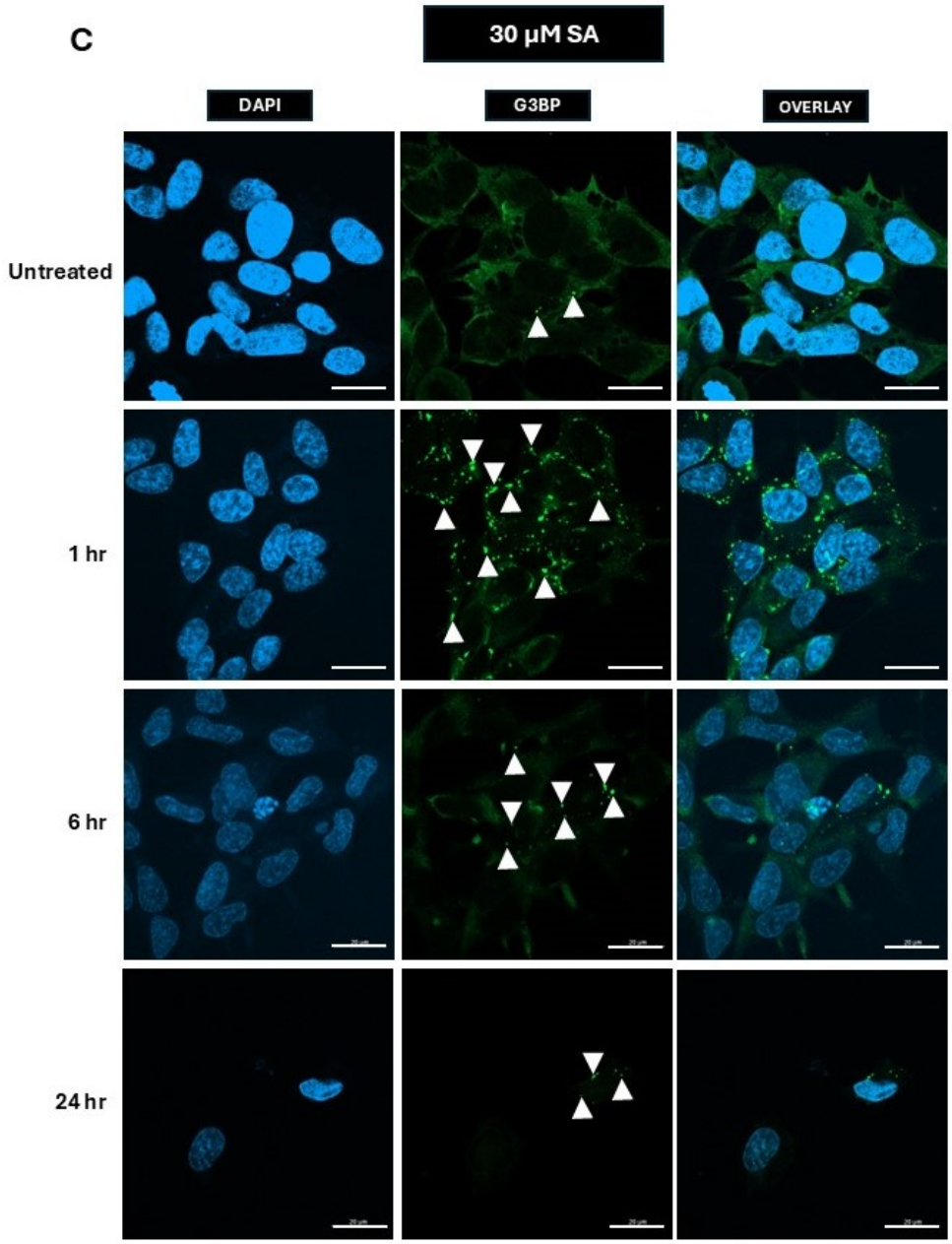

Figure 3.11 Low-dose SA and Tg-induced SGs but the number of SGs reduce in response to long-term treatment. Cells were treated with **(A)** 0.15 μM Tg (**B)** 10 μM SA and **(C)** 30 μM SA. Cell nuclei were stained using DAPI and G3BP conjugated to AF488 was used as an indicator of SG puncta. Magnification: 63x. Scale bar: 20 μm.

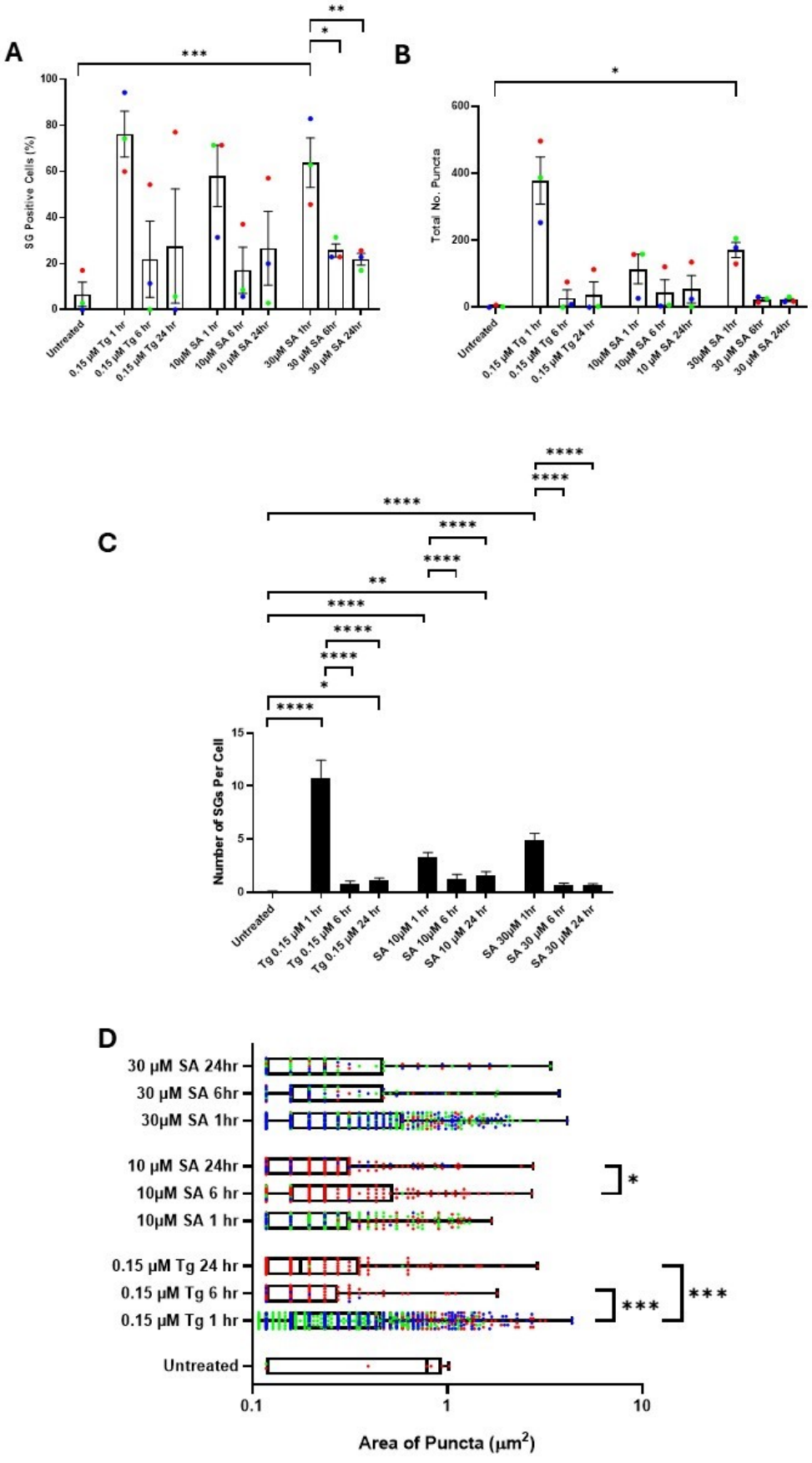
A
B
C
D
SG Positive Cells (%)
Total No. Puncta
Number of SGs Per Cell
Untreated
0.15 µM Tg 1 hr
0.15 µM Tg 6 hr
0.15 µM Tg 24 hr
10µM SA 1 hr
10µM SA 6 hr
10 µM SA 24hr
30µM SA 1hr
30 µM SA 6hr
30 µM SA 24hr
Tg 0.15 µM 1 hr
Tg 0.15 µM 6 hr
Tg 0.15 µM 24 hr
SA 10µM 1 hr
SA 10µM 6 hr
SA 10 µM 24 hr
SA 30µM 1hr
SA 30 µM 6 hr
SA 30 µM 24 hr
Area of Puncta (µm²)

Figure 3.12 Quantification of SG parameters in response to low dose SA and Tg. G3BP-positive puncta (**Figure 3.13**) were analysed by quantifying various parameters including: **(A)** percentage of cells positive for SGs**, (B)** total number of SGs across the total number of cells **(C)** the number of SGs/G3BP positive puncta per cell and **(D)** the area of SGs (μm^2). **(A, C, D**) Data was analysed by Kruskal-Wallis' test followed by Dunn's post-hoc test for multiple comparisons. **(B)** Data was analysed by one-way ANOVA followed by Tukey's post-hoc test for multiple comparisons. Significance is indicated by asterisk, P ≤0.05 (*), P≤0.0001 (****). Data without stars have been deemed as not significant. indicate individual biological replicates: **(1)** red, **(2)** green, **(3)** blue. Error bars: ± SEM (*n=3*). (35 cells per repeat).

3.2.10 SG formation in response to acute stress

Chronic stress (mild and prolonged stress) has been found to result in the reduction of SGs where there is a reduction in size and number of SGs from 1 hr to 24 hr (**Figure 3.11, 3.12**). To investigate the dynamics of SGs in response to acute stress (severe and short duration) cells were treated with 1.5 μM Tg and 250 μM SA for 1 hr. Immunocytochemistry was subsequently used to detect G3BP-positive puncta (**Figure 3.13**). Compared to the untreated condition, 1.5 μM Tg and 250 μM SA treatment for 1 hr resulted in 100 % cells positive for G3BP-positive SGs (**Figure 3.13 A**). SGs were also found to be larger in area in response to SA and Tg compared to the untreated condition (**Figure 3.13 D**). Acute and more severe stress was found to induce more and larger SGs compared to SA and Tg chronic stress conditions (**Figure 3.12**), indicating that severity of stress is a key factor in SG dynamics.

TIA-1 is another SG marker (Mackenzie et al, 2017), it was used to further validate the presence of SGs in response to SA and Tg-induced stress. Cells were treated with 1.5 μM Tg and 250 μM SA for 1 hr and immunocytochemistry was performed to detect SGs expressing TIA-1. It was found that 1.5 μM Tg and 250 μM SA resulted in 76 and 100 % of cells being positive for TIA-1 SGs respectively and 33 % of cells on average were positive for SGs in the untreated condition (**Figure 3.14 A**).

The data presented shows that SA and Tg acute stress will induce SGs positive for G3BP and TIA-1.

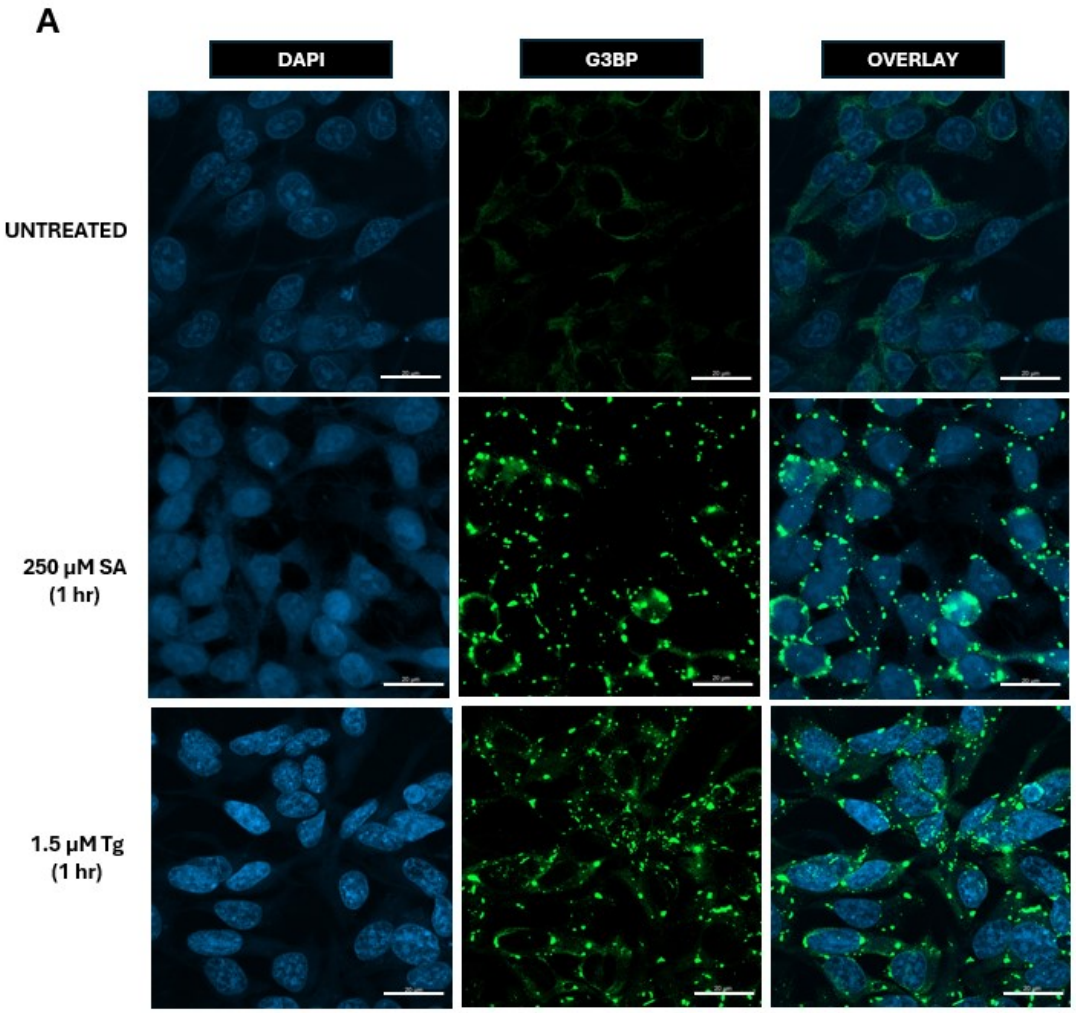
A
DAPI
G3BP
OVERLAY
UNTREATED
250 µM SA
(1 hr)
1.5 µM Tg
(1 hr)

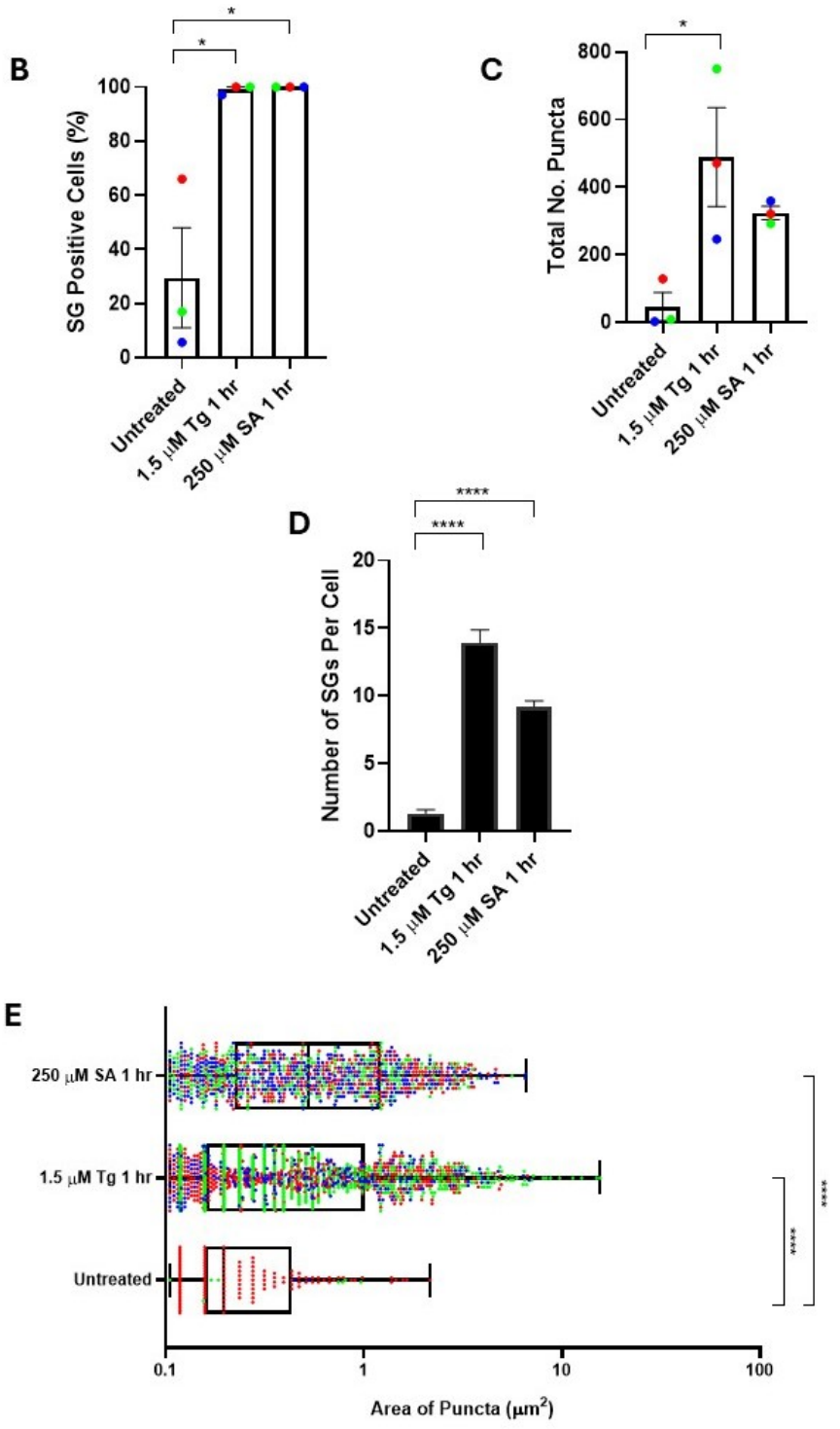
B
SG Positive Cells (%)
100
80
60
40
20
0
*
*
Untreated
1.5 μM Tg 1 hr
250 μM SA 1 hr
C
Total No. Puncta
800
600
400
200
0
*
Untreated
1.5 μM Tg 1 hr
250 μM SA 1 hr
D
Number of SGs Per Cell
20
15
10
5
0
****
****
Untreated
1.5 μM Tg 1 hr
250 μM SA 1 hr
E
250 μM SA 1 hr
1.5 μM Tg 1 hr
Untreated
0.1
1
10
100
Area of Puncta (μm²)
****
****

Figure 3.13 SA and Tg induces SG formation during short and longer duration exposure. (A) Representative images of 1.5 µM Tg and 250 µM SA treated undifferentiated SH-SY5Y cells. Cell nuclei were stained using DAPI and G3BP conjugated to AF488 was used as an indicator of SGs. Magnification: 63x. Scale bar: 20 µm. G3BP-positive puncta were analysed by quantifying various parameters including: **(B)** percentage of cells positive for SGs**, (C)** total number of SGs across the total number of cells **(D)** the number of SGs/G3BP positive puncta per cell and **(E)** the area of SGs (μm^2). Data was analysed by Kruskal-Wallis' test followed by Dunn's post-hoc test for multiple comparisons. Asterisk indicates the extent of statistical significance as reported by GraphPad Prism. The following levels of significance are P ≤0.05 (*), P ≤0.01 (**), P ≤ 0.001 (***), P≤0.0001 (****). Data without asterisk have been deemed as not significant. Colours indicate individual biological replicates: **(1)** red, **(2)** green, **(3)** blue. Error bars: ± SEM (*n*=*3*). (Total number of cells: 105/35 per repeat).

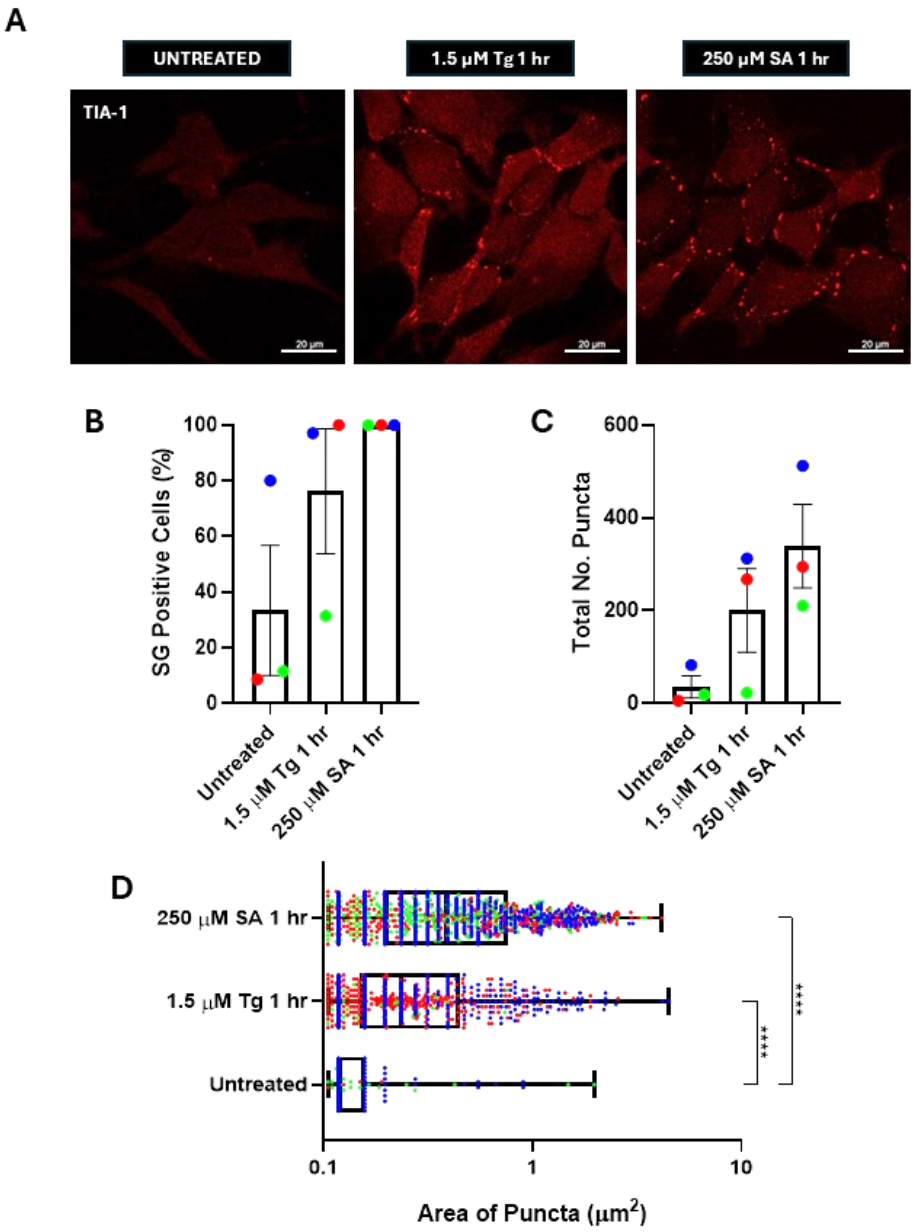

Figure 3.14 SA and Tg acute/short-term treatment also forms SGs positive for TIA-1 (A) Representative images of 250 µM SA (1 hr) and 1.5 µM Tg (1 hr) treated undifferentiated SH-SY5Y cells. Cell nuclei were stained using DAPI and AF594 was used to indicate TIA-1 positive SGs foci. Magnification: 63x. Scale bar: 20 µm. G3BP-positive puncta were analysed by quantifying various parameters including: **(B)** percentage of cells positive for SGs**, (C)** total number of SGs across the total number of cells **(D)** the area of SGs (µm^2). Data was analysed by Kruskal-Wallis' test followed by Dunn's post-hoc test for multiple comparisons. Significance is indicated by asterisk, P≤0.0001 (****). Data without asterisk have been deemed as not significant. Colours indicate individual biological replicates: **(1)** red, **(2)** green, **(3)** blue. Error bars: ± SEM (*n=3*). (35 cells per repeat).

3.2.11 MPP+ induces SG formation

With the presentation of data showing that acute and chronic SA and Tg stress induces SG formation, MPP+ was also used to treat cells to compare SG dynamics in response to the explored toxic compounds. Cells were treated with 5 mM MPP+ for 1, 6, 24 hr (**Figure 3.15**). 41 % of cells in the untreated condition were positive for G3BP-positive SGs (but on average <1 SG per cell). 1, 6, 24 hr treatment of SGs with 5 mM MPP+ resulted in 85, 18, 85 % of cells being positive for SGs (**Figure 3.15 B**). Furthermore, when looking at other parameters in the quantification of SGs in response to 5 mM MPP+ treatment, there were more and larger SGs in the 1 hr and 24 hr 5 mM MPP+ conditions (**Figure 3.15 C, D, E**).

To confirm that 5 mM MPP+ treatment could induce the formation of TIA-1-positive SGs, cells were treated with 5 mM MPP+ for 24 hr and immunocytochemistry was performed. 76 % of cells were positive for TIA-1 positive SGs in response to 5 mM MPP+ 24 hr treatment compared to the untreated condition (1.9 % of cells) (**Figure 3.16 B**). Overall, there were larger and more TIA-1-positive SGs in response to MPP+ 5 mM treatment compared to the cells that were not treated (**Figure 3.16 C, D**).

Cells were also treated with a higher concentration of 10 mM MPP+ for 1, 6, 24 hr to assess the impact of a higher concentration of MPP+ on SG dynamics. Immunocytochemistry was used to detect the presence of G3BP-positive SGs (**Figure 3.17 A**). It was found that in response to 1, 6, 24 hr treatment with 10 mM MPP+, 30, 50 and 74 % of cells respectively, had G3BP-positive SGs compared to the untreated condition (18 %) (**Figure 3.17 B**). Overall, there was an increase in the number and size (area) of SGs (**Figure 3.17 C, D, E**).

Additionally, cells were treated with 10 mM MPP+ for 24 hr and immunocytochemistry was used to detect TIA-1-positive SGs (**Figure 3.18**). 60 % of cells treated with 10 mM MPP+ were found to be positive for TIA-1 SGs compared to the untreated condition (1 %) (**Figure 3.18 B**). In general, it was found that there was more and larger (area) SGs in response to MPP+ 10 mM when compared to the untreated condition (**Figure 3.18 C, D**).

Overall, it was shown that MPP+ treatment (5 and 10 mM) was able to induce SG formation positive for G3BP and TIA-1. It appears to follow a different pattern to SA and Tg chronic stress where overtime there appears to be an increase in response to 10 mM MPP+ treatment or oscillations in SG formation as seen with 5 mM MPP+ treatment rather than a reduction in SGs overtime which was observed in the SA and Tg conditions.

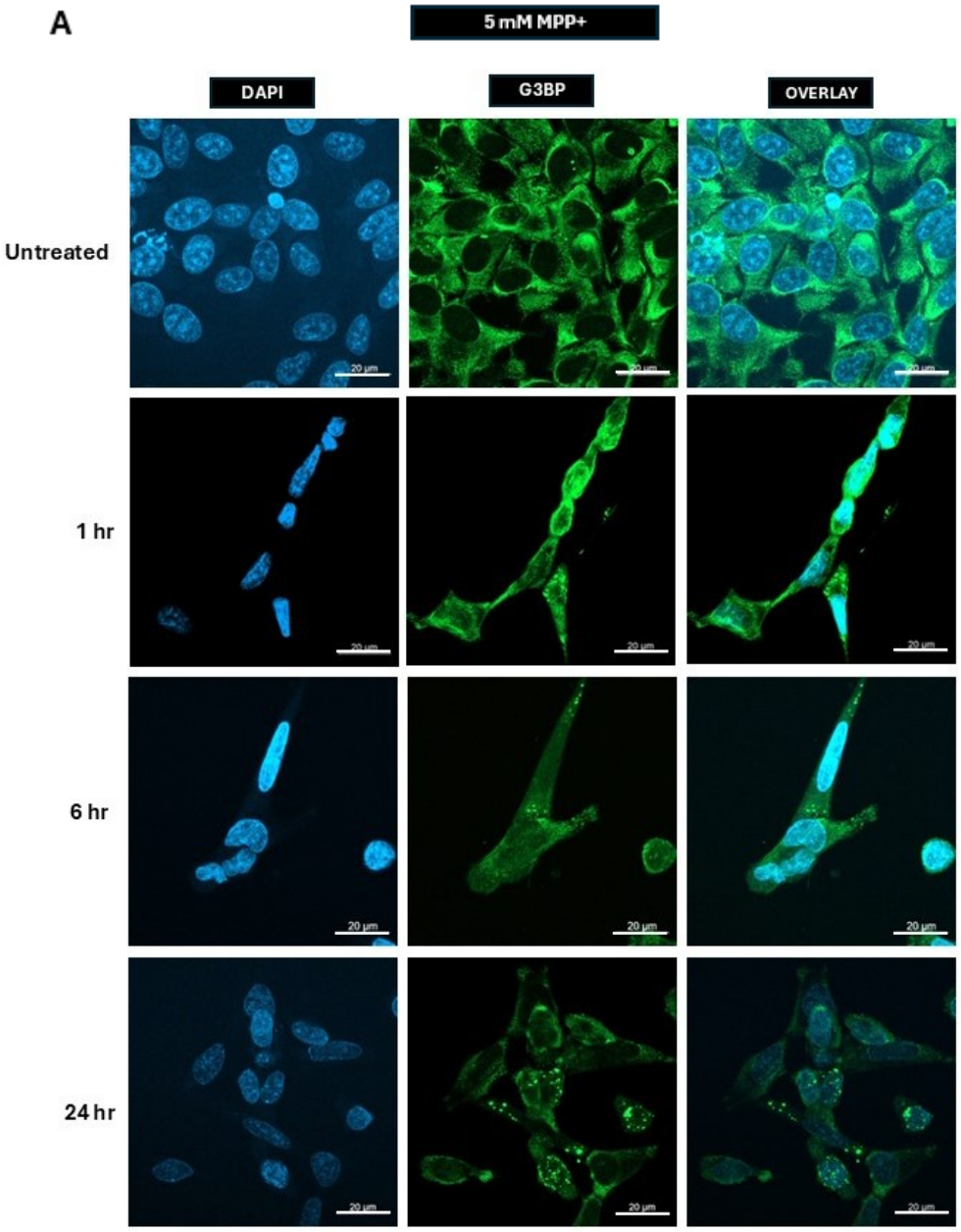
A
5 mM MPP+
DAPI
G3BP
OVERLAY
Untreated
1 hr
6 hr
24 hr

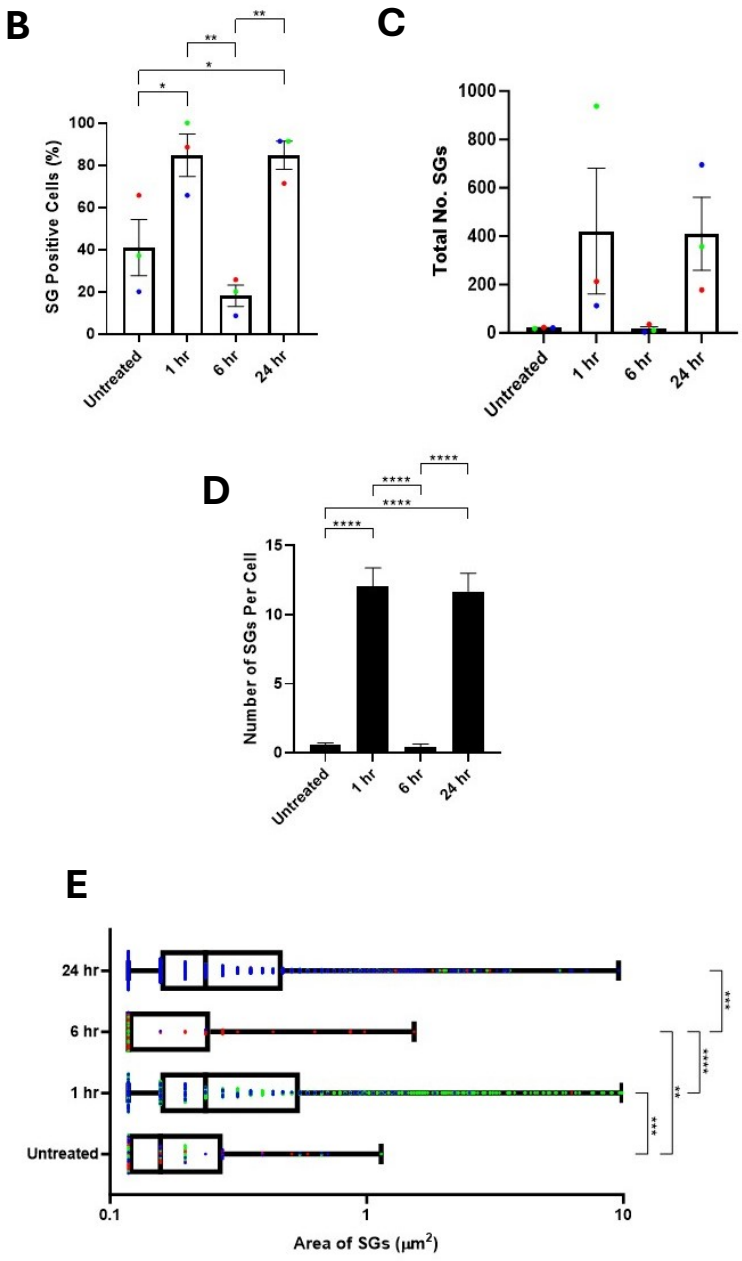

Figure 3.15 5 mM MPP+ induces SGs in both short and long-term stress. (A) Representative images of 5 mM MPP+ treated undifferentiated SH-SY5Y cells. Cell nuclei were stained using DAPI and AF488 was used to indicate G3BP positive SGs foci. Magnification: 63x. Scale bar: 20 µm. G3BP-positive puncta were analysed by quantifying various parameters including: **(B)** percentage of cells positive for SGs**, (C)** total number of SGs across the total number of cells **(D)** the number of SGs/G3BP positive puncta per cell and **(E)** the area of SGs (µm^2). Data was analysed by Kruskal-Wallis' test followed by Dunn's post-hoc test for multiple comparisons. Levels of significance was indicated by the following: P ≤0.05 (*), P ≤0.01 (**), P ≤ 0.001 (***), P≤0.0001 (****). Data without asterisk have been deemed as not significant. Colours indicate individual biological replicates: **(1)** red, **(2)** green, **(3)** blue. Error bars: ± SEM (*n=3*). (35 cells per repeat).

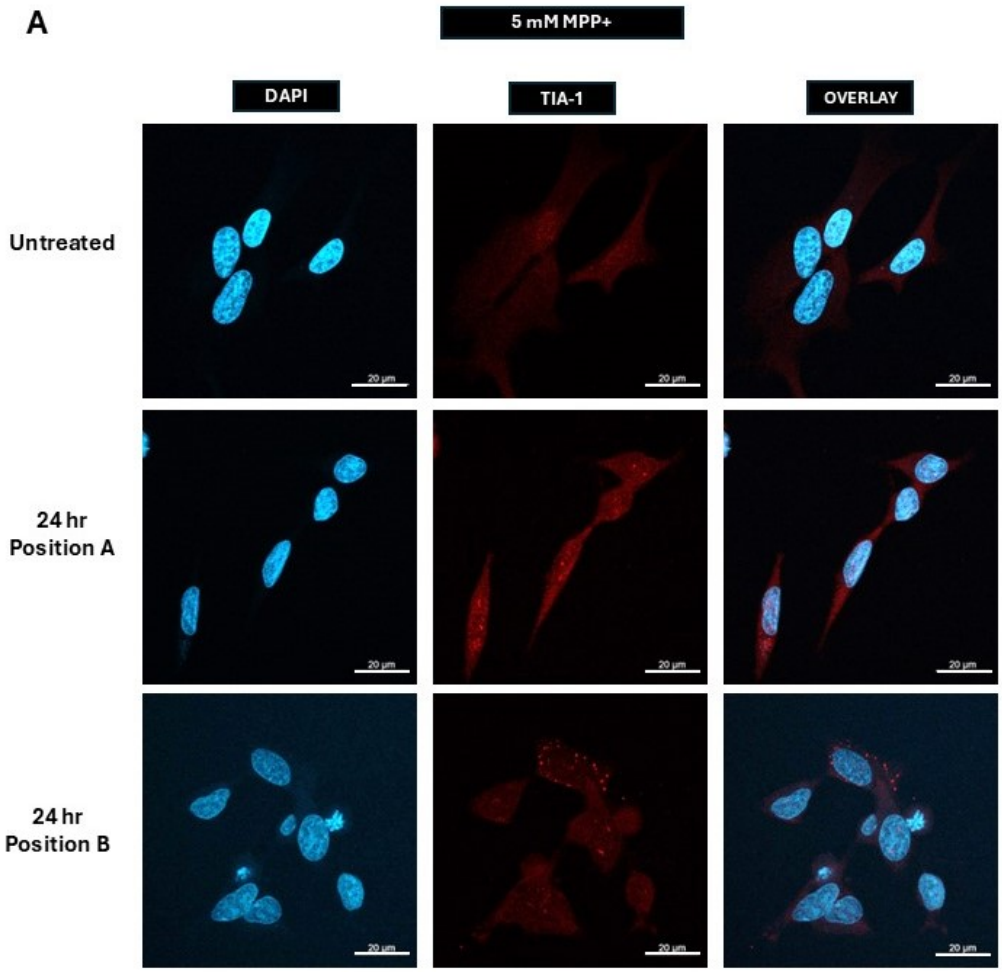
A
5 mM MPP+
DAPI
TIA-1
OVERLAY
Untreated
24 hr
Position A
24 hr
Position B
20 µm

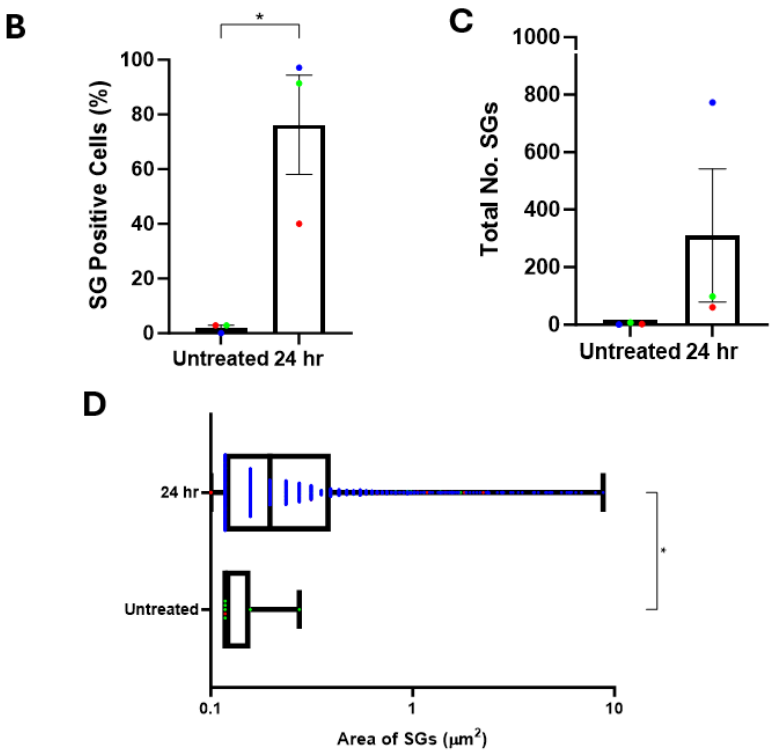

Figure 3.16 5 mM MPP+ induces TIA-1 positive SGs during long-term stress. (A) Representative images of 5 mM MPP+ treated undifferentiated SH-SY5Y cells. Cell nuclei were stained using DAPI and AF594 was used to indicate TIA-1 positive SGs foci. Magnification: 63x. Scale bar: 20 µm. Position A and B are random position taken to show the different TIA-1 puncta. TIA-1-positive puncta were analysed by quantifying various parameters including: **(B)** percentage of cells positive for SGs**, (C)** total number of SGs across the total number of cells **(D)** the area of SGs (µm^2). Data was analysed by the Mann-Whitney test. Levels of significance was indicated by the following: P ≤0.05 (*). Data without asterisk have been deemed as not significant. Colours indicate individual biological replicates: **(1)** red, **(2)** green, **(3)** blue. Error bars: ± SEM (*n=3*). (Total number of cells: 105/35 per repeat).

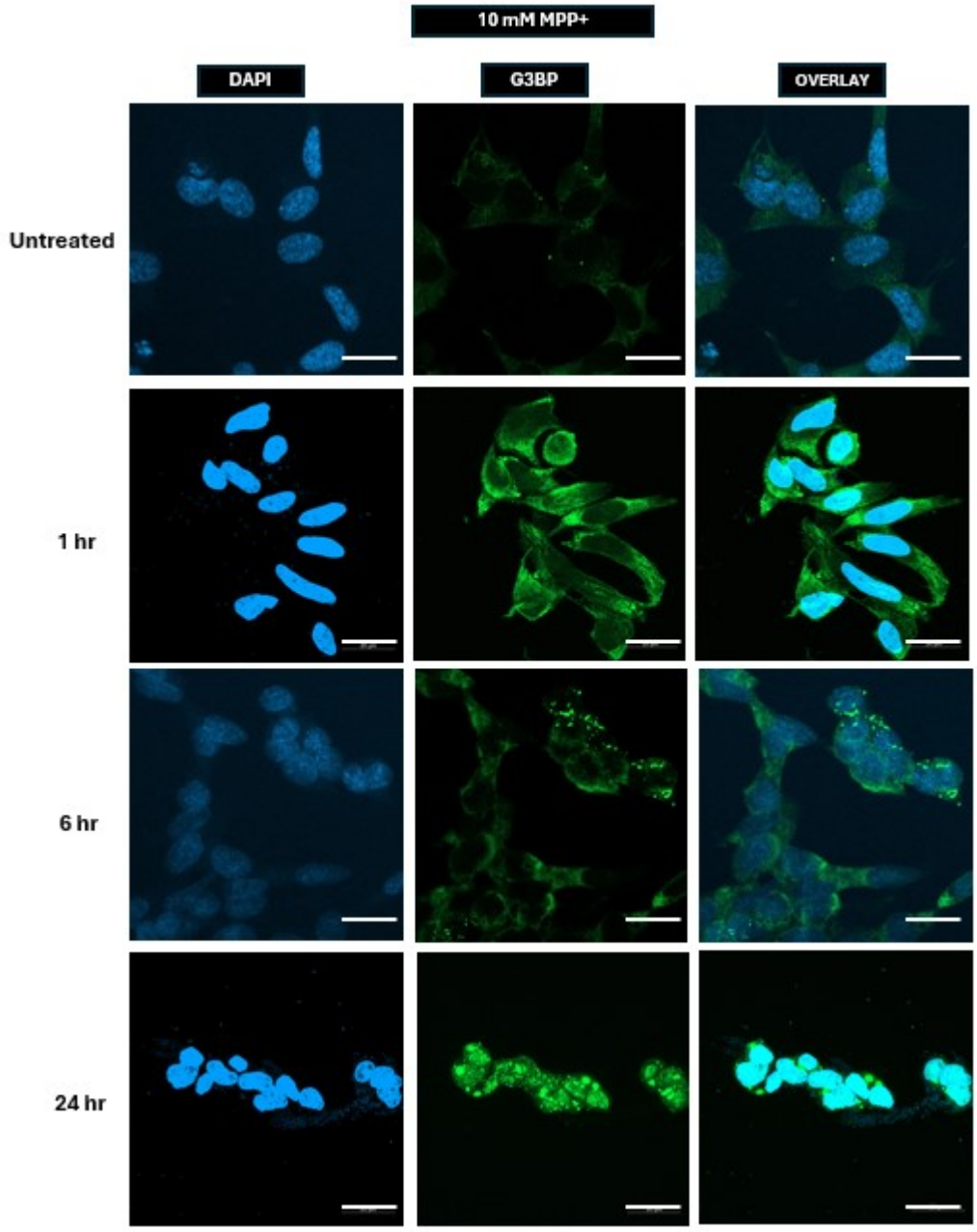
10 mM MPP+
DAPI
G3BP
OVERLAY
Untreated
1 hr
6 hr
24 hr

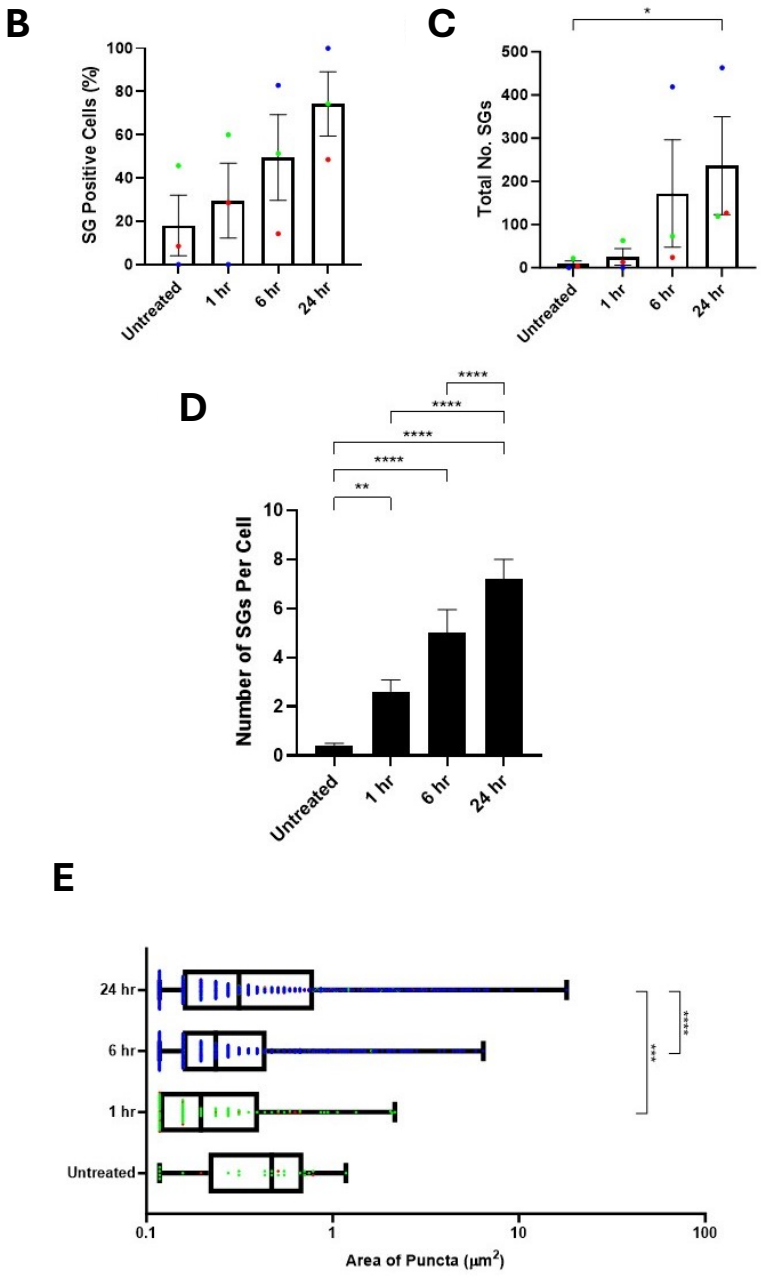

Figure 3.17 Chronic treatment of cells with 10 mM MPP+ induces. (A) Representative images of 10 mM MPP+ treated undifferentiated SH-SY5Y cells. Cell nuclei were stained using DAPI and AF488 was used to indicate G3BP positive SGs foci. Magnification: 63x. Scale bar: 20 μm. G3BP-positive puncta were analysed by quantifying various parameters including: **(B)** percentage of cells positive for SGs**, (C)** total number of SGs across the total number of cells **(D)** the number of SGs/G3BP positive puncta per cell and **(E)** the area of SGs (μm^2). Data was analysed by Kruskal-Wallis' test followed by Dunn's post-hoc test for multiple comparisons. Levels of significance was indicated by the following: P ≤0.05 (*), P ≤0.01 (**), P ≤ 0.001 (***), P≤0.0001 (****). Data without asterisk have been deemed as not significant. Colours indicate individual biological replicates: **(1)** red, **(2)** green, **(3)** blue. Error bars: ± SEM (*n=3*). (Total number of cells: 105/35 per repeat).

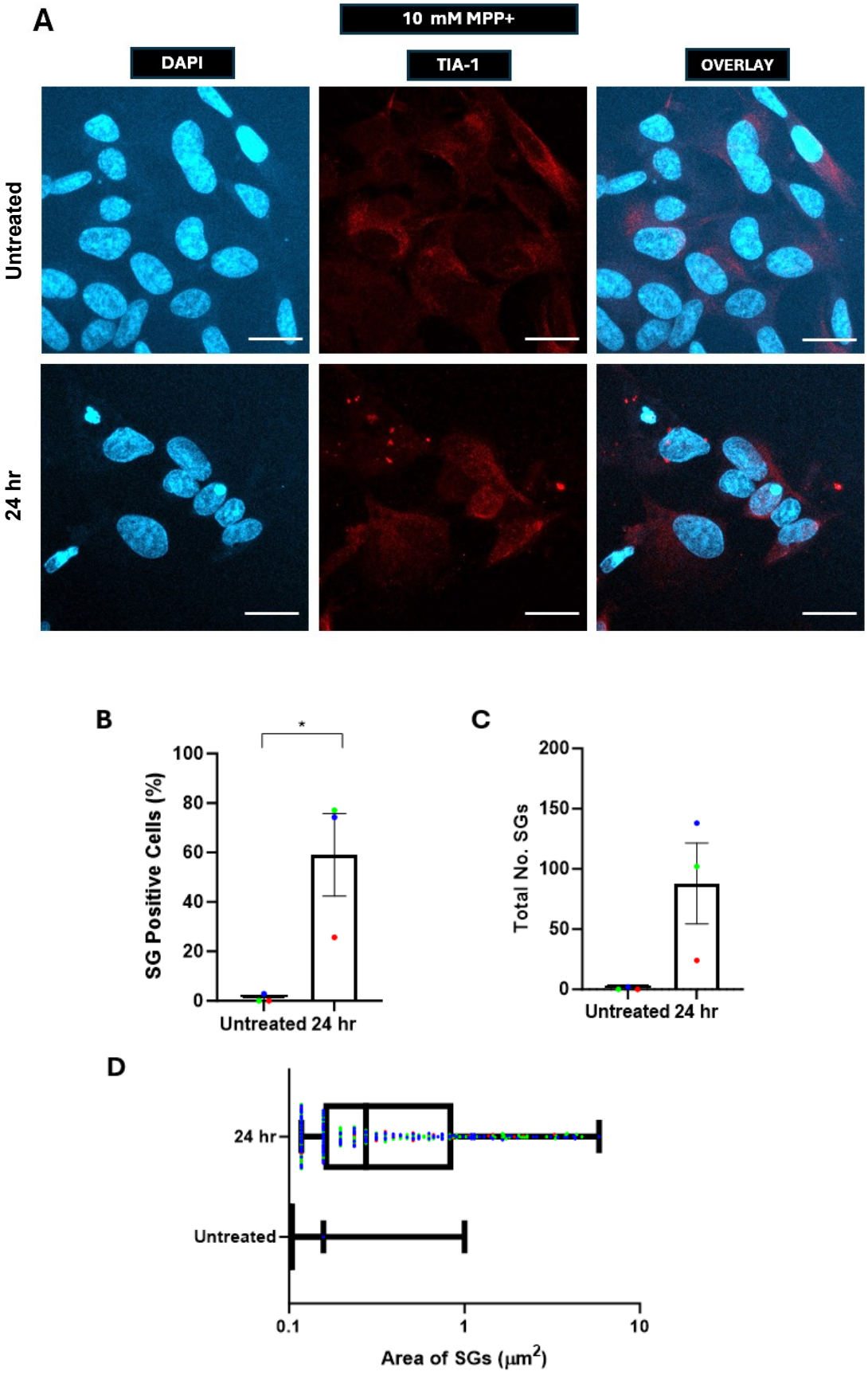
A
10 mM MPP+
DAPI
TIA-1
OVERLAY
Untreated
24 hr
B
SG Positive Cells (%)
100
80
60
40
20
0
*
Untreated 24 hr
C
Total No. SGs
200
150
100
50
0
Untreated 24 hr
D
24 hr
Untreated
0.1
1
10
Area of SGs (μm²)

Figure 3.18 10 mM MPP+ induces TIA-1 positive SGs during long-term stress. (A) Representative images of 10 mM MPP+ treated undifferentiated SH-SY5Y cells. Cell nuclei were stained using DAPI and AF594 was used to indicate G3BP positive SGs foci. Magnification: 63x. Scale bar: 20 µm. G3BP-positive puncta were analysed by quantifying various parameters including: **(B)** percentage of cells positive for SGs**, (C)** total number of SGs across the total number of cells **(D)** the area of SGs (μm^2). Data was analysed by the Mann-Whitney test. Levels of significance was indicated by the following: P ≤0.05 (*). Data without asterisk have been deemed as not significant. Colours indicate individual biological replicates: **(1)** red, **(2)** green, **(3)** blue. Error bars: ± SEM (*n=3*). (Total number of cells: 105/35 per repeat).

3.3 Discussion

3.3.1 Oxidative and ER stress activates the ISR

SA and Tg were used to explore ISR activation in response to oxidative and ER stress. It is well documented that arsenite-induced oxidative stress and Tg-induced ER stress activates the ISR (McEwen et al, 2005; Zheng et al, 2019). Treatment with SA and Tg yielded data that showed an increase in eIF2α phosphorylation (**Figure 3.1, 3.2, 3.3**). Increasing the concentration of 10 μM to 30 μM SA mirrors increasing stress severity with observations of elevated eIF2α phosphorylation as a result. It appears that the more severe the stress, the earlier the cell (if capable) will respond to the imposing stress and engage in a process of adaptation to aid cellular recovery. 6 hr treatment with 30 μM SA caused a reduction in eIF2α phosphorylation, when compared to the 1 hr treatment but was still elevated compared to the untreated condition. Due to the extensive cell death in the 30 μM SA, 24 hr condition (due to the concentration being extremely toxic as shown in LDH data), this prevented eIF2α phosphorylation quantification by western blot analysis. Cells were treated with Tg (**Figure 3.3**) to provide a comparison between ISR marker expression in conditions of oxidative and ER stress. 0.15 μM Tg, like the SA conditions, induced an increase in eIF2α phosphorylation but continues to increase when cells are subjected to 6 hr treatment. However, the characteristic reduction of eIF2α phosphorylation is observed at 24 hr which could also be a sign of cell recovery and adaptation which has been seen existing literature (Hanson et al, 2024).

Considering this information, ATF4 expression was assessed in response to the low-dose concentrations of 30 μM SA and 0.15 μM Tg at 6 and 24 hr (**Figure 3.5**). The pattern of ATF4 expression in response to SA and Tg were similar, where there were increases in expression of ATF4 at 6 hr. At 24 hr for both SA and Tg, there is a reduction in ATF4 expression. The 24 hr timepoint data shows adaptation could be taking in place which has also been observed in other literature (Hanson et al, 2024).

ATF4 expression is associated with an increase in pro-apoptotic markers (Rozpedek et al, 2016). Although, CHOP has associations with apoptosis in

ER stress conditions (Hu et al, 2019), there are other proposed functions for CHOP such as cell cycle arrest (Pan et al, 2024); cell recovery and adaptation (Liu et al, 2023) plus promotion of autophagy (Yang et al, 2021). Additionally, CHOP is a target of ATF4, where CHOP expression is dependent on ATF4 transcription (Su and Kilberg, 2008). Further, CHOP has in turn been observed to negatively regulate ATF4 activity (Su and Kilberg, 2008). CHOP expression was investigated using western blot analysis in response to 10 μM SA, 30 μM SA and 0.15 μM Tg at 1, 6 and 24 hr. It was shown that 30 μM SA induced expression of CHOP at 6 hr and 0.15 μM Tg induced moderate expression of CHOP at 6 hr (**Figure 3.7**), coinciding with the pattern of ATF4 expression observed in response to these treatments (**Figure 3.5**).

Additionally, ATF4 is associated with expression of GADD34 where GADD34 de-phosphorylates eIF2α-P, deactivating the ISR (Márton et al, 2022; Oliveira et al, 2024). Western blot analysis shows that GADD34 was expressed in response to 6 hr treatment with 30 μM SA and 24 hr treatment with 0.15 μM Tg. But this was not the case with 10 μM SA (**Figure 3.9**). At the timepoints where GADD34 was expressed, there was reduction in eIF2α phosphorylation at 30 μM SA, 6 hr (**Figure 3.2**) and 0.15 μM Tg, 24 hr (**Figure 3.3**) compared to their respective earlier timepoints. Which is indicatory of GADD34 activity (deactivating the ISR) and suggestive of cellular adaptation.

GADD34 expression is low in unstressed cells but will increased upon induction of cellular stress. However, when stress dissipates, the cellular content of GADD34 will experience a rapid decline that occurs through 26S proteasomal mediated degradation (Brush and Shenolikar, 2008). GADD34 expression was assessed by western blot in our study to establish if ISR deactivation was an occurrence in the oxidative and ER (chemically induced) stress conditions. However, with the rapid decay of GADD34, the assessment of GADD34 decay rates and/or stability would have provided better context of GADD34 expression in response to the stressors utilised in this study. An example of this is the quantification of cellular levels of green fluorescent protein fused with GADD34 to assess decay rates (Brush and Shenolikar, 2008).

An intrinsic event of the activation of the ISR is the attenuation of translation by the inhibition of GEF activity of eIF2B resulting in the reduction of ternary complexes (Wek et al, 2023). It has been demonstrated that Tg resulted in a reduction of puromycin incorporation indicating translation inhibition (**Figure 3.10**). However, the incorporation of puromycin did not change in response to 6 hr treatment with 30 μM SA compared to the untreated. This marries with the GADD34 data where GADD34 is expressed in response to 30 μM SA at 6 hr indicatory of ISR de-activation.

3.3.2 High-dose MPP+ activates the ISR but does not enhance ATF4 expression.

Understanding MPP+'s ability to not only induce stress but to also activate the ISR was important in establishing a link between the ISR and PD pathology in our cell model along with validating existing findings in literature.

10 mM MPP+ induced moderate eIF2α phosphorylation (**Figure 3.5**) but did not enhance ATF4 expression at this concentration (**Figure 3.6**). 0.1 and 5 mM MPP+ was able to induce ATF4 expression at 6 hr compared to the untreated condition (**Figure 3.6**). Similar to SA and Tg, (**Figure 3.5**), there was a comparative reduction in ATF4 expression at 24 hr compared to the 6 hr timepoint when cells were treated with MPP+ (at all explored concentrations). Suggesting that cellular adaptation is taking place when cells are treated with 0.1 and 5 mM MPP+ for sustained durations. It would be beneficial to observe eIF2α phosphorylation at 0.1 and 5 mM MPP+ for comparative purposes to understand why 10 mM MPP+ did not increase the expression of ATF4 when compared to the untreated condition.

10 mM MPP+ treatment did not induce CHOP expression also (**Figure 3.7**). Despite the absence of enhanced ATF4 and CHOP expression, puromycin incorporation was lowered compared to the untreated condition indicating reduced protein synthesis (**Figure 3.10**), a marker of ISR activation. Considering that 10 mM MPP+ induces phosphorylation of eIF2α and reduces puromycin incorporation (indication of translation inhibition) at 6 hr, it was interesting that ATF4 and CHOP expression was not enhanced. The absence of CHOP expression in response to 10 mM MPP+ could mean other pro-death markers being expressed. Caspase-3 was shown to be expressed in response

to MPP+ (Kaul et al, 2003) as well as melastatin-like transient receptor potential (TRPM) 2 (Sun et al, 2018). Absence of ATF4 and CHOP expression was also seen when mouse embryonic fibroblast (MEF) cells were subjected to UV irradiation (UV-B and UV-C) (Dey et al, 2012). There were also observations of increased eIF2α phosphorylation along with attenuation of translation (Dey et al, 2012). Although UV radiation differs from MPP+ induced stress, it is plausible to suggest that during specific stresses, a mechanism to suppress CHOP expression could be utilized to promote survival. However, further research is needed to investigate this in cases of MPP+ stress conditions.

The data collected indicates that MPP+ at a concentration of 10 mM can induce GADD34 expression at both 6 and 24 hours (**Figure 3.9 D**). This induction correlates with moderate increases in phosphorylation of eIF2α at 6 and 24 hr (**Figure 3.4**). Which suggests that the 10 mM MPP+ condition leads to GADD34 induction independent of increased ATF4 and CHOP expression. GADD34 induction was shown to occur independently of enhanced ATF4 and CHOP expression during mild hyperosmotic stress (Krokowski et al., 2015). MEFs were treated with 500 mosmol medium to induce hyperosmotic stress, which caused an increase in eIF2α phosphorylation and GADD34 expression but no expression of ATF4 and CHOP (Krokowski et al, 2015). These observations were also seen when SH-SY5Y cells were treated with trehalose, an inducer of autophagy (Dimasi et al, 2017). It would be beneficial to investigate the mRNA levels of ATF4, GADD34, and CHOP at the time points investigated (1, 6, and 24 hours) in response to 10 mM MPP+ treatment of SH-SY5Y cells to provide further context for the findings presented.

3.3.3 Stress granules dynamics differ depending on stress conditions

It has been demonstrated that acute and severe (high concentration) stresses, as indicated by SA and Tg, lead to large SGs, often resulting in 100% of quantified cells having SGs (**Figure 3.13**). Chronic stress (lower concentrations/milder concentrations) induced by SA and Tg, resulted in SGs that were smaller and fewer in number (**Figure 3.11, 3.12**). This suggests that the SGs may have different characteristics due to differing stress conditions or

the SGs being smaller could be due to the cell being subjected to milder stress conditions. Within the chronic stress condition (mild, prolonged), there were more and larger SGs at 1 hr compared to longer timepoints (**Figure 3.11**). The observed reduction of SGs (number and size) overtime suggests stress adaptation. This is supported by expression of GADD34 in response to 6 hr treatment with 30 μM SA and 24 hr treatment with 0.15 μM Tg (**Figure 3.9**). Similar patterns of SG reduction in response to chronic stress has been seen in other literature where SGs reduce at timepoints after 1 hr treatment with low doses of SA (e.g. 50 μM) (Adachi et al, 2024).

SG dynamics were also explored in response to MPP+ treatment. Data presented showed that 5 mM and 10 mM induced the formation of SGs (**Figure 3.15, 3.16, 3.17, 3.18**). These SGs were shown to be positive for both G3BP and TIA-1. There appears to be a difference in SG dynamics in response to MPP+ (**Figure 3.15, 3.17)** when compared to SA and Tg (**Figure 3.11**). Like SA and Tg, there also appears to be increases in SGs at 1 hr in response to 5 mM MPP+ followed by a decrease at 6 hr. However, the number and size of SGs increased again at 24hr (**Figure 3.15**). The oscillating SG formation seen in response to 5 mM MPP+ has been seen in other stress conditions. It has been shown that SGs can assemble and disassemble in an oscillating manner as seen with viral infection-induced stress (Ruggieri et al, 2012). Regarding, 10 mM MPP+, this condition was shown to induce more SGs overtime with the size and number of SGs peaking at 24 hr (**Figure 3.17**).

Expression of GADD34, in cases of SA and Tg-induced stress, appears to coincide with a reduction of cells positive for SGs (**Figure 3.9**). Similar observations were seen with hepatitis C virus infected-Huh7 cells where GADD34 expression correlated with reduced phosphorylated eIF2α levels and decreased SGs (Klein et al, 2022). Considering the current understanding that GADD34 de-phosphorylates eIF2α-P, which is an indicator of cell recovery (Goh et al, 2018), it is expected that SG disassembly should occur (Hoffmann et al, 2022). This does not appear to be the case with 10 mM MPP+. GADD34 was shown to be expressed at 1, 6 and 24 hr (**Figure 3.9 D**) and SGs increased overtime (**Figure 3.17**) which suggests an alternative link between GADD34 and SGs that should be explored. Moreover, despite both SA and

MPP+ having the capacity to induce oxidative stress (Anantharam et al, 2007; Ruiz-Ramos et al, 2009), SG dynamics differs between the explored treatment conditions, indicating that the SGs dynamics will vary in response to different compounds with variances in their mechanism of action.

SGs will typically only form under conditions of stress. There were observations of minimal amounts of SGs present in the untreated condition (**Figure 3.11 – 3.18**). This could be due to fluctuations in cell culture conditions resulting in moderate stress induction. Some cancer cell lines may be inherently stressed as cellular stress has been found to be key to tumorgenesis and cancer proliferation (Redding and Grabocka, 2023), potentially enhancing basal levels of SGs. Additionally, SG components such as G3BP1 have been found to be overexpressed in certain cancer cells altering SG dynamics (Redding and Grabocka, 2024).

3.4 Summary

The aim of chapter three was to validate the activation of the ISR in response to compounds that have been explored in existing literature such as SA, Tg and MPP+, to build a foundation of expectation in the selected cell line, SH-SY5Y.

This study further explored the impact of duration, severity and type of stress treatments on ISR marker expression. The data presented confirms SA and Tg are able to increase expression of the following ISR markers: eIF2α phosphorylation, ATF4, GADD34 and CHOP expression (**Figure 3.19**). It can also be confirmed that MPP+ can induce ISR marker expression. But in the condition of high doses of MPP+ (10 mM) there is observation of ISR activation independent of increased ATF4 and CHOP expression (**Figure 3.20**) which requires further exploration.

Treatment with these stress-inducing compounds shows the capacity of cells to adapt to various stresses (oxidative and ER stress) through the reduction of ISR markers overtime as shown with the reduction of eIF2α phosphorylation and ATF4 expression as well as increased GADD34 expression despite the observation of increased cytotoxicity.

It is common knowledge that SA and Tg triggers SG formation, but it has not been shown in existing literature that MPP+ can induce SG formation which has been demonstrated with G3BP and TIA-1 immunocytochemistry. Further, SGs formed in response to MPP+ exhibits different dynamics when compared to SA and Tg.

Furthermore, the data explored in this chapter uses techniques focused on protein expression of ISR, it would be informative to investigate how stress induced by SA, Tg and MPP+ alters gene expression of various ISR markers. Exploration of additional timepoints and concentrations of the toxic compounds used would be helpful in understanding how time and concentration impacts the ISR. Also, further investigation into additional adaptive and apoptosis markers downstream of ATF4 would provide a more in-depth picture of the stress response induced by the stress conditions investigated.

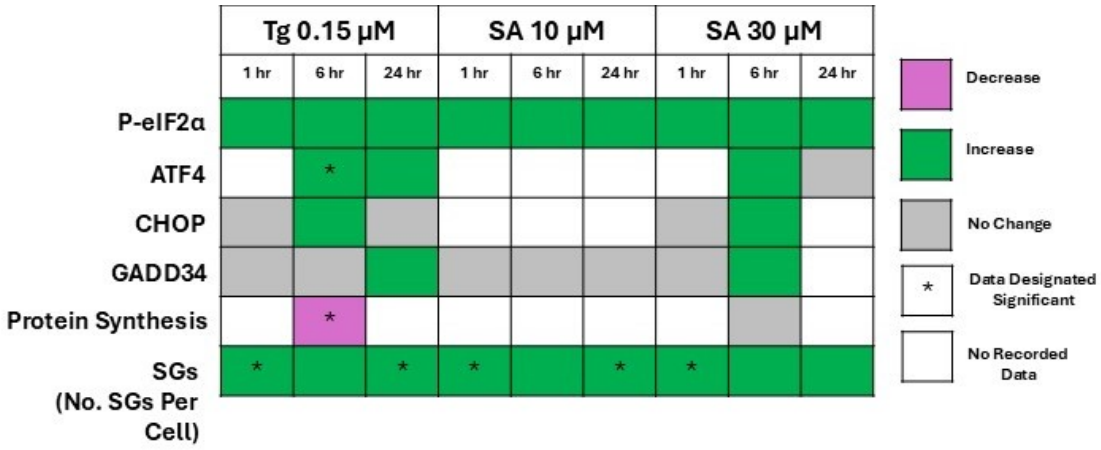

Figure 3.19 A summary of data exploring SA and Tg of ISR marker expression. The diagrams summarise the findings presented throughout the chapters in response to low-dose SA and Tg. With specific focuses on how expression changes compared to the prior timepoint.

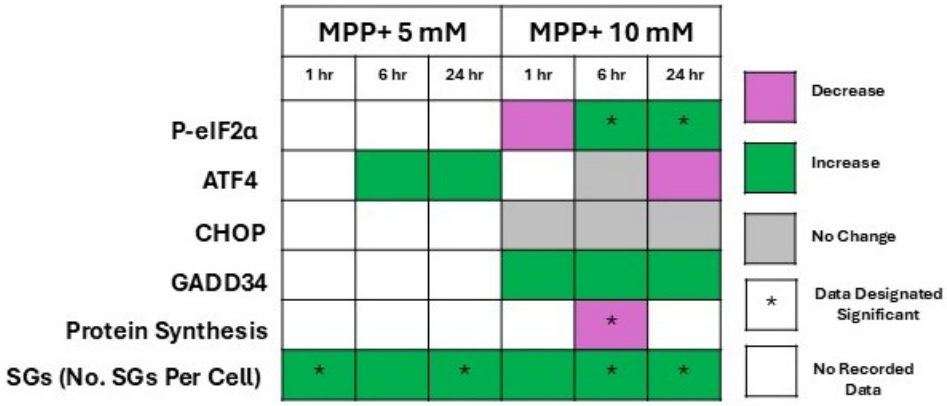

Figure 3.20 MPP+ timeline of ISR marker expression. The diagrams summarise the findings presented throughout the chapters in response to MPP+. With specific focuses on how expression changes compared to the prior timepoint.

4 Chapter Four: The production and characterisation of α-synuclein aggregates

4.1 Introduction

α-Synuclein aggregation is a hallmark in PD pathology (Hijaz and Volpicelli-Daley, 2020) and has been studied in other diseases such as DLB, PDD, MSA, pure autonomic failure and rapid eye movement sleep behaviour (Calabresi et al, 2023). Due to its association with various conditions and mechanisms, the production and characterisation of α-synuclein aggregates has been key to studying PD (Danzer et al, 2007; Howe et al, 2021; Taylor-Whiteley et al, 2019; Woerman and Luk, 2024). Aggregates of α-synuclein exist in many forms as discussed in **Sections 1.5, 1.6** with oligomers and PFFs being implicated in PD-associated cellular stress (Russo et al, 2019; Taylor-Whiteley et al, 2019; Zeng et al, 2024). The activation of the ISR in response to oligomers and PFF will be explored to determine a link between the ISR, stress and PD pathology. Therefore, production and characterisation of α-synuclein oligomers and PFFs will be intrinsic to investigating this.

4.2 Objectives

The aim of this chapter is to focus on the production of seeding (Type C) oligomers and PFFs for subsequent cellular treatment to explore cellular stress as well as the effects of α-synuclein aggregates on sEV proteomic cargo. Therefore, to achieve this, the following will be carried out:

- the production and characterisation of WT monomeric α-synuclein.
- inducing aggregation of monomeric α-synuclein into oligomers, fibrils and PFFs.
- characterising oligomers and PFFs/fibrils using various techniques.
- exploration of alternative techniques (use of novel fluorescent dyes) to detect intracellular aggregation upon exposure to PFFs.

4.3 Results

4.3.1 The production and characterisation of monomeric α-synuclein

The production of monomeric α-synuclein is required when synthesising oligomers and PFFs. Monomeric α-synuclein was produced in a bacterial expression system using the BL21 (DE3) *E.coli* strain. Bacterial cells were subjected to expansion steps as described in **Section 2.3**. Samples at all stages of crude purification were collected and subjected to SDS-PAGE. Gels were then stained using the Imperial Protein Stain to detect presence of proteins. It was observed that there were proteins at various molecular weights (**Figure 4.1 A**).

To purify the acquired bacterial protein samples and obtain the desired recombinant protein, samples were then subjected to FPLC using anion exchange and gel filtration/size exclusion chromatography (SEC) (**Section 2.3**). Recombinant protein samples were dissolved in sodium phosphate and purity was confirmed by the presence of a single protein band detected by SDS-PAGE and subsequent staining of proteins present on the gel (**Figure 4.1 B**). The detected protein band was higher than 15 kDa, this is due to α-synuclein monomers being intrinsically disordered proteins (IDP) (Tong et al, 2024). IDPs will migrate on gels slower due to a lower binding affinity to SDS resulting in protein bands appearing higher than the expected molecular weight (MW) (Trivedi and Nagarajaram et al, 2022).

The presence of α-synuclein in lyophilised samples was confirmed with dot blots utilising an antibody that targets α-synuclein, alongside a BSA only control (**Figure 4.1 C**).

To further validate the presence of full-length α-synuclein in synthesised samples, electrospray ionisation mass spectrometry (ESI-MS) was performed to determine the MW. It was found that the resulting sample had a MW of 14,460 Da (14.5 kDa, rounded) which is the expected mass of WT monomeric α-synuclein (**Figure 4.2**).

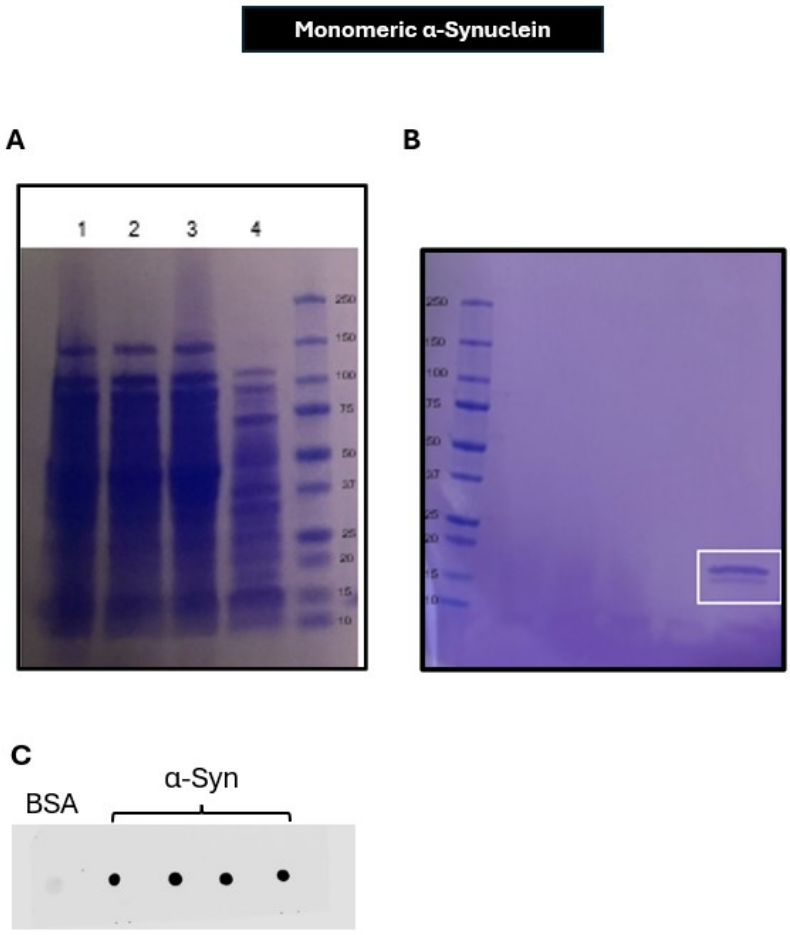

Figure 4.1 α-Synuclein positive SEC samples. (A) Imperial staining (protein stain) of gels acquired from SDS-PAGE, show that samples collected throughout the crude purification steps contain proteins with varying molecular weight. The following are the steps at which samples were collected: **(A1)** aliquots collected from sonicated BL21 pellets, **(A2)** samples collected from supernatant after centrifugation of BL21, **(A3)** post-centrifugation supernatant was acidified to PH 4.0 using 1 M HCl and **(A4)** acidified supernatant was centrifuged and neutralised using 1 M NaOH. **(B)** Lyophilised samples subjected to both anion exchange and SEC show a protein band of 14-15 kDa. **(C)** Dot blot analysis of the BSA control and SEC/freeze-dried samples shows that samples prepared are positive for α-synuclein (technical repeats, *n=4*).

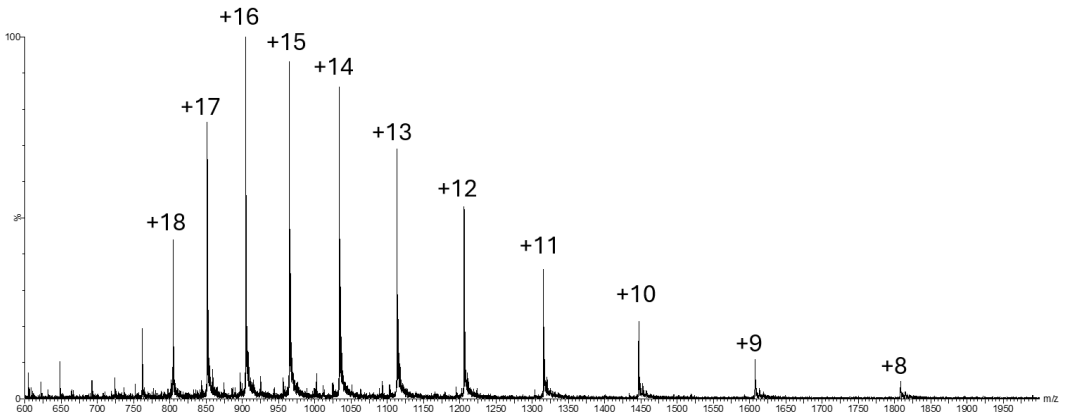

Figure 4.2 ESI-MS analysis of intact monomeric α-synuclein. ESI-MS spectra of 800 – 2000 range of recombinant proteins demonstrate the charge state distribution envelope of α-synuclein. Each peak within the spectra represents an individual charge state of the protein, with the relevant charges noted. The mass of the protein was determined to be 14,460.63 Da (ESI performed by Prof. David P Smith).

4.3.2 Using ThT to report presence of amyloid conformations

1 mg/mL monomeric α-synuclein was agitated over a 7-day period as described in **Section 2.5** to induce amyloid fibril formation of α-synuclein as done in other literature (Volpicelli-Daley et al, 2011). A common practice in the characterisation of fibrils is using fluorescent dyes such as Thioflavin T (ThT) to detect the presence of the cross-linked b-sheet conformation present in amyloid structures/α-synuclein fibrils (Li et al, 2018; Sulatskaya et al, 2018; Xue et al, 2017). ThT fluorescence was compared between monomers, oligomers and fibrils (**Figure 4.3**). It was found that ThT fluorescence was highest in response to the fibrils compared to the monomer and oligomers (**Figure 4.3 B**), indicating that the synthesised α-synuclein fibrils had an amyloid structure.

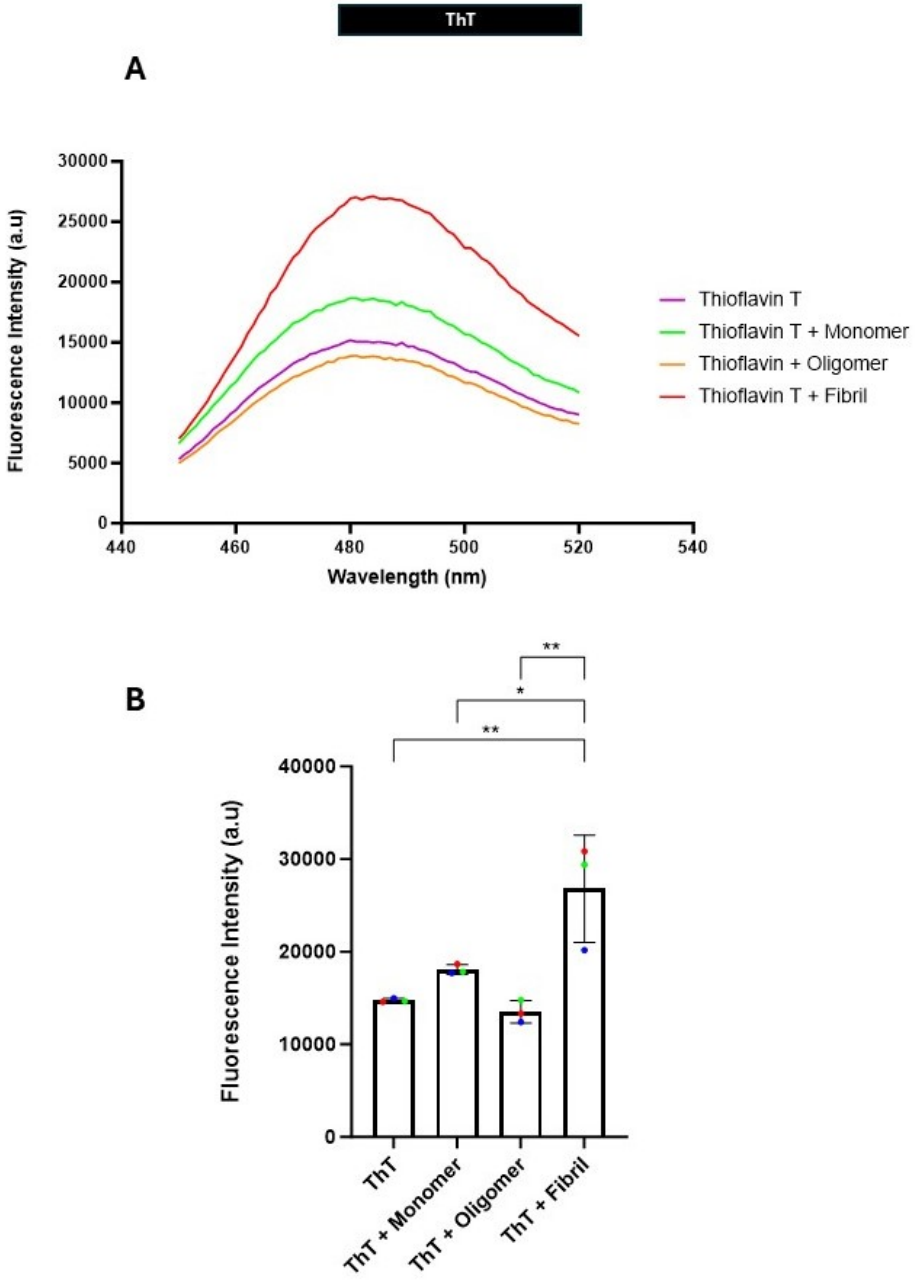

Figure 4.3 ThT indicates highest fluorescent intensity in response to α-synuclein fibrils. (A) Spectral reading of ThT fluorescence across 450 – 520 nm shows increased fluorescence in response to fibril samples. **(B)** ThT fluorescence intensity at 485 nm was highest in response fibrillar α-synuclein compared to monomeric and oligomeric α-synuclein. Data was analysed by one-way ANOVA followed by Tukey's post-hoc test for multiple comparisons. Levels of significance as indicated by the following: P ≤0.05 (*), 0.01 (**). Data without asterisk have been deemed as not significant. Colours indicate individual biological replicates. Error bars: ± SEM (*n*=*3*) (biological repeats/separate preparations, *n*=*3*).

4.3.3 ThT detects α-synuclein amyloid formation occurs overtime

ThT was used to measure the aggregation rate of α-synuclein overtime (**Figure 4.4**) to provide information on the dynamics of α-synuclein fibril assembly. 1 mg/mL (70 μM) α-synuclein was agitated continuously for over 5 (5.4) days for 37 °C as described in **Section 2.5** (**Figure 4.4 A**). A large increase in ThT fluorescence was seen between days 1 and 3. No increase was seen with the ThT control (**Figure 4.4 A**). This pattern of formation is characteristic of nucleation and elongation kinetics associated with amyloid fibril formation.

The discontinuous method as described in **Section 2.5** (**Figure 4.4 B**) was also utilised to measure ThT fluorescence in response to monomeric α-synuclein assembly overtime at a higher concentration of 2 mg/mL (140 μM). The discontinuous method involved the collection of aliquots for daily measurement during sustained agitation of samples. A similar pattern to the continuous method was observed, where an increase in ThT fluorescence occurred between days 1 and 3 and tapers off after day 3 (**Figure 4.4 B**).

Together, the data presented demonstrates that α-synuclein fibril formation is occurring in accordance with the expected nucleation and elongation kinetic pathway.

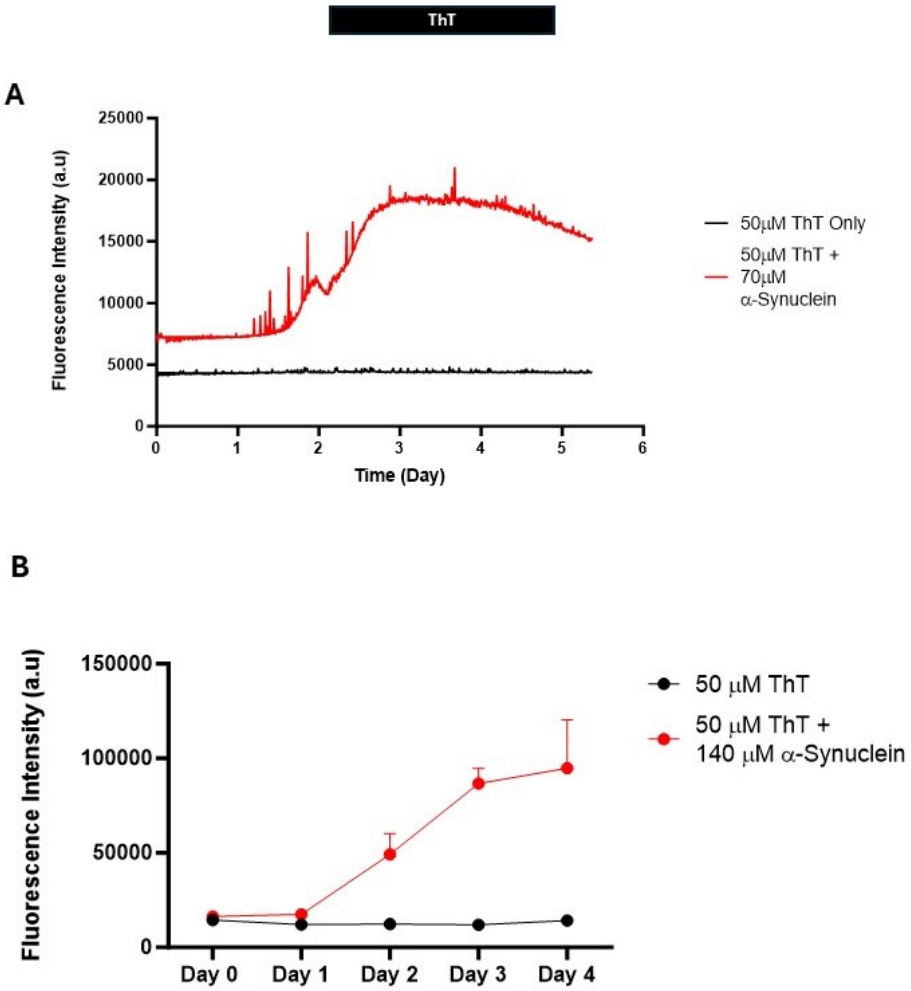

Figure 4.4 ThT fluorescence increases overtime when α-synuclein is agitated to induce aggregation. (A) Monomeric α-synuclein (1 mg/mL, 70 μM) in 96-well black, clear bottom plates were left to agitate for 5.4 days resulted an increase in fluorescence intensity of ThT. The increase in fluorescence can be observed after day 3 to slight taper off (technical repeats, *n*=*3*). **(B)** Aliquots of α-synuclein (2 mg/mL, 140 μM) was collected during agitation of α-synuclein and ThT fluorescence was measured the same time daily. It was found fluorescence increased overtime (technical repeats, *n*=*3*). **(B)** Data was featured in the following scientific article, Owyong et al (2024).

4.3.4 Using NIAD-4 derivatives to assess presence of amyloid fibrils

For the furtherance of providing additional methods for the detection of intracellular aggregation, synthesis and characterisation of derivatives of the [5'-(4-Hydroxyphenyl) [2,2'-bithiophen]-5-yl] methylene]-propanedinitrile (NIAD-4) dye was carried out to formulate a method to discriminate cells that experience intracellular α-synuclein aggregation in response to PFF treatment (Owyong et al, 2024). NIAD-4 is a dye, like ThT, that has the ability to bind to amyloid fibrils (Peccati et al, 2015) and has been reported to detect *in vivo* protein deposits (Naganuma et al, 2023). It was found that along with NIAD-4, NIAD CNEOT (one of the synthesised derivative dyes) preformed best in measuring amyloid formation (Owyong et al, 2024).

The discontinuous method used in measuring ThT fluorescence (**Figure 4.5 B**) was used to measure NIAD-4 and NIAD CNEOT fluorescence overtime in response to 2 mg/mL (140 μM) monomeric α-synuclein subjected to agitation (**Section 2.5**). Aggregates were agitated in Eppendorf tubes for 4 days as done previously (**Figure 4.5**). It was shown that NIAD-4 and NIAD CNEOT's fluorescence increased over the 4-day period compared to the dye-only controls. NIAD-4 primarily showed an increase in fluorescence between days 1 and 3 followed by a tapering off after day 3, like ThT (**Figure 4.5 A**). NIAD CNEOT showed an increase in fluorescence from day 1 to 4 in response to α-synuclein (**Figure 4.5 B**). Data indicates that NIAD-4 and NIAD CNEOT can be used as an alternative dye to ThT in the measurement of α-synuclein amyloid formation.

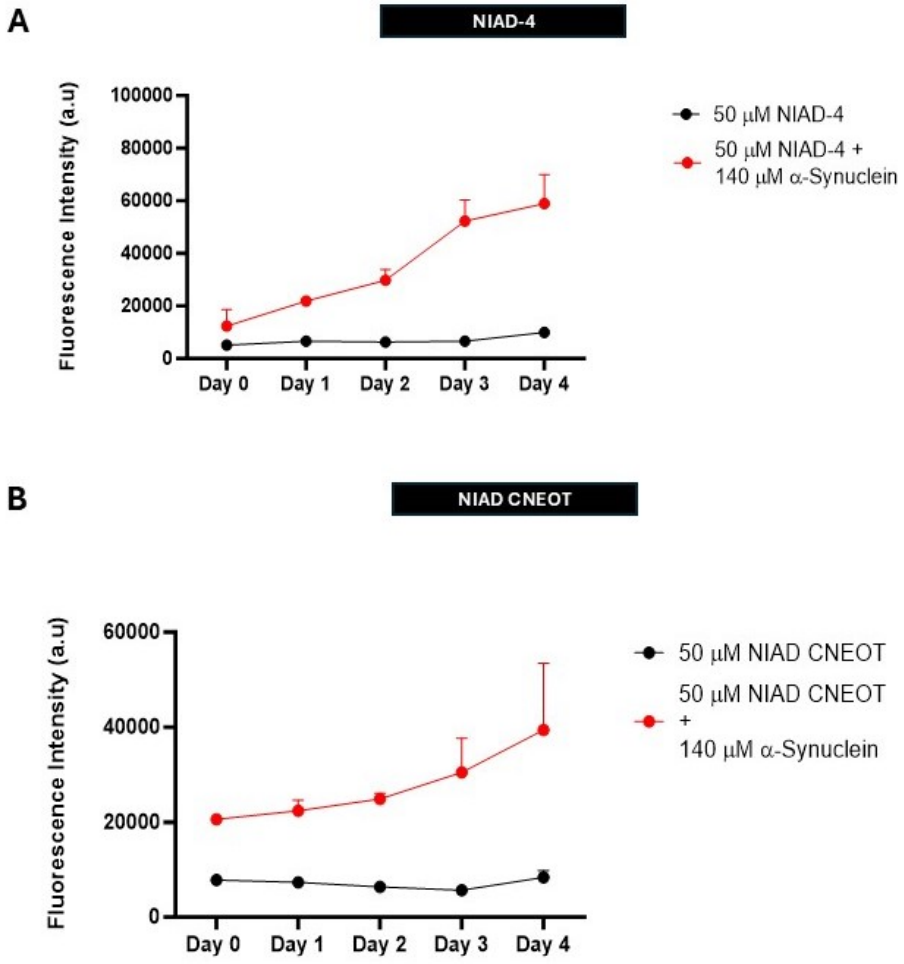

Figure 4.5 NIAD-4 and NIAD CNEOT dyes are able to detect aggregation overtime of α-synuclein. Synthesis, characterisation and validation of NIAD dyes were described in the following scientific article, Owyong et al (2024). As done previously the discontinuous method was utilised to assess NIAD dyes fluorescence in response to α-synuclein (140 μM, 2mg/mL) agitated over a 4-day period. Aliquots of α-synuclein was collected during agitation of α-synuclein and ThT fluorescence was measured the same time daily. It was found fluorescence in response **(A)** NIAD-4 **(B)** NIAD CNEOT increased overtime (technical repeats, *n=3*).

4.3.5 NIAD-4 and NIAD CNEOT detected α-synuclein PFFs

Evidence collected suggested that both NIAD-4 and NIAD CNEOT have similar capabilities to ThT in the detection of α-synuclein fibrils/amyloid. Both dyes were used to compare monomeric α-synuclein samples to PFFs. It was shown that both NIAD-4 and NIAD CNEOT fluorescence was higher in response to PFFs compared to monomers and the dye only control (**Figure 4.6**). Data indicates that α-synuclein PFFs has an amyloid structure. Further, the NIAD CNEOT derivative exhibits similar capabilities to NIAD-4 by fluorescing more in response to PFFs.

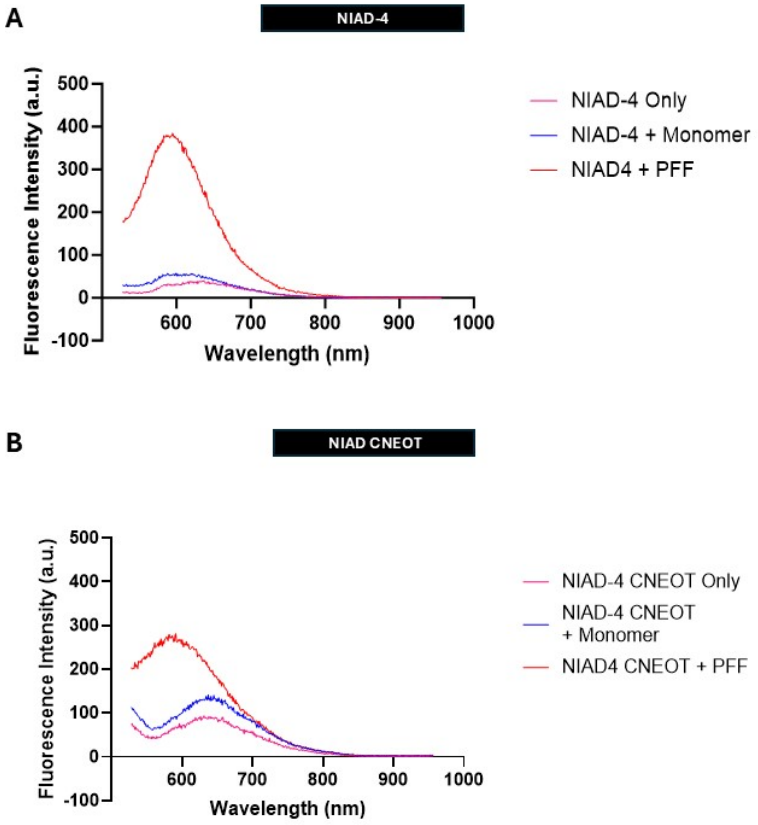

Figure 4.6 NIAD-4 and NIAD CNEOT dyes are able to detect aggregation overtime of α-synuclein. Synthesis, characterisation and validation of NIAD dyes were described in the following scientific article, Owyong et al (2024). Fluorometric spectrometry was used to assess **(A)** NIAD-4 and **(B)** NIAD CNEOT fluorescence in response to α-synuclein monomers and PFFs (70 μM, 1 mg/mL), it was found both dyes had the most fluorescence intensity in response to PFFs compared to monomers and the dye only (technical repeats, *n=3*).

4.3.6 Structural and size characterisation of α-synuclein fibrils

Monomeric α-synuclein was stimulated to aggregate as described in **Section 2.4** to form fibrils. Atomic force microscopy (AFM) was carried out to validate the structure of fibrils produced at the end of the preparative process (4-day agitation) (**Figure 4.8**). The fibrils found in these samples exhibit a branched morphology and display structural similarities to fibrillar aggregates reported in other literature (Bharathi et al, 2007; Smith et al, 2008). These fibrils do not display a typical tubular morphology instead they have a branched structure, which may indicate that these fibrils are not mature but may have more “ends” present which is usually associated with inducing cellular toxicity.

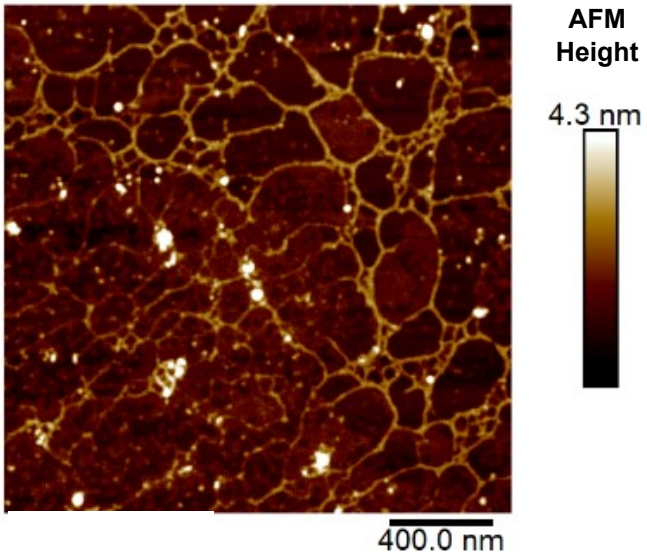

Figure 4.7 AFM images of day 4 fibrils. Fibrils were left agitating for 4 days and representative AFM images were taken of fibrillar α-synuclein samples (*n=1*). Similar morphology has been seen in other literature (Smith et al, 2008) at day 3 and 4 of fibril formation. Image was featured in the following scientific article, Owyong et al (2024).

4.3.7 Detecting intracellular aggregation using NIAD-4 and NIAD CNEOT fluorescent dyes

SH-SY5Y cells were treated with PFFs for 24 hr and subsequently stained with either NIAD-4 or NIAD CNEOT and SYTOX blue. SYTOX blue stains cells that are dead for later exclusion so that data is representative of live cells only. Cells were subjected to flow cytometry analysis where untreated cells were compared to cells treated with PFFs to establish the corresponding fluorescence intensity of live cells in response both dyes (NIAD-4 and NIAD CNEOT). Raw data was gated and analysed using FlowJo software (**Figure 4.8**).

Intracellular aggregation was indicated by cells that had a higher fluorescence intensity in response NIAD-4 and NIAD CNEOT. It was found when cells were treated with PFFs for 24 hr, they had a higher fluorescence intensity when stained with the NIAD dyes compared to the untreated cells (**Figure 4.9**). This indicates the presence of intracellular aggregation in response to PFFs detectable by NIAD-4 and NIAD CNEOT.

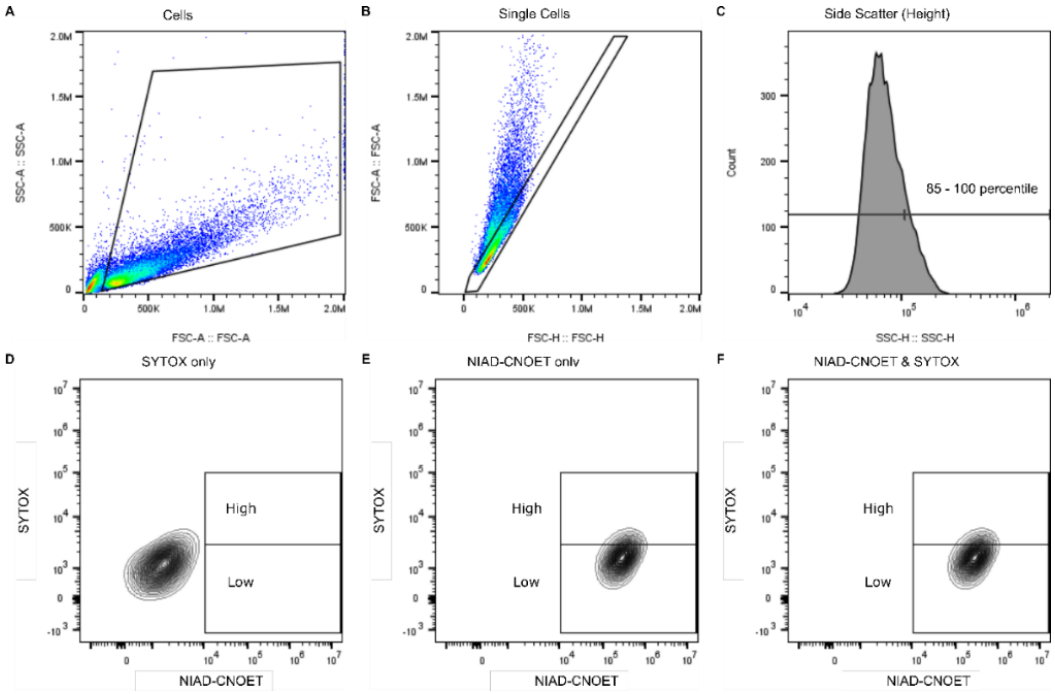

Figure 4.8 Flow cytometry gating strategy for NIAD-4 and NIAD CNEOT experiment. General flow cytometry gating strategy and control conditions – example shown for NIAD-CNOET and corresponding conditions. **(A)** Cells were first gated followed by **(B)** single cells. **(C)** Cells were then gated based on their side scatter (height) at 0 – 85 and 85 – 100 percentiles. **(D – F)** The cells gated by their side scatter profile and counted by their intensity, with focus on the 85 – 100 percentiles of side scatter profiles in the high gate population count. (Taken from the supplementary evidence of the Owyong et al, 2024 – second author of paper (Laura E. Shippey) and performed this experiment).

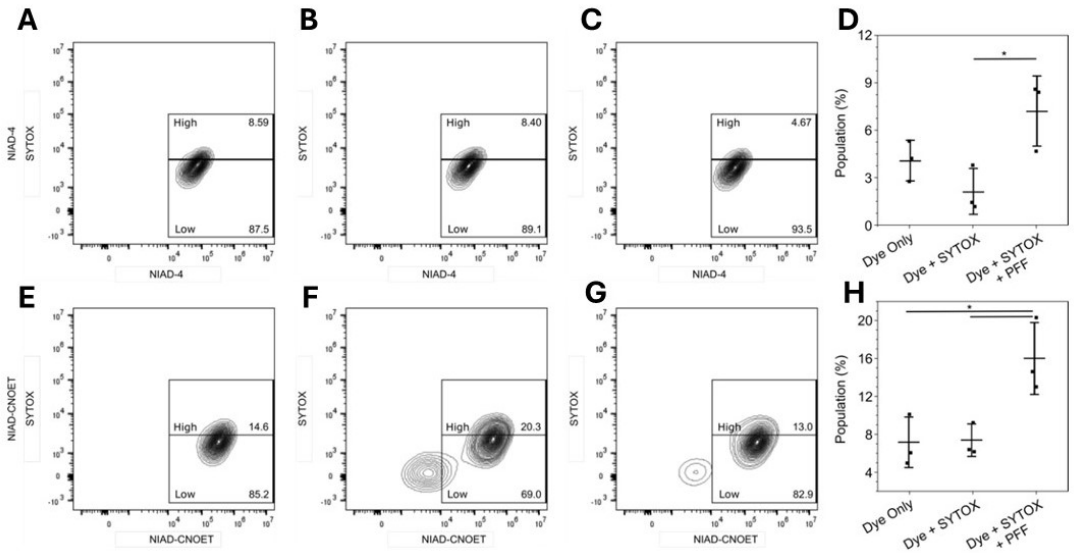

Figure 4.9 NIAD-4 and NIAD CNEOT detects intracellular aggregation in response to PFFs. Flow cytometry gating showing PFF treated cells stained by **(top)** NIAD-4 and **(bottom)** NIAD-CNOET with SYTOX as the counter dead-stain. **(A, E)** Dye only conditions in response to NIAD-4 and NIAD CNEOT. **(B, F)** Dye + SYTOX staining conditions. **(C, G)** Dye + SYTOX staining subsequent to PFF treatment. **(D, H)** Quantification of populations of cells positive for NIAD-4/NIAD CNEOT. (Total events: 10,000) (*n=3*, technical replicates). (Taken from the supplementary evidence of the Owyong et al, 2024 – second author (Laura E. Shippey) of paper and preformed this experiment).

4.4 Discussion

The production of human WT α-synuclein from BL21 cells was confirmed by using diverse methods including SDS-PAGE with subsequent protein staining and immunoblotting (dot blot) experiments to detect α-synuclein (**Figure 4.1 A, B, C**). ESI was used to determine the MW of the sample, and it was confirmed that it was the expected MW of α-synuclein (**Figure 4.2**) (Abeliovich et al, 2000; Lashuel et al, 2013; Siddiqui et al, 2016).

The confirmation of synthesised α-synuclein allowed for production of oligomers, fibrils and PFFs. ThT, a commonly used dye in the detection of amyloid, was used differentiate between monomers, oligomers and fibrils, where fibrils were able to induce the highest amount of fluorescence suggesting a high composition of β-pleated sheets (**Figure 4.3**).

ThT fluorescence was also used to show changes in aggregation/ increased fibril formation overtime during the agitation of monomeric α-synuclein (**Figure 4.4**). When using the discontinuous method, NIAD-4 and NIAD CNEOT had a similar pattern to the ThT dye, where fluorescence intensity in response to sustained agitation of monomeric α-synuclein over a 4-day period (**Figure 4.5**).

When comparing PFFs to monomeric α-synuclein, NIAD-4 and NIAD CNEOT fluoresced more in response to PFFs compared to monomeric α-synuclein indicatory of PFFs being an amyloid structure (**Figure 4.6**). The data presented show that NIAD-4 and NIAD CNEOT could be a useful method in fibril detection and aggregate characterisation. This also demonstrates that PFFs will retain its amyloid structure after sonication.

Fluorescent dye data was confirmed by AFM imaging which visualised the morphology of day 4 fibrils (**Figure 4.7**); the day after which ThT and NIAD dyes fluorescence was highest. Day 4 fibrils also mirrored the branched structure seen in other literature (Bharathi et al, 2007; Smith et al, 2008).

To assess the ability of NIAD dyes to detect intracellular aggregation, flow cytometry analysis was used to measure fluorescence intensity. It was found that cells treated with PFFs had a higher level of fluorescence compared to

untreated cells (**Figure 4.8**) showing that NIAD dyes are a useful method in the detection of intracellular aggregation which is valuable in demonstrating the seeding nature of PFFs.

4.5 Summary

The aim of this chapter was to produce, prepare and characterise α-synuclein aggregates for the purpose of later use in the investigation of cellular stress and ISR activation. We demonstrated that ThT and the NIAD dyes (NIAD-4 and the newly synthesised NIAD CNEOT derivative) were able to differentiate between α-synuclein structures (monomers and PFFs) plus show changes in aggregation overtime. Here, it is shown that NIAD CNEOT is able to detect presence of aggregation in response to 24 hr cellular treatment with PFFs. It would be beneficial to improve robustness of this claim by co-staining NIAD CNEOT with thioflavin S for example, another dye used to detect intracellular amyloid formation (Flock et al, 2023). Future work on the characterisation of α-synuclein should involve exploring structural differences between oligomers and PFFs which can be done using techniques such as AFM and transmission electron microscopy (TEM).

5 Chapter Five: α-Synuclein oligomers and preformed fibrils activate the ISR

5.1 Introduction

Chapter three explored oxidative and ER stress-induced activation of the ISR using toxic compounds such as SA, Tg and MPP+. The data presented shows that there is expression of numerous ISR markers including eIF2α phosphorylation (**Figure 3.3-5**) and increased ATF4 expression (**Figure 3.7**) in response to chemically induced stress. In addition, validating ISR activation with well-known stress inducing compounds, MPP+ was used to connect the ISR to PD pathology. With the establishment that the ISR is activated in response to oxidative and ER stress (stresses implicated in PD) plus a PD neurotoxin (MPP+), it was of particular interest to explore if aggregated and pathological forms of α-synuclein could activate the ISR to elucidate whether the eIF2α/ATF4 pathway was associated with α-synuclein aggregation patho-mechanisms.

5.1.1 Oligomers and PFFs induce cellular stress

The failure of cellular systems to prevent aggregation of α-synuclein (Bayati et al, 2024; Kumar et al, 2018) contributes to cell stress and eventual death (Feng et al, 2022; Marques and Outeiro, 2012). Oligomers and PFFs have been observed to induce oxidative and ER stress (Domingues et al, 2022; Jiang et al, 2010). This has been demonstrated in a dose-response assay where treatment of iPSC-derived cortical neurons with α-synuclein oligomers induced an increase in ROS and lipid peroxidation (Deas et al, 2016). Moreover, when mice-derived primary hippocampal neurons were treated with PFFs for 14 days, increased phosphorylated α-synuclein (at Ser129) was observed along with higher MW α-synuclein species and mitochondrial dysfunction (Tapias et al, 2017). The UPR specifically the PERK pathway has been shown to be activated in PARK20 fibroblasts (a mutation that gives rise to a juvenile form of recessive PD) (Amodio et al, 2019). Overexpression of A53T α-synuclein in PC12 cells resulted in an increase in the expression of GRP78 and phosphorylated eIF2α, altogether indicatory of UPR activation (Jiang et al, 2010). α-Synuclein has been linked to nutrient deprivation related stress,

where α-synuclein is believed to mediate glucose deprivation activation of the UPR pathway in differentiated SH-SY5Y cells (Bellucci et al, 2011). Overall, literature indicates that α-synuclein aggregation triggers cellular stress responses. However, throughout literature different aggregate conformations have been used in cell treatments and there are no definitive studies comparing various α-synuclein aggregates and the manner in which they induce stress plus activate stress pathways.

5.1.2 Objectives

This chapter aims to understand how ISR activation occurs as a result of cellular exposure to oligomers and PFFs, with the additional purpose of providing a comparison to previously studied stresses explored in chapter three. To establish a link between α-synuclein aggregates and the eIF2α/ATF4 pathway (ISR), the following will be performed:

- confirm intracellular aggregation in response to oligomer and PFF treatment.
- assessment of oxidative stress and cytotoxicity upon exposure to oligomers and PFFs.
- investigate the activation of the ISR and SG formation in response to α-synuclein aggregates.

5.2 Results

5.2.1 Oligomers and PFFs induces intracellular aggregation

α-Synuclein aggregates have been well documented to have prion-like characteristics specifically exhibiting the ability to engage in cell-to-cell transmission activities (Choi et al, 2021; Lee et al, 2010; Neupane et al, 2023). Cells were treated with oligomers and PFFs to determine whether intracellular aggregation of α-synuclein would take place. Undifferentiated SH-SY5Y cells were treated with 0.1 mg/mL oligomers and PFFs (monomeric equivalent) for 1, 6, 24 and 48 hr. Immunocytochemistry was used to detect α-synuclein positive puncta in response to oligomer and PFF treatment (**Figure 5.1**). Percentage of cells with intracellular aggregates, total number of α-synuclein and area of aggregates were subsequently quantified (**Figure 5.2 A, B, C**). It was found that 24 hr treatment with oligomers resulted in the largest percentage of cells positive for α-synuclein intracellular aggregates – 95.22 ± 3.43 %. Within the PFF conditions, it was observed that PFF treatment for 24 and 48 hr resulted in the highest amount of aggregation –72.37 ± 14.02 % and 76.20 ± 6.26 % respectively (**Figure 5.2 A**). Overall, oligomers and PFF treatment of SH-SY5Y cells are able to induce intracellular aggregation indicating that the synthesised α-synuclein aggregates (oligomers and PFFs) are able to exhibit seeding/prion-like characteristics.

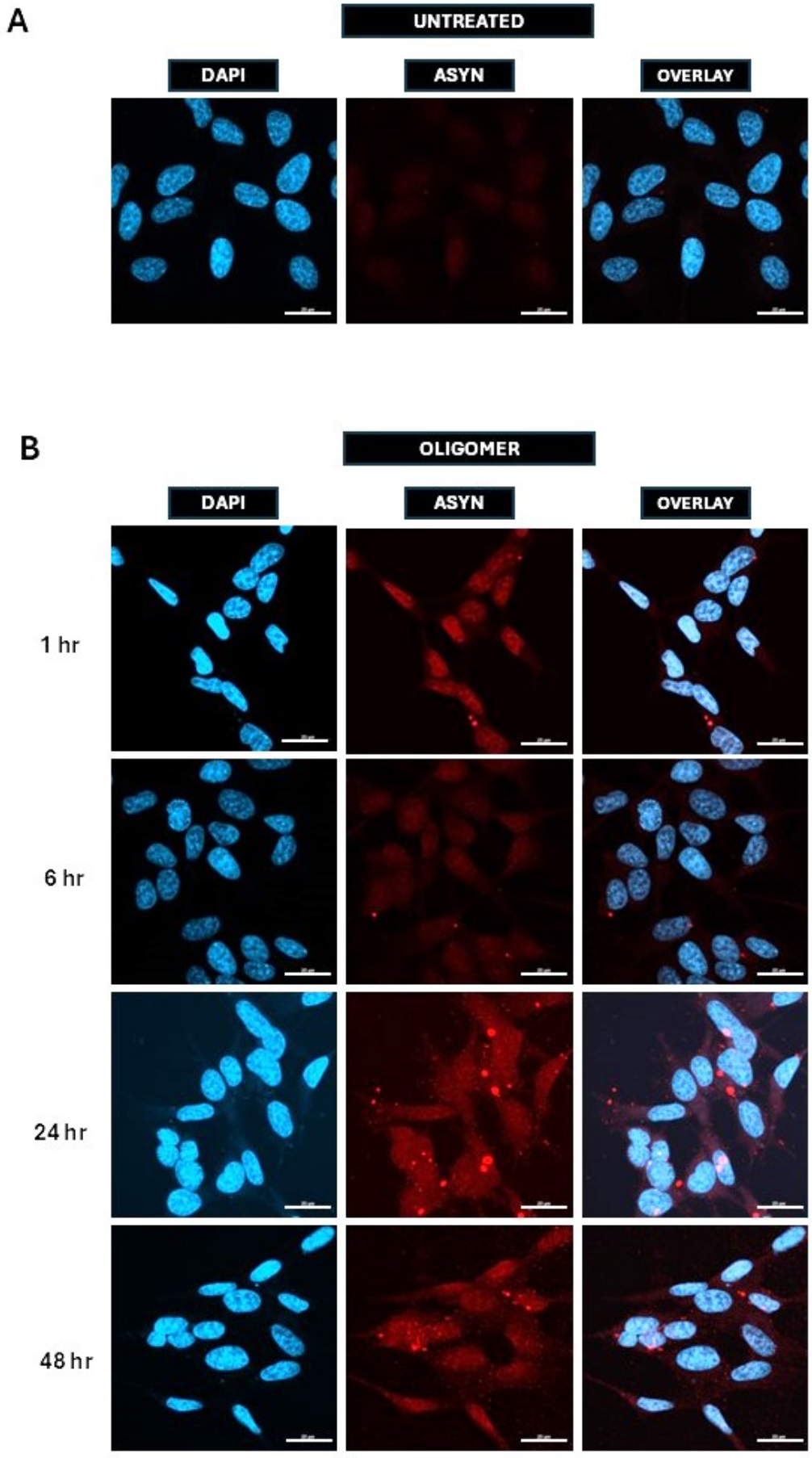
A
UNTREATED
DAPI
ASYN
OVERLAY
B
OLIGOMER
DAPI
ASYN
OVERLAY
1 hr
6 hr
24 hr
48 hr

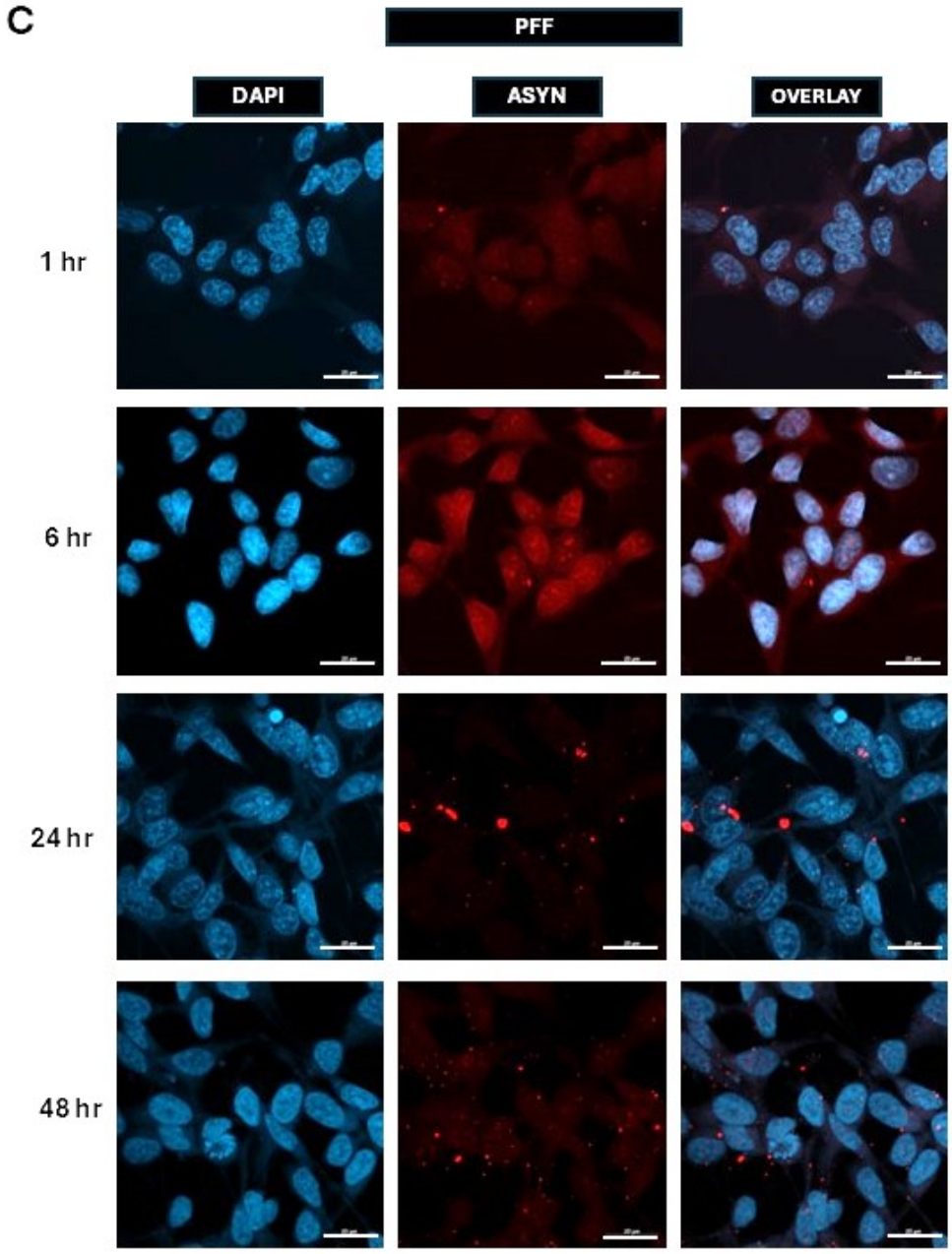

Figure 5.1 Intracellular α-synuclein aggregation takes place in response to cellular exposure to oligomers and PFFs. Cells were treated with **(B)** oligomers and **(C)** PFFs at concentration of 0.1 mg/mL for 1, 6, 24, 48 hr. Cell nuclei were stained using DAPI and TexRed was used as an indicator of intracellular α-synuclein aggregates. Magnification: 63x. Scale bar: 20 μm.

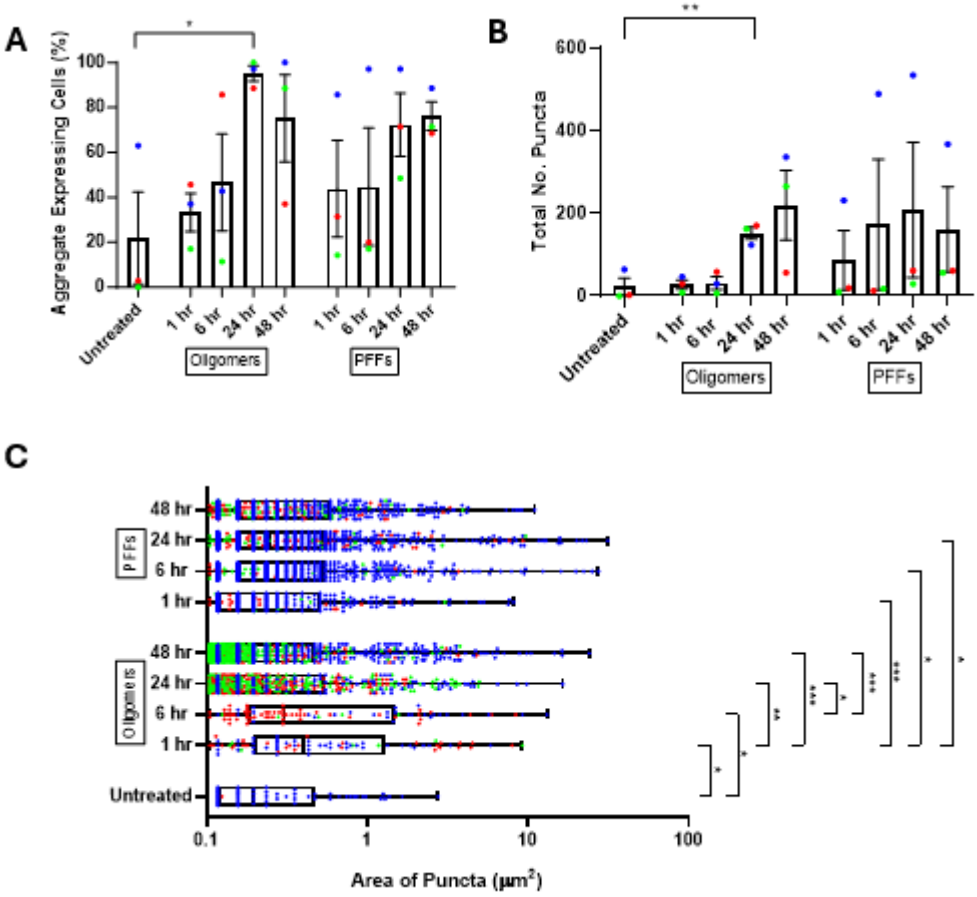

Figure 5.2 Quantification of intracellular α-synuclein aggregation in response to cellular exposure to oligomers and PFFs. α-Synuclein-positive puncta (as shown in **Figure 5.1**) were analysed by quantifying various parameters including: **(A)** percentage of cells positive for α-synuclein aggregates**, (B)** total number of α-synuclein across the total number of cells **(C)** the area of α-synuclein intracellular aggregates (µm^2). **(A)** Data was analysed by one-way ANOVA followed by Tukey's post-hoc test for multiple comparisons. **(B, C)** Data was analysed by Kruskal-Wallis' test followed by Dunn's post-hoc test for multiple comparisons (across all oligomers and PFF conditions). Significance is indicated by asterisk, P ≤0.05 (*), P≤0.01 (**) and P≤0.001 (***). Data without stars have been deemed as not significant. Colours indicate individual biological replicates: **(1)** red **(2)** green **(3)** blue. Error bars: ± SEM (*n=3*). (Total number of cells: 105/35 per repeat).

5.2.2 α-Synuclein aggregates increase oxidative stress

The most intracellular α-synuclein aggregation takes place at 24 and 48 hr when treated with 0.1 mg/mL oligomers and PFFs (**Figure 5.1, 5.2**). To establish whether intracellular aggregation coincided with oxidative stress, flow cytometry was performed using the CellROX Green assay subsequent to cell treatment with 0.1 mg/mL oligomers and PFFs for 24 and 48 hr. TBHP treatment for 30 min was used as a positive control and it was found that nearly 100% of cells were ROS-positive and the unstained condition (where no dye was used) had 0% of cells that were ROS-positive. It was found compared to the untreated (no treatment, but stained with dye) conditions, that all oligomer and PFF treatments were able to induce an increase in ROS-positive cells compared to the untreated condition (**Figure 5.3**). It was observed that the oligomer 48 hr treatment had the most ROS-positive cells (19.55 ± 8.05 %) compared to oligomer 24 hr treatment. PFF 24 hr treatment resulted in 27.81 ± 11.42 % ROS-positive cells, which was higher than the PFF 48 hr treatment. However, the untreated condition had 6.45 ± 4.35 % ROS-positive cells (**Figure 5.3 B**). The data indicates both oligomers and PFFs are able to induce an increase ROS-positive cells indicating oxidative stress induction. It was found ROS-positive cells increased from 24 to 48 hr in response to oligomer treatment. PFFs were able to induce more ROS-positive cells at 24 hr compared to the PFF 48 hr timepoint. Overall, PFFs induced more ROS-positive cells compared to oligomer treated cells at both timepoints. This suggests that oxidative stress induction differs in response to oligomers and PFFs and PFFs are able to trigger more oxidative stress compared to oligomer treatment.

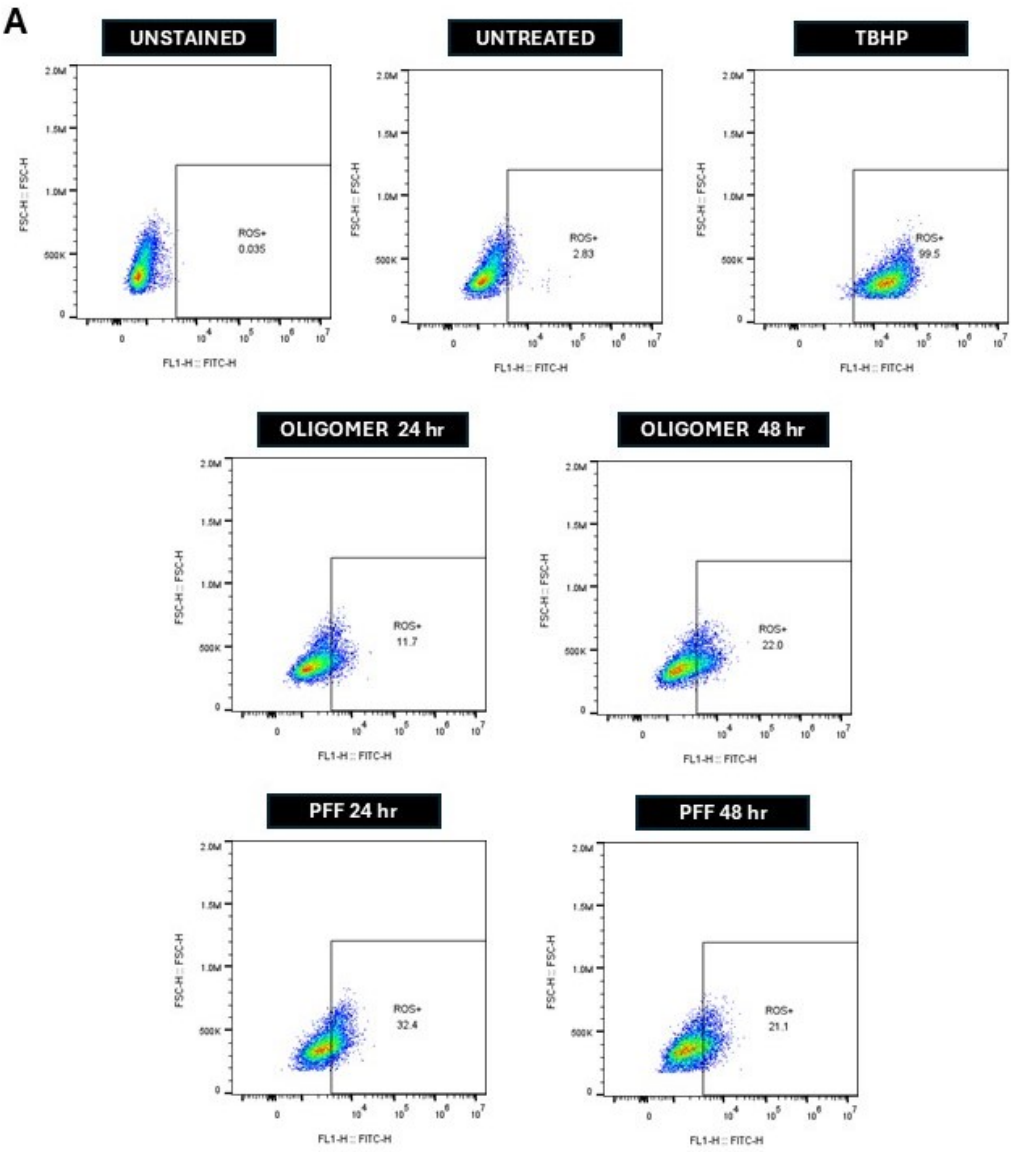
A
UNSTAINED
UNTREATED
TBHP
OLIGOMER 24 hr
OLIGOMER 48 hr
PFF 24 hr
PFF 48 hr
ROS+
0.035
2.83
99.5
11.7
22.0
32.4
21.1
FSC-H :: FSC-H
FL1-H :: FITC-H

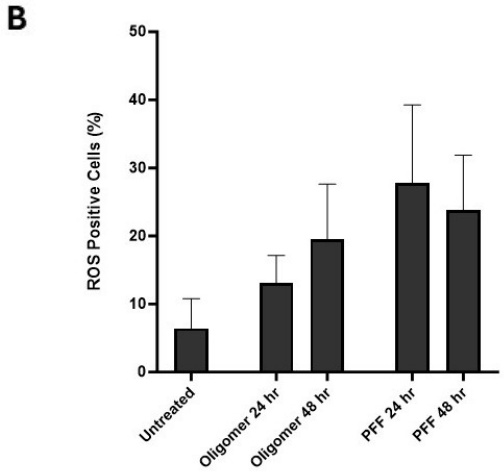
B
ROS Positive Cells (%)
50
40
30
20
10
0
Untreated
Oligomer 24 hr
Oligomer 48 hr
PFF 24 hr
PFF 48 hr

Figure 5.3 Oligomers and PFFs induces ROS formation. Cells treated with oligomer and PFFs was subjected to flow cytometry to assess presence of ROS using the CellROX Green assay. Oligomers and PFFs at 24 and 48 hr resulted in an increase in ROS-positive cells. **(A)** Flow cytometry analysis software, FlowJo, generated representative graphical diagrams showing populations positive for ROS. **(B)** Quantification of ROS-positive cells in response to oligomer and PFF treatment. Total events: 10,000 per repeat. ANOVA followed by Tukey's post-hoc test for multiple comparisons. Data without asterisks have been deemed as not significant. Error bars: ± SEM (*n=3*).

5.2.3 α-Synuclein oligomers and PFFs aggregates are cytotoxic

Oligomers and PFFs are known to cause a wide range of stresses (Du et al, 2020; Niskanen et al, 2025; Zeng et al, 2024). With the consideration that cellular exposure to oligomers and PFFs induces an increase in ROS (**Figure 5.3**), which coincides with increased intracellular α-synuclein aggregation (**Figure 5.1, 5.2**), the assessment of cytotoxicity in response these treatments were of interest. The LDH assay was performed as described in **Section 2.8** to assess cytotoxicity in response to 0.1 mg/mL oligomers and PFFs 1, 6, 24 and 48 hr treatment. All conditions were found to result in an increase in LDH levels compared to the spontaneous (control) condition with the highest LDH activity seen with oligomer and PFF treatment for 48 hr (**Figure 5.4**). As such both oligomers and PFFs were demonstrated to cause cell toxicity at all timepoints which corresponds with the observation that oligomers and PFFs induce oxidative stress (**Figure 5.3**).

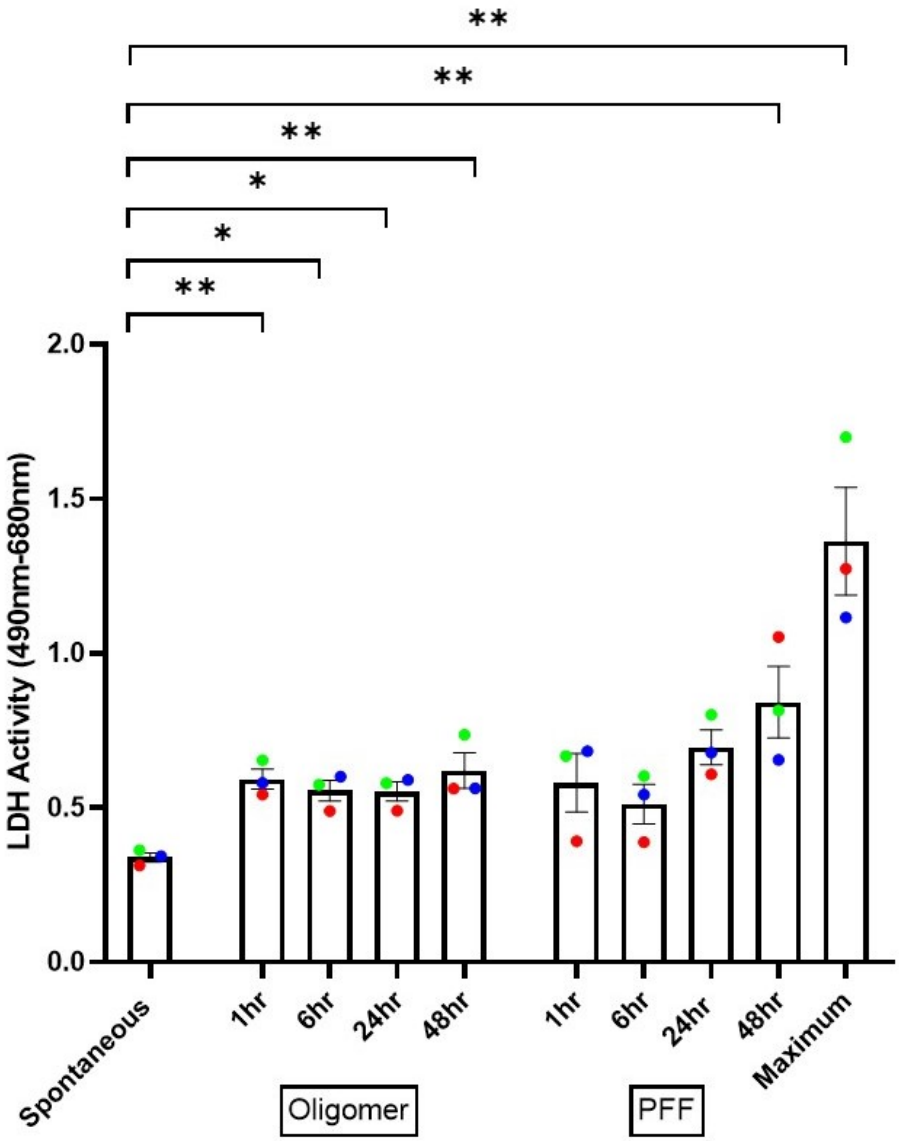

Figure 5.4 Oligomers and PFFs are cytotoxic. Cell culture medium was collected subsequent to oligomer and PFF (0.1 mg/mL) treatment and subjected to the LDH cytotoxicity kit where LDH activity was quantified. The spontaneous functions as control condition (ultrapure water added to culture medium overnight) and the maximum condition are produced as result of lysis buffer treatment for 15 mins. Data was analysed using one-way ANOVA followed by Dunnett's post-hoc test for multiple comparisons (untreated vs treatment conditions). Significance is indicated by asterisk, P ≤0.05 (*), P≤0.01 (**). Data without asterisks have been deemed as not significant. Colours indicate individual biological replicates: **(1)** red, **(2)** green, **(3)** blue. Error bars: ± SEM (biological replicates, *n=3*).

5.2.4 EIF2α phosphorylation upon exposure to oligomers and PFFs

SA, Tg and MPP+ were found to induce the phosphorylation of eIF2α (**Figure 3.4-6**) and in conjunction with increased oxidative stress in response to oligomers and PFFs (**Figure 5.3**), western blotting analysis was carried out to establish if eIF2α phosphorylation occurs in response to oligomer or PFF treatment. Cells were treated with oligomers and PFFs for 6 and 24 hr. EIF2α phosphorylation was quantified in comparison to total eIF2α. A moderate 1.6-fold increase in eIF2α phosphorylation was observed in response to oligomer treatment for 24 hr. Whereas PFF 6 and 24 hr treatment induced a 1.3-fold change on average compared to the untreated cells, however data was not deemed to be significant (**Figure 5.5**). Although the data is variable oligomers at 24 hr and PFFs at 6 and 24 hr were able to moderately increase phosphorylation of eIF2α.

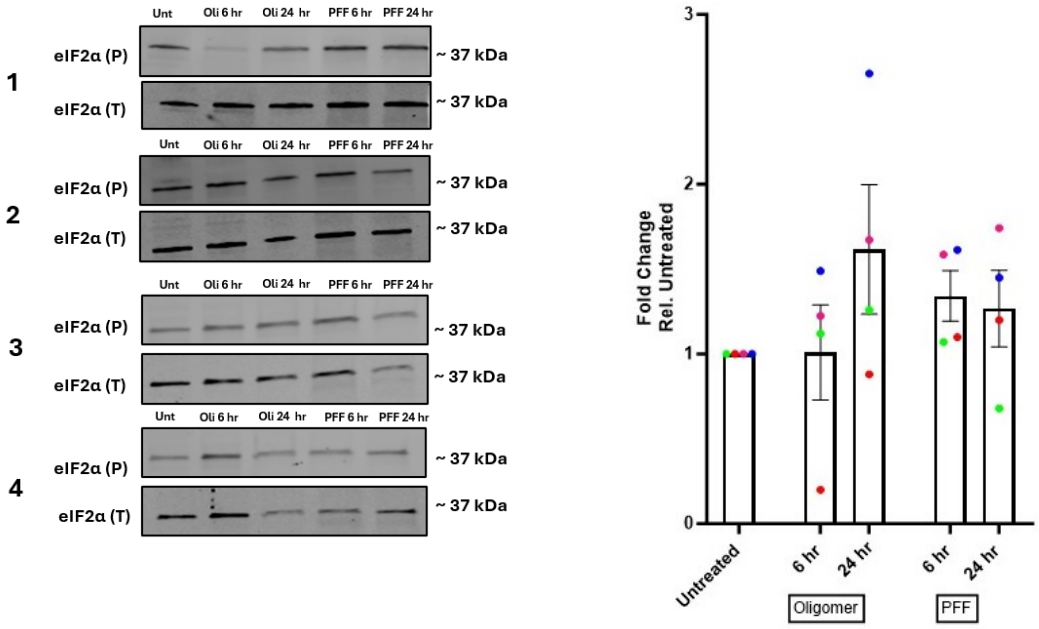

Figure 5.5 EIF2α phosphorylation in response to oligomers and PFFs. Cells were treated with oligomers and PFFs for 6 and 24 hr. ImageJ densitometry analysis was used to process immuno-stained blots. Data was analysed by one-way ANOVA followed by Tukey's post-hoc test for multiple comparisons. Data without asterisk have been deemed as not significant. Error bars: ± SEM (biological replicates, *n=4*). Colours indicate individual biological replicates: **(1)** red, **(2)** green, **(3)** blue **(4)** orange.

5.2.5 Oligomers and PFFs moderately increases ATF4 gene expression

Moderate eIF2α phosphorylation occurred in response to oligomers and PFFs. To determine if there are downstream effects indicatory of eIF2α phosphorylation, ATF4 expression was also assessed in the same oligomer and PFF treatment conditions at 6 and 24 hr. 0.15 μM Tg was used as a comparative stress-inducing treatment in the assessment of oligomer and PFFs induction of ATF4 expression. qRT-PCR was carried out to establish changes in gene expression of ATF4 (**Figure 5.6 A**). Tg resulted in the largest change in ATF4 expression compared to the untreated control with a 4.6 and 3.11-fold increase seen in response to 6 and 24 hr treatment respectively. Increases in ATF4 gene expression was also seen in response to oligomers and PFFs for 6 and 24 hr. Oligomers resulted in a 2.83 and 1.74-fold increase compared to the untreated condition. PFFs induced a 2.67 and 1.51-fold increase (**Figure 5.6 A**). Though oligomer and PFF datapoints were deemed to not be significant. Altogether suggesting that α-synuclein oligomers and PFFs are able to increase ATF4 mRNA levels suggestive of ISR activation.

To assess whether increases in gene expression would coincide with an increase ATF4 protein expression, an ELISA was also performed after cell treatment with oligomers and PFFs for 6 and 24 hr as done previously with SA, Tg (**Figure 3.7**) and MPP+ (**Figure 3.8**). It was found that oligomer and PFFs particularly at 24 hr yielded the largest increases in ATF4 expression where 1.31-fold and 1.44-fold increase, but data was not deemed to be significant at any timepoint explored (**Figure 5.6 B**). The data presented was variable but shows that oligomers and PFFs are able to induce moderate increases in ATF4 expression.

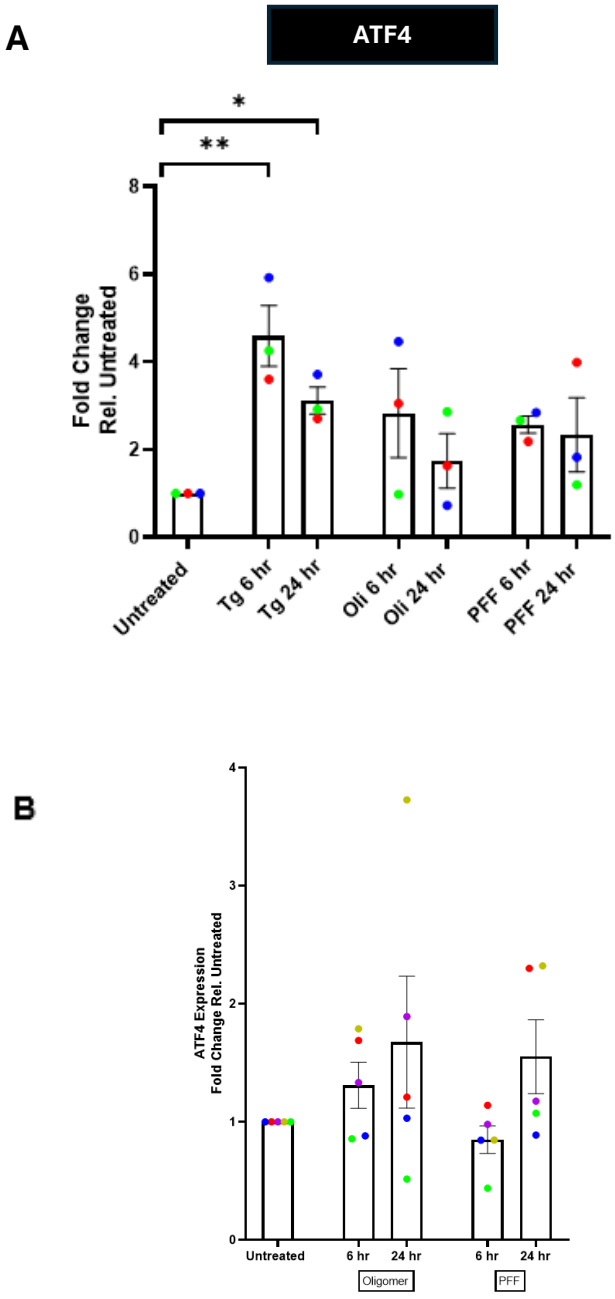

Figure 5.6 ATF4 RNA expression is enhanced in response to oligomers and PFFs. **(A)** qRT-PCR was used assess changes in ATF4 gene expression change in response to 6 and 24 hr treatment with 0.15 µM Tg, oligomers (0.1 mg/mL) and PFFs (0.1 mg/mL). **(B)** Oligomers and PFFs was used to treat undifferentiated SH-SY5Y cells for 6 and 24 hr. The ATF4 ELISA assay kit was used to establish pg/mL concentrations of ATF4 from cell lysates. Data was analysed by one-way ANOVA followed by Tukey's post-hoc test for multiple comparisons. Levels of significance was indicated by the following: P ≤0.05 (*) and P ≤0.01 (**). Data without asterisk have been deemed as not significant. Error bars: ± SEM (biological replicates, **(A)** *n=3,* ***(B)*** *n=5*). Colours indicate individual biological replicates: **(1)** red, **(2)** green, **(3)** blue **(4)** purple **(5)** dark yellow.

5.2.6 ATF5 is not expressed in response to ER stress and moderately expressed upon treatment with PFFs

CellROX Green data indicated an increase in ROS in response to oligomer and PFF treatment (**Figure 5.3**) paired with observations of increased eIF2α phosphorylation (**Figure 5.5**) plus enhanced ATF4 gene and protein expression (**Figure 5.6**). ATF5 is associated with the mitochondrial UPR pathway, specific to the mitochondria (Fiorese et al, 2016) and is known to be expressed as a result of ATF4 expression (Teske et al, 2013). Mitochondrial dysfunction and genetic mutations in *PINK1* and *PARK2* have been associated with dysregulation of mitochondria proteins and has been implicated in early-onset, autosomal PD (Ashraf et al, 2024). Further PINK1 has been found to regulate the mitochondrial UPR in cells (da Costa et al, 2020) which suggests that the mitochondrial UPR may be linked to PD pathology in some manner.

qRT-PCR was used to assess gene (mRNA) expression of ATF5 in response to Tg, oligomer and PFF treatment. It was found that 0.15 μM Tg treatment for 6 and 24 hr was able to induce an increase in ATF5 expression – 2.00-fold and 3.46-fold increase respectively. Whereas oligomers and PFFs (0.1 mg/mL) did not induce noticeable increases in ATF5 expression except PFF treatment for 6 hr that resulted in a moderate fold change (1.50 ± 0.51) but not deemed to be significant (**Figure 5.7**). Altogether showing that Tg treatment can induce the expression of ATF5. However, there were only minor increases in ATF5 gene expression in response to PFF 6 hr treatment but not enough to confidently conclude ATF5 expression in response to PFFs at the timepoints explored.

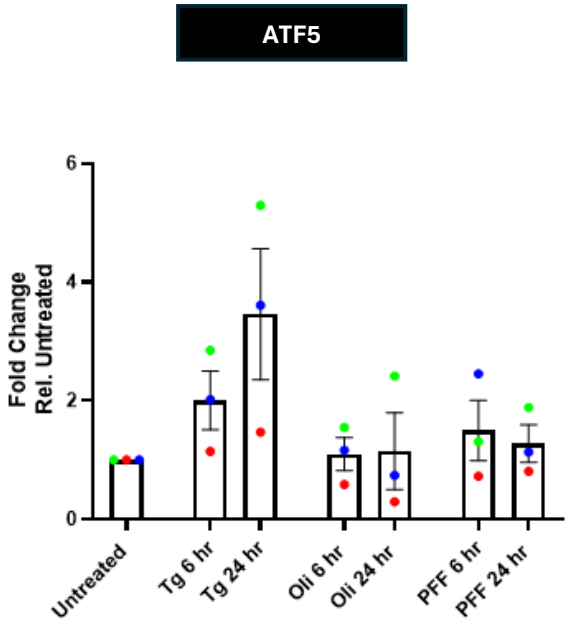

Figure 5.7 ATF5 expression is not enhanced in response to PFFs. qRT-PCR was used assess changes in gene expression changes in ATF5 in response to 6 and 24 hr treatment with 0.15 μM Tg, oligomers (0.1 mg/mL) and PFFs (0.1 mg/mL). Data was analysed by one-way ANOVA followed by Tukey's post-hoc test for multiple comparisons. Data without asterisk have been deemed as not significant. Error bars: ± SEM (biological replicates, *n*=3). Colours indicate individual biological replicates: **(1)** red, **(2)** green, **(3)** blue.

5.2.7 CHOP expression was not induced by oligomers and PFFs

Oligomers and PFFs-associated stress have been found to enhance ATF4 gene expression (**Figure 5.6 A**). As CHOP is a target of ATF4 (Hu et al, 2019), CHOP gene expression was assessed in response to oligomers and PFFs. Cells were also treated with oligomers and PFFs for 6 and 24 hr and compared to 0.15 µM Tg treatment (6 and 24 hr). It was found that Tg treatment for 6 hr caused the highest fold change in CHOP gene expression (27.65-fold increase) but comparatively reduced at 24 hr (11.75-fold increase compared to the untreated condition). It was found that the treatment conditions involving both oligomers and PFFs did not result in an increase in CHOP gene expression compared to the untreated condition (**Figure 5.8 A**)

To confirm the gene expression data, where CHOP expression did not increase in response to oligomer and PFFs, western blot analysis of CHOP expression subsequent to oligomer and PFFs treatment (6 and 24 hr) was carried out. It was found that oligomers and PFFs cell treatment for 6 and 24 hr did not induce the expression of CHOP (**Figure 5.8 B**).

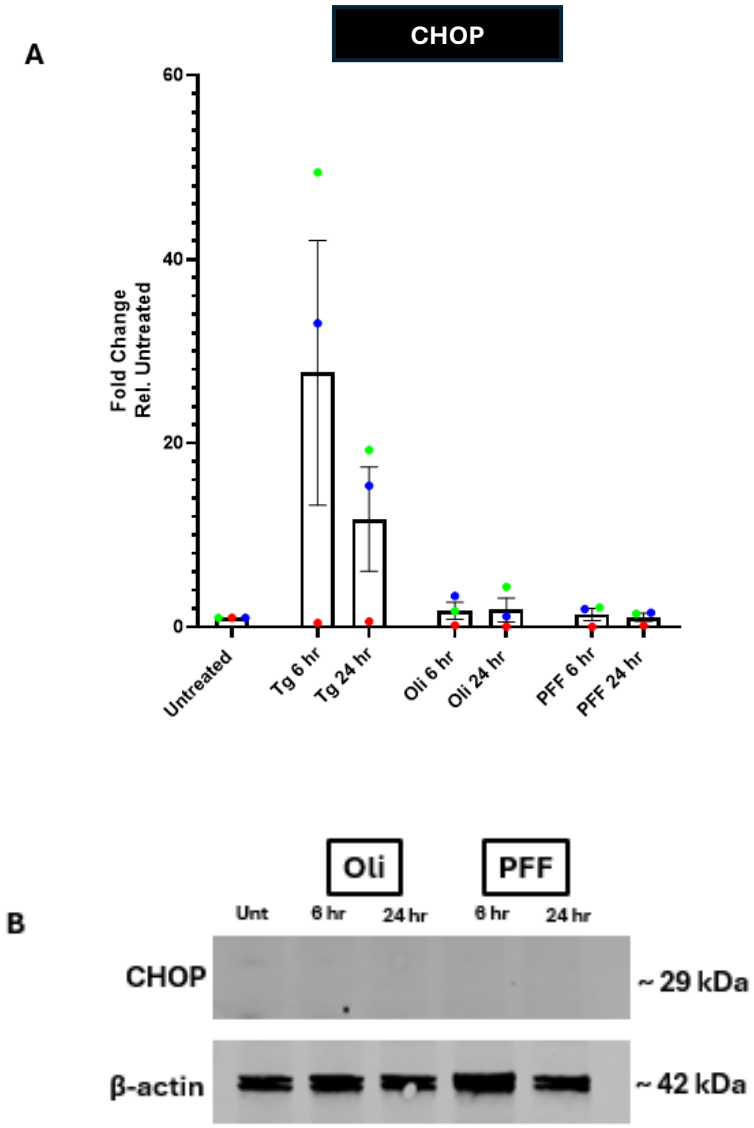

Figure 5.8 Enhancement of CHOP expression does not occur in response to oligomers and PFFs. (A) qRT-PCR was used assess changes in gene expression changes in CHOP in response to 6 and 24 hr treatment with 0.15 μM Tg, oligomers (0.1 mg/mL) and PFFs (0.1 mg/mL). Data was analysed by one-way ANOVA followed by Tukey's post-hoc test for multiple comparisons. Data without asterisk have been deemed as not significant. Error bars: ± SEM (biological replicates, *n=3*). Colours indicate individual biological replicates: **(1)** red, **(2)** green, **(3)** blue. **(B)** Oligomers and PFFs were used to treat cells for 1, 6, 24 hr. ImageJ densitometry analysis was used to process immuno-stained blots. (biological replicates, *n=3*).

5.2.8 GADD34 is expressed in response to ER stress and moderately in response to α-synuclein aggregates

GADD34 is intrinsic to the de-activation of the ISR and important in the regulation of cell stress (Oliveira et al, 2024) and was found to be expressed in response to SA and Tg induced stress (**Figure 3.11**). It has been reported that CHOP directly activates GADD34 during instances of ER stress for the purposes of cell recovery particularly to re-establish protein synthesis (Marciniak et al, 2004). GADD34 is a target of ATF4 (Márton et al, 2022) and with the consideration that oligomers and PFFs can enhance ATF4 expression (**Figure 5.6**).

qRT-PCR was used to quantify GADD34 gene expression in response to Tg, oligomer and PFF (6 and 24 hr) treatment. It has been previously demonstrated that 0.15 μM Tg induces GADD34 expression according to western blot analysis (**Figure 3.11**). It was found that 0.15 μM Tg treatment resulted in an increase in the expression of GADD34 at both 6 and 24 hr (8.53-fold and 4.63-fold increase). Oligomers and PFFs were also able to induce expression of GADD34. GADD34 expression was found to increase in response to 6 hr treatment with oligomers (2.55-fold increase) and PFFs (3.68-fold increase). Additionally, it was observed there was a decrease in GADD34 gene expression at 24 hr when compared 6 hr in all treatment conditions, though no oligomer and PFF datapoints were not deemed to be significant. The data presented shows that oligomers and PFFs can induce GADD34 expression but more so with PFF treatment (**Figure 5.9**). However, as treatment/stress is sustained, GADD34 expression will decrease.

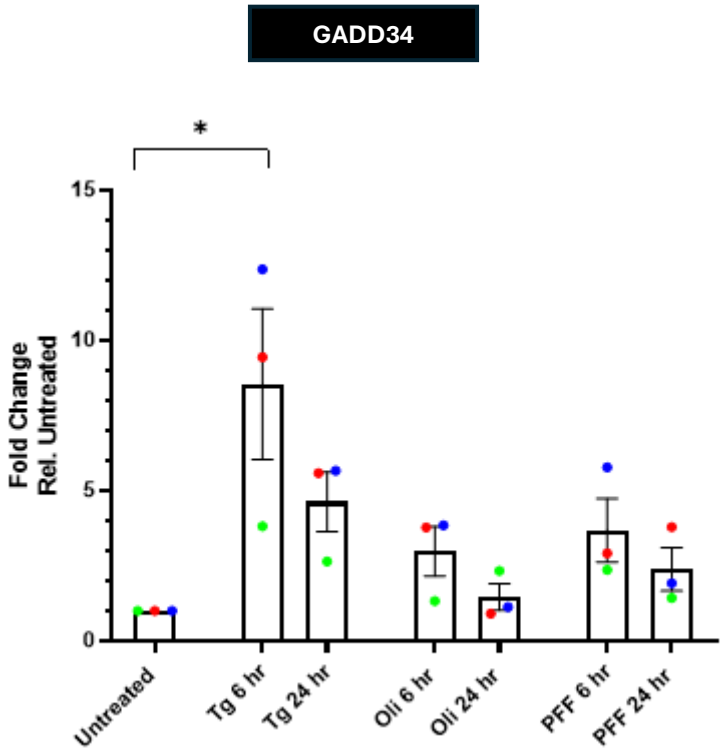

Figure 5.9 GADD34 expression increased in response to oligomers and PFFs. qRT-PCR was used assess changes in gene expression changes in CHOP in response to 6 and 24 hr treatment with 0.15 μM Tg, oligomers (0.1 mg/mL) and PFFs (0.1 mg/mL). Data was analysed by one-way ANOVA followed by Tukey's post-hoc test for multiple comparisons. Levels of significance was indicated by the following: P ≤0.05 (*). Data without asterisk have been deemed as not significant. Error bars: ± SEM (biological replicates, *n=3*). Colours indicate individual biological replicates: **(1)** red, **(2)** green, **(3)** blue.

5.2.9 PFFs inhibit cellular translation

Oligomers and PFFs activates the ISR as shown with increases in eIF2α phosphorylation (**Figure 5.5**) and enhanced ATF4 expression (**Figure 5.6**). The puromycin incorporation assay was performed subsequent to cell treatment (as described in **Section 2.10**). It was found that oligomers and PFF treatment conditions (at both 6 and 24 hr) were able to result in a reduction in puromycin incorporation when compared to the untreated condition. Specifically, PFF treatment for 24 hr caused a significant reduction in puromycin incorporation compared to the untreated condition (**Figure 5.10**). Data presented shows protein synthesis is inhibited in response to oligomers and PFFs particularly when cells were treated with PFFs for 24 hr. This data can be explained by PFFs inducing more oxidative stress (**Figure 5.3**), triggering cytotoxicity (**Figure 5.4**) along with enhanced eIF2α phosphorylation (**Figure 5.6**) and ATF4 gene expression data (**Figure 5.7 A**) when compared to oligomers.

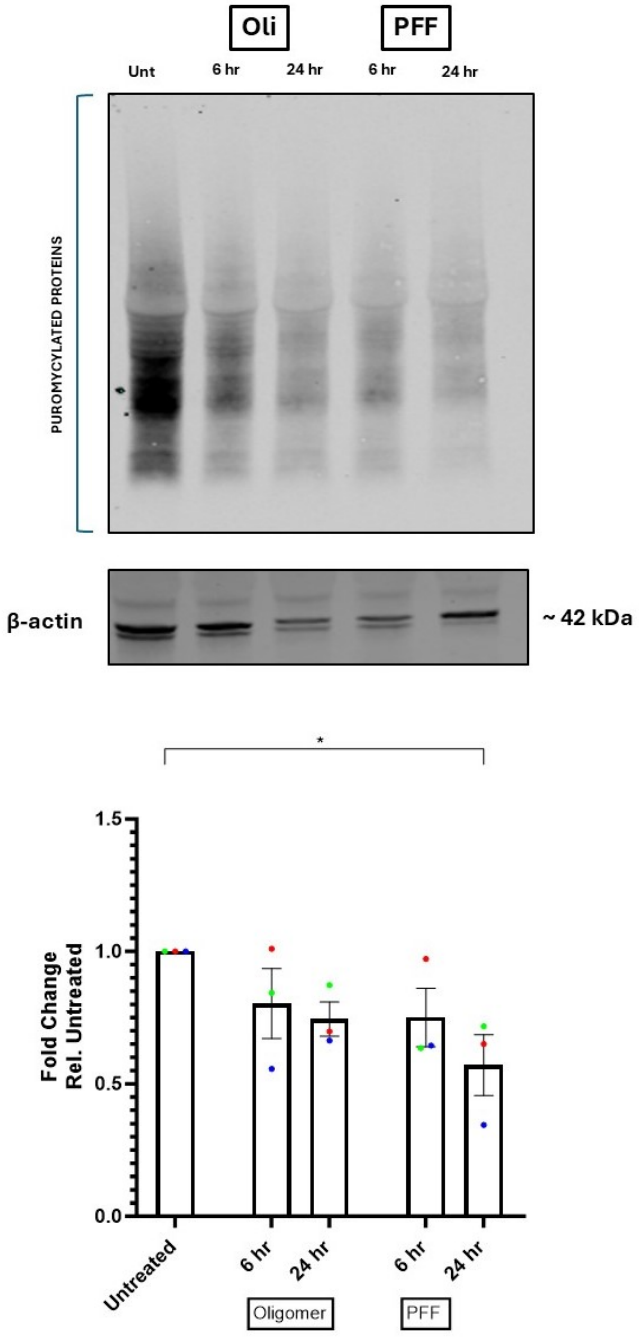

Figure 5.10 Oligomers and PFFs attenuate cellular translation. Oligomers and PFFs (0.1 mg/mL) were used to treat cells for 6 and 24 hr. The puromycin incorporation assay was performed and subsequent ImageJ densitometry analysis was used to process resulting immuno-stained blots. Data was analysed by one-way ANOVA followed by Tukey's post-hoc test for multiple comparisons. Levels of significance was indicated by the following: P ≤0.05 (*). Data without asterisk have been deemed as not significant. Error bars: ± SEM (*n=3*). Colours indicate individual biological replicates: **(1)** red, **(2)** green, **(3)** blue.

5.2.10 Stress granules form in response to oligomers and PFF treatment

α-Synuclein aggregates activate the ISR (**Figure 5.5, 5.6, 5.10**). The formation of SGs can be dependent on eIF2α phosphorylation (McInerney et al, 2005). With this in consideration, the presence of SGs was investigated in response to oligomer and PFF treatment. The same treatment conditions used in the assessment of SG formation was used previously to observe α-synuclein aggregation (**Figure 5.1, 5.2**). Immunocytochemistry was preformed to detect G3BP-positive puncta. Data presented shows that oligomers (**Figure 5.11 A**) and PFFs (**Figure 5.11 B**) induce the formation of SGs. Parameters pertaining to SGs were quantified such as percentage of SG positive cells, total number of G3BP-positive puncta, the number of SGs per cell and area of SGs (**Figure 5.12 A, B, C, D**). It was found that oligomer 24 hr treatment and PFF 6 hr triggered the largest percentage of cells positive for SGs - 53.34 ± 11.59 % and 58.10 ± 22.40 %, respectively. Oligomer and PFF treatment for 24 hr and 6 hr induced the highest total number of puncta and number of SGs per cells respectively when compared to the other investigated timepoints within their respective conditions (**Figure 5.12 A, B, C**). Additionally, SGs were largest in response to 24 and 48 hr treatment with oligomers and PFFs (**Figure 5.12 D**). But when comparing oligomers to PFF, PFFs were able to induce more SGs at 6 hr compared to all investigated conditions. This shows that despite oligomers and PFFs being aggregates of α-synuclein, the manner in which they induce stress/impact SG dynamics varies which is also supported by oxidative stress, eIF2α, ATF4 and protein synthesis data previously shown.

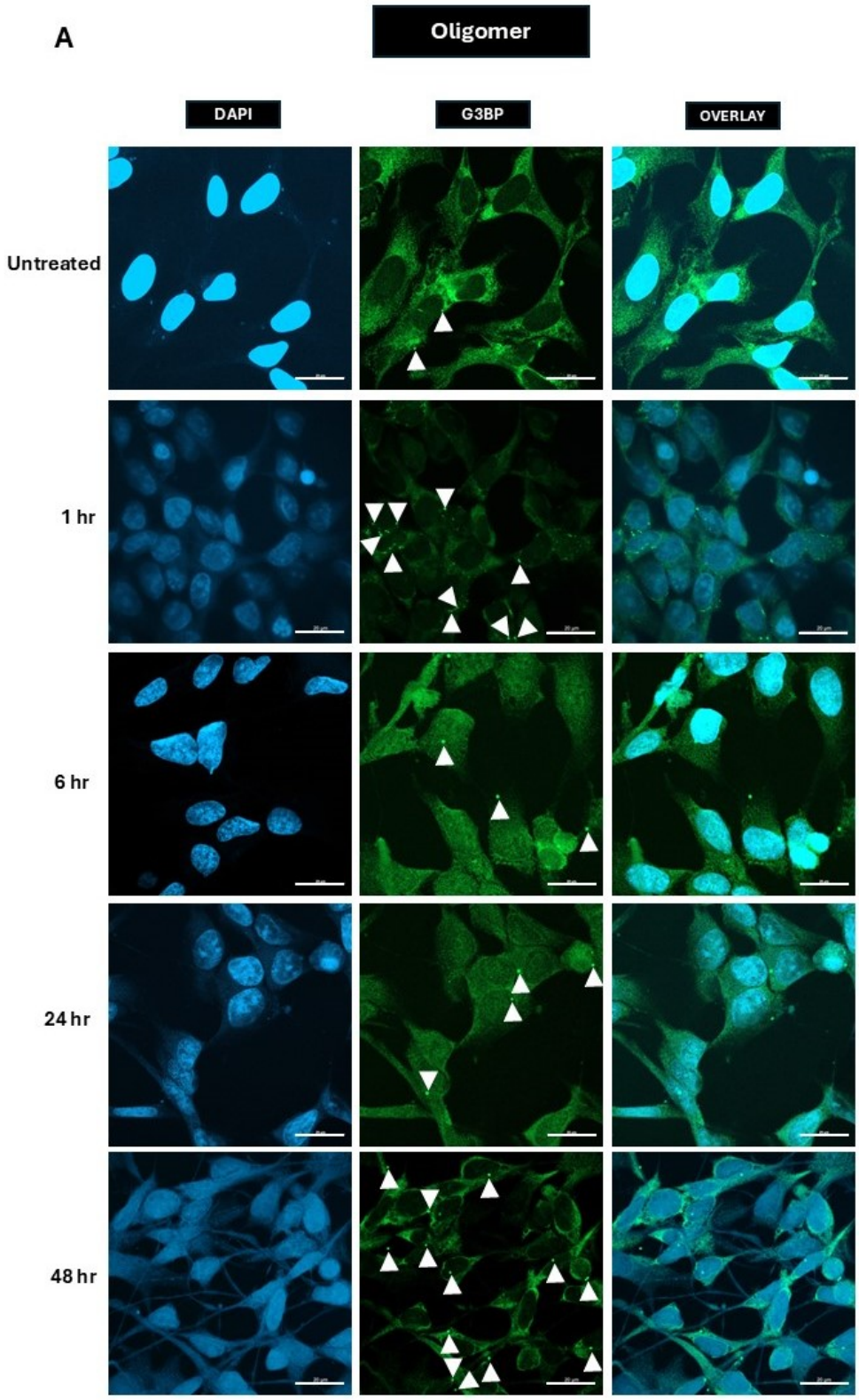
A
Oligomer
DAPI
G3BP
OVERLAY
Untreated
1 hr
6 hr
24 hr
48 hr

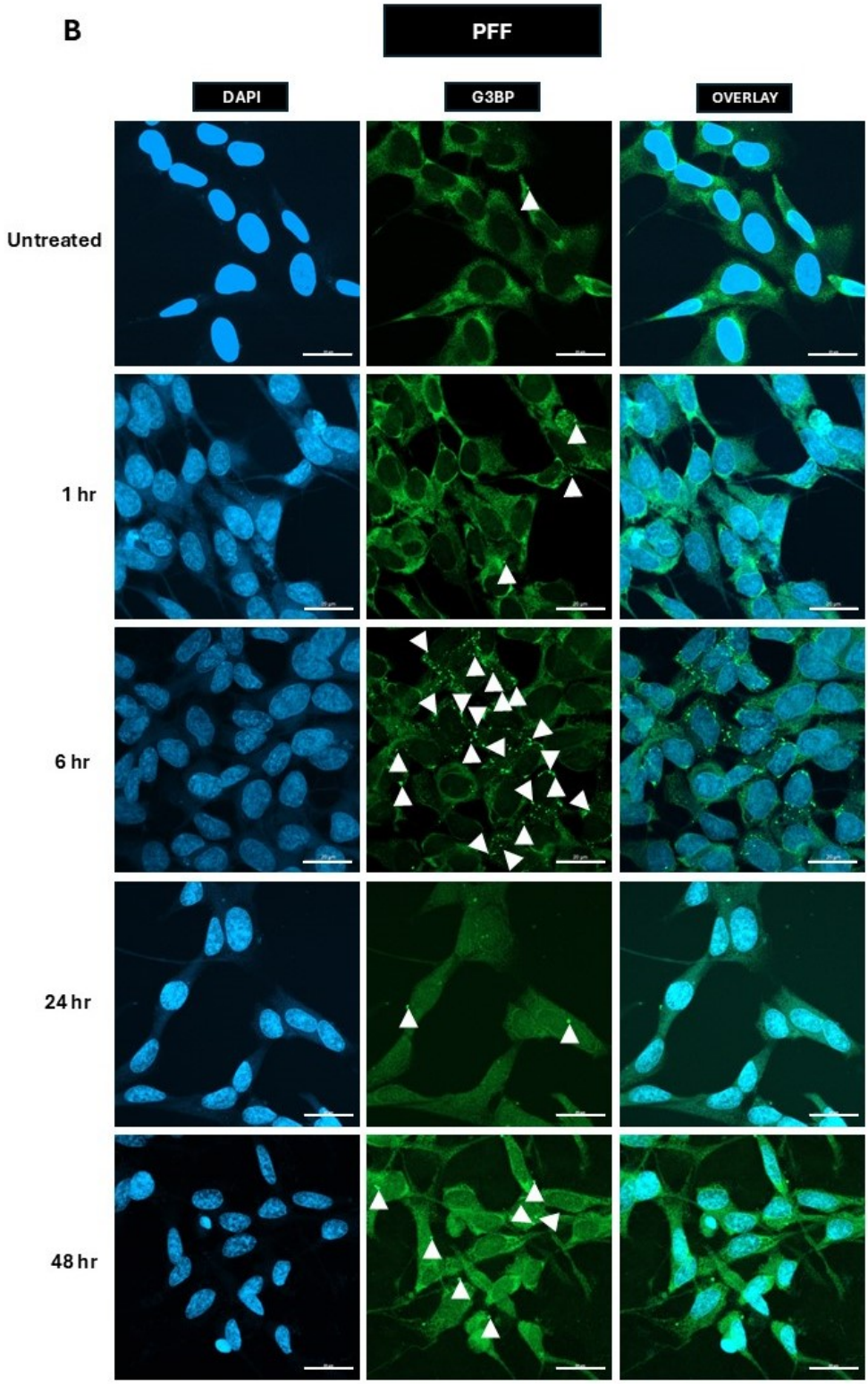

Figure 5.11 Oligomers and PFFs trigger SG formation. Cells were treated with 0.1 mg/mL **(A)** oligomers and **(B)** PFFs for 1, 6, 24 and 48 hr. Cell nuclei were stained using DAPI and G3BP conjugated to AF488 was used as an indicator of SG puncta. Magnification: 63x. Scale bar: 20 µm.

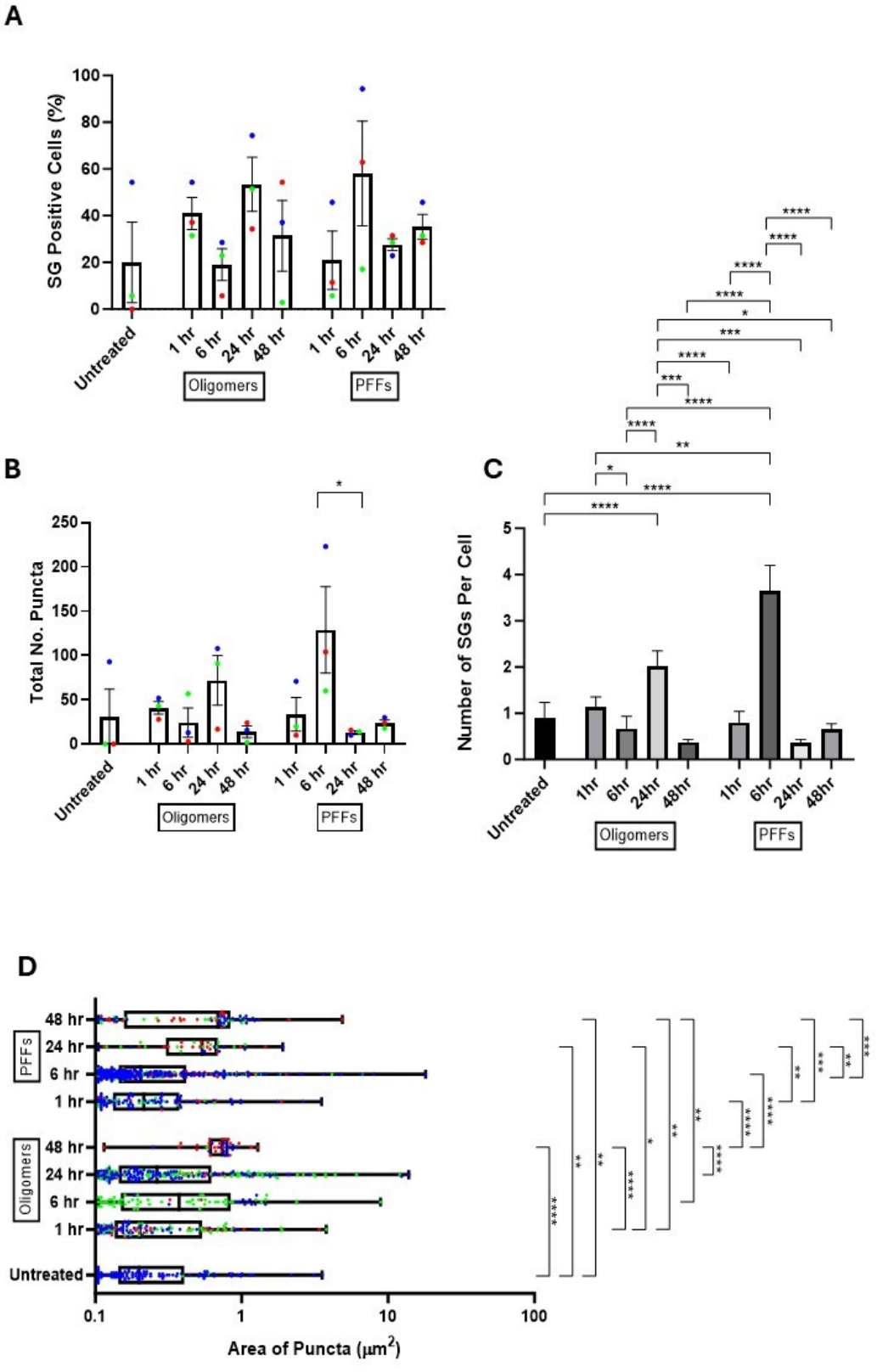
A
SG Positive Cells (%)
Untreated
1 hr
6 hr
24 hr
48 hr
Oligomers
PFFs
B
Total No. Puncta
C
Number of SGs Per Cell
1hr
6hr
24hr
48hr
D
Area of Puncta (μm²)

Figure 5.12 Oligomers and PFFs trigger SG formation. G3BP-positive puncta were analysed by quantifying various parameters including: **(A)** percentage of cells positive for SGs**, (B)** total number of SGs across the total number of cells **(C)** the number of SGs/G3BP positive puncta per cell and **(D)** the area of SGs (μm^2). **(A, C, D)** Data was analysed by Kruskal-Wallis' test followed by Dunn's post-hoc test for multiple comparisons (across all oligomers and PFF conditions). **(B)** Data was analysed by one-way ANOVA followed by Tukey's post-hoc test for multiple comparisons (across all oligomers and PFF conditions). Significance is indicated by asterisk, P ≤0.05 (*), P≤0.01 (**), P≤0.001 (***) and P≤0.0001 (****). Data without stars have been deemed as not significant. Error bars: ± SEM (*n=3*). (Total number of cells: 105/35 per repeat). Colours indicate individual biological replicates: **(1)** red, **(2)** green, **(3)** blue.

5.2.11 SGs co-localisation with intracellular α-synuclein aggregates increases in response to oligomer and PFF treatment

It has been demonstrated that oligomer and PFF treatment is able to induce intracellular aggregation of α-synuclein (**Figure 5.1, 5.2**) and trigger SG formation (**Figure 5.11, 5.12**). Intracellular aggregation was highest at 24 hr and 48 hr treatment with oligomers and PFFs. Further SG formation was highest in response to oligomer treatment at 24 hr. Therefore, as it has been previously demonstrated that aggregates of TDP-43 and SGs co-localise and interact (Mori et al, 2023), it was of interest to investigate if α-synuclein aggregates and SGs interact. Cells were treated with oligomers and PFFs for 24 hr, where intracellular aggregation of α-synuclein and SG formation was previously observed (**Figure 5.1, 5.11**). To establish if SGs co-localised with intracellular α-synuclein aggregates, immunocytochemistry was performed subsequent to treatment to visualise α-synuclein and SG positive puncta as well as any co-localisation that may occur. α-Synuclein aggregates and SGs were present in all conditions but at different capacities (**Figure 5.13**). Co-localisation was determined by the use of the confocal analysis processing system overlaying images positive for α-synuclein (red, AF594) and SGs/G3BP (green, AF488). Foci found to have a yellow/orange colour indicated co-localisation in this experiment. Co-localisation was increased in oligomer and PFF 24 hr treatment conditions – 26.73 % and 22.22 % compared to the untreated condition - 10 % but the data was not deemed to be significant (**Figure 5.12 B**). The data suggests that oligomer and PFFs cell treatment exacerbates α-synuclein co-localisation with SGs.

A

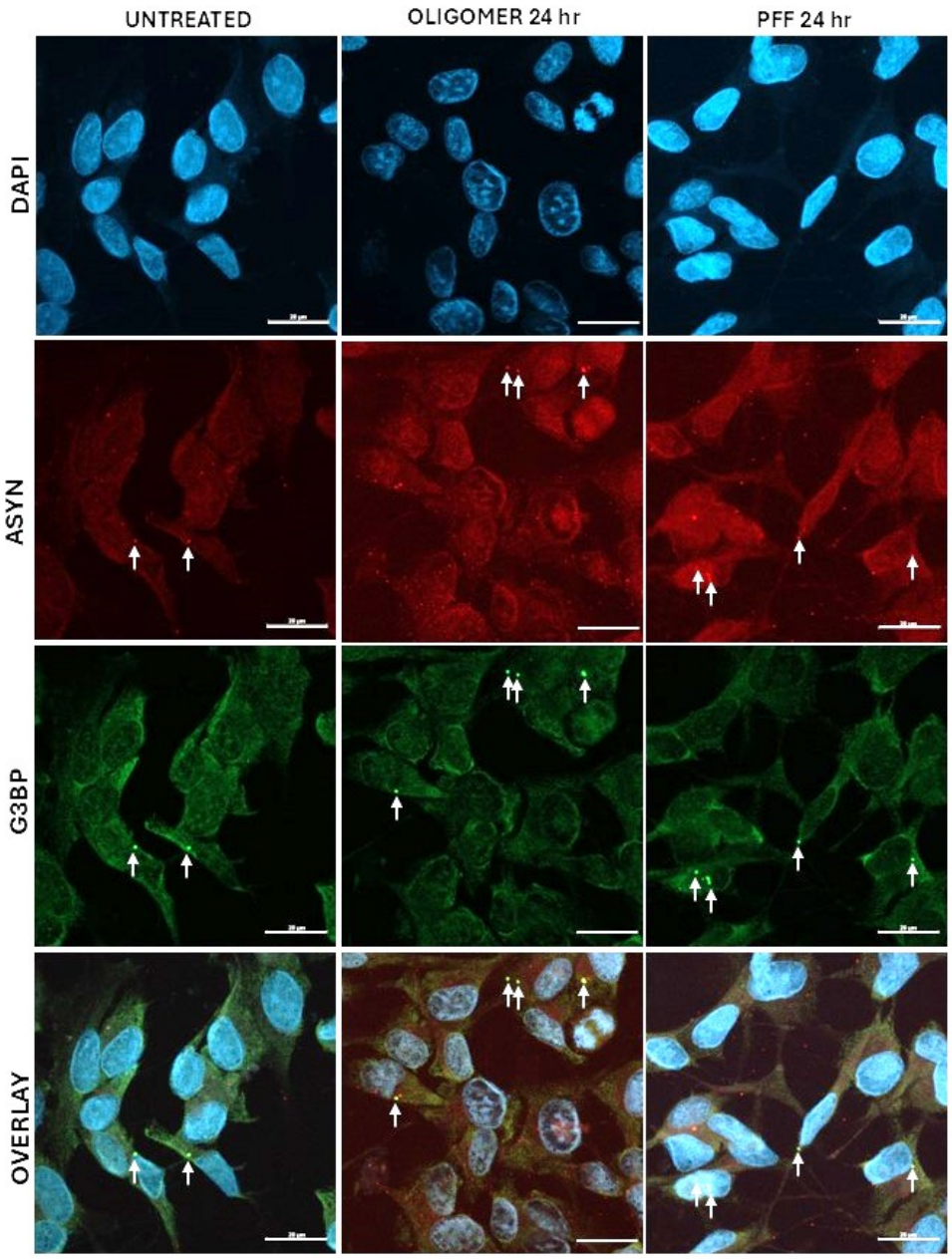

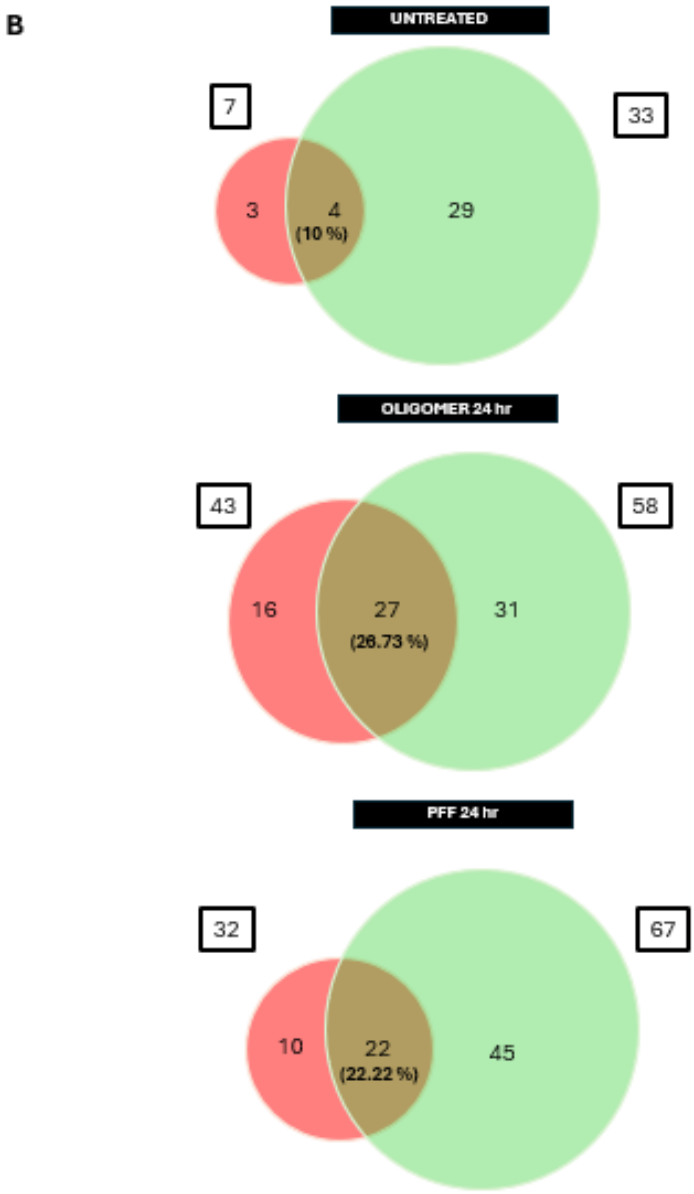

Figure 5.13 Oligomers and PFFs increases SG co-localisation to α-synuclein intracellular aggregates. Cells were treated with 0.1 mg/mL **(A)** oligomers and PFFs for 24 hr. Cell nuclei were stained using DAPI and G3BP conjugated to AF488 was used as an indicator of SG puncta. Magnification: 63x. Scale bar: 20 µm. **(B)** Co-localisation of α-synuclein and SGs positive puncta were quantified in Venn diagrams in cells positive for SGs where the red circle represents the number of α-synuclein puncta and the green represents the G3BP-positive puncta. The centre of the Venn diagram represents puncta with overlapping signal indicating co-localisation (Total number of cells: 45/15 per repeat).

5.3 Discussion

5.3.1 Oligomers and PFFs induce intracellular α-synuclein aggregation that induces cellular stress

It was found at the later timepoints of 24 and 48 hr that both oligomers and PFFs induced intracellular aggregation (**Figure 5.1, 5.2**), showing oligomers and PFFs ability to seed aggregation. It is a well-known concept that α-synuclein aggregates can induce cellular stress including oxidative stress (Deas et al, 2016). It was confirmed that at 24 and 48 hr that both oligomers and PFFs resulted in an increase in ROS-positive cells (**Figure 5.3**). It is also an important consideration that there may also be other stresses induced by these aggregates, but this was not explored within the scope of this research. Furthermore, to provide a more global context for the consequence of the cell stress induced by oligomers and PFFs, LDH activity levels (indicatory of cytotoxicity) was measured (**Figure 5.4**). It was found that PFFs at 48 hr, out of all the explored treatment conditions, was able to result in the highest amount of released LDH. This corresponds with ROS data which showed that PFFs were able to trigger more ROS-positive cells compared to oligomer-treated and untreated cells. Altogether, it can be surmised that oligomers and PFFs are cytotoxic in accordance with their demonstrated ability to induce oxidative stress. One could also suggest that PFFs may be more toxic than oligomers, but more experimental investigation would be required to confirm this.

5.3.2 Oligomers and PFFs induces expression of specific ISR markers

Chapter three demonstrated that SA and Tg are toxic to cells and activate the ISR/eIF2α-ATF4 pathway. It was also found that eIF2α phosphorylation occurs during MPP+ induced stress (**Figure 3.6**). MPP+ activates the ISR differently when compared to SA and Tg, indicating that ISR activation varies in different stress conditions. Given that α-synuclein aggregate-induced stress is a crucial element of PD-associated pathology, the consequences of oligomers and PFF induced cell stress was examined by investigating ISR activation. The core focus of the ISR is the phosphorylation of eIF2α, which was investigated through cell treatment with oligomers and PFFs at 6 and 24 hr (**Figure 5.5**).

These time points were chosen to align with the stress-inducing compounds discussed in chapter three. The results showed that both oligomers (at 24 hr) induced phosphorylation of eIF2α (**Figure 5.1, 5.2**). This indicates a link between intracellular aggregation-induced stress and eIF2α phosphorylation. It is important to note that the eIF2α phosphorylation data exhibited considerable variability. Such fluctuations can be attributed to batch-to-batch variability in the production of aggregates as well as influenced by their varying interactions with cellular organelles (Devi et al, 2008; Iyer and Claessens, 2019; Srinivasan et al, 2021), potentially resulting in inconsistent/varied cellular responses. An alternative consideration is the timing of the investigations into the effects of α-synuclein treatment. Many studies examining α-synuclein and PD focus on longer time frames, ranging from days to weeks (Demmings et al., 2021; Ferrari et al., 2023; Tapias et al, 2017). Observations of phosphorylation at Ser129, was observed at longer timepoints (Demmings et al., 2021; Tapias et al, 2017), which is a hallmark of PD pathology (Parra-Rivas et al, 2023; Samuel et al 2016). Whereas Ser129 phosphorylation was not seen at shorter timepoints of α-synuclein aggregate treatment (Taylor-Whiteley, 2019). Phosphorylation at Ser129 has been connected to enhanced fibrillar networks (Samuel et al, 2016); reduced cell viability; increased ROS and enhanced caspase-3 activity (Ma et al, 2016). It might be reasonable to expect more considerable increases in eIF2α phosphorylation in response to prolonged exposure to oligomers and PFFs due to an increased likelihood of cells being positive for intracellular phosphorylated α-synuclein aggregates that corresponds to increased cytotoxicity.

Downstream of eIF2α, is the enhanced expression of ATF4 which has been shown to occur in response to SA and Tg (**Figure 3.7**). It was shown that Tg was able to result in an increase in ATF4 expression at both 6 and 24 hr (**Figure 3.7**) with minimal comparative cytotoxicity (**Figure 3.10**), making Tg 0.15 μM an appropriate positive control. It was shown that oligomers and PFFs at 6 and 24 hr along with Tg were able to enhance ATF4 gene expression (**Figure 5.6 A**). All treatment conditions had higher ATF4 gene expression compared to the untreated but there appeared to be a reduction in ATF4 gene

expression when comparing the 24 hr to the 6 hr timepoint. As discussed in chapter three, there appears to be an element of cellular adaptation to the explored to chemical induced stress as well as α-synuclein aggregate stress. To confirm the data showing increased ATF4 gene expression in response to oligomers and PFFs, ATF4 protein expression was also shown to increase in response to oligomers and PFFs but data was deemed not significant enough to confidently show an increase in ATF4 protein expression (**Figure 5.6 B**).

ATF4 interacts with many proteins (Neill and Masson, 2023), which affects how cells respond to various stresses (Wu and Liang, 2024). ATF5 is one of the many targets of ATF4 (Teske et al, 2013). ATF5 is intrinsic to the mitochondrial UPR (Fiorese et al, 2016) and has been found to be pro-apoptotic in certain cases through its ability to induce the transcription of BCL-2 (Fiorese et al, 2016). The mitochondria UPR and the ER UPR (as discussed in **Section 1.9.3**) have both been implicated in the neurodegenerative diseases (Xu et al, 2023). The mitochondria are essential in production of ATP and cell growth/function. Mitochondrial stress responses can lead to increases misfolded, unfolded and damaged proteins resulting in the activation of the mitochondrial UPR (Xu et al, 2023). Under normal circumstances there are chaperones (e.g. heat shock protein 60) available in the mitochondria to correctly restore appropriate folding of various proteins as well as proteases (e.g. mitochondrial Lon protease-like 1) that degrade damaged and/or misfolded proteins. The mitochondrial UPR has different stands including: ATF4-ATF5-CHOP; AKT-Erα-NRF and Sirt3-FOXO2a-SOD2 catalase. These stands promote protein folding/degradation, increased quality of proteins and enhanced antioxidant capacity respectively (Xu et al, 2023). The ER UPR and mitochondrial UPR both have the capacity in conditions of ER stress to maintain protein homeostasis through the stimulation of protein degradation and promoting protein folding as well triggering other processes to achieve this. When both are dysfunctional or prolonged, it can lead to cellular death (Xu et al, 2023). The gene expression assay demonstrated that Tg 0.15 μM at 6 and 24 hours resulted in an increase in ATF5 expression (**Figure 5.7**) as observed in other studies (Ma et al, 2023). Oligomers (6 and 24 hr) and PFF (24 hr) did not result in an increase in ATF5 gene expression compared to the

untreated condition but PFF treatment for 6 hr was able to induce a moderate increase in ATF5 expression but not significant enough to indicate a legitimate change (**Figure 5.7**).

Additionally, CHOP acts as a transcription factor under the control of ATF4 (Teske et al, 2013). As α-synuclein aggregates were shown to induce ATF4 expression, CHOP gene expression was assessed in response to oligomer and PFF treatment for 6 and 24 hr. Oligomers and PFFs did not result in an increase in CHOP expression (**Figure 5.8 A, B**). This has been supported by other studies where CHOP was not expressed but rather other death markers such as PUMA (Demmings et al, 2021).

Oligomers and PFFs have been demonstrated to induce a minor enhanced activation of the eIF2α/ATF4 pathway (more so ATF4 expression than P-eIF2α) but with the absence of CHOP expression. To establish whether there was expression of other ATF4 targets, GADD34 expression was explored. GADD34 gene expression was examined following treatments with Tg, oligomers, and PFFs at 6 and 24 hr. It was observed that all treatment conditions led to an increase in the gene expression of GADD34, (**Figure 5.9**) with PFF 6 hr treatment inducing the highest amount of GADD34 gene expression when comparing the aggregate treatment conditions (**Figure 5.9**). Across all the treatment conditions explored, GADD34 gene expression reduced at 24 hr when compared to 6 hr (**Figure 5.9**) indicating that stress adaptation and/or recovery is taking place.

The attenuation of global protein synthesis is a key event and indicator of ISR activation (Ryoo and Vasudevan, 2017). It was demonstrated that in response to stress inducing compounds such as Tg and MPP+ that ISR activation corresponds to inhibited protein synthesis at 6 hr (**Figure 3.12**). It was shown that cells treated with oligomers and PFFs for 6 and 24 hr resulted in a reduction in puromycin incorporation compared to the untreated condition, particularly when cells were treated with PFFs for 24 hr (**Figure 5.10**). This can be linked to data showing PFFs inducing more ROS and toxicity when compared to oligomers.

5.3.3 Oligomers and PFFs triggers SG formation that co-localise with α-synuclein

During ISR activation and cellular stress, SGs are commonly observed due to their role in storing untranslated RNA (Glineburg et al, 2023). Oligomers and PFFs were shown to induce oxidative stress (**Figure 5.3**), so observation of SGs were of interest. It was shown that treatment with oligomers and PFFs induced the formation of SGs (**Figure 5.11**). The highest number of SG-positive cells was observed in response to a 6 hr treatment with PFFs (**Figure 5.12 A**). Since SGs are a marker of ISR activation, this finding further supports the evidence that oligomers and PFFs can trigger ISR activation plus reprogramme translation. The number of SGs and the percentage of SG-positive cells peaked at different time points for oligomers (at 24 hr) and PFFs (at 6 hr). This highlights that oligomers and PFFs induce varied stress responses which could be due to structural differences of oligomers and PFFs altering the manner in which it enters the cell and interacts with cellular components.

SGs have been implicated in pathological protein aggregation associated with ALS (Dudman and Qi, 2020). TDP-43 has been associated with ALS neuropathology where TDP-43 are able to form aggregates (Kon et al, 2022). Patient studies have shown presence of phosphorylated TDP-43 in the cytoplasm leading to aggregation (Kon et al, 2022) as seen with α-synuclein in PD (Lee et al, 2012). The presence of TDP-43 aggregates has been found in senescent neuronal cells (Kon et al, 2022). TDP-43 aggregates have been observed to co-localise with SGs, specifically the SG marker HuR, in the early stages of TDP-43 aggregation (Mori et al, 2023). Here, we investigated whether intracellular aggregates of α-synuclein co-localises with SGs (G3BP-positive SGs). Treatment with oligomers and PFFs induced more than double the amount of co-localisation (%) between SGs and intracellular α-synuclein aggregates compared to the untreated condition (**Figure 5.13 B**). As the number of SGs were highest for oligomers at 24 hr and PFFs at 6 hr (**Figure 5.11 and 5.12**), it would be of interest to explore co-localisation between α-synuclein aggregations and SGs at other timepoints (e.g. 1, 6 and 48 hr). A limitation of fluorescent imaging in co-localisation analysis is this method only

determines signal overlap of two probes (Dunn et al, 2011). Therefore, it cannot be robustly concluded that SGs and α-synuclein intracellular aggregates interact and to what capacity they may do so. However, α-synuclein is associated with numerous SG-associated proteins such as DJ-1 (Xu et al, 2017) and TDP-43 (Dhakal et al, 2021). Additionally, α-synuclein and TDP-43 are found to form hybrid fibrils (Dhakal et al, 2021), which further supports the idea that α-synuclein and SGs could interact. Further studies will be of importance to determine the extent of this interaction and the associated consequences for cellular function and health.

5.4 Summary

Synthesized oligomers and PFFs demonstrate a prion-like ability to induce and promote intracellular aggregation of α-synuclein, which is associated with cellular stress and toxicity.

While it is known that oligomers and PFFs causes cellular stress, the exploration of multiple ISR markers in response to oligomers and PFFs has not been previously explored. This chapter illustrates that both oligomers and PFFs can induce expression of specific ISR markers as summarised in **Figure 5.14**. It appears PFFs may incur a more robust stress response compared to oligomers (in certain cases) which is supported by the presence of more ROS-positive cells in response to PFFs when compared to oligomers. This is also supported by PFFs inducing more cytotoxicity as shown by LDH activity data. Oxidative stress and toxicity data coincides with PFFs triggering more SGs as well as a stronger attenuation of protein synthesis when compared to oligomers.

To further substantiate the ability of oligomers and PFFs to activate the ISR, it would be beneficial to investigate oxidative stress markers downstream of ATF4, such as NOXA (Albert et al, 2014) and markers upstream of eIF2α related to mitochondrial stress, like HRI (Chakrabarty et al, 2024). Additionally, examining the effects of higher concentrations of oligomers and PFFs as well as longer treatment durations could provide more information regarding the effects of α-synuclein-induced chronic stress, to better reflect the prodromal phase of PD.

Overall, chapter five shows that oligomers and PFFs alters the ISR where specific markers experienced enhanced expression (e.g. ATF4 and GADD34 gene expression) and induces SG formation, which establishes a connection between the ISR, SGs and PD.

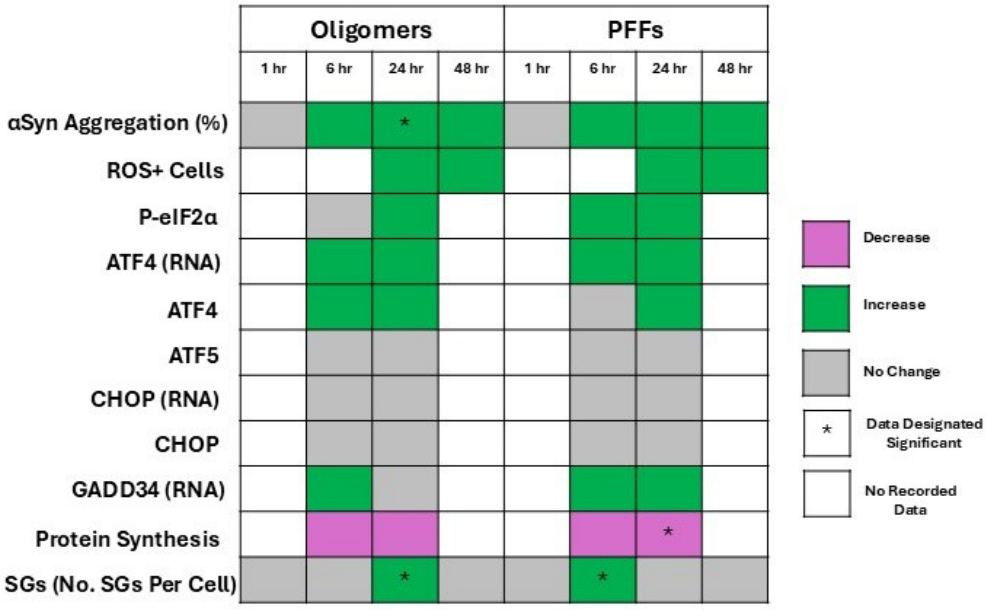

Figure 5.14 Timeline of ISR marker expression in response to oligomer and PFF treatment. The diagrams depict and summarises the findings presented throughout the chapters in response to PFF treatment at 1, 6, 24 and 48 hr. With specific focuses on how gene and protein expression changes compared to the prior timepoint.

6 Chapter Six: The effect of α-synuclein aggregates on the extracellular vesicle proteome

6.1 Introduction

6.1.1 The structure and function of extracellular vesicles

Extracellular vesicles (EVs) have been implicated in the propagation of pathological proteins in neurodegenerative diseases (Ananbeh et al, 2021; Ferrara et al, 2021; Garcia-Contreras and Thakor, 2023; Shippey et al, 2022; Soukup et al, 2023; Upadhya and Shetty, 2021). EVs are released from cells during various biological processes and are found in biofluids such as serum, plasma, cerebrospinal fluid and cell culture supernatant (Zeng et al, 2022). EVs have been categorised into various groups including exosomes (30-150 nm) formed through the endosomal pathway, microvesicles (100 – 1000 nm) formed through the outward budding of the plasma membrane and apoptotic bodies (larger than 1000 nm) formed during apoptosis (Rizzo et al, 2021). Small extracellular vesicles (sEVs) is a general term often used to class exosomes and other nanosized membranous particles with diameters less than 200 nm (Abhange et al; 2021; Jia et al, 2022) and are defined by surface protein markers such as CD63 and CD81 (Zhou et al, 2024). The general composition of EV's include tetraspanin proteins; adhesion proteins; tissue specific proteins membrane fusion and trafficking proteins; endosomal and vascular body proteins; transmembrane proteins and sphingolipids (Rashed et al, 2017).

There are numerous mechanisms involved in the biogenesis of EVs (Hadizadeh et al, 2022; Tricarico et al, 2016; Yu et al, 2024). An example is the biogenesis of exosomes, which begins with the early endosome being formed by the process of plasma membrane invagination where the early endosome can fuse with endocytic vesicles. As a result, the content of these vesicles can then be with recycled, degraded or secreted (Abels and Breakefield, 2016). Early endosomes that remain will develop into late endosomes which will accumulate intraluminal vesicles (ILVs) formed by the inward budding of the endosomal membrane which allows for proteins, nucleic

acids and lipids to be sorted into vesicles (Abels and Breakefield, 2016; Fonseka and Mathivanan, 2023). The late endosomes are called multivesicular bodies (MVBs) which are able to fuse with the lysosome to allow degradation of content or fuse with the membrane to allow release of ILVs as exosomes into the extracellular space (Abels and Breakefield, 2016) in a process termed exocytosis.

EVs are also taken up by cells in a process called endocytosis via a number of documented mechanisms such as membrane fusion, caveolin-mediated endocytosis, clathrin-mediated endocytosis, lipid raft-mediated endocytosis and others (Mulcahy et al, 2014). When taken up by recipient cells, molecular and signalling pathways can be initiated, reflective of EV roles in cell-to-cell communication (Fonseka and Mathivanan, 2023). The contents of EVs are released into the cellular cytoplasm and have the ability to modify transcription and translation (Abhange et al; 2021). Additionally, EVs are known to have roles in tissue maintenance and repair, inflammation regulation, stimulation of cell differentiation, waste removal and neurotransmission (Rashed et al, 2017).

6.1.2 EVs role in neurodegenerative disease

sEVs/exosomes have been associated with neurodegenerative disorder pathology, particularly in the spread of cytotoxic proteins that play integral roles in causing cellular death (Gomes et al, 2023). However, they have been found to carry miRNAs (Beatriz et al, 2023) and lipids (Ghadami and Dellinger, 2023) which influences the progression of numerous disease types.

In a meta-analysis pertaining to sEVs (reported as exosomes) isolated from PD patients' plasma, there is evidence of increased total α-synuclein associated with EVs (Xylaki et al, 2023). The presence of EV-associated α-synuclein has been proposed as a method to effectively differentiate healthy controls and PD patients (Xylaki et al, 2023). A cross comparison of EVs isolated from patients diagnosed with progressive nuclear palsy (PSP), DLB and PD, showed increased levels of EV positive α-synuclein in PD and a reduction in the number of particles compared to plasma acquired from controls, PSP and DLB patients (Stuendi et al, 2021). By contrast, when α-synuclein aggregates were used to treat the neonatal mouse cerebral cortex,

there was evidence of increased secretion of EVs as indicated by increased ALIX expression (an EV marker) compared to controls (Wang et al, 2023). Evidence has been presented showing the uptake of PFFs by neuroglioma H4 cells (Ishiguro et al, 2024). Further, when free PFFs and PFF-positive EVs derived from H4 cells were added to cell culture medium of iPSCs, PFFs within EVs were more rapidly taken up by iPSC-derived dopaminergic neurons (Ishiguro et al, 2024). This shows that EVs are a vessel for cellular transmission of α-synuclein aggregates. LDH levels were also investigated to assess cellular viability of primary cortical neurons in response to α-synuclein-positive EVs compared to α-synuclein-negative EVs derived from HEK cells. It was found that LDH levels increased in response to α-synuclein positive EVs (Zhang et al, 2019) indicating that EVs containing α-synuclein can induce cellular toxicity.

6.1.3 Objectives

Literature has shown that EVs mediates the cell-to-cell transmission of α-synuclein (Ishiguro et al, 2024; Stuendi et al, 2021) and it is known that treatment of cells with aggregated or mutated forms of α-synuclein results in increased α-synuclein-positive EVs and EV secretion (Shippey et al, 2022; Xylaki et al, 2023). Thesis chapters, three and five, investigated stress induction (specifically ISR activation) following exposure to stress-inducing compounds and α-synuclein aggregates (oligomers and PFFs). To further this work, changes in sEV proteomic cargo in response to stress-inducing compounds and α-synuclein aggregate exposure will be investigated to provide an understanding for how stress impacts the sEV proteome. To investigate this, the following will be conducted:

- verification of SH-SY5Y cell differentiation.
- isolation and characterisation of sEVs from undifferentiated and differentiated SH-SY5Y cells.
- analysis of sEV protein expression by LC-MS in response to oxidative and ER stress by treating undifferentiated cells with SA and Tg.
- analysis of protein expression in sEVs derived from to oligomer and PFF treated undifferentiated and differentiated SH-SY5Y cells.

6.2 Results

6.2.1 Characterising the morphology of undifferentiated and differentiated SH-SY5Y neuroblastoma cells

SH-SY5Y cells are commonly used in the research of neurological/neurodegenerative diseases such as PD (Magalingham et al, 2022; Xicoy et al, 2017). Undifferentiated SH-SY5Y cells have two reported states: the 'S' type which refers to epithelial-like cells and 'N' type which refers to the neuronal-like cells (Kovalevich and Langford, 2016). These cells have been reported to have attributes like dopaminergic neurons and stem cells (Avola et al, 2018). It has been demonstrated that differentiation of SH-SY5Y cells using compounds such as all-trans retinoic acid (ATRA) will result in the expression of markers indicatory of neuronal differentiation and expression of neuronal markers such as TH, MAP2 and β-tubulin III (Avola et al, 2018). It is common practice in the differentiation of SH-SY5Y cells to use ATRA in low serum conditions (Kovalevich and Langford, 2016). ATRA-differentiation of SH-SY5Y cells induces changes in neuronal marker expression that can be seen as early as 2 days (Cuende et al, 2008). Morphological changes such as neurite out-growth have been observed when SH-SY5Y cells were treated for 4 days (Xun et al, 2013). Additionally, cells subjected to differentiation exhibit less capacity to proliferate than undifferentiated cells as observed by a decrease in the proliferation marker, Ki67 (Taylor-Whiteley et al, 2019).

To differentiate SH-SY5Y cells into a more neuronal cell type, undifferentiated SH-SY5Y cells were treated with 10 μM ATRA in low serum media (1 % FBS) for 4 days. Prior to ATRA treatment (day 0) and the last day of differentiation (day 4), brightfield images were taken to observe morphological changes of SH-SY5Y cells which showed an increase in neurite length (**Figure 6.1**).

Immunocytochemistry was also performed to detect expression of Ki67 which was found to decrease in response to ATRA treatment (**Figure 6.2**). This shows that proliferation will reduce in response to ATRA treatment in alignment with existing literature.

Together the results indicate that ATRA induced differentiation of SH-SY5Y cells.

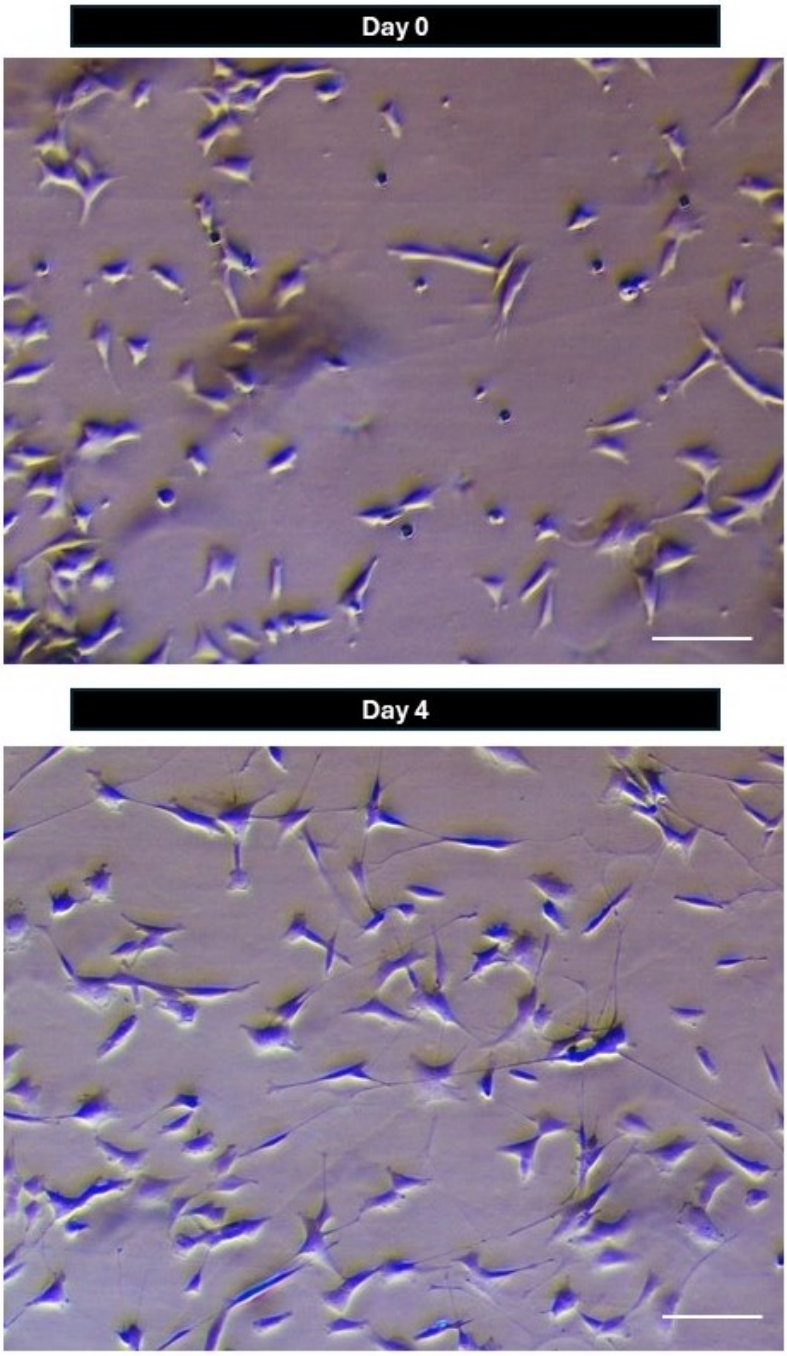

Figure 6.1 Morphology changes upon prolonged exposure to RA. Brightfield images were taken at day 0 and day 4. Day 0 is characteristic of undifferentiated cells where neurites are comparatively shorter. Day 4 images of RA-treated cells to have longer neurites indicatory of differentiation. Scale bar: 100 μm.

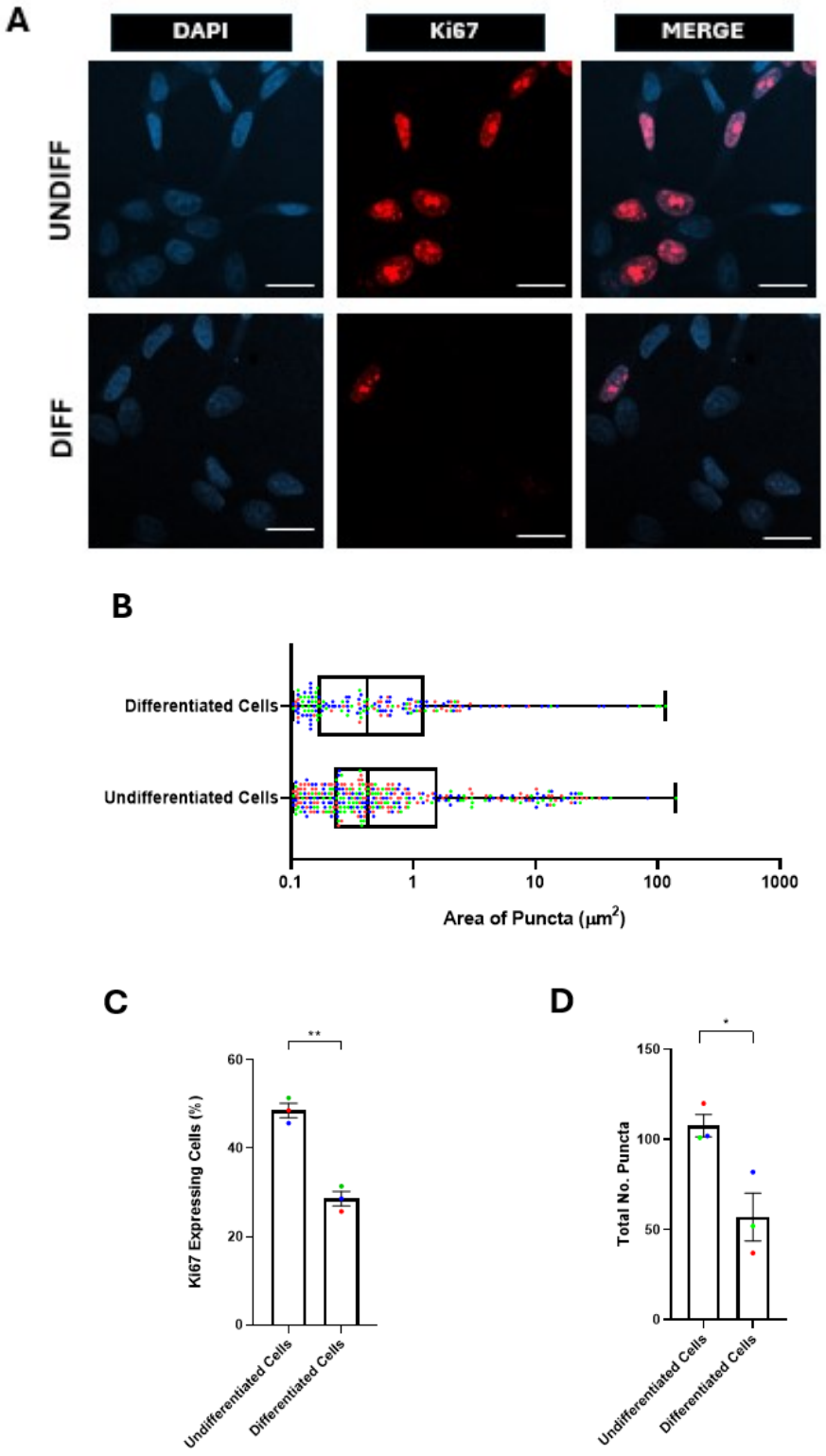
A
DAPI
Ki67
MERGE
UNDIFF
DIFF
B
Differentiated Cells
Undifferentiated Cells
0.1
1
10
100
1000
Area of Puncta (μm²)
C
Ki67 Expressing Cells (%)
60
40
20
0
**
Undifferentiated Cells
Differentiated Cells
D
Total No. Puncta
150
100
50
0
*
Undifferentiated Cells
Differentiated Cells

Figure 6.2 Ki67 expressed reduces during prolonged exposure to RA. (A) Representative fluorescent images were taken of undifferentiated and RA-differentiated cells to quantify Ki67 expression. Cell nuclei were stained using DAPI and Anti-Ki67/AF594 was used as an indicator of Ki67. Magnification: 63x. Scale bar: 20 μm. **(B)** Quantification of Ki67 puncta. **(C)** Percentage of cells expressing Ki67 was quantified and **(D)** the number of Ki67 puncta was quantified across the total number of cells. Data was analysed by student t test. Asterisk indicates the extent of statistical significance as reported by GraphPad Prism. The following levels of significance are P ≤0.05 (*), P ≤0.01 (**). Data without asterisk have been deemed as not significant. Colours indicate individual biological replicates: **(1)** red **(2)** green **(3)** blue. Error bars: ± SEM (*n*=*3*). (35 per repeat).

6.2.2 α-Synuclein aggregation in differentiated cells

α-Synuclein oligomers and PFFs have been shown to induce intracellular aggregation in undifferentiated SH-SY5Y cells particularly at 24 and 48 hr (**Figure 5.1**). Cells were treated with 0.1 mg/mL oligomers and PFFs for 48 hr to confirm the presence of intracellular aggregation in differentiated cells. Immunocytochemistry was performed to detect α-synuclein-positive puncta/intracellular aggregation. Data showed presence of α-synuclein intracellular aggregation at 48 hr within the differentiated cells in response to oligomer and PFF treatment (**Figure 6.3**). Oligomers induced aggregation with an area of 2.8 ± 0.73 μm^2 compared to the PFFs 1.8 ± 0.35 μm and both conditions resulted in 100% of cells being positive for α-synuclein aggregates (**Figure 6.3**). Altogether the data is accordance with previous observations, where intracellular aggregation is seen to occur upon exposure to oligomers and PFFs in undifferentiated cells (**Figure 5.1**) and differentiated cells (**Figure 6.3**). Which is also in alignment with existing literature.

.

A

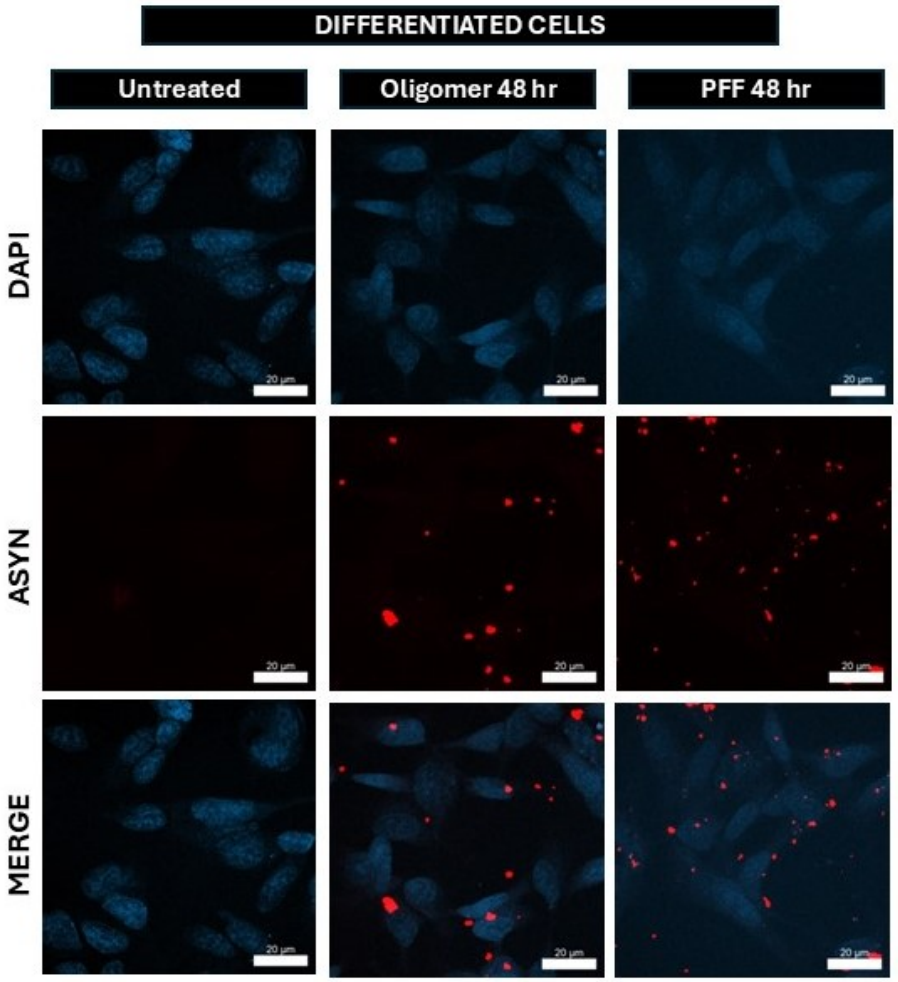
DIFFERENTIATED CELLS
Untreated
Oligomer 48 hr
PFF 48 hr
DAPI
ASYN
MERGE
20 µm

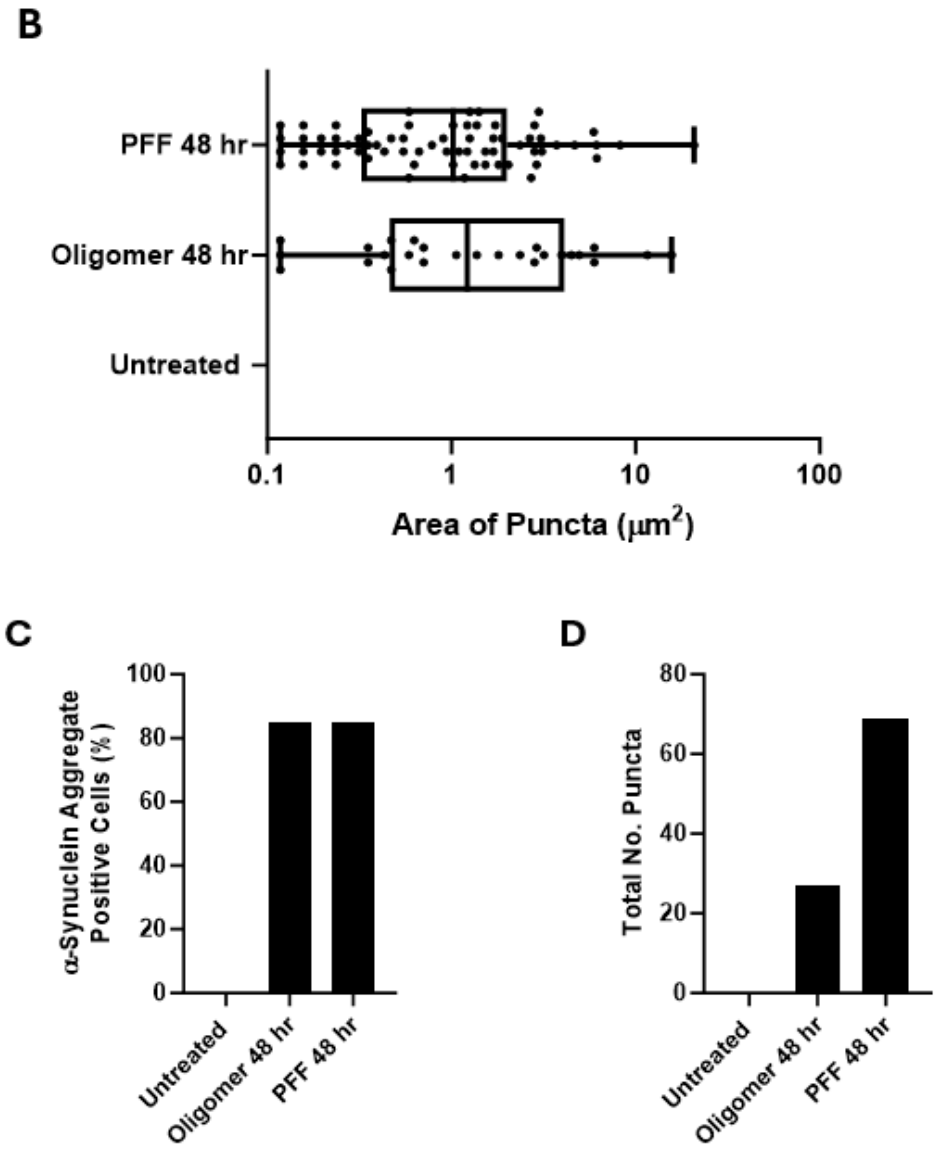

Figure 6.3 α-Synuclein aggregation in undifferentiated cells when treated with oligomers and PFFs. (A) Representative images of 0.1 mg/mL oligomer and PFF treated differentiated SH-SY5Y cells (48 hr). Cell nuclei were stained using DAPI and anti-MJFR1/AF594 was used as an indicator of α-synuclein aggregates. **(B)** The area of α-synuclein positive puncta. **(C)** The percentage of cells positive for α-synuclein aggregates. **(D)** Total number of α-synuclein puncta over the total number of cells counted. Magnification: 63x. Scale bar: 20 μm. Data without asterisk have been deemed as not significant. Error bars: ± SEM (*n=1*). (Total Cells: 20 Cells).

6.2.3 ROS increases in cells exposed to oligomers and PFFs

Oligomers and PFFs have been shown to induce intracellular aggregation in both undifferentiated and differentiated cells (**Figure 5.1, 6.3**). Additionally, oligomers and PFFs were demonstrated to induce an increase ROS in undifferentiated cells (**Figure 5.2**). To confirm that oligomers and PFFs can induce oxidative stress in differentiated cells, CellROX Green flow cytometry was used to measure ROS. TBHP was used as a known oxidative stress inducer (positive control) which resulted in 98.5 % of cells being ROS-positive (**Figure 6.4**). The percentage of differentiated SH-SY5Y cells that were ROS-positive cells increased in response to oligomer (19.1 %) and PFF (14.8 %) treatment compared to the untreated condition (0.16 %) (**Figure 6.4**). This shows that oligomers and PFFs induces oxidative stress in differentiated cells as shown with α-synuclein treatment of undifferentiated cells.

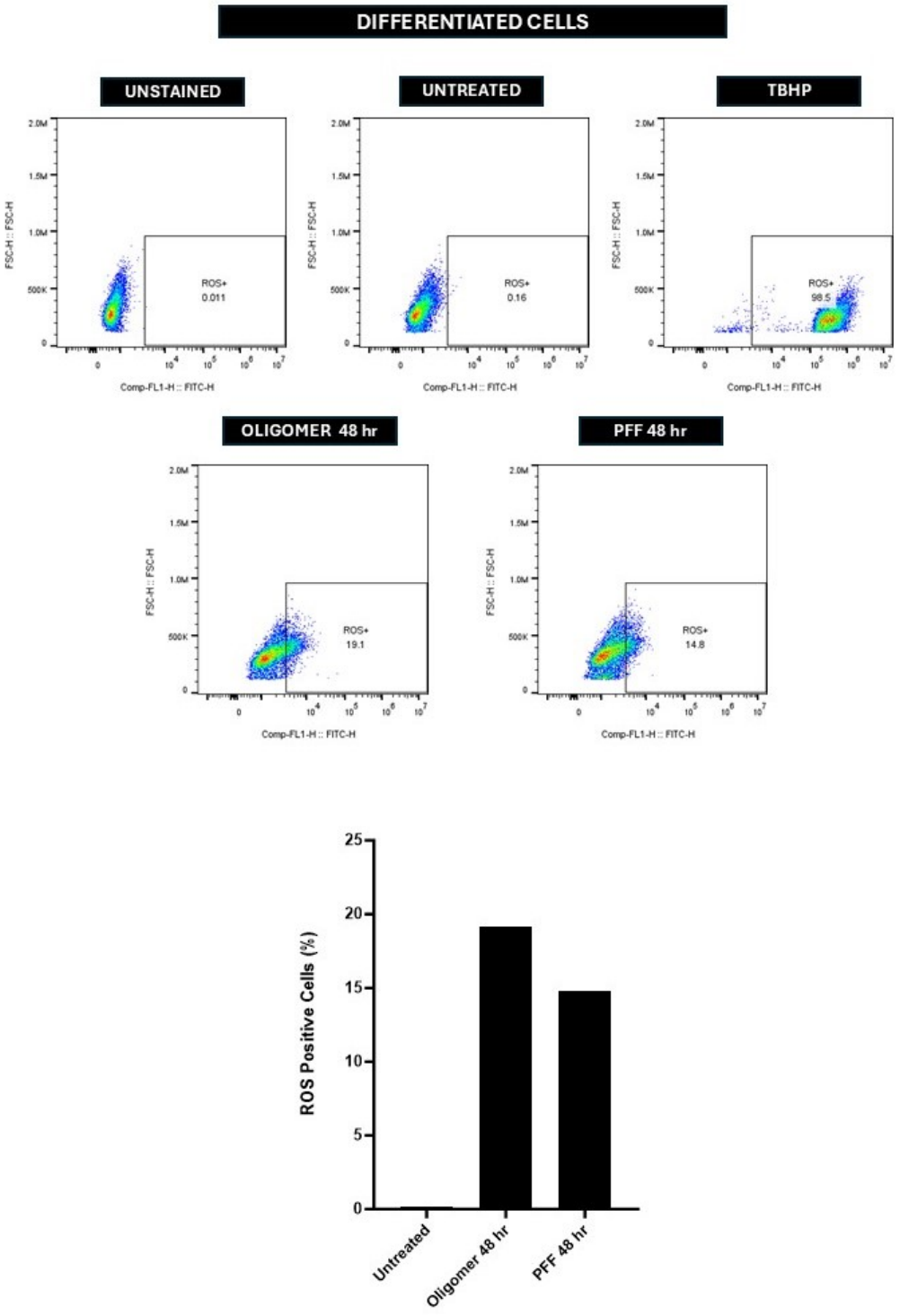

Figure 6.4 Oligomers and PFFs increases ROS positive cells. Flow cytometry graphs showing CellROX Green stained cells in different conditions including differentiated cells treated with 0.1 mg/mL oligomers and PFF for 48 hr. Data without asterisk have been deemed as not significant (*n=1*). (Total Events: 10,000).

6.2.4 Characterising the size of sEVs isolated from SH-SY5Y cells

The isolation of sEVs from conditioned cell media can be performed using various techniques including microfluidics, precipitation techniques, immunoaffinity based capture, ultrafiltration and SEC (Dilsiz, 2024). Here, sEVs were isolated from SH-SY5Y cells by differential ultracentrifugation of conditioned medium collected from undifferentiated SH-SY5Y following cell treatment with 10 μM SA and 0.15 μM Tg.

Once isolated, EVs were characterised by NTA to provide information on size, number and charge of particles within a sample (Comfort et al, 2021). The ZetaView instrument was used to determine the number of particles collected and if these fall within the size range considered to be sEVs. Particles isolated from untreated undifferentiated cells had a mean diameter of 137.03 ± 2.91 nm within the expected range of sEVs. The average (mean) diameter of particles acquired from SA treated cells were 136.8 ± 3.73 nm. Particles acquired from the Tg treated cells, had mean diameter of 141.27 ± 1.24 nm (**Figure 6.5 B**). The diameter of particles from each condition were within the exosome/sEV size range and there appeared to be no significant differences in diameter between particles isolated from each condition. The untreated conditioned media contained 6.57 ± 2.69 x 10^{10} particles/mL (**Figure 6.5 B**) with comparable levels acquired from SA and Tg treated cells, 5.97 ± 1.4 x 10^{10} particles/mL and 2.8 ± 1.14 x 10^{10} particles/mL respectively.

Using identical methods to isolate and measure particle diameter and particle/mL, sEVs were isolated from undifferentiated cells treated with oligomers and PFFs. The particle diameter for all conditions was within the expected sEV size range. Oligomer-derived particles were on average 128.2 ± 3.15 nm and the PFF condition had particles that were 133.4 ± 1.75 nm compared to the untreated condition which had particles with an average diameter 118.5 ± 5.96 nm (**Figure 6.6 B**). Approximately 10-fold less particles/mL were observed in the treated conditions 5.30 ± 1.39 x 10^{10} and 4.83 ± 2.2 x 10^{10} for the oligomers and PFF respectively compared to the control (20.33 ± 9.84 x 10^{10}) (**Figure 6.6 C**).

The particle parameters were also assessed in differentiated SH-SY5Y cells treated with oligomers and PFFs with no significant change in diameter compared to the undifferentiated cells (**Figure 6.7 B**). Isolated sEVs also appeared to be within exosomal/sEV range. But sEVs derived from differentiated SH-SY5Y cells appeared to be smaller in diameter compared to sEVs collected from the medium of undifferentiated cells. In addition, quantification of particles/mL in the oligomer and PFF treated conditions were similar to the particles/mL derived from undifferentiated cells (**Figure 6.7 C**).

As such sEVs derived from undifferentiated and differentiated SH-SY5Y cells were within the size range of exosomes/sEVs. Treatment with SA and Tg did not significantly alter the size of sEVs and did not result in a significant difference in the particles/mL. Additionally, treatment of undifferentiated and differentiated cells with oligomers and PFFs did not have a significant impact on particle diameter or the total particle/mL count (to note the particle/mL parameter was not normalised to a cell viability/death count).

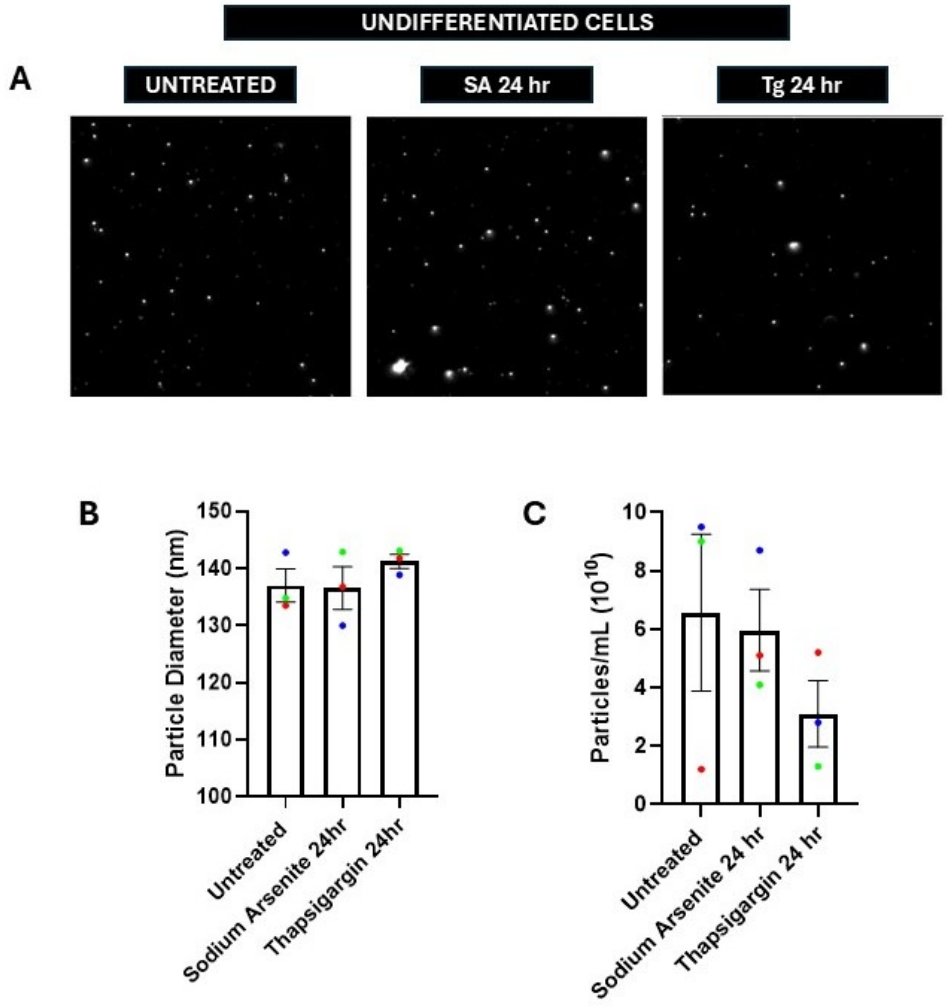

Figure 6.5 NTA of EV samples derived the conditioned medium from undifferentiated cells treated with SA and Tg. (A) NTA images of particle samples post-isolation from cell treated with 10 µM SA and 0.15 µM Tg. **(B)** Particle diameter of particles was assessed **(C)** as well as the particles per mL (mean ± SEM, *n=3*). Statistical analysis was carried out using the One-way ANOVA. Colours indicate individual biological replicates: **(1)** red **(2)** green **(3)** blue.

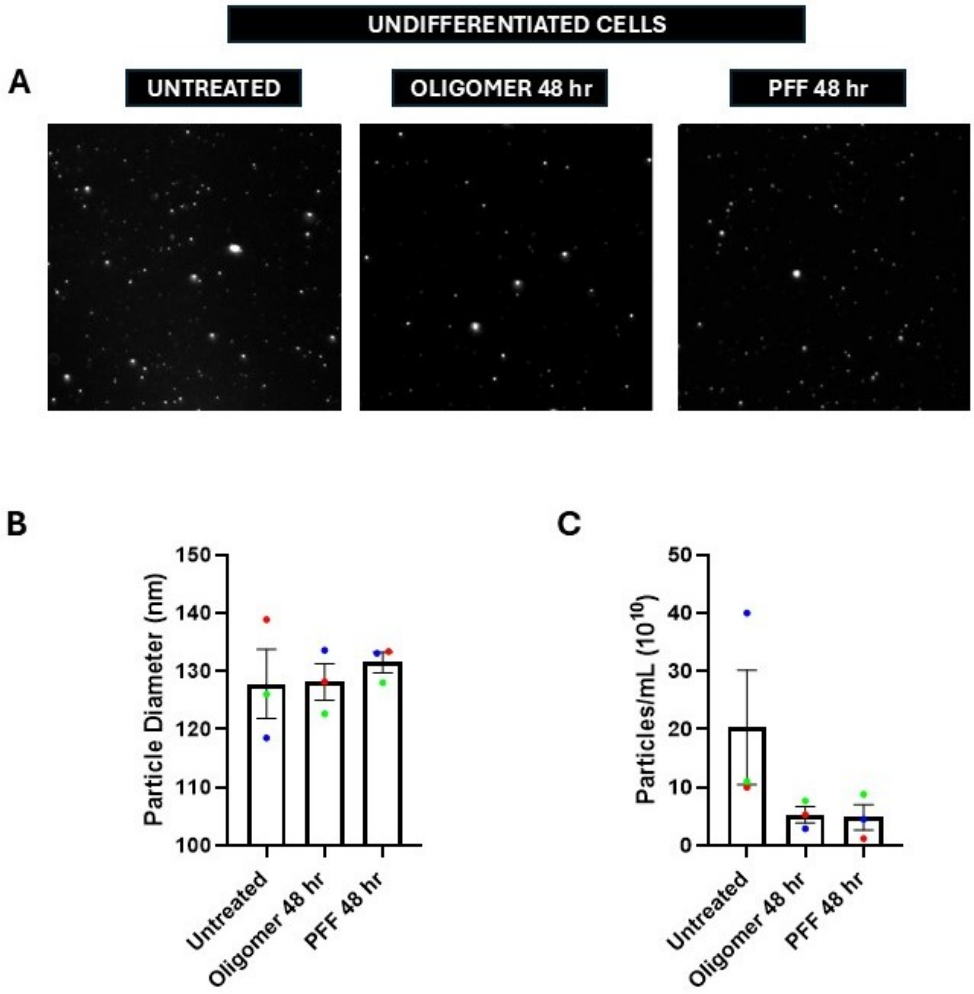

Figure 6.6 NTA of EV samples derived from undifferentiated cells treated with α-synuclein aggregates. (A) NTA images of particle samples post-isolation from cell treated with 0.1 mg/mL oligomers and PFFs. **(B)** Particle diameter of particles was assessed. **(C)** Particles per mL of sEV samples were also measured. (mean ± SEM, *n=3*). Statistical analysis was carried out using the One-way ANOVA. Colours indicate individual biological replicates: **(1)** red **(2)** green **(3)** blue.

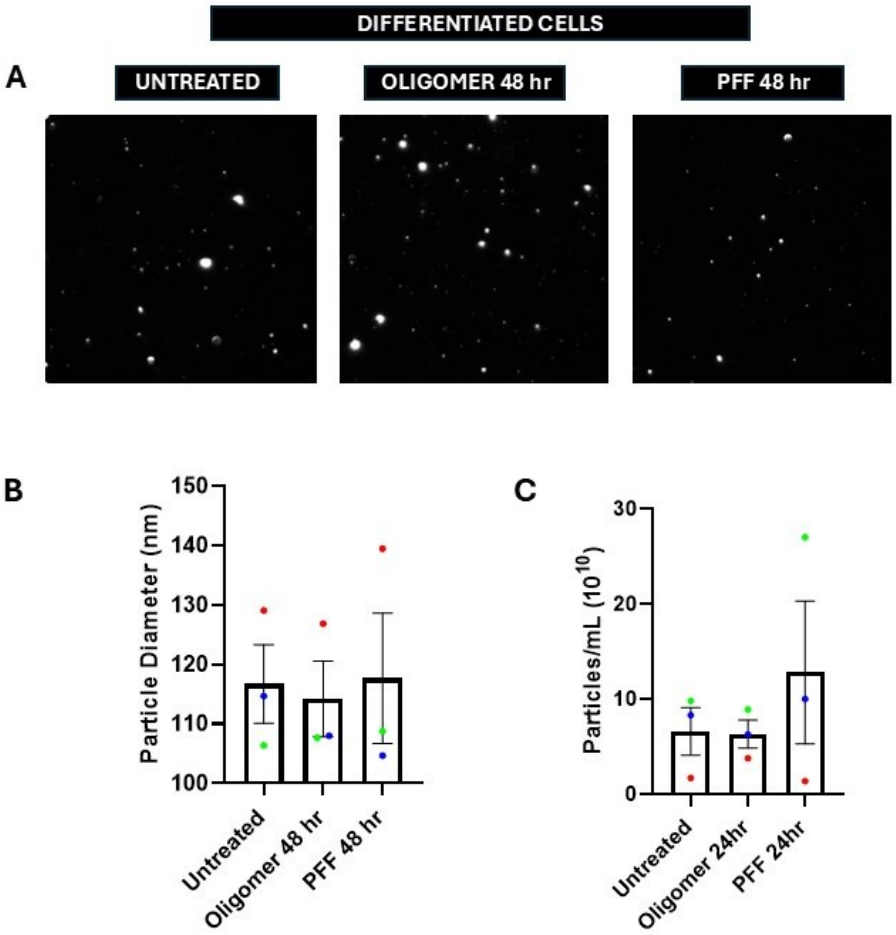

Figure 6.7 NTA of EV samples derived from differentiated cells treated with α-synuclein aggregates. (A) NTA images of particle samples post-isolation from cell treated with 0.1 mg/mL oligomers and PFFs. **(B)** Particle diameter of particles was assessed. **(C)** Particles per mL of sEV samples were also measured. (mean ± SEM, *n=3*). Statistical analysis was carried out using the One-way ANOVA. Colours indicate individual biological replicates: **(1)** red **(2)** green **(3)** blue.

6.2.5 Validation of isolated SH-SY5Y derived sEVs

In addition to characterising the size and amount of isolated sEVs, visualisation of the particles by negative stain TEM was performed. Images confirm sEV were present in all conditions (**Figure 6.8**) which mirrors other literature's sEV TEM images (Rikkert et al, 2019). The TEM preparation of sEV causes the EV structure to somewhat collapse forming a cup-like structure that is typically seen across TEM images in literature (Rikkert et al, 2019) which was also characteristic of the sEVs presented.

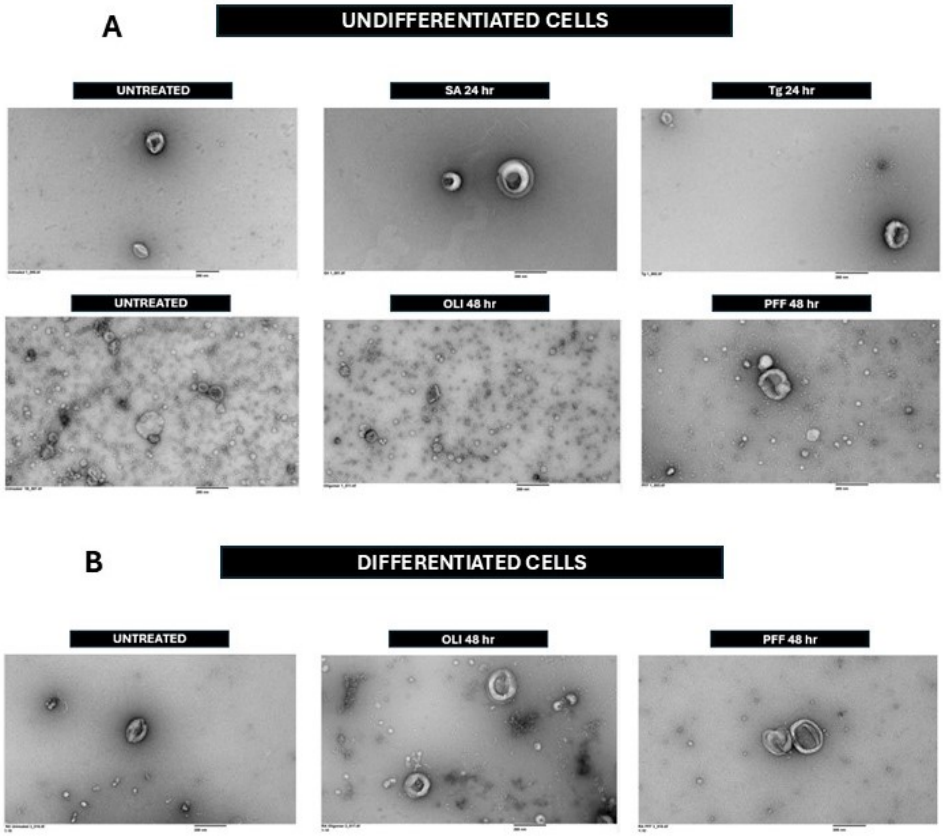

Figure 6.8 TEM of EV samples derived from undifferentiated and differentiated cells subjected to stress treatments. TEM images of: **(A)** sEVs derived from undifferentiated cells treated with 10 μM SA and 0.15 μM Tg for 24hr. 48 hr oligomer and PFF (0.1 mg/mL) treated undifferentiated cells sEVs. **(B)** sEVs acquired from differentiated SH-SY5Y cells treated with oligomers and PFFs for 48 hr (*n=3*). Scale bar 200 nm.

6.2.6 Detecting sEV markers

To further validate the presence of sEVs, western blotting was carried out on cell lysates and sEV samples to determine the expression of the following markers: ALIX, CD9 and the sEV negative control marker, β-actin. CD9 is a tetraspanin and associated with various cell functions including differentiation, proliferation, adhesion as well as others (Reyes et al, 2018) and is necessary for the uptake of EVs (Nigri et al, 2022; Tognoli et al, 2023). ALIX has been found to be cytoplasmic protein that is also enriched in sEVs (Yang et al, 2021).

Expression of both ALIX and CD9 was observed in both the cell lysate and sEV samples (**Figure 6.9**). To aid in the distinction between cell lysates and sEV samples, a negative marker was used. It was shown that β-actin was not expressed in sEV samples but present in cell lysates as shown by western blot analysis. Data presented further validates the isolation of sEVs.

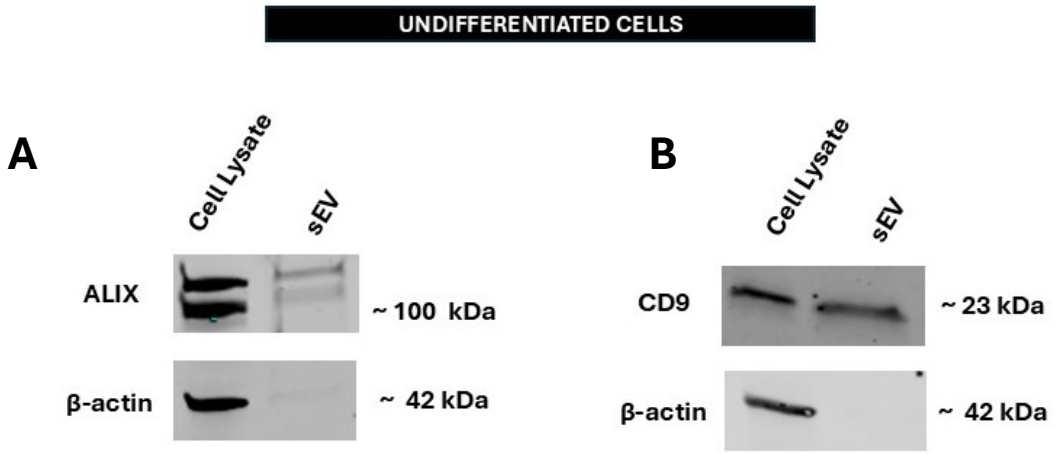

Figure 6.9 ALIX and CD9 but not β-actin is expressed in sEV sample. Cell and sEV lysates were subjected to western blotting **(A)** ALIX was expressed in response to cell lysates and sEVs, but β-actin was not expressed in sEV samples. **(B)** CD9 was expressed in response to cell lysates and sEVs but β-actin was not expressed in sEV samples.

6.2.7 Protein expression is altered in response to oxidative stress

To elucidate the effects of cell stress on sEVs' proteomic cargo, cells were treated with 10 μM SA and 0.15 μM Tg for 24 hr. Cell supernatant was then collected and subjected to a number of centrifugation steps to remove cell debris and isolated sEVs (by ultracentrifugation specifically). LC-MS analysis was used to detect proteins expressed in sEVs derived from untreated and treated conditions as summarised in **Figure 6.10**.

Cells treated with 10 μM SA for 24 hr yielded a number of proteins where expression was either reduced or increased (**Figure 6.11**). Information regarding the function and associated signalling pathways were provided about the detected proteins with decreased and increased expression (**Table 6.1 and 6.2**).

Profiling was carried out, as described in **Section 2.13**, on isolated sEVs from undifferentiated SH-SY5Y cells subjected to numerous stress conditions. The normalised fold change in proteins expression between conditions was plotted as $-\log_2$ fold change against the $-\log^{10}$ of the significance value. Volcano plot diagrams provided information on expression of proteins where the higher the protein is located on the y-axis of the diagram, the more significant the result. Whereas the x-axis shows magnitude of change compared to the control. Therefore, the left panel will show proteins with reduced expression, and the right panel indicated proteins with increased expression in response to treatment. Proteins were referred to using their gene symbol and identified through user defined threshold to display/visualise proteins on the volcano plot: alpha (0.5) which is the statistical significance level and $\log_2$ fold change (0.5). In addition to this, proteins indicated on the volcano plots included proteins identified in all three replicates of one condition and were determined to have more than one unique peptide. The one unique peptide rule is defined by a peptide sequence that appears exclusively in a single protein within a specific proteomic database (Zhao and Lin, 2010).

To further understand the context behind sEV expressed proteins, STRING analysis was used to establish networks or associations between proteins, the proteins with reduced expression or increased expression was inputted.

It was found that the proteins with reduced expression such as SRP14 and PSMA2 (**Figure 6.12**) were connected by a black line according to STRING analysis indicating co-expression of proteins (**Figure 6.12**). SRP14 acts as a signal recognition molecule involved in the recognition of the scaffold particle RNA, 7SL (Gussakovsky et al. 2024). Whereas PSMA2, a component of the 20S and 26S proteosome, is involved in the recycling of damaged proteins (Rashid et al, 2023). There is not an abundance of information regarding exact connections between these two proteins but through autoantigen analysis in various human cell lines, it was found that both these proteins were expressed in HS-Sultan cells (Wang et al, 2022). Autoantigens are associated with viral infection, translation vesicle processing, cell stress and apoptosis. They are released during cell death which can stimulate immune cells (Wang et al, 2022).

Additionally, GNG12 and RRAS found to be reduced in expression in response to SA treatment were found to have interactions according to STRING analysis (**Figure 6.12**). GNG12 belongs to the G protein family and regulates signalling cascades associated with inflammation (Li et al, 2020). RRAS is a small GTPase necessary in the aid of cell survival and important in the process of cell adhesion (Komatsu and Ruoslahti, 2005). The link between these proteins within neurodegeneration has not been elucidated. But proteomic analysis for reoccurrence predicting of non-small cell lung cancer reported that amongst 411 patients there was lower expression of several proteins including GNG12 and RRAS (Huang et al, 2023).

Gene ontology analysis of the sEV proteins found to have reduced expression showed that the proteins were associated with EVs (**Figure 6.13**).

SERPIN B12, DSG1, FLG2 and BLMH were identified to have increased expression and had associations according to STRING (**Figure 6.14**). SERPIN B12, DSG1, FLG2 and BLMH are involved in epidermal differentiation processes according to cluster analysis of identified proteins. These proteins were found to be abnormally expressed in the skin of individual's diagnosed with atopic dermatitis (Goleva et al, 2025). The connections between these proteins within neurodegenerative diseases have not yet been explored.

XPO7, USO1 and LMAN1 were also found to have increased expression and were linked using STRING (**Figure 6.14**). Affinity purification and mass spectrometry analysis of A549 lung carcinoma cells expressing SARS-CoV-2 and SARS-CoV proteins revealed that XPO7, USO1 LMAN1 were among a number of other proteins identified as viral protein host binders (Stukalov et al, 2020). This suggests that these proteins are essential to the viral infection process and disease progression. In more general instances these proteins (as discussed in **Table 6.2**) have been linked to nucleocytoplasmic transport, molecule recognition and vesicular transport (Dommett et al, 2006; Mingot et al, 2004; Yoon et al, 2021).

AP2B1, RPS6KA3, KIF5B had increased expression in response to SA cell treatment and interact according to STRING (**Figure 6.14**). AP2B1 and RPS6KA3 were identified as enriched differentially expressed genes involved in cellular repair when ATRA-differentiated SH-SY5Y cells were treated with amyloid-$\beta_{1\text{-}42}$ (Silvestro et al, 2021). Further, the connection between RPS6KA3 and EIF5B hinges on the observation that depletion of EIF5B, important in canonical translation, also resulted in the reduction of RPS6KA3 (Bressler et al, 2021). This suggest that sEVs will carry translation-associated markers.

HNRNPA3, HNRNPL and RALY, proteins with increased expression in sEVs, had detected connections according to STRING (**Figure 6.14**). HNRNPA3 was found to associate with RNA packaging proteins important in nucleocytoplasmic shuttling and mRNA processing such as HNRNP complexes (Ma et al, 2002). Pull down assays revealed association of HNRNPA3 to HNRNPL in HeLa nuclear and cytoplasmic extracts (Ma et al, 2002) but associations to neurodegeneration and neurological conditions have not yet been found.

Gene ontology analysis indicated that the linked proteins that increased in expression in response to SA stress were associated with the extracellular matrix (**Figure 6.15**).

Altogether, the sEV proteomic data derived from cells treated with SA for 24 hr indicates the SA stress has the ability to alter the proteome of sEVs to exhibit

proteins associated with cellular processes necessary for normal function e.g. translation and mRNA shuttling but the proteins identified had associations with disease.

There were no proteins determined to be significant when comparing the sEV proteome derived from cells treated with 0.15 μM Tg 24 hr to untreated cell sEVs (**Figure 6.16**).

Log_2 centred intensity was calculated and compared for each of the sEV proteins detected in SA, Tg and untreated conditions (**Figure 6.17**). It was observed that sEV proteins in the SA condition had the most difference compared to the untreated condition. Detected proteins in **Figure 6.17** when comparing the SA to the untreated condition, found to have increased and decreased expression were discussed in **Tables 6.1 and 6.2**. The additional proteins found to increase in response to SA when compared to the Tg condition were the following:

- distinct subgroup of the Tas family member 2 (DIRAS2) - it may have roles in cell growth and morphology (Grünewald et al, 2018).
- ephrin B4 (EPHB4) – receptor proteins involved in cell-to-cell communication (Chen et al, 2019).
- Ras family GTPase 1 (RAP1A) – involved in the integrin pathway necessary for cell adhesion (Sayyah et al, 2014).
- serpin family B member 12 (SERPINB12) – serine protease inhibitor involved in matrix remodelling (Niehaus et al, 2015).

When comparing the Tg condition to the SA condition, poly(A) binding protein cytoplasmic 4 (PABPC4) involved in cell development and survival (Liu et al, 2012) was found to increase in sEV samples.

Clustered heatmaps based on log_2 centred intensity was used to summarise protein expression in the different treatment conditions (untreated, SA and Tg) (**Figure 6.18**).

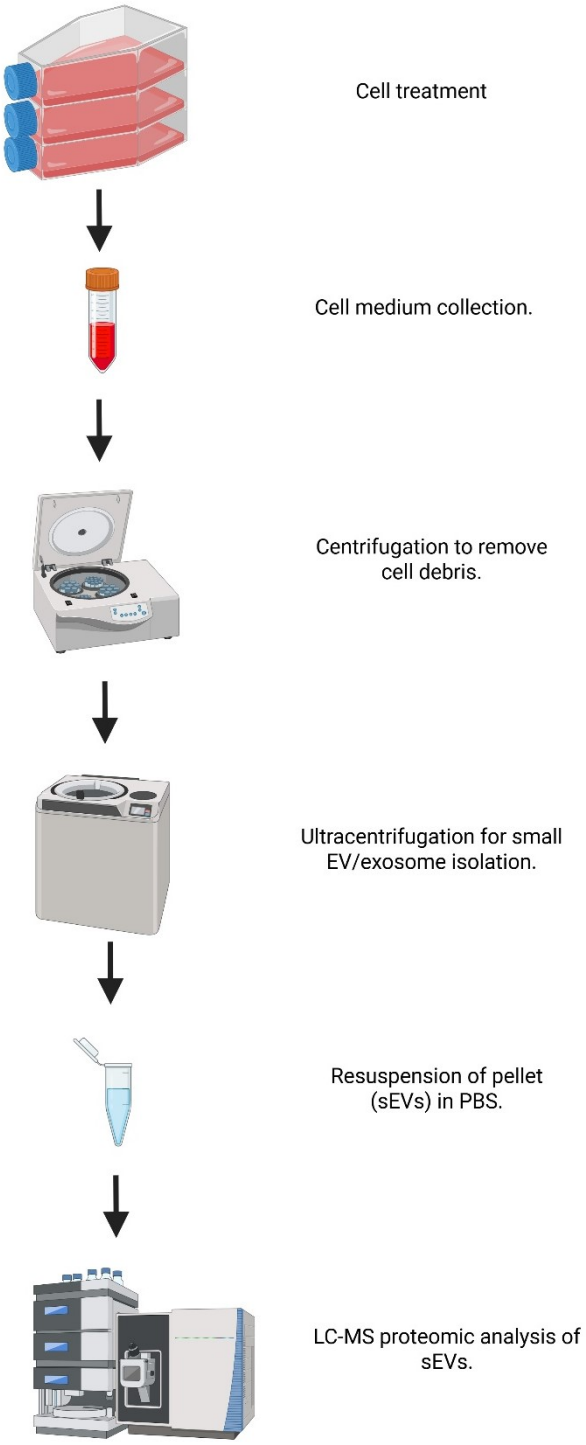

Figure 6.10 Experimental workflow of EV isolation and proteomic analysis. Cell medium is transferred to falcon tubes subsequent to cellular treatment in T175 flasks. Centrifugation of medium is preformed to remove cell debris. Ultracentrifugation is preformed to isolated sEVs. The resulting pellet (sEVs) is resuspended in PBS and then subjected to preparation for LC-MS analysis.

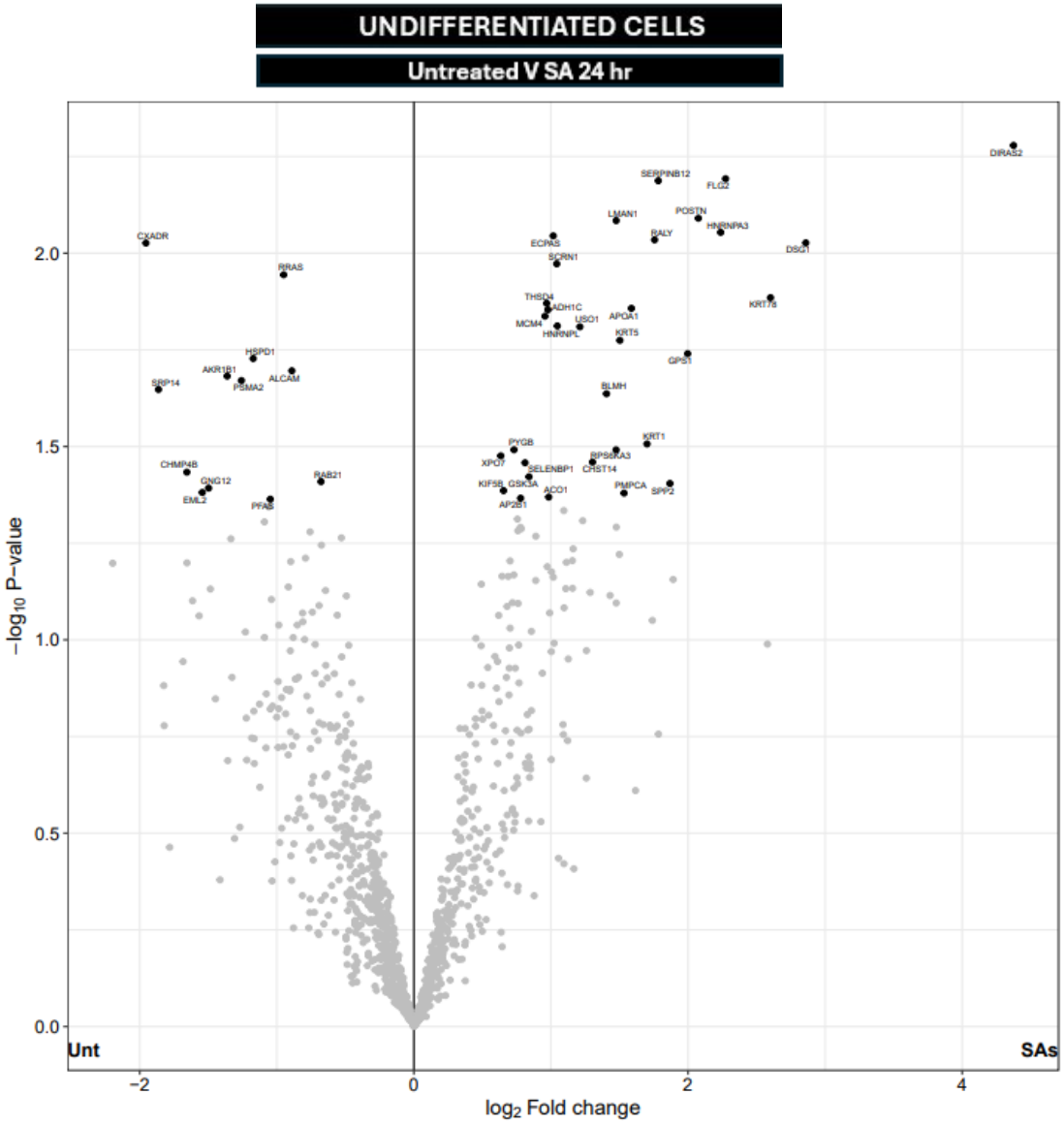

Figure 6.11 LC-MS analysis of sEV proteins derived from cells treated with SA 24 hr. A number of proteins were found to experience an increase in expression in response to 24 hr of SA treatment as seen in the right section of the volcano plot. The left section also shows proteins with reduced expression in response to the SA treatment. (*n*=*3*). Protein have been disclosed in **Table 6.1 and 6.2**. Proteins were made visible by cutoffs for alpha (0.5) and log fold change (0.5).

Table 6.1 Decreased expression of sEV proteins. The proteins found to have reduced expression in the sEV sample when comparing the SA 24 hr treatment condition to untreated conditions (**Figure 6.10**). As described in **Section 2.13.5**, proteins included in the table were identified as significant and made visible in volcano plots through cutoffs for alpha (0.5) and log_2 fold change (0.5).

Undifferentiated Cells (SA 24 hr)	
Protein	**Reported role/Disease association**
Aldo-keto reductase family 1 member B1 (AKR1B1)	It is an enzyme that converts nicotinamide adenine dinucleotide phosphate (NADPH) into $NADP^+$ involved in numerous metabolic and physiological processes such as glucose metabolism, inflammation and prostaglandin synthesis. It has been associated with the mTOR pathway and has been implicated in colorectal, breast and various cancers due to its overexpression in these diseases which has been linked to increases in ROS and other cellular events (Khayami et al, 2020).
Activated leukocyte cell adhesion molecule (ALCAM) or CD166	Cell adhesion molecule that is involved in the activation of T-cells, inflammation and the propagation of tumours. It is often linked to the grade and stage of cancers. It is associated with melanoma, colorectal, breast, prostate, bladder and many other cancers. The knocking down of ALCAM has been associated with autophagy activation (Darvishi et al, 2020).
Charged multivesicular body protein 4b (CHMP4B)	Probable core component of the endosomal sorting required for transport complex III (ESCRT-III) which is involved in multivesicular bodies (MVBs) formation and sorting of endosomal cargo proteins into MVBs. It has been found to be increased in the neuronal nuclei of ALS cell models (induced human pluripotent stem cell

	derived spinal neurons) (Coyne and Rothstein, 2021).
Coxsackievirus and adenovirus receptor (CXADR also CAR)	Component of the epithelial apical junction complex that may function as a homophilic cell adhesion molecule and is essential for tight junction integrity. It has been demonstrated to be involved in neurite extension and neuronal development (Patzke et al, 2010).
Echinoderm microtubule-associated protein-like 2 (EML2)	Tubulin binding protein that inhibits microtubule nucleation and growth, resulting in shorter microtubules. It has been linked to cell growth, the immune response, apoptosis as well as other physiological processes (Sun et al, 2024).
Guanine nucleotide-binding protein G(I)/G(S)/G(O) subunit gamma-12 (GNG12)	Guanine nucleotide-binding proteins (G proteins) are involved in various transmembrane signalling systems. It has been found to be linked to the activation of the NF-kB signalling pathway which is connected cancer proliferation and angiogenesis (Alausa et al, 2022).
60 kDa heat shock protein D (HSPD1)	Chaperonin involved in the folding of mitochondrial proteins that ultimately becomes imported into the mitochondrial matrix (Cömert et al, 2020)
Phosphoribosylformylglycinamidine synthase (PFAS)	Necessary for the de novo synthesis of purine but interacts with various proteins such as carbamoyl-phosphate synthetase (synthesis of pyrimidine), chaperonin containing TCP1, subunit 2 (chaperonin) and peroxiredoxin 1 (antioxidant enzyme) specifically through allowing for these proteins post-translational modifications (Lu et al, 2019).

Proteasome subunit alpha type-2 (PSMA2)	A protein responsible for the degradation or recycling of proteins considered to be defective. It has been linked with the influenza A virus, acting as a host factor for this virus' maturation (Rashid et al, 2022).
Ras-related protein Rab-21 (RAB21)	Linked to neurodegenerative disorders such as AD as well as cancers such as glioma. It is involved in membrane trafficking, endosomal function, cell adhesion as well as endosomal cargo sorting (Liu et al, 2022).
Ras-related protein R-Ras (RRAS)	Studies have identified RRAS as having links to cell adhesion, differentiation, migration, invasion, neurite growth and phagocytosis. It preforms inside-out signalling which allows for integrin signalling (Liu et al, 2017).
Signal recognition particle 14 kDa protein (SRP14)	SRP14 influences elongation arrest activity via effects on the ribosome and has the ability to alter the tertiary structure of RNA (Thomas et al, 1997).

Table 6.2 Increased expression of sEV proteins. The proteins found to have increased expression in the sEV sample when comparing the SA 24 hr treatment condition to untreated conditions. (**Figure 6.10**). As described in **Section 2.13.5**, proteins included in the table were identified as significant and made visible in volcano plots through cutoffs for alpha (0.5) and log_2 fold change (0.5).

Undifferentiated Cells (SA 24 hr)	
Protein	**Reported role/Disease Association**
Aconitase 1 (ACO1)	Within the mitochondria, this enzyme converts citrate to isocitrate in the tricarboxylic acid (TCA) cycle. Mitochondrial ACO1 is involved in cellular respiration and ATP level modulation (Cho et al, 2021).
Adaptor Protein Complex 1 (AP2B1)	AP2B1 is linked to the mediation of intracellular trafficking specifically the shuttling of vesicles within the trans/Golgi network and recycling endosomes (Moreno et al, 2022).
Alcohol dehydrogenase 1C (ADH1C)	An isoenzyme that belongs to a family of enzymes responsible for alcohol metabolism. It has been found that individuals carrying the homozygous allele for ADH1C have increased risk for alcohol-induced organ damage (Homann et al, 2006). Additionally, ADH1C has been linked to a higher risk of colorectal adenomas according to a Dutch case study (Homann et al, 2009).
Apolipoprotein A1 (APOA1)	One of the main apolipoproteins of the plasma high-density lipoproteins and is a co-factor of lecithin:cholesterol transferase, an enzyme that produces plasma cholesteryl esters (Cochran et al, 2021).
Bleomycin Hydrolase (BLMH)	A protease enzyme that targets cysteine, expressed in a number of tissues. It is involved in the degradation of citrullinated filaggrin monomers into free amino acids necessary for skin hydration (Riise et al, 2019).
Carbohydrate Sulfotransferase 14 (CHST14)	CHST14 has been linked to Ehlers-Danlos Syndrome (inherited condition that affects the connective tissue) (Kosho, 2016). It linked to a variety of functions specific

	to the nervous system including inhibition of neural regeneration and cell proliferation (Akyüz et al, 2013).
Desmoglein-1 (DSG1)	DSG1 is a constituent of desmosomes which connects the cell surface to the keratin cytoskeleton. DSG1 plays roles in numerous diseases including pemphigus foliaceus (autoimmune blistering disorder) as well as other skin conditions (Samuelov et al, 2013).
DIRAS family GTPase 2 (DIRAS2)	DIRAS2 or Di-Ras2 has been associated with ADHD as well as neurodevelopment. It is unclear what pathways this protein effects due to minimal available information but due to its labelling as a Ras kinase, it may have roles in cell growth and morphology. It appears to be primarily expressed in the hippocampus, cerebral cortex and cerebellum of the human brain (Grünewald et al, 2018).
Ecm29 Proteasome Adaptor (ECPAS)	A proteosome-interacting protein that plays roles in the remodelling of the 26S proteosome in human cells in conditions of oxidative stress (Wang et al, 2017).
Exportin 7 (XPO7)	This exportin protein has been found to be involved in nucleocytoplasmic transport (Mingot et al, 2004).
Filaggrin 2 (FLG2)	Filaggrin (FLG) contributes to the maintenance of the barrier function of the skin. However, FLG2, a variation of FLG, which is found in the stratum corneum is reported to be important for skin barrier function. Reduction of FLG2 is often associated with skin inflammation and atopic dermatitis (Margolis et al, 2014).
G Protein Pathway Suppressor 1 (GPS1)	GPS1 has been identified as a matrix protein 2-interacting host protein. It has also been found to be a component of COP9 signalsome, which regulates the NF-kB signal pathway involved in inflammation and the immune response (Kuwahara et al, 2019).
Glycogen phosphorylase B (PYGB)	PYGB is one of two forms with the other form being glycogen phosphorylase A. PYGB is the dephosphorylated low activity form of glycogen phosphorylase which regulates glycogen concentration in the muscle and liver (Oikonomakos et al, 2000).

	Glycogen phosphorylases are also found in the brain and regulates oxidative stress (Mathieu et al, 2019).
Glycogen Synthase Kinase 3 Alpha (GSK3A)	GSK3A regulates fatty acid metabolism and involved in the accumulation of lipids within the heart (Nakamura et al, 2020). It has also been linked to inflammation and apoptosis plus regulating oxidative stress (Rana and Singh, 2018).
Heterogeneous nuclear ribonucleoprotein A3 (HNRNPA3)	HNRNPA3 belongs to a family of proteins involved in mRNA processing and transport, transcription, DNA repair and others. It has been linked to the early stages of cortical development (Ou et al, 2020).
Heterogenous Nuclear Ribonucleoprotein L (HNRNPL)	An RNA-binding protein that is associated with DNA repair (Hu et al, 2019).
Kinesin Family Member 5B (KIF5B)	A motor adaptor protein that along with syntabulin (a syntaxin-binding protein), regulates the anterograde transport of syntaxin-1 to neuronal processes (Cai et al, 2007).
Lectin, Mannose Binding 1 (LMAN1)	LMAN1 belongs to a family of collectin proteins and acts as a major-recognition molecule of the innate immune system. This protein has been connected to inflammation and apoptotic cell clearance (Dommett et al, 2006).
Minichromosome Maintenance Complex Component 4 (MCM4)	One of six MCM proteins, which forms part of the pre-replicative complex that binds to the replicative origins in the cell cycle's G1 phase and is essential for DNA replication. MCM4 has been evidenced to be a marker of non-small cell lung cancer (Kikuchi et al, 2011).
Peptidase Mitochondrial Processing Subunit Alpha (PMPCA)	PMPCA processes mitochondrial proteins specifically by cleaving the extension peptides at the amino termini of precursor proteins synthesised in the nucleus that have been imported into the mitochondria (Nagao et al, 2000).
Periostin (POSTN)	POSTN also known as osteoblast-specific factor 2 is a vitamin K-dependent protein belongs to a family of fasciclins. It is believed to interact with integrins and activate numerous signalling pathways such as NF-

	kB/STAT3, PI3K/Akt and FAK signalling. It has been linked to tissue repair and inflammation (Conway et al, 2013).
RBP associated with lethal yellow mutation (RALY)	RBP forms RNP complexes and the protein arginine N-methyltransferase (PRMT1) has found to be enriched in these RNP complexes. A target of PRMT1 is Fused in Sarcoma (FUS) which is associated with transcriptional regulation, DNA repair and damage response. In neurons, FUS plays roles in RNA transport, mRNA stability and synaptic homeostasis (Gasperini et al, 2018).
Ribosomal Protein S6 Kinase A3 (RPS6KA3)	RPS6 is linked to the mTOR pathway specifically acting as an effector of TORC1 (Magnuson et al, 2012). RPS6KA3 has been found to be a downstream substrate of the extracellular signal-regulated kinase (ERK) pathway and an activator of CREB1 (Pan et al, 2023). It is also a component of SGs (Sfakianos et al, 2018).
Secernin-1 (SCRN1)	An amyloid plaque associated protein that has the ability to interact with phosphorylated tau, a major component of NFTs – a hallmark of AD. There is evidence that SCRN1 plays roles in ER signalling and synaptic vesicle cycling (Pires et al, 2019).
Secreted Phosphoprotein 2 (SPP2)	SPP2 is a bone matrix protein that inhibits bone morphogenetic proteins and acts as an inhibitor of tumour cell growth in cases of prostate, pancreatic and hepatocellular cancer. Improved survival in breast and lung cancer patients was connected to increased SPP2 expression. However, its overexpression has been linked to poor prognosis in patients diagnosed with ovarian cancer. (Tu et al, 2019).
Selenium Binding Protein 1 (SELENBP1)	SELENBP1 covalently binds to selenium and plays roles in protein degradation, intra-Golgi transport as well as modulating cellular redox reactions (Elhodaky and Diamond, 2018).

Serpin Family B Member 12 (SERPINB12)	A human clade B/intracellular inhibitor of trypsin-like proteinases found in various tissues including the cerebellum and has been found to primarily localised in the epithelium of most organs and alveolar macrophages. It may have roles in processing of proteins and host defence through inhibiting bacterial and viral proteases (Niehaus et al, 2015).
Thrombospondin type 1 domain containing 4 (THSD4).	THSD4 encodes ADAMTSL6, a microfibril-associated protein that binds to fibrillin-1 promoting fibrillin-1's matrix assembly (Elbitar et al. 2021).
USO1 Vesicle Transport Factor (USO1)	A vesicle transport factor which regulates vesicle trafficking from the ER to the Golgi apparatus. Expression of USO1 has been linked to colon, breast and gastric cancer (Yoon et al, 2021).

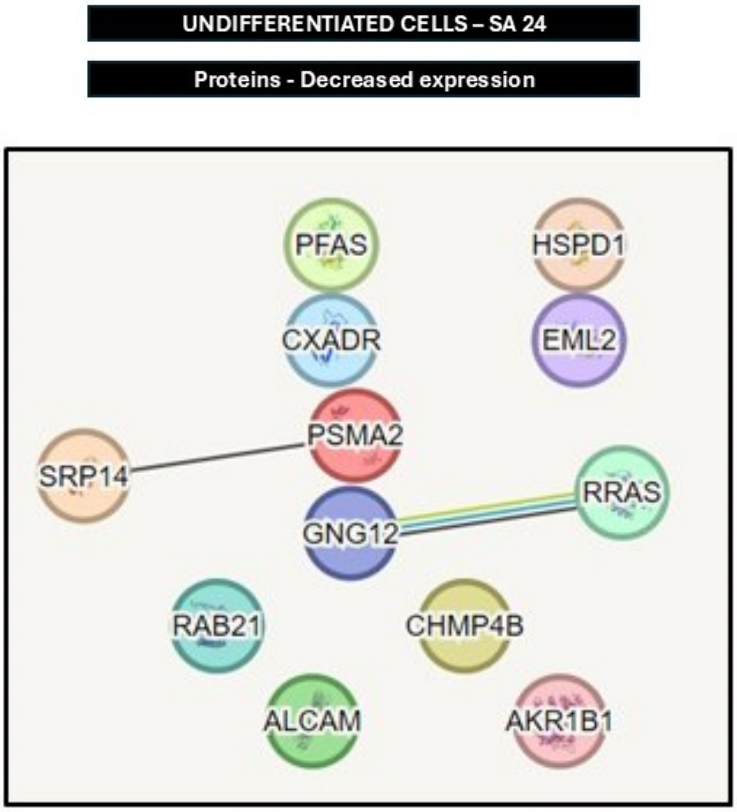

Figure 6.12 STRING analysis of sEV proteins found to have reduced expression in response to SA 24 hr treatment. Proteins found to have decreased expression upon 24 hr treatment with SA according to LC-MS proteomic analysis were entered into the STRING software to provide information regarding connections between the proteins. STRING analysis colour definitions: red – fusion evidence; green – neighbourhood evidence; blue: co-occurrence; purple - experimental evidence; yellow – text-mining evidence; light blue – evidence sourced from other databases; black line – proteins found to be co-expressed.

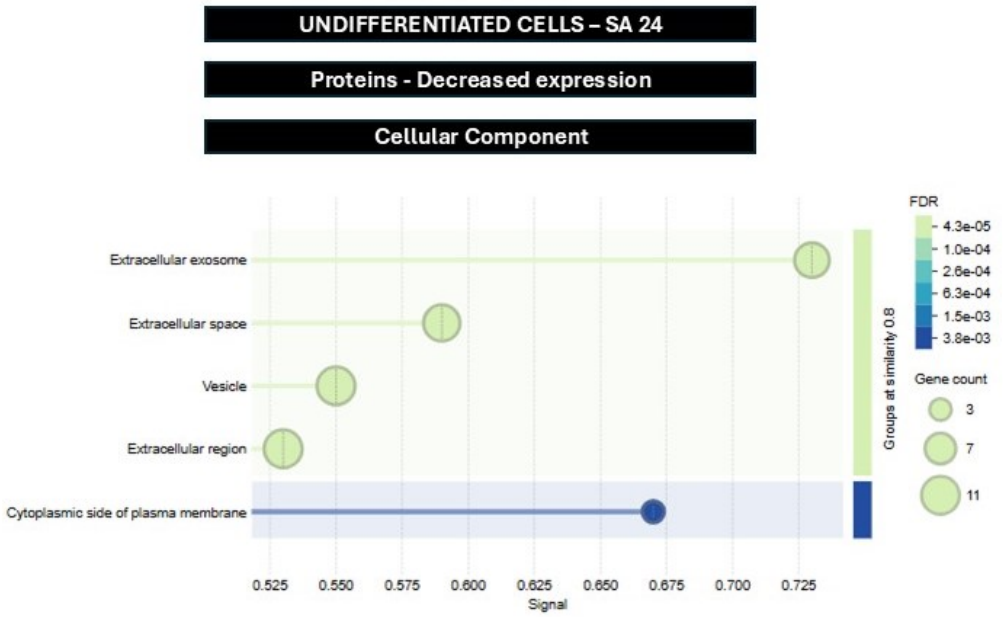

Figure 6.13 Gene ontology analysis of sEV proteins with reduced expression in response to SA 24 hr treatment. Proteins found to have decreased expression upon 24 hr treatment with SA was subjected to gene ontology analysis via STRING software. The connections between the detected sEV proteins yielded significant enrichment in various cellular components associated with EVs and the extracellular sspace.

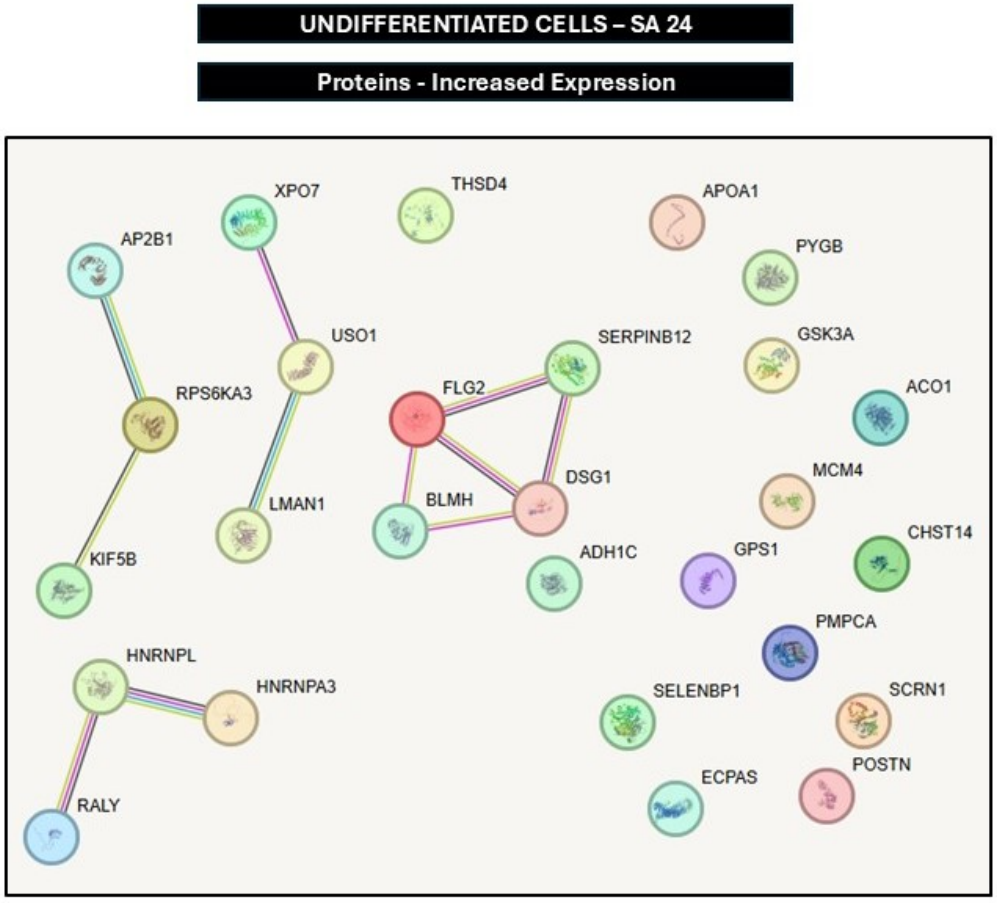

Figure 6.14 STRING analysis of sEV proteins with increased expression in response to SA 24 hr treatment. Proteins found to have increased expression upon 24 hr treatment with SA according to LC-MS proteomic analysis were entered into the STRING software to provide information regarding connections between the proteins. STRING analysis colour definitions: red – fusion evidence; green – neighbourhood evidence; blue: co-occurrence; purple - experimental evidence; yellow – text-mining evidence; light blue – evidence sourced from other databases; black line – proteins found to be co-expressed.

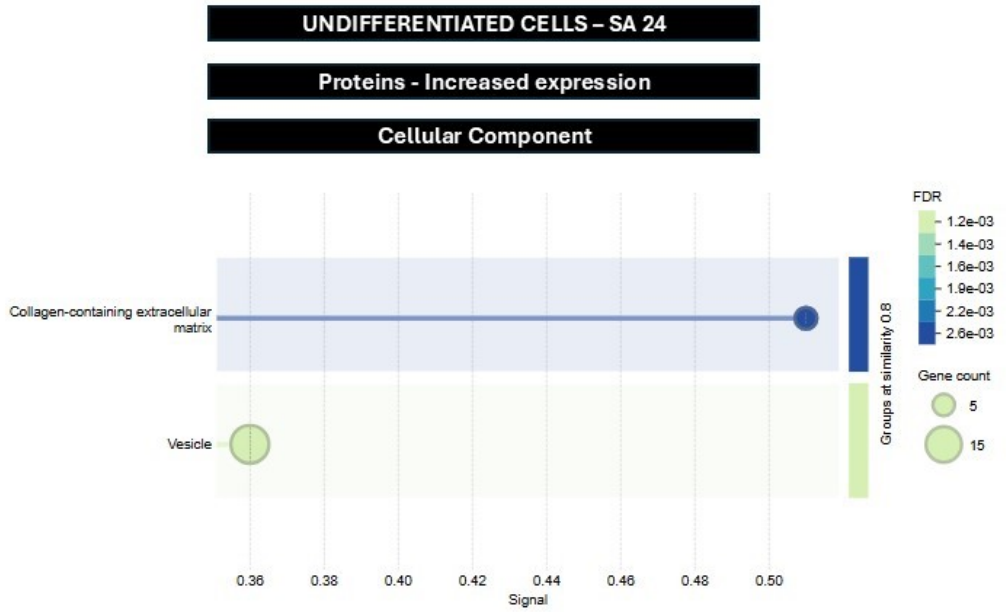

Figure 6.15 Gene ontology analysis of sEV proteins with increased expression in response to SA 24 hr treatment. Proteins found to have increased expression upon 24 hr treatment with SA was subjected to gene ontology analysis via STRING software. The connections between the detected sEV proteins yielded significant enrichment in various cellular components and had associations with female organ tissues.

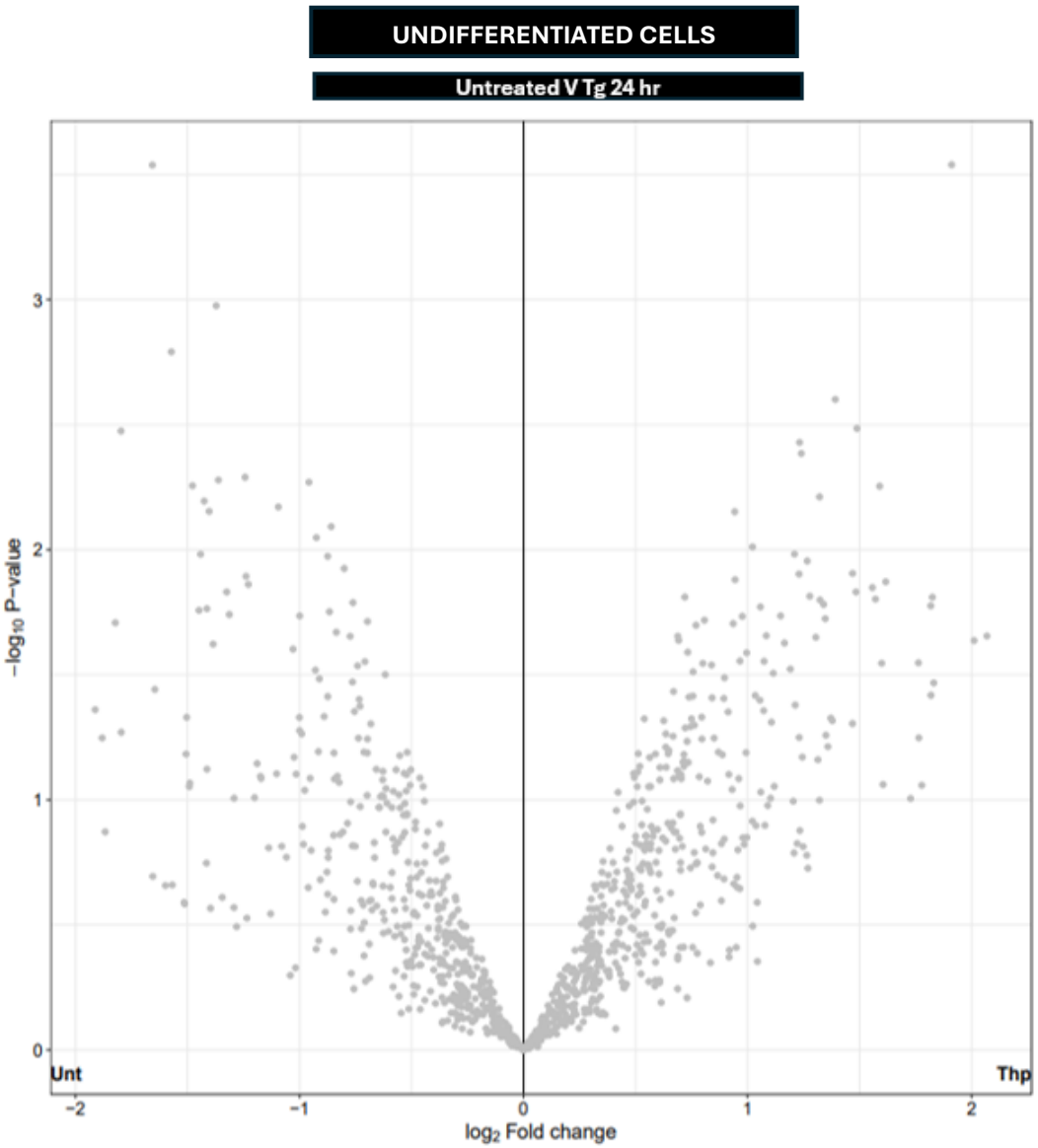

Figure 6.16 LC-MS analysis of sEV proteins derived from cells treated with Tg 24 hr. When proteins found in sEVs derived from the Tg condition was compared to the untreated condition, there appeared to be no significantly different changes in the expression of proteins found in the isolated EVs. (*n=3*). Proteins included in the volcano plot were identified as significant through and made visible on the volcano plot by cutoffs for alpha (0.5) and log fold change (0.5). In this case no proteins were identified.

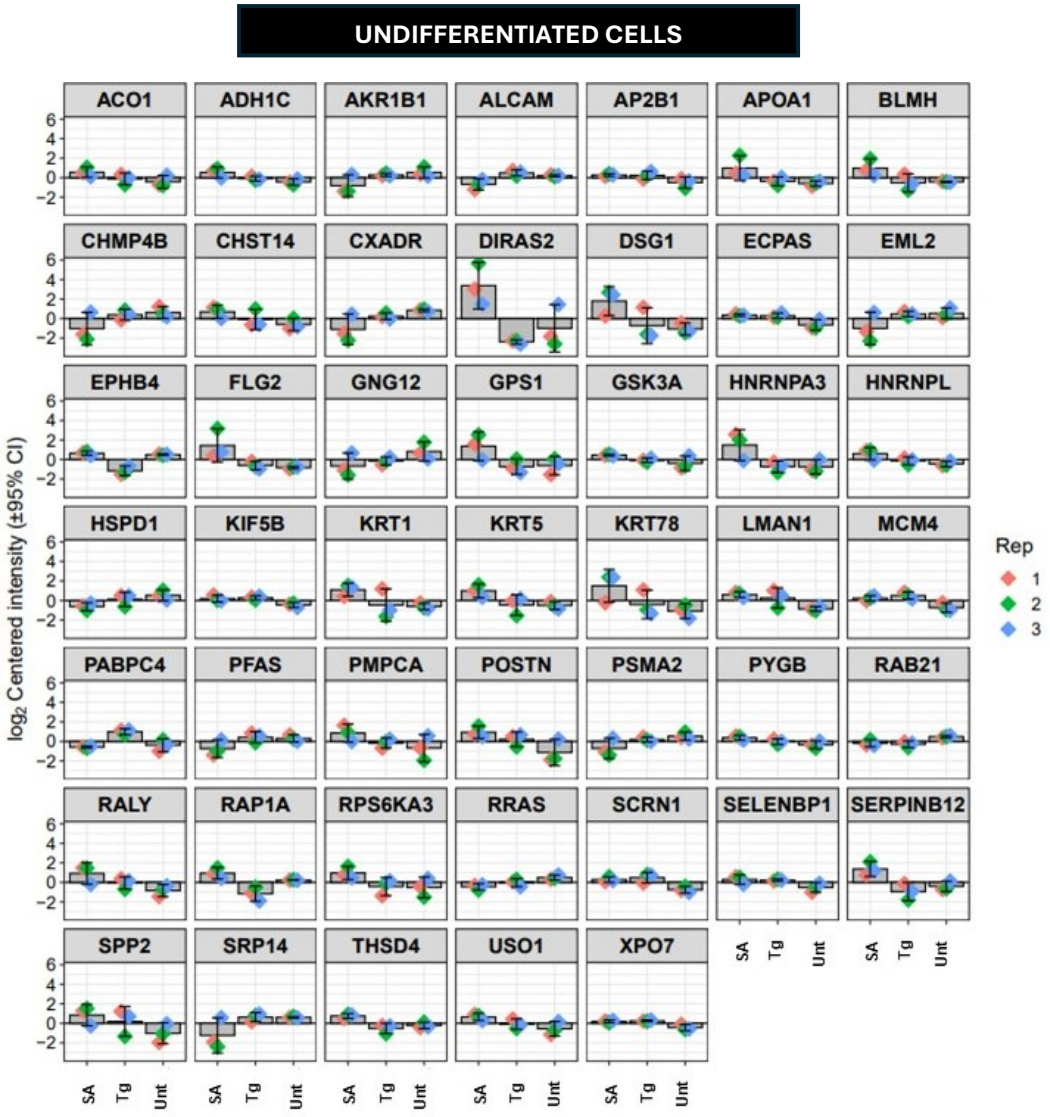

Figure 6.17 Log_2 centred intensity of sEV proteins derived from cells treated with undifferentiated SA and Tg. Undifferentiated cells were treated with 10 μM SA and 0.15 μM Tg for 24 hr. The log_2 centred intensity was calculated of significant proteins. These proteins were included by user defined cutoffs for alpha (0.5) and log fold change (0.5). In this case no proteins were identified.

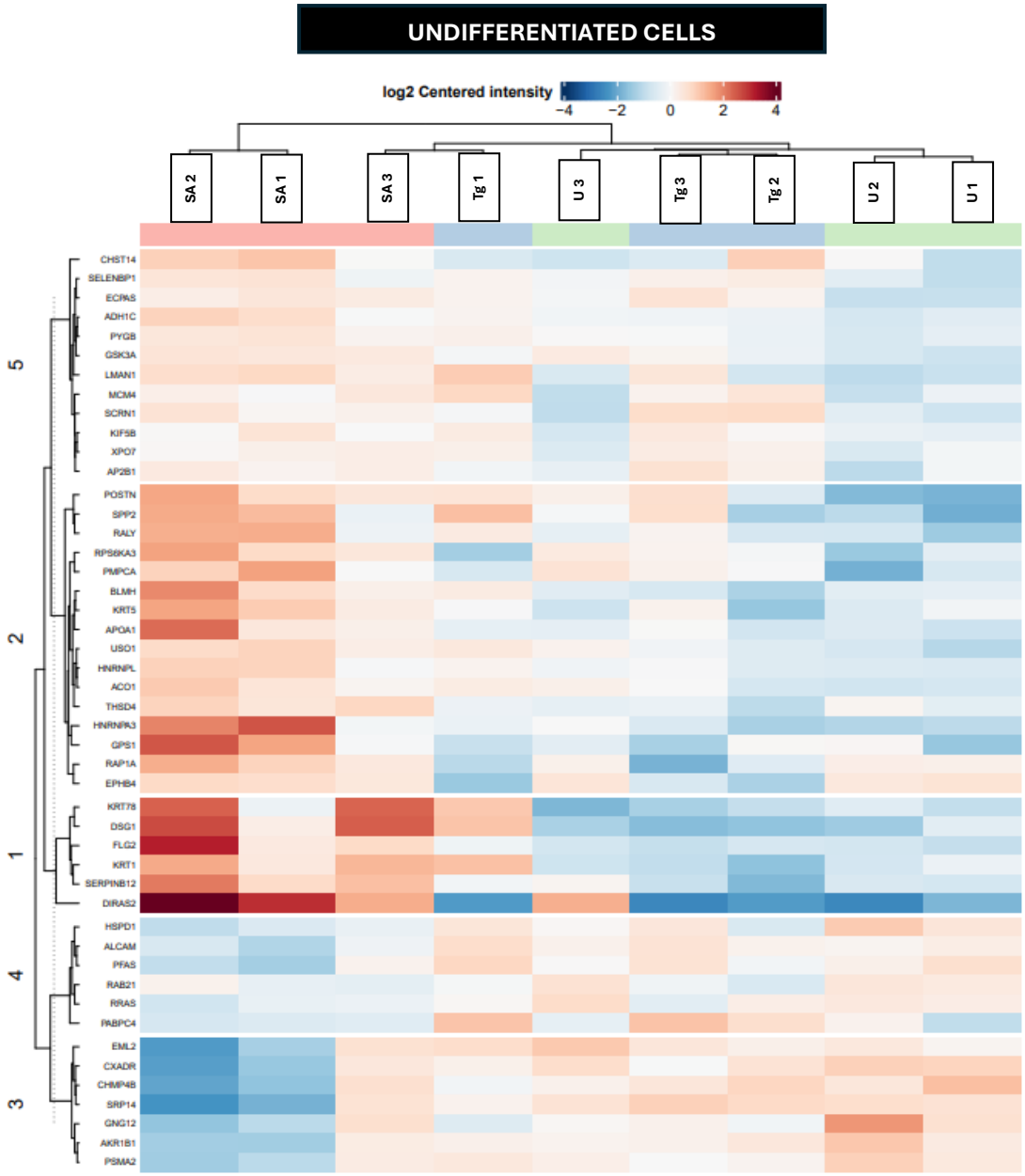

Figure 6.18 sEV protein expression in response to SA and Tg treatment of undifferentiated SH-SY5Y cells. Clustered heatmap presents LC-MS proteomic analysis of sEVs derived from undifferentiated SH-SY5Y cells subjected to SA and Tg 24 hr treatment. Proteins shown have been determined to be significant and log2 centred intensity normalisation is used to determine proteins with reduced expression (blue to white) and increased (orange to burgundy/purple) expression in individual conditions. Colour coded condition is indicated on the top of the heatmap: SA (pink), untreated (green), Tg (blue).

6.2.8 Oligomer and PFF treatment of undifferentiated SH-SY5Y cells are positive for α-synuclein as well as proteins indicatory of stress induction

LC-MS analysis was also carried out on sEVs derived from oligomer and PFF (48 hr) treated undifferentiated cells to understand how α-synuclein aggregates would alter protein expression in sEVs derived from SH-SY5Y cells. It was shown that oligomers and PFFs are able to induce intracellular aggregation in undifferentiated cells (**Figure 5.1**). With this in consideration establishing if sEVs are a vehicle for transmission of α-synuclein was of particular interest. SNCA (α-synuclein) was found to have increased expression in response to 0.1 mg/mL oligomer 48 hr treatment (**Figure 6.19**). Further, other proteins identified to have altered expression in response to oligomer treatment was reported in **Table 5.3 and 5.4**.

LAMC1 and LAMB1 were proteins detected to reduce in sEV samples derived from cells treated with oligomers (**Figure 6.20**). Both proteins are laminins shown to be both important in development, where LAMC1 has been found in adaxial cells during somitogenesis and LAMB1 is detected in all cells localised around the notochord (Sztal et al, 2011).

0.1 mg/mL PFFs treatment for 24 hr yielded similar result where there was a significant increase in the expression of SNCA (**Figure 6.21**)**.** Other proteins identified alongside SNCA that had increased expression in sEVs in response to PFF treatment (48 hr) were reported in **Table 6.5 and 6.6**.

It is also important to consider the presence of SNCA in sEVs in response to oligomer and PFF cell treatment could also be attributed to the input material used to treat cells (oligomers and PFFs) being detected by LC-MS.

Moreover, STRING analysis indicated that amongst the proteins identified to have reduced expression in sEVs in response to PFF exposure was MACROH2A2, MACROH2A, H2BC18, H1-0, H3-3B, H2BC21, H1-5, H1-3 and FEN1 had connections (**Figure 6.22**). These are histone proteins involved in gene expression and chromatin stabilisation (Costanzi and Pehrson, 2001; Ojaimi et al, 2025). FEN1 was linked to H3-3B and H2BC21 (**Figure 6.22**); FEN1 is a nuclease that removes 5’ flaps involved in DNA repair and

degradation, it also is an important contributor to histone modifications (Zhang et al, 2016).

Gene ontology analysis also showed that the linked proteins with decreased expression are involved in the regulation of DNA and gene expression (**Figure 6.23**).

PTK7 and SCRIB were proteins identified to increase in expression in sEVs upon PFF treatment (**Figure 6.24**). It was reported that PTK7 and SCRIB double heterozygous variants were identified in a spina bifida case when investigating neural tube defect conditions (Lei et al, 2018) suggesting that both proteins are important in cellular development.

Log_2 centred intensity was calculated for each of the sEV proteins detected in oligomer, PFF and untreated conditions that were also determined to be significant (**Figure 6.25**). α-Synuclein (SNCA) expression was found to experience the largest fold change in response to oligomers and PFFs compared to the untreated condition but more so in response to oligomer treatment. Detected sEV proteins mentioned in **Figure 6.25** found to have increased and decreased expression specifically when comparing oligomers to the untreated condition was discussed in **Tables 6.3 and 6.4**. Proteins detected in sEVs, when comparing PFFs to untreated were discussed in **Tables 6.5 and 6.6**. Additional proteins were found to increase in response to the oligomer condition compared to PFF condition:

- eukaryotic translation initiation factor 2 subunit 3 (EIF2S3) – encodes the gamma subunit of the translation initiation factor eIF2 and important in the translation mechanism (Gregory et al, 2019).
- flap endonuclease (FEN1) - enzyme essential in DNA replication and repair (Guo et al, 2020).
- macroH2A.2 histone (MACROH2A2) - a histone variant that contributes to the chromatin shaping (Nikolic et al, 2023).
- reticulon 4 (RTN4) - ER protein that regulates the morphology of the ER (Konno et al, 2024).
- stathmin 4 (STMN1) - promotes the disassembly of the mitotic spindle, necessary for cell cycle and differentiation (Jing et al, 2024).

The following sEV proteins were found to increase in response to PFFs when compared to the oligomer condition:

- collectin 11 (COLEC11) – involved in innate defence mechanisms (Farrar et al, 2016).
- intracellular adhesion molecule 1 (ICAM1) – cell surface protein important in inflammation (Bui et al, 2021).
- peptidoglycan recognition protein 1 (PGYRP1) – a pattern recognition protein that is necessary for antibacterial responses and involved in immune mechanisms.
- tenascin-C (TNC) – an extracellular matrix protein that has been linked to chronic inflammation (Yilmaz et al, 2022).

Clustered heatmaps based on $\log_2$ centred intensity was used to summarise protein expression in the different treatment conditions (untreated, oligomer and PFF) (**Figure 6.26**).

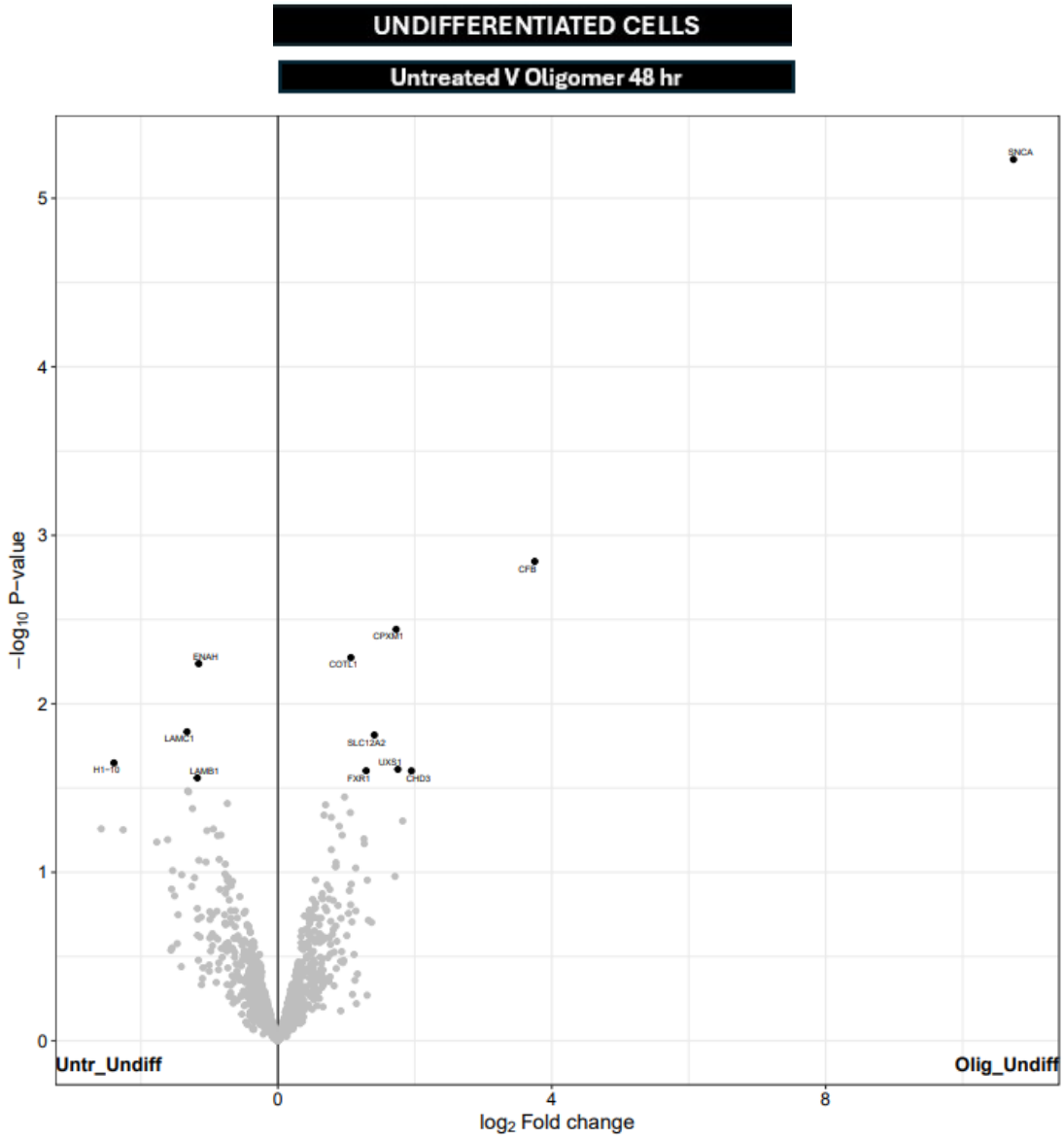

Figure 6.19 LC-MS analysis of sEV proteins in response to cell treatment with oligomer 48 hr. A number of proteins were found to experience an increase in expression in response to 48 hr of oligomer treatment as seen in the right section of the volcano plot. The left section however shows proteins with reduced expression in response to the oligomer treatment. (*n=3*). Proteins have been disclosed in **Table 6.3 and 6.4**. Proteins included in the volcano plot were identified as significant and made visible on the volcano plot through cutoffs for alpha (0.5) and log fold change (0.5).

Table 6.3 Decreased expression of oligomer treated cellular sEV proteins. The proteins found to have decreased expression in the sEV sample when comparing the oligomer 48 hr treatment condition to untreated conditions. Proteins included in the table were identified as significant and made visible on the volcano plot through cutoffs for alpha (0.5) and log_2 fold change (0.5).

Undifferentiated Cells (Oligomers 48 hr)	
Protein	**Reported role/Disease Association**
Enabled homolog (ENAH)	ENAH is a member of the enabled/vasodilator stimulated phosphoprotein gene family that binds to actin. It has been linked to a variety of cancer types including but not limited to gastric and breast cancer (Deng et al, 2022).
Histones 1-10 (H1-10)	These histones are expressed in somatic cells and has been linked to remodelling of chromatin as well as establishing cell state specificity (Izzo et al, 2017).
Laminin subunit beta-1 (LAMB1)	LAMB1 is an extracellular matrix protein present in most tissues that is linked to MAPK pathway (Lee et al, 2021).
Laminin subunit gamma-1 (LAMC1)	LAMC1 is an extracellular matrix protein (Durham et al, 1995) that is now considered an oncogene linked to the cell-to-cell signal transduction in the tumour microenvironment as well as tumour cell invasion (Fang et al, 2021).

Table 6.4 Increased expression of oligomer treated cellular sEV proteins. The proteins found to have increased expression in the sEV sample when comparing the oligomer 48 hr treatment condition to untreated conditions. Proteins included in the table were identified as significant and made visible on the volcano plot through cutoffs for alpha (0.5) and log_2 fold change (0.5).

Undifferentiated Cells (Oligomer 48 hr)	
Protein	**Reported role/Disease Association**
Carboxypeptidase X, M14 Family Member 1 (CPXM1)	CPXM1 belongs to the carboxypeptidase family and is believed to regulate adipogenesis and regulate extracellular matrix remodelling. It has been demonstrated to be a biomarker of various cancers including breast and ovarian cancer (Gu et al, 2024).
Chromodomain Helicase DNA Binding Protein 3 (CHD3)	CHD3 remodels chromatin plus facilitates the nucleosome mobilization, it has also been shown to be inactivated in numerous cancers (Mills, 2017).
Coactosin Lie F-Actin Binding Protein 1 (COTL1)	COTL1 belongs to the ADF-H domain protein superfamily and linked to the stabilisation of actin filaments. Additionally, COTL1 has been linked to TGF-β signalling pathway inhibition (Lechuga et al, 2024).
Complement Factor B (CFB)	CFB is a serine protease that acts as C3 convertase and has been linked to the activation of the complement alternative pathway which is linked to inflammation and immunologic regulation (Huang et al, 2002).
FMR1 Autosomal Homolog 1 (FXR1)	One of a group of Fragile-X-related RNA binding proteins that is associated with mRNA metabolism, transport, translation and degradation (Méndez-Albelo et al, 2024). It has also been found to be recruited into SGs during stressed SH-SY5Y cells as shown when cells were treated with SA (Valina et al, 2025).
Solute Carrier Family 12 Member 12 (SLC12A2)	Studies have shown that SLC12A2 is a transporter protein involved in corticogenesis and brain development (McNeill et al, 2020).
UDP-Glucuronate Decarboxylase 1 (UXS1)	UXS1 catalyses the reaction from UDP-glucuronrate to UDP-xylose where UDP-xylose is essential for the biosynthesis of glycosaminoglycan found in proteoglycans core proteins. Proteoglycans themselves are important in numerous signalling

	pathways particularly to allow for successful development (Moriarity et al, 2002).
α-Synuclein (SNCA)	SNCA is localised in the nerve terminals and has been linked to the regulation of the synaptic vesicles specifically inhibiting neurotransmitter release. It is primarily known for its links to PD (Bendor et al, 2013).

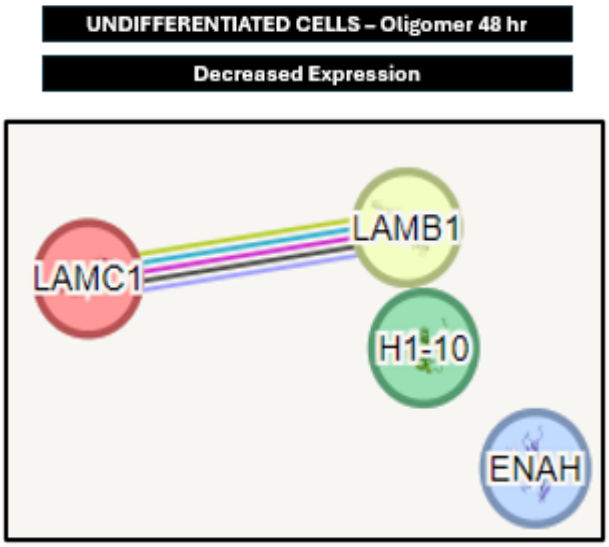

Figure 6.20 STRING analysis of sEV proteins found to have decreased expression in response to oligomer 48 hr treatment. The proteins identified to have a connection that was of interest had reduced expression compared to the control in response to oligomer treatment. STRING analysis colour definitions: red – fusion evidence; green – neighbourhood evidence; blue: co-occurrence; purple - experimental evidence; yellow – text-mining evidence; light blue – evidence sourced from other databases; black line – proteins found to be co-expressed.

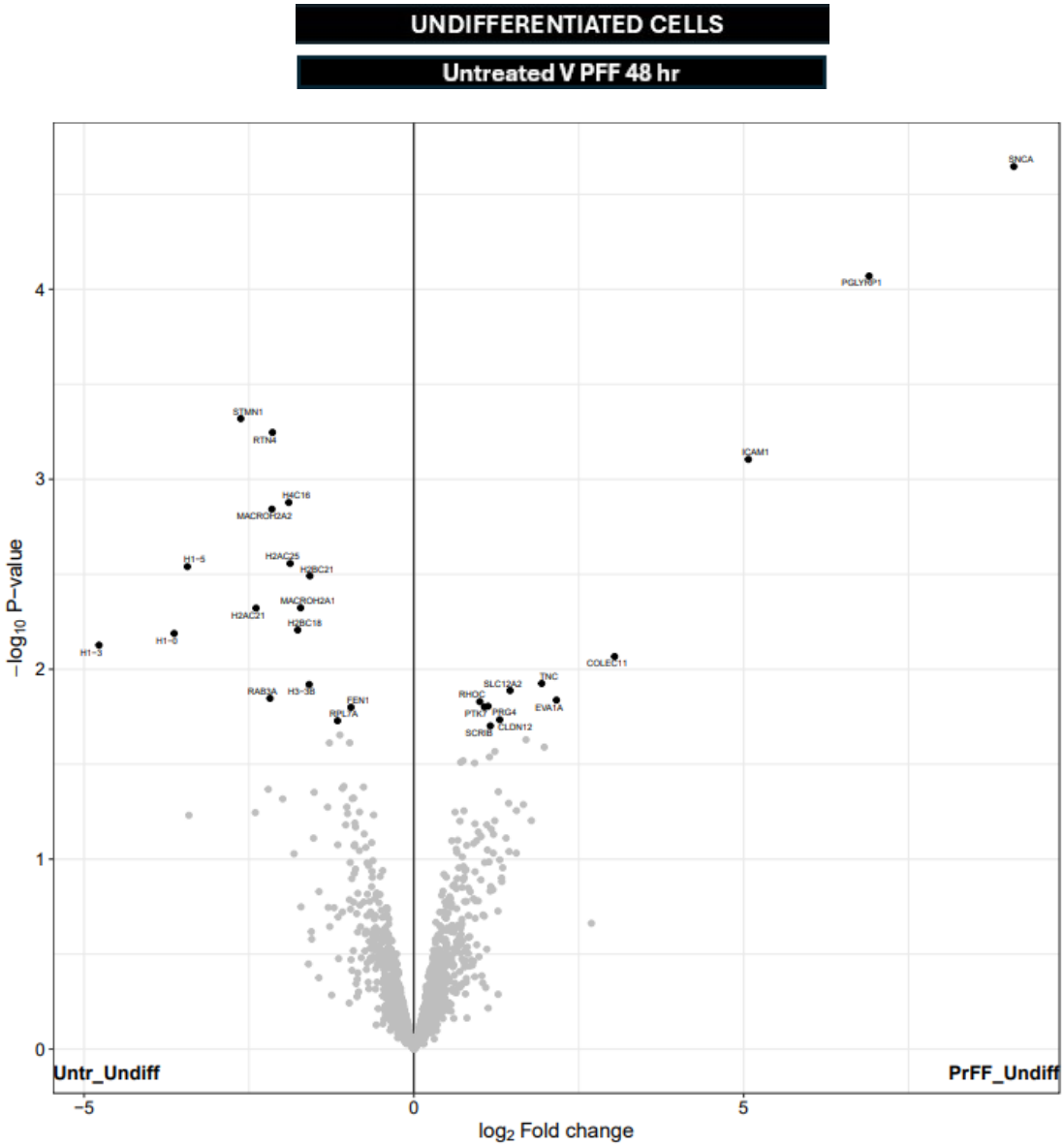

Figure 6.21 LC-MS analysis of sEV proteins isolated from cells treated with PFF 48 hr. A number of proteins were found to experience an increase in expression in response to 48 hr of PFF treatment as seen in the right section of the volcano plot. The left section however shows proteins with reduced expression in response to the oligomer treatment (*n=3*). Proteins have been disclosed in **Table 6.5 and 6.6**. Proteins included in the volcano plot were identified as significant and made visible on the volcano plot through cutoffs for alpha (0.5) and log fold change (0.5).

Table 6.5 Decreased expression of PFF treated cellular sEV proteins. The proteins found to have decreased expression in the sEV sample when comparing the PFF 48 hr treatment condition to untreated conditions. Proteins included in the table were identified as significant and made visible on the volcano plot through cutoffs for alpha (0.5) and log_2 fold change (0.5).

Undifferentiated Cells (PFF 48 hr)	
Protein	**Reported role/Disease Association**
Core histone macro-H2A.1 (MACROH2A1)	A histone variant that regulates mitochondrial respiration through the modulation of poly (ADP-ribose) polymerase (PARP) activity.
Core histone macro-H2A.2 (MACROH2A2)	MACROH2A2 encodes the core histone H2A variant that is involved in the repair of double-stranded breaks and differentiation modulation. The downregulation or loss of MACROH2A2 has been linked to numerous malignancies such as bladder, lung cancer as well as glioblastoma (Nikolic et al, 2023).
Flap endonuclease 1 (FEN1)	An enzyme important in the maintenance of eukaryotic genome stability, specifically through its participation of DNA replication and repair. It has also been identified as a protein essential to the suppression of tumours (Henneke et al, 2003).
Histone 1.0 (H1-0)	A linker histone classified as a DNA-binding protein involved in the formation of higher order structures of chromatin (Liegro et al, 2018).
Histone 1.5 (H1-5)	A linker histone which organises chromatin and has been linked to mammalian development. It is also believed to be a factor in carcinogenesis (Behrends and Engmann, 2020).
Histone H2B type 2-E (H2BC21)	Belongs to the H2B Clustered Histone family with roles in cell cycle distribution. H2BC21 has been linked to glioma categorised to have a poor prognosis (Jia et al, 2022).
Histone H2B type 2-F (H2BC18)	A clustered histone variant of H2B which forms part of the core of the chromatin's nucleosome essential to processes such as DNA replication, repair and recombination (Jiang et al, 2020).
Histone H3.3 (H3-3B)	Encodes H3.3 expressed in embryonic and differentiated cells plus implicated in a variety of cancers. It is a DNA-binding protein involved in repair of DNA damage (Okur et al, 2021).

Histones 1.3 (H1-3)	H1-3 is a canonical, somatic histone essential to chromatin remodelling and correct development (Izzo et al, 2013)
Ras-related protein Rab-3A; (RAB3A)	RAB3A regulates neurotransmitter release and influences calcium-induced synaptic vesicle exocytosis (Yang et al, 2010).
Reticulon-4 (RTN4)	Essential to the structure of the ER. It has been found that the loss of RTN4 does not affect ER functions as such nor does it result in activation of the UPR, but store-operated calcium entry is altered (Jozef et al, 2014).
Ribosomal protein L7a (RPL7A)	RPL7A has been linked to alcohol (consumption) linked breast cancer. It is an ethanol-response factor in the breast cancer cells; its expression is increased in response to ethanol.
Stathmin (STMN1)	STMN1 regulates the microtubule skeleton and engages microtubule depolymerisation - processes necessary in the regulation of the cell cycle particularly mitosis. Dysfunction of STMN1 leads to a reduction in cell proliferation (Rubin and Atweh, 2004).

Table 6.6 Increased expression of PFF treated cellular sEV proteins. The proteins found to have increased expression in the sEV sample when comparing the PFF 48 hr treatment condition to untreated conditions. Proteins included in the table were identified as significant and made visible for the volcano plot through cutoffs for alpha (0.5) and log_2 fold change (0.5).

Undifferentiated Cells (PFF 48 hr)	
Protein	**Reported role/Disease Association**
Claudin-12 (CLDN12)	A member of the claudin protein family and claudin-12 is considered to be an atypical member. It is involved in paracellular Ca^{2+} transients. It has been linked to cancer cell migration and invasion plus cancer metastasis (Apostolova et al, 2024).
Collectin subfamily member 11 (COLEC11)	A pattern recognition receptor which belongs to the C-type lectin superfamily (Wang et al, 2023). Its primary roles are host defence, development of the embryo, fibrosis and autoimmunity. It is linked to proliferation and growth of cancer cells (Wang et al, 2023)
Inactive tyrosine-protein kinase 7 (PTK7)	PTK7 is also known as a colon carcinoma kinase-4 and regulates the wnt (canonical and non-canonical) signalling pathways. It is important in the tumorigenesis of certain cancers particularly oesophageal squamous cell carcinoma. This protein promotes the proliferation, migration and invasion of different cell types but has been found to be a tumour suppressor in some instances (Shin et al, 2022).
Intercellular adhesion molecule 1 (ICAM1)	A cell surface glycoprotein found in immune, epithelial and endothelial cells. Its expression increases during inflammation particularly induced by inflammatory cytokines. It also regulates the barrier function of epithelial and endothelial cells. (Bui et al, 2020).
Peptidoglycan Recognition Protein 1 (PGLYRP1)	PGLYRP1 is linked to the invasive nature of pancreatic cancer cells. In mammals PGLYRP1 is primarily produced by neutrophils and has been associated with immune evasive mechanisms in T cells secreted from tumours (López-Gil et al, 2024).
Protein eva-1 homolog A (EVA1A)	A lysosome and ER associated protein that has the ability to co-localise with the autophagosome. It promotes autophagy, apoptosis as well as differentiation. It has been found to be expressed in various cancer cells (Canham et al, 2023).

Protein scribble homolog (SCRIB)	SCRIB plays a part in the regulation of cellular polarity which is essential in maintaining not only the morphology of cells but their general function (Su et al, 2012).
Proteoglycan 4 (PRG4)	A mucin-like glycoprotein that is primarily expressed in cells found in the joint and chondrocytes. It plays a role in the lubrication of ocular surfaces and regulate the inflammatory response (Das et al, 2019).
Rho-related GTP-binding protein RhoC (RHOC)	A Rho GTPase sub-family member which regulates signal transduction such as cell shape, division, migration, proliferation and vesicular trafficking. A typical Rho GTPase will mediate the exchange from GDP to GTP and has been determined to be important to cancer pathogenesis (Eckenstaler et al, 2022).
Solute carrier family 12 member 2 (SLC12A2)	Refer to **Table 6.4**
Synuclein Alpha (SNCA)	Refer to **Table 6.4**
Tenascin-C (TNC)	An extracellular matrix protein that belongs to the tenascin family. It regulates cell surface receptors, cell adhesion, migration, proliferation plus differentiation (Gremlich et al, 2020).

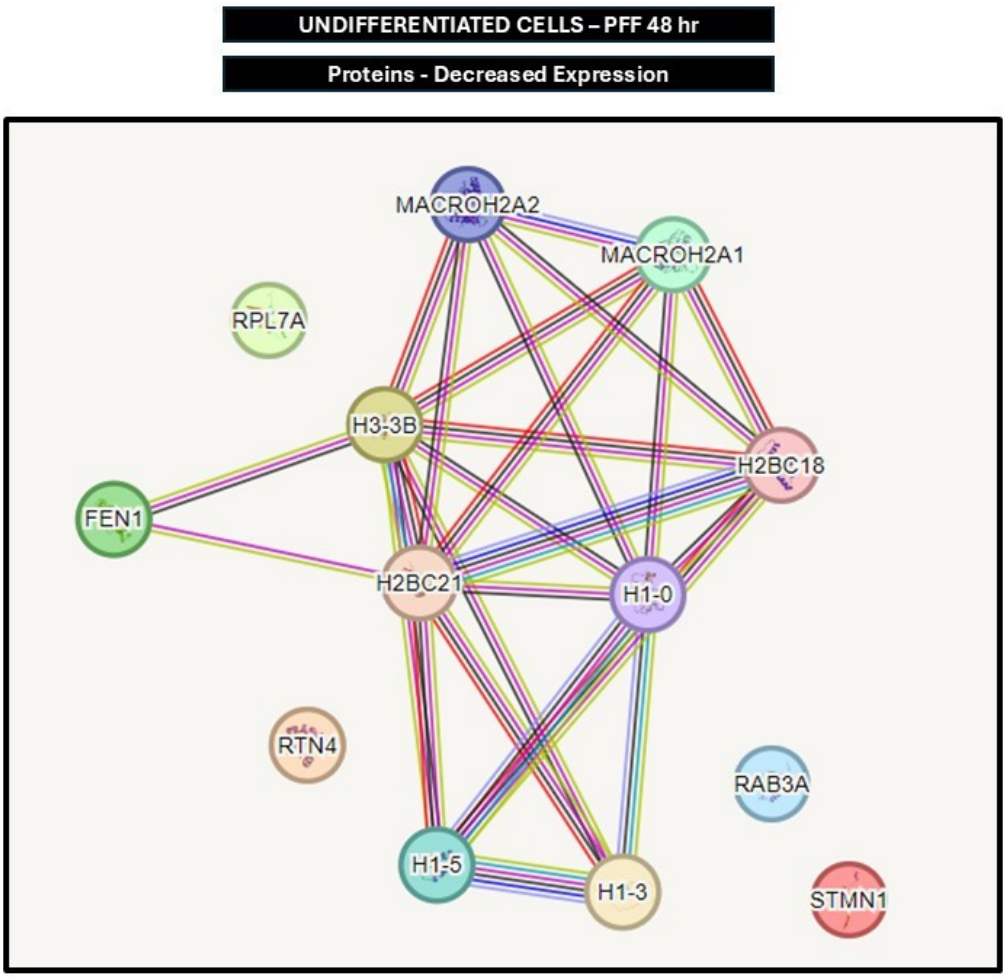

Figure 6.22 STRING analysis of sEV proteins with decreased expression derived from cells treated with PFF 48 hr. The proteins identified to have a connection that was of interest had reduced expression compared to the control in response to PFF treatment. STRING analysis colour definitions: red – fusion evidence; green – neighbourhood evidence; blue: co-occurrence; purple - experimental evidence; yellow – text-mining evidence; light blue – evidence sourced from other databases; black line – proteins found to be co-expressed.

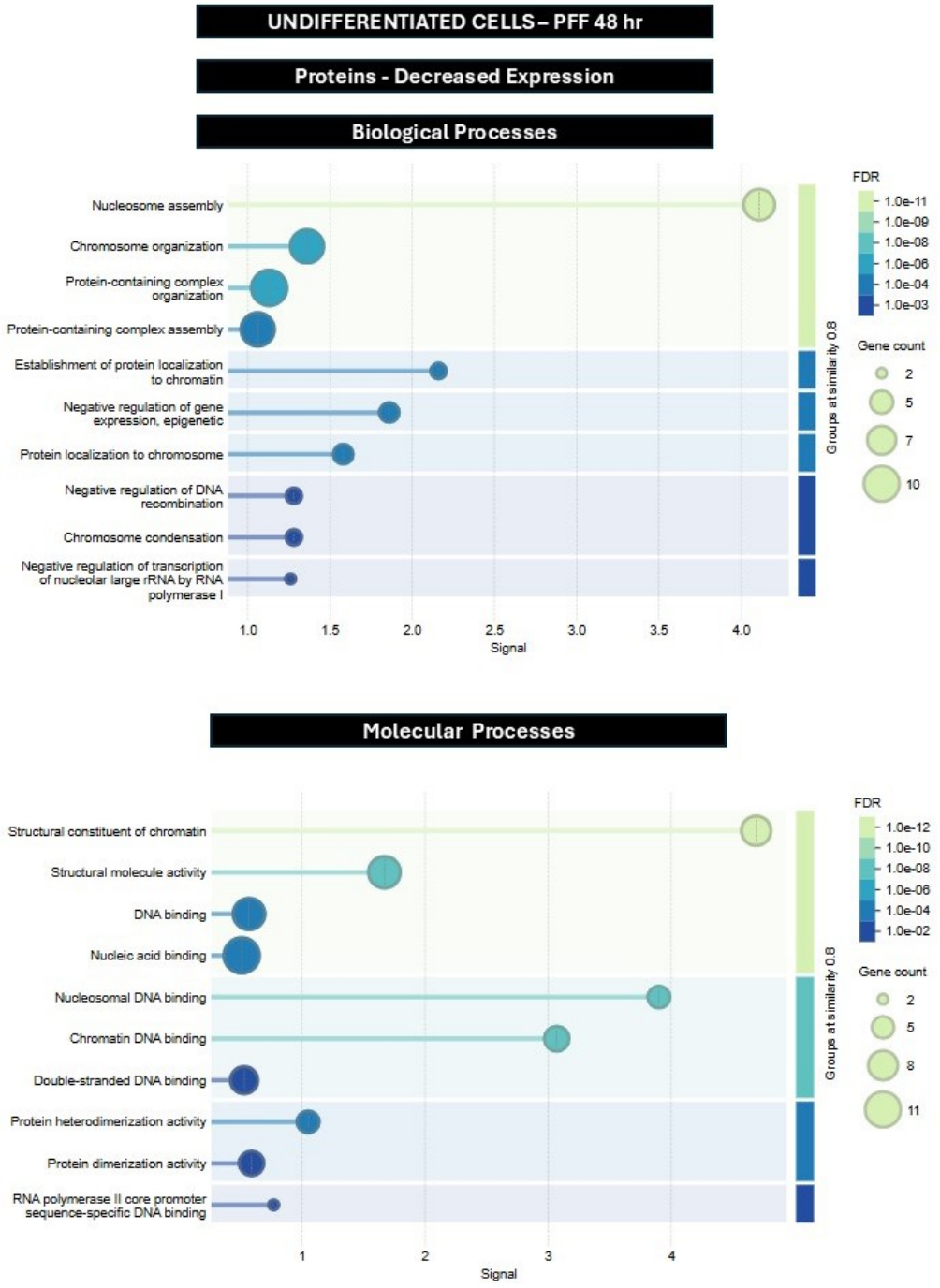

Figure 6.23 Gene ontology analysis of sEV proteins found to have reduced expression isolated from cells subjected to PFF 48 hr treatment. Proteins found to have decreased expression upon 48 hr treatment with PFFs were subjected to gene ontology analysis. The connections between the detected sEV proteins yielded significant enrichment in various biological and molecular processes.

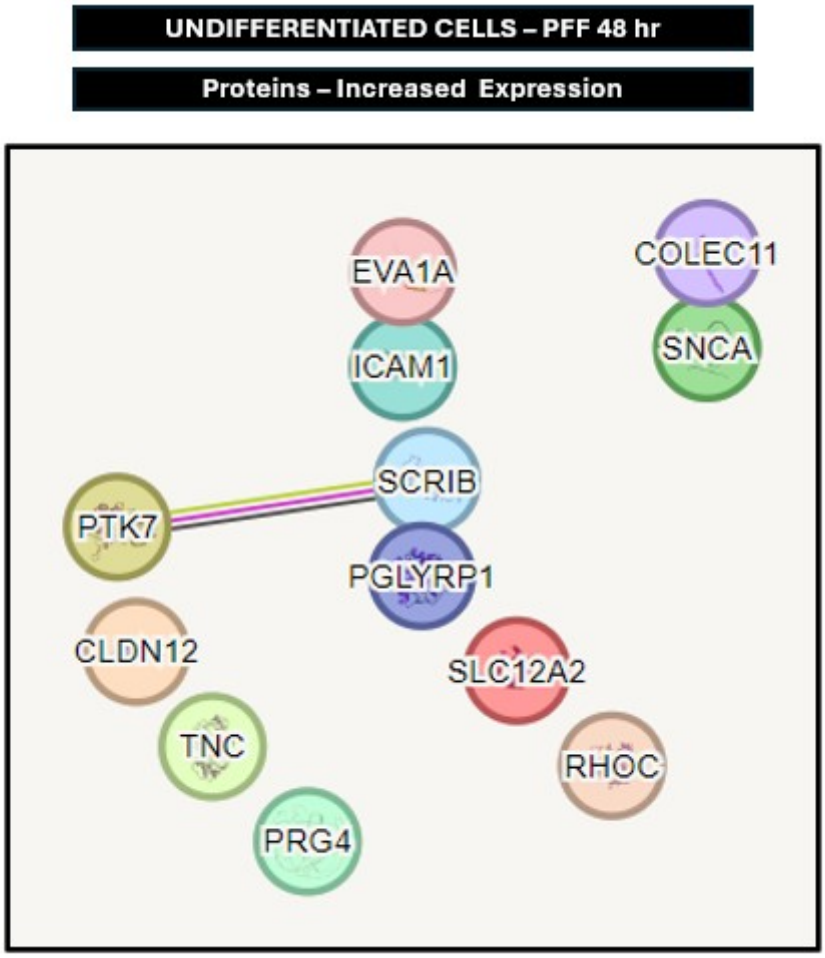

Figure 6.24 STRING analysis of sEV proteins identified to have increased expression isolated from cells treated with PFF 48 hr. The proteins identified to have a connection that was of interest had increased expression compared to the control in response to PFF treatment. STRING analysis colour definitions: red – fusion evidence; green – neighbourhood evidence; blue: co-occurrence; purple - experimental evidence; yellow – text-mining evidence; light blue – evidence sourced from other databases; black line – proteins found to be co-expressed.

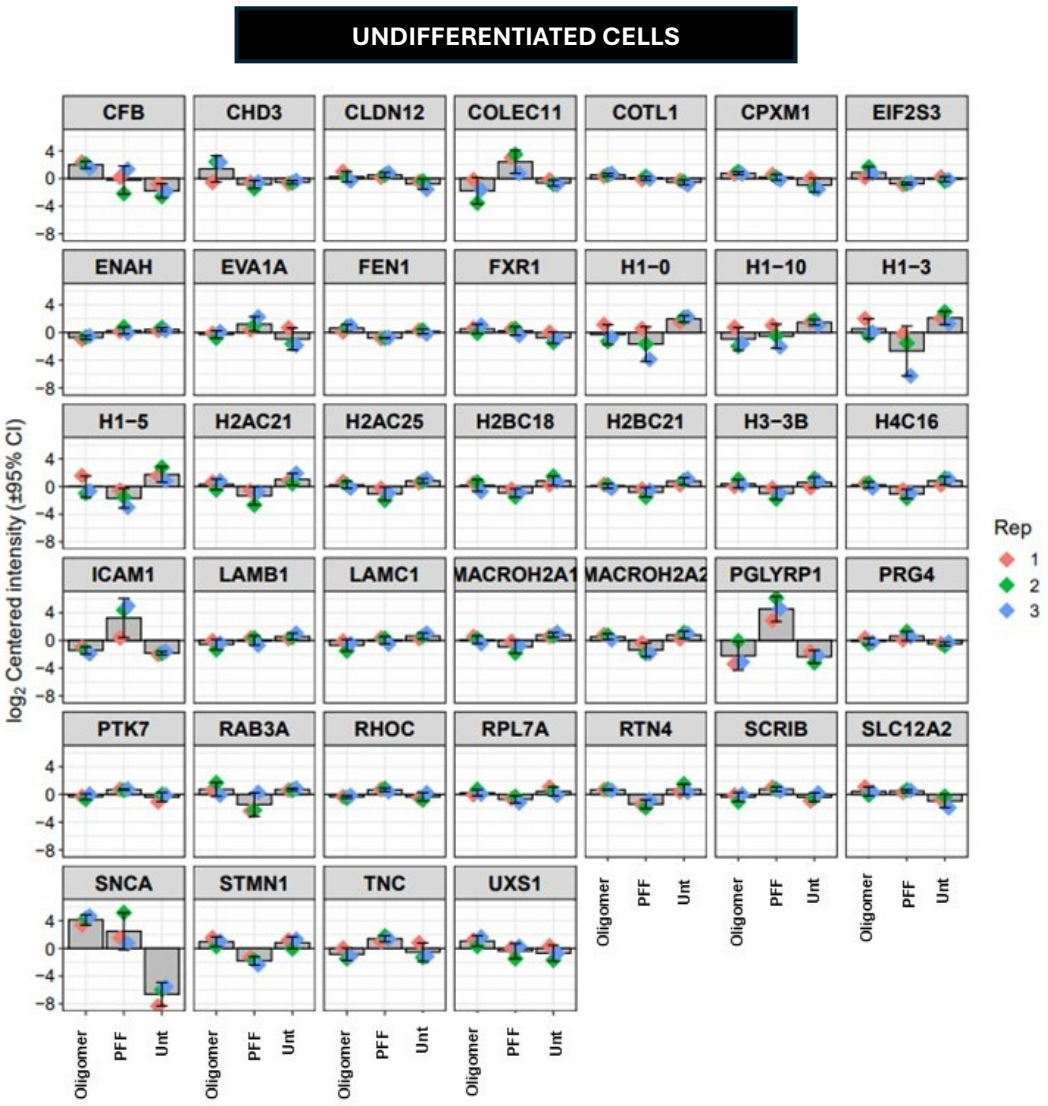

Figure 6.25 Log_2 centred intensity of sEV proteins derived from undifferentiated cells treated with oligomers and PFFs. Undifferentiated cells were treated with 0.1 mg/mL oligomers and PFFs for 48 hr. The log_2 centred intensity was calculated of significant proteins. These proteins were included by user defined cutoffs for alpha (0.5) and log fold change (0.5). In this case no proteins were identified.

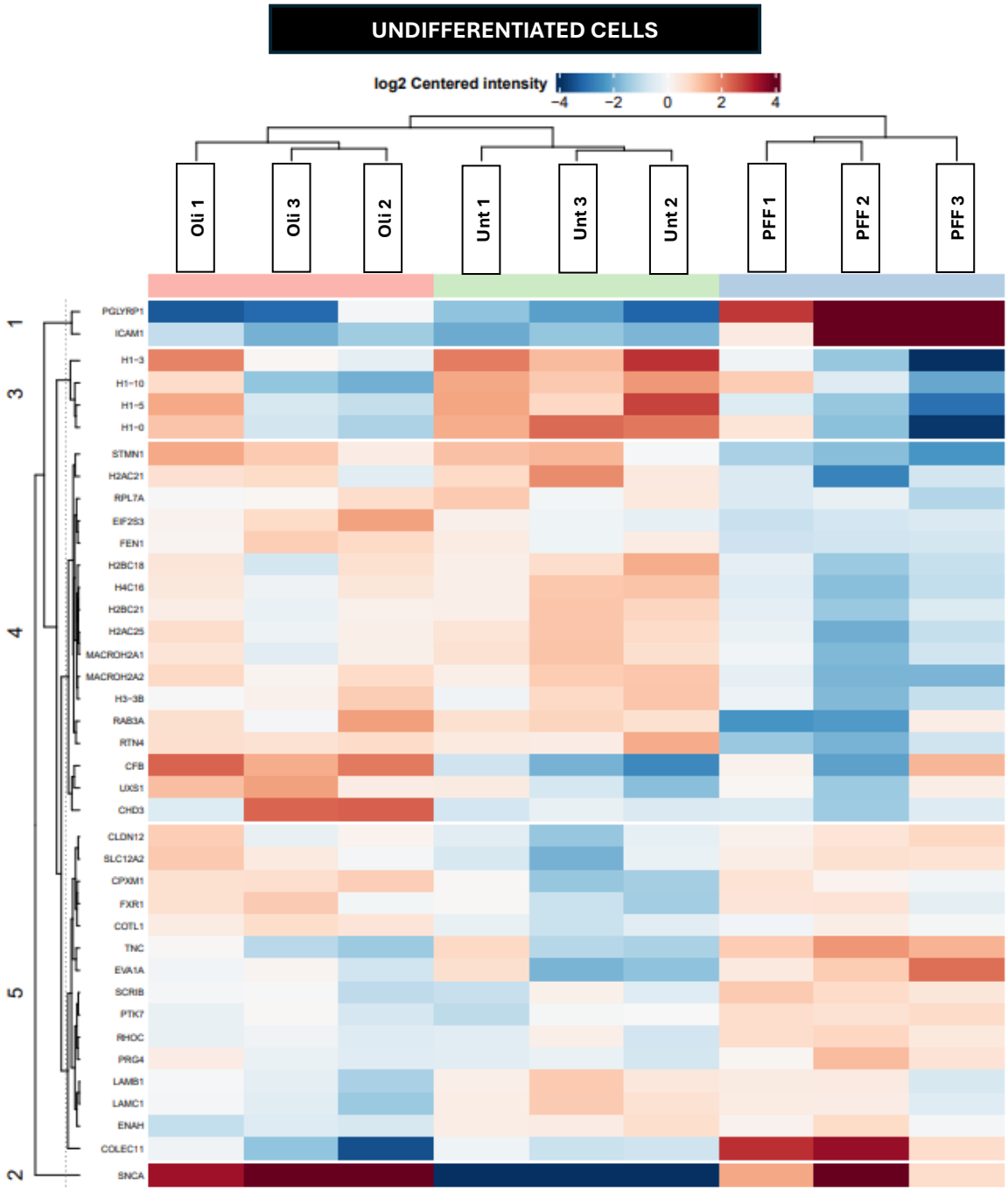

Figure 6.26 sEV protein expression in response to oligomer and PFF treatment of undifferentiated cells. Clustered heatmap presents LC-MS proteomic analysis of sEVs derived from undifferentiated SH-SY5Y cells subjected to oligomer and PFF 48 hr treatment. Proteins shown have been determined to be significant and log2 centred intensity normalisation is used to determine proteins with reduced (blue to white) and increased (orange to burgundy/purple) expression in individual conditions. Colour coded conditions are indicated on the top of the heatmap: oligomers (pink), untreated (green), PFFs (blue).

6.2.9 Mitochondrial and PD associated proteins and α-synuclein are present in sEVs in response to oligomer and PFF treatment of differentiated SH-SY5Y cells

sEVs were isolated from ATRA-differentiated cells treated with either oligomers or PFFs (0.1 mg/mL) for 48 hr. LC-MS proteomic analysis was carried out on sEVs to determine how α-synuclein aggregates would affect sEV proteomic cargo derived from differentiated cells. SNCA was found to have increased expression in sEV samples in response to both oligomer and PFF treatment of differentiated cells (**Figure 6.27 and 6.30**) in a similar manner to the undifferentiated cell line.

Other proteins found to have a reduction or an increase in expression in oligomer-treated cell sEV samples were reported in **Table 6.7 and 6.8**.

STRING analysis of proteins with increased expression in response to oligomer exposure showed connections between SNCA, NDUFB9 and PARK7, which has direct links to PD (**Figure 6.28**). Both SNCA and PARK7 were identified as PD associated genes with identified missense mutations (Nuytemans et al, 2010). When investigating proteins with altered expression in eight brains of individuals diagnosed with PD, it was found that SNCA, NDUFB9, and PARK7 were among 202 mitochondrial proteins (> 1.5-fold) found to have altered expression compared to controls (Toomey et al., 2022).

Gene ontology reported that these linked proteins had roles in synaptic transmission, regulation of the mitochondria's electron transport chain as well as cuprous ion binding (**Figure 6.29**).

Proteins with reduced and increased expression in response to PFF treatment was reported in **Table 6.9 and 6.10**.

SNCA and NDUFS7 were found to have increased expression and linked according to STRING analysis (**Figure 6.31**). Both proteins were identified as mitochondrial proteins reported to have altered expression in PD brains compared to controls (greater than 1.5-fold) (Toomey et al., 2022).

No significant pathway enrichments were identified in the dataset for the PFF 48 hr condition, so gene ontology was not presented.

Log_2 centred intensity was calculated for each of the sEV proteins detected in the oligomer, PFF and untreated conditions that were also determined to be significant (**Figure 6.32**). sEV proteins found to experience a change in expression when comparing the treatment condition to the untreated condition were discussed in **Tables 6.7, 6.8, 6.9 and 6.10.** α-Synuclein/SNCA expression was found to increase in response to oligomers and PFFs compared to the untreated condition but more so in response to oligomer treatment. PARK7 was found to increase in response to oligomers when compared to PFFs and the untreated condition. Large fold changes were seen in the expression of mitochondrial subunits NDUFB9 and NDUFS7 in response to oligomers and PFFs respectively, when compared to the untreated condition. This suggests that in addition to α-synuclein, sEVs will carry mitochondrial subunits and markers of oxidative stress when cells are exposed to oligomers and PFFs. Furthermore, the following sEV proteins were found to increase in response to oligomers when compared to PFFs as seen in **Figure 6.32**:

- Aggrecanase-1 (ADAMTS4) – a metalloproteinase that targets proteoglycans particularly the degradation of proteoglycans in the extracellular matrix (Lemarchant et al, 2017).
- Eps15 homology domain (EHD4) – involved in endocytic trafficking (Sharma et al, 2008).
- G protein subunits 11 (GNA11) - forms the alpha subunit of G proteins allowing for a range of signalling processes to take place (Pilch et al, 2024).
- Glutamyl-prolyl-tRNA synthetase 1 (EPRS1) – allows for the binding of certain amino acids to their respective tRNA (Yang et al, 2023).
- Integral membrane protein 2 B (ITM2B) – is involved in amyloid β metabolism (Wohlschlegal et al, 2021).
- NADH dehydrogenase [ubiquinone] 1 beta subcomplex subunit 9 **(**NDUFB9) - an accessory subunit of the mitochondria's respiratory chain (Li et al, 2015).
- Peptidase inhibitor 15 **(**PI15) - acts as a serine protease inhibitor (Prusty et al, 2018).

- Platelet-activating factor acetyl hydrolase 1B1 (PAFAH1B12) – involved in neuronal migration and layer formation in cells essential to development (Feng et al, 2024).
- Protein/nucleic acid deglycase DJ-1 (PARK7) – involved in the regulation of oxidative stress (Skou et al, 2024).
- Ras-related protein Rab-5A (RAB5A) – involved in neuronal endocytosis (fusion of enodcytic vesicles to early endosomes (Hoop et al, 1994).
- Scribble (SCRIB) – a polarity protein important in cell differentiation and synaptic function (Qin et al, 2005).
- Transforming growth factor beta regulator 4 (TBRG4) – involved in regulating the cell cycle by the stabilisation of regulatory proteins involved in the cell cycle (Tao et al, 2024).
- Valine aminoacyl-tRNA synthetase (VARS1) – involved in the esterification of amino acids to their respective tRNA (Hiz et al, 2022).

The following sEV proteins were found to increase in response to PFFs when compared to oligomers as seen in **Figure 6.32**:

- 2,3-bisphosphoglycerate mutase (BPGM) – regulates glycolysis (Kulow et al, 2024).
- Erbin (ERBIN) – an adaptor protein linked to autophagy and apoptosis (Qiu et al, 2024).
- Glucosylceramidase Beta 1 (GBA1) – linked to PD, is a lysosomal enzyme essential to the function of the lysosome and neuroinflammation (Bo et al, 2022).
- NADH dehydrogenase [ubiquinone] iron-sulfur protein 7, mitochondrial (NDUFS7) - a subunit of complex I and has been linked to processes such as myogenesis (Hong et al, 2014)
- Signal peptidase complex subunit 2 (SPCS2) – forms part of the ER SPase and is believed to be important in viral processing and packaging (Cui et al, 2015) and associated with overall ER function (Hu et al, 2022).

- Tight junction protein 1 (TJP1) – modulates the mTOR pathway (Liu et al, 2020).

Clustered heatmaps based on log_2 centred intensity was used to summarise protein expression in the different treatment conditions (untreated, oligomer and PFF) (**Figure 6.33**).

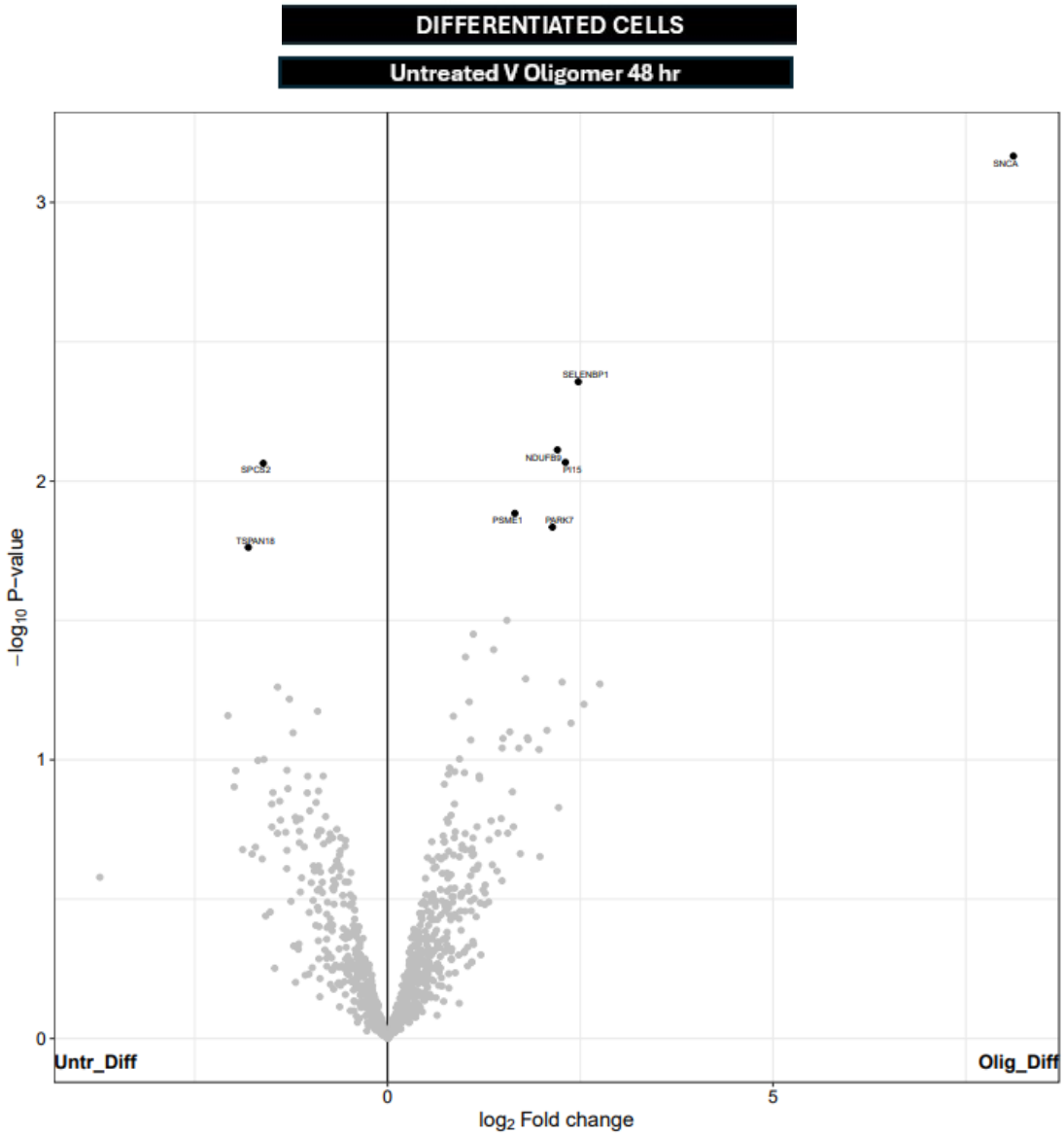

Figure 6.27 LC-MS analysis of sEV proteins from cells treated with oligomers 48 hr. The right panel shows proteins of high significance with increased expression in response to oligomers compared to the untreated. The left shows proteins with reduced expression compared to the control when cells were treated with oligomers for 48 hr (*n*=3). Protein have been disclosed in **Table 6.7 and 6.8**. Proteins included in the volcano plot were identified as significant and made visible on the volcano plot through cutoffs for alpha (0.5) and log fold change (0.5).

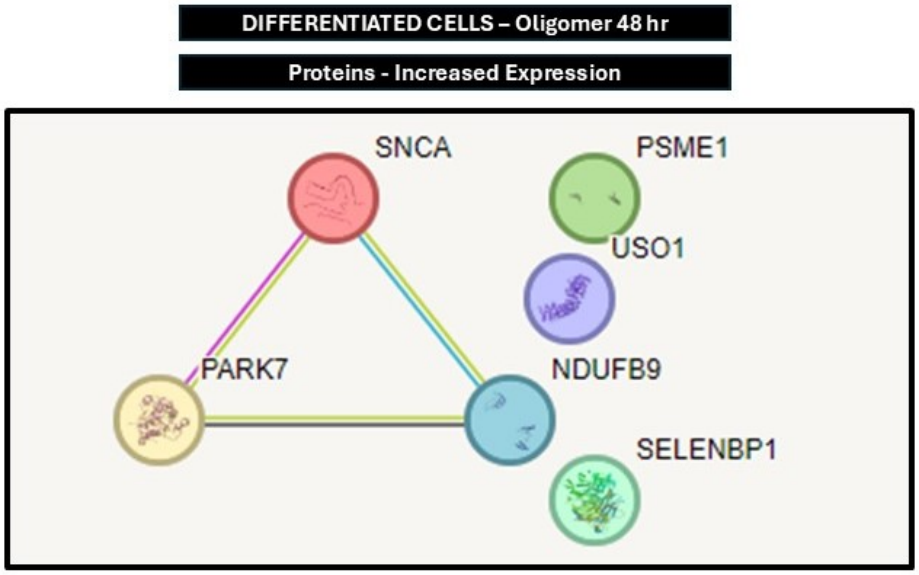

Figure 6.28 String analysis of sEV proteins with increased expression derived from cells treated with oligomers 48 hr. The protein group with increased expression in response to oligomers were inputted in STRING software and some proteins were found to have connections. STRING analysis colour definitions: red – fusion evidence; green – neighbourhood evidence; blue: co-occurrence; purple - experimental evidence; yellow – text-mining evidence; light blue – evidence sourced from other databases; black line – proteins found to be co-expressed.

Table 6.7 Decreased expression of oligomer treated cellular sEV proteins. The proteins found to have increased expression in the sEV sample when comparing the oligomer 48 hr treatment condition to untreated conditions. Proteins included in the table were identified as significant and made visible on the volcano plot through cutoffs for alpha (0.5) and log_2 fold change (0.5).

Differentiated Cells (Oligomer 48 hr)	
Protein	**Reported role/Disease Association**
Signal peptidase complex subunit 2 (SPCS2)	SPCS2 is found in all eukaryotes and is responsible for the cleavage of signal peptides and is a crucial component of the UPR. The deletion of SPCS2 has been found to activate the ER and UPR (Chung et al, 2024).
Tetraspanin 18 (TSPAN18)	TSPAN18 is present primarily in endothelial cells and has been found to regulate the Orai1/Ca^{2+} signalling pathway (Gavin et al, 2020).

Table 6.8 Increased expression of oligomer treated cellular sEV proteins. The proteins found to have increased expression in the sEV sample when comparing the oligomer 48 hr treatment condition to untreated conditions. Proteins included in the table were identified as significant through cutoffs for alpha (0.5) and log_2 fold change (0.5).

Differentiated Cells (Oligomer 48 hr)	
Protein	**Reported role/Disease Association**
NADH dehydrogenase [ubiquinone] 1 beta subcomplex subunit 9 (NDUFB9)	NDUFB9 is an accessory subunit of the mitochondria specifically the mitochondria's membrane respiratory chain nicotinamide adenine dinucleotide (NADH) dehydrogenase (complex I). Loss of this subunit has been shown to result in increased mitochondrial ROS (Li et al, 2015).
Peptidase inhibitor 15 (PI15)	PI15 belongs to antigen 5 and pathogenesis-related 1 proteins superfamily and acts as a serine protease inhibitor (Prusty et al, 2018).
Proteasome activator complex subunit 1 (PSME1)	PSME1 is a regulator of various intracellular proteolytic pathways and has been linked to HIV infection particularly initial stages of infection. It is believed that PSME1 has the ability to influence viral RNA (Liu et al, 2024). It is also associated with oxidative stress and the immune response (Koçberber et al, 2023).
Protein/nucleic acid deglycase DJ-1 (PARK7)	PARK7 encodes the protein DJ-1, which is found in the cytoplasm, mitochondria and nucleus. It will localise to the mitochondria's outer membrane in conditions of oxidative stress. It is linked to autosomal recessive PD (Skou et al, 2024).
SELENBP1	Refer to **Table 6.2**
α-Synuclein (SNCA)	Refer to **Table 6.4**

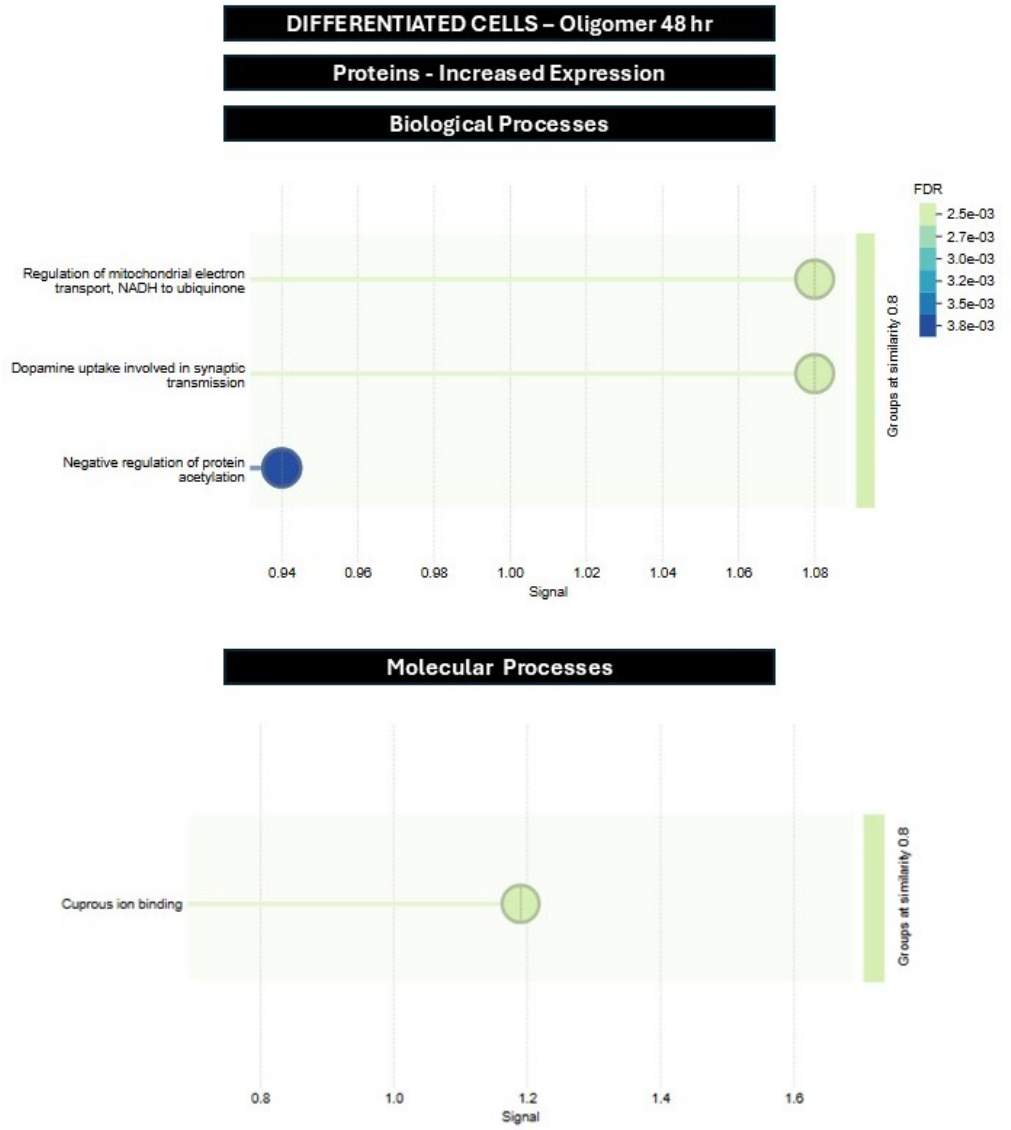

Figure 6.29 Gene ontology analysis of sEV proteins found to have increased expression in response to oligomer 48 hr treatment. Proteins found to have increased expression upon 48 hr treatment with oligomers was subjected to gene ontology analysis via STRING software. The connections between the detected sEV proteins yielded significant enrichment in various cellular components and had associations with female organ tissues.

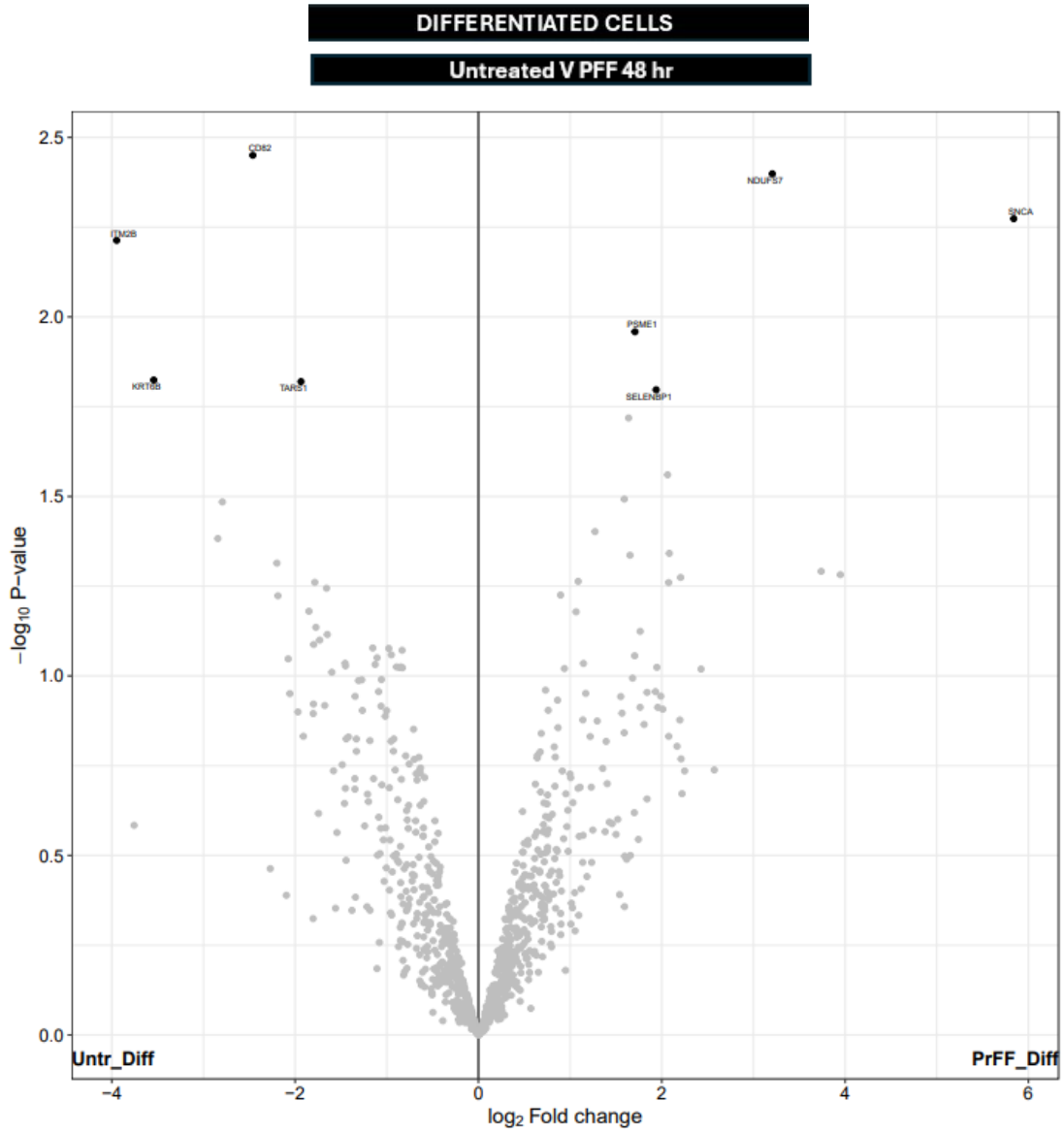

Figure 6.30 LC-MS analysis of sEV proteins isolated from cells treated with PFF 48 hr. The proteins found to have increased expression in response to PFF treatment were shown in the right panel and reduced expression in the left panel (*n=3*). Proteins have been disclosed in **Table 6.9 and 6.10**. Proteins included in the volcano plot were identified as significant and made visible on the volcano plot through cutoffs for alpha (0.5) and log fold change (0.5).

Table 6.9 Decreased expression of PFF treated cellular sEV proteins. The proteins found to have increased expression in the sEV sample when comparing the PFF 48 hr treatment differentiated SH-SY5Y to the untreated condition. Proteins included in the table were identified as significant and made visible on the volcano plot through cutoffs for alpha (0.5) and $\log_2$ fold change (0.5).

Differentiated Cells (PFF 48 hr)	
Protein	**Reported role/Disease Association**
CD82 antigen (CD82)	A tetraspanin linked to cell adhesion and T-cell activation (Shibagaki et al, 1998) and has been used as a marker for muscle cells (Alexander et al, 2016). CD82 has been linked to proliferation of myoblasts (Alexander et al, 2016). It also has the ability to activate mTORC1 (Ye et al, 2021).
Integral membrane protein 2B (ITM2B)	ITM2B is a membrane protein which has been connected to familial dementia and has been found to facilitate the glutamate transmission (Yao et al, 2019).
Threonine--tRNA ligase 1, cytoplasmic (TARS1)	A peripheral member of the multiple tRNA synthase complex. When TARS1 was deleted in mice models they were found to exhibit dysfunctional development in both the bone, muscle and in general but not protein synthesis itself (Zeng et al, 2023).

Table 6.10 Increased expression of PFF treated cellular sEV proteins. The proteins found to have increased expression in the sEV sample when comparing the PFF 48 hr treatment of differentiated SH-SY5Y to the untreated condition. Proteins included in the table were identified as significant and made visible on the volcano plot through cutoffs for alpha (0.5) and log_2 fold change (0.5).

Differentiated Cells (PFF 48 hr)	
Protein	**Reported role/Disease Association**
NADH dehydrogenase [ubiquinone] iron-sulfur protein 7, mitochondrial (NDUFS7)	NDUFS7 is a subunit of complex I and has been linked to processes such as myogenesis (Hong et al, 2014) as well as encephalopathy, pyramidal and extrapyramidal symptoms when mutated (Lebon et al, 2007).
Proteasome activator complex subunit 1 (PSME1)	Refer to **Table 6.8**
SELENBP1	Refer to **Table 6.2**
α-Synuclein (SNCA)	Refer to **Table 6.4**

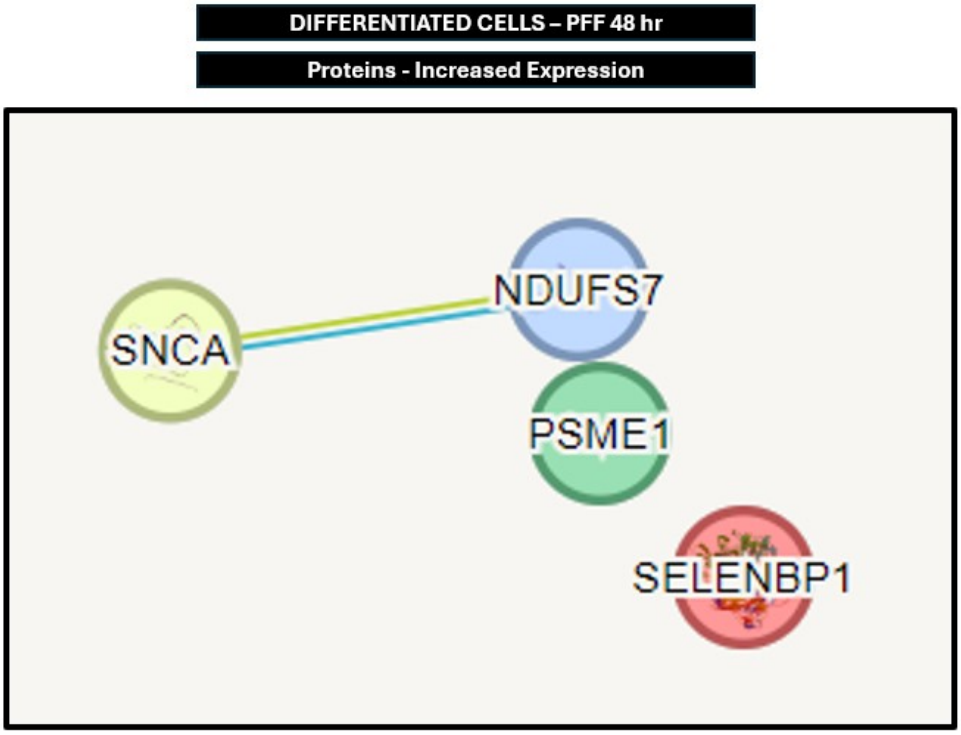

Figure 6.31 LC-MS analysis of sEV proteins. The proteins found to have increased expression sEVs derived from PFF treated cells. STRING analysis colour definitions: red – fusion evidence; green – neighbourhood evidence; blue: co-occurrence; purple - experimental evidence; yellow – text-mining evidence; light blue – evidence sourced from other databases; black line – proteins found to be co-expressed.

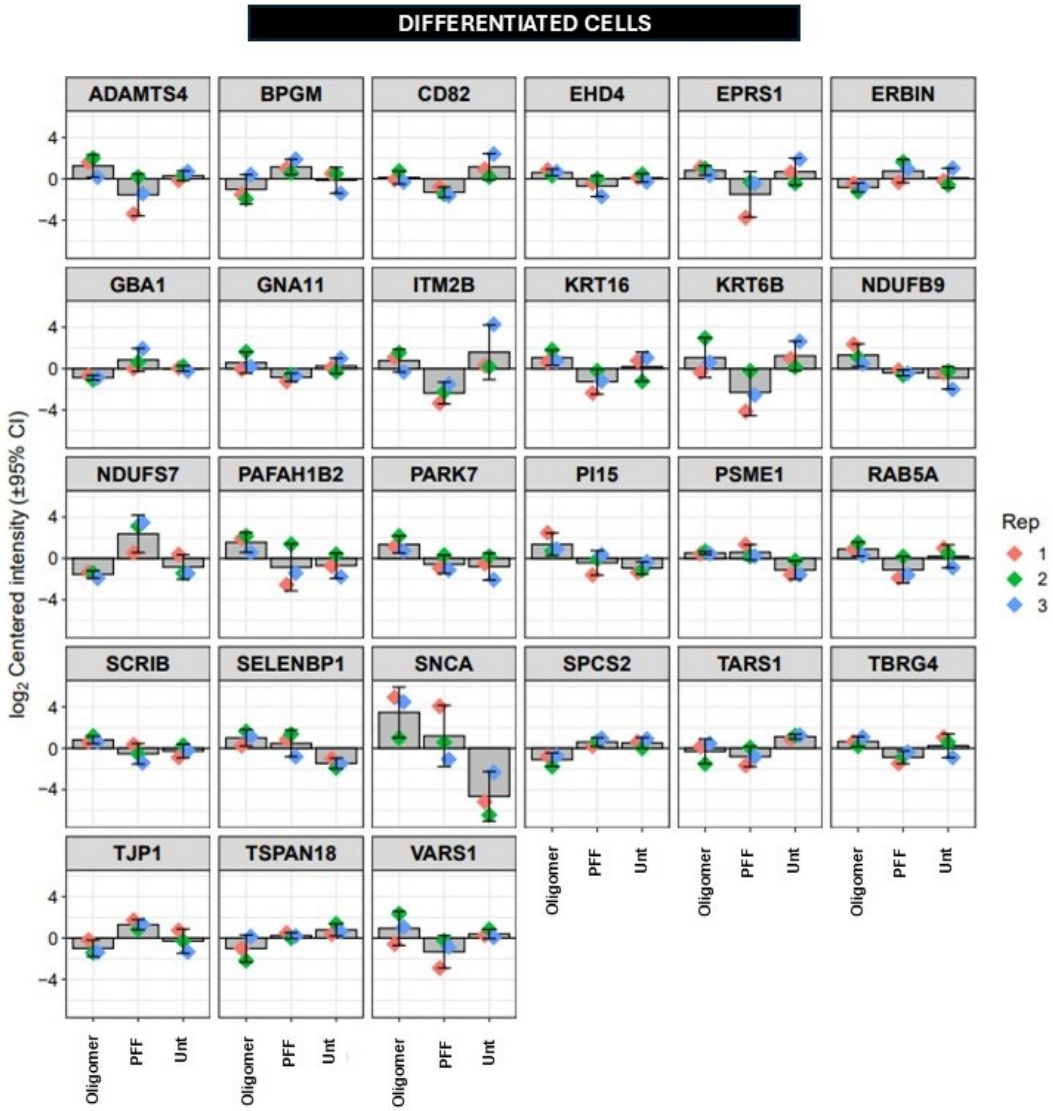

Figure 6.32 Log_2 centred intensity of sEV proteins derived from differentiated cells treated with oligomers and PFFs. Differentiated cells were treated with 0.1 mg/mL oligomers and PFFs for 48 hr. The log_2 centred intensity was calculated of significant proteins. These proteins were included by user defined cutoffs for alpha (0.5) and log fold change (0.5). In this case no proteins were identified.

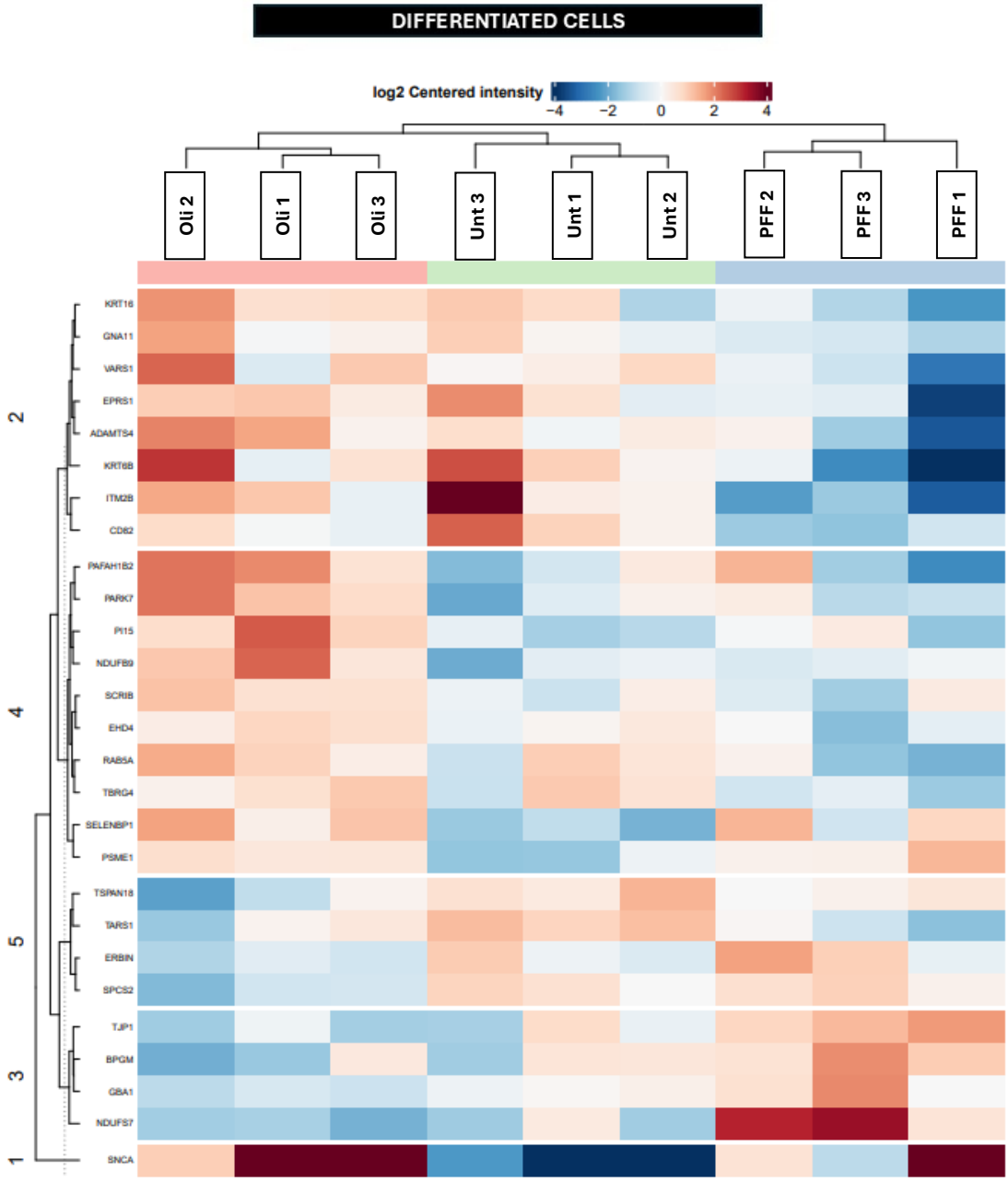

Figure 6.33 sEV protein expression in response to oligomers and PFFs treatment of differentiated cells. Clustered heatmap presents LC-MS proteomic analysis of sEVs derived from differentiated SH-SY5Y cells subjected to oligomer and PFF 48 hr treatment. Proteins shown have been determined to be significant and log2 centred intensity normalisation is used to determine proteins with reduced expression (blue to white) and increased (orange to burgundy/purple) expression in individual conditions. Colour coded condition is indicated on the top of the heatmap: oligomers (pink), untreated (green), PFFs (blue).

6.3 Discussion

6.3.1 Differentiated SY5Y cells experience intracellular aggregation upon exposure to α-synuclein oligomers and PFFs

Treatment with oligomers and PFFs at various timepoints (1, 6, 24, 48 hr) induces intracellular aggregation in undifferentiated cells (**Figure 5.1**). A similar increase in α-synuclein-positive puncta was seen in differentiated cells at 48 hr in response to both oligomers and PFFs (**Figure 6.3**). Oligomers and PFFs at this timepoint were shown to also cause oxidative stress in differentiated cells (**Figure 6.4**) as demonstrated in undifferentiated cells. These findings are established and in accordance with previous literature (Taylor-Whiteley et al, 2019). To further our understanding of the biological effect and prion-like ability of these aggregates, the next step was to be assess how cellular exposure to oligomers and PFFs effects the proteomic cargo of sEVs.

6.3.2 The characterisation of sEVs derived from SH-SY5Y cells

Characterising EVs is a common practice prior to conducting experimental work with EVs. Using NTA on sEV samples derived from undifferentiated and differentiated cells subjected to untreated and treatment conditions show that the EV samples fall within the sEV/exosome range as samples were on average between 114 – 141 nm (**Figure 6.5 B, 6.6 B, 6.7 B**). Whereas differentiated SH-SY5Y sEVs were comparatively smaller (**Figure 6.7**). Regarding the quantification of the number of sEVs in response to untreated and treated conditions, no significant differences were observed (**Figure 6.5C, 6.6C, 6.7C**). However, when looking at the undifferentiated sEV samples, SA, Tg, oligomer and PFF treatments resulted in a decrease in particles/mL (or less sEVs) when compared to the untreated condition. This could be explained by the increased cellular death which was shown in cytotoxicity data in chapter three and five which would cause a decrease in total cell number. Therefore, concurrent live/death cell assays would be helpful in understanding why this decrease in sEVs was observed and to normalise data.

6.3.3 Oxidative stress impacts the proteins expressed in sEVs

Oxidative stress has been shown to result in the expression of markers associated with the ISR (**Figure 3.1, 3.2**), cell death markers (**Figure 3.7**) and induces toxicity (**Figure 3.8**) which has been demonstrated by SA treatment of undifferentiated SH-SY5Y cells. It is understood that in instances of stress, the cargo of sEVs will change in some manner. Oxidative stress has been shown to result in the presence of antioxidant proteins in EVs such as SOD1 (Chiaradia et al, 2021). It is believed that this process not only helps cells remove toxic or damaged proteins from its intracellular space (Chiaradia et al, 2021) but it can help transmit proteins from a donor cell to recipient cells to modulate the recipient cells response to an imposing stress (Chiaradia et al, 2021). Using SA treatment at a concentration of 10 μM for 24 hours, LC-MS proteomic analysis revealed that the cargo was altered (**Figure 6.11**). The proteins found to have decreased expression in response to SA treatment were shown to be proteins involved in transport and trafficking, development and cell structure maintenance as well as many other roles (**Table 6.1**). Instances where protein expression was increased in response to SA 24 hr, proteins detected had different roles ranging from cell signalling, RNA processing and metabolism (**Table 6.2**). In accordance with the idea that sEVs carry proteins as a marker of oxidative stress, we observed increased expression of ECPAS, a protein involved in remodelling the 26S proteosome during oxidative stress (**Figure 6.11, Table 6.2**). Additionally, markers of apoptosis were detected as indicated by the expression of LMAN1 (**Table 6.2**), which aligns with the LDH cellular toxicity results. SELENBP1, a protein involved in redox regulation, was shown to increase in sEV samples which acts as an indicator of cellular oxidative stress. Furthermore, the connection of sEV to specialised stress pathways was shown in the expression of the RPS6KA3 protein, which influences activation of the mTOR pathway (Magnuson et al, 2011). Additionally, RPS6KA3 acts as a kinase where ATF4 is one of its targets (Field et al, 2009). RPS6KA3 has also been shown to localise to SGs during SA treatment (Sfakianos et al, 2018). Altogether, the sEVs' (derived from SA stress cells) proteomic data supports the concept that sEVs derived from stress conditions will carry molecules that have the capacity to target key protein substrates likely to have associations with stress

regulation and alter cellular processes in neighbouring cells. An additional example of this is EVs will carry high levels of program-death-ligand 1 and cancer-associated receptors involved in angiogenesis as well as disease progression (Kumar et al, 2024).

6.3.4 Oligomers and PFFs results in increased α-Synuclein sEV loading plus alterations in sEVs proteomics in undifferentiated and differentiated SH-SY5Y cells.

Data presented shows oligomers and PFFs can induce cellular stress and toxicity in undifferentiated cells (**Figure 5.3, 5.4**). LC-MS analysis showed oligomer and PFF altered sEV proteomics. Treatment of undifferentiated SH-SY5Y cells with 0.1 mg/mL oligomers and PFFs for 48 hours resulted in increased SNCA-positive sEV samples, as determined by LC-MS proteomic analysis (**Figures 6.19, 6.21**). However, given the nature of the protocol it cannot be determined if the α-synuclein is present within or on the membrane of the sEV. The association of α-synuclein with sEVs is supported by wider literature and EVs have been found to be positive for α-synuclein aggregates in response to α-synuclein aggregate treatment (e.g. PFFs) (Ishiguro et al, 2024).

Use of LC-MS analysis to identify key proteins within sEVs that are involved in stress response pathways derived from α-synuclein aggregate treated cells has not been previously shown in literature. Oligomer 48 hr treatment resulted in an increased expression of CFB, an inflammatory associated protein, in sEVs (**Figure 6.19**). It was shown that when SH-SY5Y cells were maintained in the absence doxycycline, they secreted oligomeric α-synuclein. The collected conditioned medium was able to activate microglia, indicatory of an inflammatory response (Leandrou et al, 2024) - a key marker of PD (Pajares et al, 2020).

PFFs were also used to treat SH-SY5Y cells, sEVs showed reduced expression of a range of histones H1-0, H1-3, H1-5, H3-3B, H2AC18, H2BC21, and MACROH2A1 and MACROH2A2 (**Figure 6.21**) which were found to have associations via STRING analysis (**Figure 6.22**). Similarly, a decrease in histone expression (H1-10) was also seen is sEVs derived from cells treated with oligomers (**Figure 6.19**). Amyloid material has been shown

to bind to histones in other contexts (Smith et. al 2008). This interaction is due to repeating net negative charges found on the surface of both DNA and amyloid. Core (H3, H4) and linker (H1) histones have been found to interact with WT α-synuclein via the N-terminal flexible histone tails and the C-terminal of α-synuclein (Jos et al, 2021). Mutations of α-synuclein have been found to have a higher affinity for histones (Jos et al, 2021). Which could explain the reduction in histones expressed in sEVs released by cells treated with PFFs. In other cases, core histones such as H2A, H2B, H3 and H4 plus the linker histone, H1 are released into extracellular space by damaged cells (Richards et al, 2023). In other instances, the presence of histones in EVs has been recognised as an indicator of neuroinflammation (Richards et al, 2023). Further, phagocytes exposed to extracellular histones have been found to result in inflammation, toxicity, and ROS (McRae et al, 2024). Exploration into the link between α-synuclein aggregates and histone dynamics is required to provide more context for this work.

EVA1A, ICAM1 and PRG4 were found to have increased expression in sEV samples as a result of PFF cell treatment (**Figure 6.21**). These proteins are associated with apoptosis and inflammation (**Table 6.6**). This data supports findings that show sEVs have the ability to propagate PFF/α-synuclein-linked cellular toxicity (Quiroz-Baez et al, 2020)

sEVs derived from oligomer and PFF treated cells, were positive for increased expression of PSME1 which has been linked to oxidative stress and SELENBP1, also increased in sEV samples, is involved in the maintenance of redox reactions (**Figure 6.29**). This evidence coincides with the oxidative stress-inducing capabilities of oligomers and PFFs (**Figure 6.4**).

STRING analysis showed links between key proteins implicated in PD namely, NDUFB9 (mitochondrial protein) and PARK7, expressed in sEV samples derived from oligomer-treated differentiated cells (**Figure 6.27**). This links to commonly investigated associations between α-synuclein aggregates, mitochondrial insults (Thorne and Tumbarello, 2022) and the presence of antioxidant machinery present in EVs during stress (Chiaradia et al, 2021). sEVs being positive for PARK7 supports this idea but also links sEVs to the

ISR and SGs. PARK7 has been found to localise to SGs in HEK293T cells specifically in conditions of stress (hyperosmotic shock) (Repici et al, 2018). This corresponds with evidence that oligomers have been found to induce SG formation (**Figure 5.11**). Furthermore, in support of data presented showing sEVs being positive for PARK7, EVs taken from PD patients were also found to be positive for PARK7 (Valencia et al, 2022)

Overall, the cellular stress induced by oligomers and PFFs appear to result in expression of proteins within sEV samples associated with oxidative stress regulation, inflammation and the mitochondria.

6.4 Summary

Oxidative stress and toxicity have been shown to be induced by both SA, α-synuclein aggregates, the data presented in this chapters shows the sEV proteome will mirror the stress experienced by the cell it is derived from.

The sEV proteins found to experience an increase in expression within treatment conditions (SA 24 hr, oligomer 48 hr and PFF 48 hr) are connected to oxidative stress, antioxidant modulation, inflammation and apoptosis. There were also increased expression of proteins in sEVs associated with SGs,

sEVs acquired from α-synuclein aggregate treatment conditions were positive for SNCA but this was not the case for sEVs acquired from the SA and Tg condition. Altogether supporting that sEVs mediates α-synuclein transmissibility.

It is also a valuable consideration that input α-synuclein (oligomers and PFFs used to treat cells) could be a contributor to the high levels of detected α-synuclein. It would be beneficial to explore this using tagged α-synuclein aggregates when treating cells to determine if sEV-associated α-synuclein is due to simply treating cells with oligomers/PFFs or rather sEVs engaging in the transmission of endogenous α-synuclein.

sEVs derived from SH-SY5Y cells exposed to aggregated α-synuclein shares some similarities to the proteins identified in patient-derived EVs. This indicates that the method and model adopted in this study is appropriate in further understanding α-synuclein aggregate transmission and potential consequences associated with this process.

Overall, the release of sEVs positive for α-synuclein and stress-associated proteins is linked to the intracellular aggregation and oxidative stress induced by oligomers and PFFs (**Figure 6.34)** which suggests that stress underpins the sEV-mediated cell-to-cell transmission.

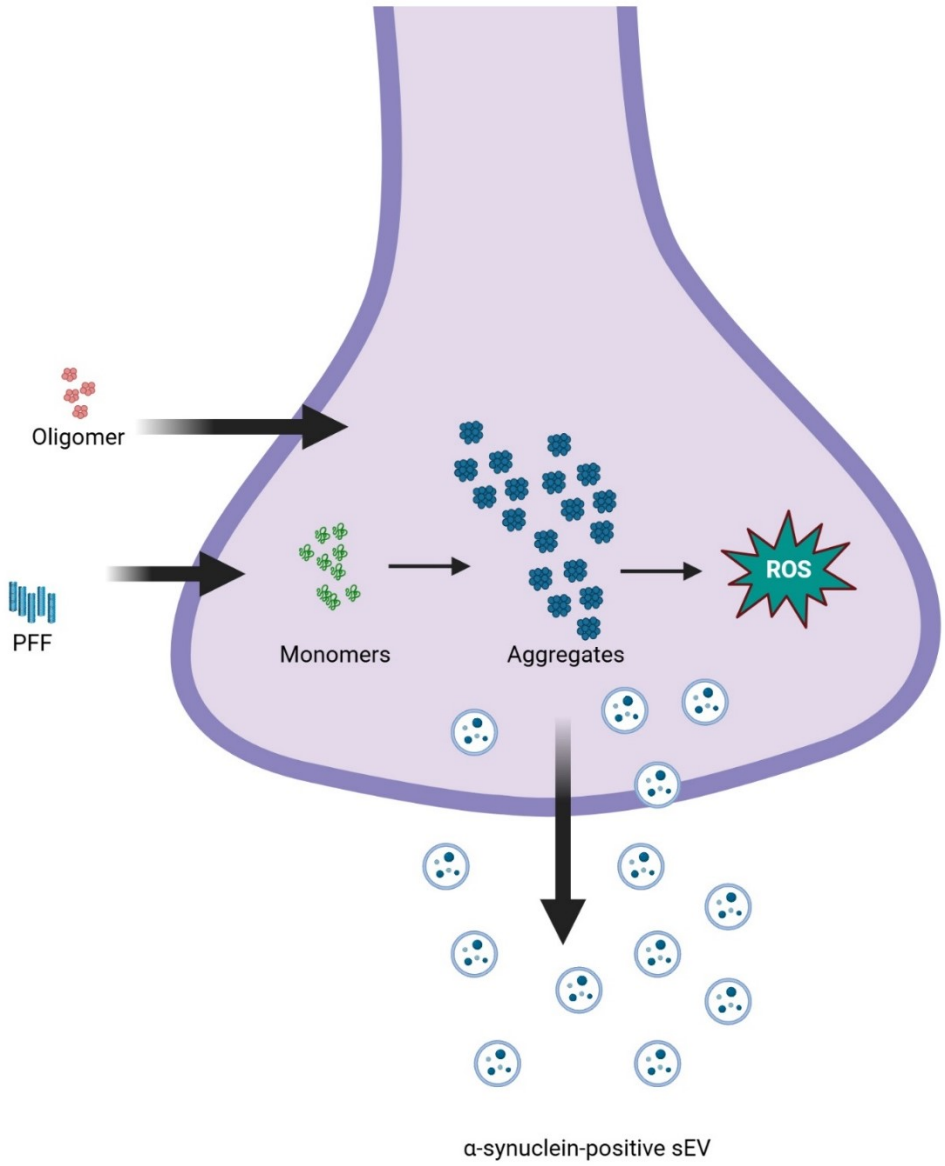

Figure 6.34 α-Synuclein-positive sEVs are released from cells treated oligomers and PFFs. A summary figure of data presented. Cellular exposure to oligomers and PFFs that results in intracellular aggregation of α-synuclein that has been shown to induce oxidative stress. As a result of either intracellular aggregation and/or oxidative stress induced by said aggregation this results in α-synuclein-positive sEVs being released from neuronal cells (in this case undifferentiated and differentiated SH-SY5Y cells).

7 Chapter Seven: Discussion, conclusion and future work

7.1 Introduction

Cellular stress has been explored as a major contributor in PD progression (Dias et al, 2013) and has been closely linked to the pathology exhibited by α-synuclein-associated neurodegeneration (Hsu et al, 2000). Previous research has linked PD to the ISR by showing expression of ATF4 in response to MPP+ and PFFs (Demmings et al, 2021). The activation of the ISR has not been shown in response to both oligomers and PFFs. Therefore, investigations were carried out to determine if α-synuclein oligomers and PFFs could activate the ISR which would provide further context into α-synuclein-induced cellular stress. Furthermore, EVs have been highlighted as a mediator in the cell-to-cell transmission process of α-synuclein (Shippey et al, 2022). It was of interest to also explore how cellular stress could alter the proteins expressed in sEVs to further understand the mechanism of sEV-mediated cellular transmission.

To explore ISR activation and changes in the sEV proteome upon exposure to α-synuclein-induced stress, the research aims of this thesis were:

- to validate ISR activation and SG formation in response to SA, Tg and MPP+ iodide for later comparisons when investigating α-synuclein-induced stress.
- to determine the ability oligomers and PFFs to induce cellular stress, activate the ISR and induce SG formation.
- to link α-synuclein-induced stress to alterations in the sEV proteome.

7.2 Discussion

7.2.1 Cellular adaptation occurs in conditions of chronic chemically induced stress.

The activation of the ISR was studied using chemical inducers such as SA, Tg and MPP+. The use of toxic compounds was important in validating appropriate utilisation of molecular techniques to allow for comparison to existing research findings and establishing a baseline of expectation pertaining to the stress response in undifferentiated SH-SY5Y cells. The main ISR markers studied in this research were eIF2α phosphorylation, ATF4, CHOP, GADD34 expression and protein synthesis inhibition along with the formation of SGs. It was demonstrated that all markers of the ISR, investigated in this study, was expressed in response to SA and Tg (**Figure 3.2, 3.5**). It was shown that expression of these markers is dependent on both time and concentration of the stress-inducing compound used for treatment. Increased eIF2α phosphorylation (**Figure 3.2, 3.3**) and ATF4 protein expression (**Figure 3.5**) was observed but overtime there would be a reduction in both molecular events. This could be attributed to stress adaptation in chronic stress conditions (Avelar et al, 2024; Ryoo, 2024). ATF4 may modulate various genes to manage stress adaptation or induce apoptosis (Demmings et al; 2021; Ok et al, 2023; Wek et al, 2023; Wortel et al, 2017). GADD34 is a target of ATF4 and intrinsic to stress adaptation (Krokowski et al, 2015). It was found that reductions in eIF2α phosphorylation coincided with an expression of GADD34 when cells were treated with SA and Tg (**Figure 3.9**). The expression of GADD34 provides an explanation for the eventual reductions in the expression of ISR markers (eIF2α phosphorylation, ATF4 and CHOP expression) in response to SA and Tg treatment.

Attenuation of protein synthesis is a key outcome of ISR activation, Tg treatment was found inhibit protein synthesis (**Figure 3.10)**. This coincides with Tg treatment enhancing eIF2α phosphorylation, ATF4 and CHOP expression. SA treatment at 6 hr did not result in attenuation of protein synthesis (**Figure 3.10**), which is explained by the expression of GADD34 at this timepoint (**Figure 3.9**) which inactivates the ISR and restores protein synthesis (Oliveira et al, 2024).

7.2.2 High dose MPP+ activates the ISR but does not enhance ATF4 expression.

MPP+ which has been extensively used in the research of PD-associated neurodegeneration (Chun et al, 2001; Kalivendi et al, 2003; Kim-Han et al, 2011; Mapa et al, 2018; Marti et al, 2017; Yee et al, 2014) was introduced to establish a connection between the ISR and PD. Evidence shows 10 mM MPP+ induced eIF2α phosphorylation but ATF4 expression did not increase (**Figure 3.6**). In response to 10 mM MPP+, ATF4 expression was found to reduce at 24 hr compared to the 6 hr timepoint, despite the 6 hr timepoint not showing enhanced ATF4 expression compared to untreated condition (**Figure 3.5**). There could be a mechanism of ATF4 suppression in conditions of chronic, severe MPP+ stress. TRIB3, found to be expressed in response to MPP+ (Demmings et al, 2021), acts as an inhibitor of ATF4 during Bortezomib treatment of HepG2 cells (Örd et al, 2021). ATF4 was seen to mildly increase when cells were treated with 0.1 and 5 mM MPP+ for 6 hr (**Figure 3.6**), suggesting that ATF4 expression is concentration dependent.

10 mM MPP+ did not induce CHOP expression (**Figure 3.6**). This could be due to the concentration of MPP+ used or the cell model used for this experiment. Different cell types will respond differently to the same stress-inducing compound as shown through variations in ISR marker expression (Hanson et al, 2024). This is valuable to note as MPP+ has been shown at lower concentrations, 25 μM (16 hr treatment), to induce expression of CHOP, TRIB3 and PUMA mRNA levels in mice mesencephalic neurons (Demmings et al, 2021). Additionally, an increase in ATF4 protein expression was observed in cortical neurons treated with 50 μM MPP+ (Demmings et al, 2021).

GADD34 was expressed in response to 10 mM MPP+ treatment for 1, 6 and 24 hr (**Figure 3.9**), indicating an ATF4-independent mechanism of GADD34 expression. This indicates that recovery mechanisms are still taking place despite the severity of 10 mM MPP+ treatment.

7.2.3 MPP+ SG dynamics differs to that of SA and Tg.

The ISR is activated in response to SA, Tg and MPP+. SGs can form in response to the activation of the ISR. The low-dose concentrations used when

looking at 30 μM SA and 0.15 μM Tg induced an initial increase of SGs at 1 hr but reduced at 6 and 24 hr. Treatment of cells with 10 mM MPP+ caused the number and size of SGs to increase overtime, peaking at 24 hr (**Figure 3.17**). Which suggests differing mechanisms in SG dynamics in these explored stress conditions.

Stress severity could be key to understanding the variation in dynamics seen to these different stresses. When treating U2OS cells with 50 μM SA, it was found that there was an initial increase at 1 hr but then the percentages of SG positive cells began to decrease at 4 hr, with no SGs observed at 12 and 24 hr (Adachi et al, 2024). However, when cells were treated with 100 and 500 μM SA, SGs could once again be seen at 1 hr with reductions at 4, 12 and 24 hr but as the concentration of SA increased the time taken to for all observable SGs to disassemble took longer (Adachi et al, 2024). These observations indicate that the presence of SGs, may act as an initial responder to stress but overtime through adaptive mechanisms SGs will disassemble at different rates depending on the severity of the stress/concentration of drug.

According to the data presented, enhanced eIF2α phosphorylation leads to SG formation but eventually SGs will reduce in both size and number that can be attributed to GADD34 activity/expression as shown when cells are treated with SA and Tg. In the 10 mM MPP+ condition, the increased percentage of cells with SGs coincides with an increase in eIF2α phosphorylation also. Which indicates that SGs formed in response to these stresses are influenced by the phosphorylation of eIF2α (Wang et al, 2019).

7.2.4 Oligomers and PFFs alters the eIF2α/ATF4 pathway

Equipped with the knowledge that ISR activation looks different depending on the type of stress the cell is subjected to, understanding if synthesised oligomers and PFFs activate the ISR was of primary interest.

α-Synuclein aggregates exhibit prion-like activity, specifically through the recruitment, misfolding and aggregation of initially natively folded α-synuclein (Leak et al, 2019). Fluorescent imaging showed when undifferentiated SH-SY5Y cells were treated with oligomers and PFFs, that the size and number of α-synuclein aggregated increased (**Figure 5.1, 5.2**) an indicator of prion-like

activity. The observed intracellular aggregation coincided with oxidative stress (ROS formation) (**Figure 5.3**) and increased cytotoxicity (**Figure 5.4**).

When exploring ISR activation upon exposure to oligomers and PFFs, it was found that both oligomers and PFFs induced moderate phosphorylation of eIF2α but not significant enough to confidently determine a biologically relevant change (**Figure 5.5**). Gene expression data showed that oligomers and PFFs increased ATF4 and GADD34 levels (**Figure 5.6, 5.9**), indicating ISR activation. ATF4 has been explored in neurodegeneration (Pitale et al, 2017) where increased ATF4 expression was observed in the SNpc of rat models. This correlated with a loss of tyrosine hydroxylase (TH) positive cells (Pitale et al, 2017) which are able to synthesise catecholamine needed for production of dopamine, epinephrine and other neurotransmitters (Daubner et al, 2011) - all found to be implicated in PD and neurodegenerative diseases (Barone, 2010). This shows that ATF4 expression is key to the apoptosis associated with neurodegeneration which has been previously demonstrated (Demmings et al, 2021). We also present evidence of oligomer and PFF treatment inhibiting translation (**Figure 5.10**), further supporting the link between α-synuclein pathology and the ISR. The protective and pathological implications of α-synuclein aggregate inhibition of protein synthesis was not explored but it would be of interest to investigate this.

Other downstream markers associated with ISR activation upon oligomer and PFF treatment were explored to understand the implications of the ISR being activated. ATF5 and CHOP gene expression was investigated upon oligomer and PFF treatment to determine whether the mitochondrial-UPR and ER stress mechanisms were activated. However, it was found that ATF5 (**Figure 5.7**) and CHOP (**Figure 5.8**) were not expressed. This suggests that the synthesised oligomers and PFFs does not induce mitochondrial-UPR and ER stress in this cell model or at these timepoints. Exploring expression of eIF2α kinases (e.g. PERK and HRI) in response to oligomers and PFFs would be helpful to confirm this.

In conjunction with oligomers and PFFs activating the ISR, G3BP-positive SGs were formed (**Figure 5.11, 5.12**). PFFs were found to induce more SGs

compared to oligomers which indicates PFFs triggering a higher level of cellular stress. PFFs resulted in higher percentage of cells positive for SGs overall and earlier than oligomers. Further, PFFs induced more SGs per cell (double) compared to oligomers. Oligomers and PFFs had the largest SGs at 48 hr suggesting that the size of SGs in response to oligomers and PFF treatment increases overtime.

There were less G3BP-positive SGs induced by oligomers and PFFs compared to SA, Tg and MPP+. The distribution of SGs (percentage of cells positive and SGs per cell) overtime in response oligomers and PFFs were different when compared to SA, Tg and MPP+. Which indicates that the SG dynamics in conditions of SA, Tg, a neurotoxin (MPP+) and α-synuclein varies considerably.

TDP-43 forms aggregates which is a known marker of ALS, has been found to interact with SGs (Mori et al, 2023). SG co-localisation with intracellular α-synuclein aggregates was explored to garner more understanding of the link between SGs and α-synuclein. SGs were shown to co-localise with intracellular α-synuclein aggregates particularly in response to oligomer and PFF treatment (**Figure 5.13**). Pull-down assays would be helpful in robustly confirming that there is an interaction between SGs and α-synuclein. It would be of interest to explore how this alters the kinetics of SG assembly and disassembly plus if this exacerbates α-synuclein aggregation.

7.2.5 Small EVs carry proteins associated with the imposing cell stress

EVs are important contributors to cellular stress (Kumar et al, 2024). The release of EVs is enhanced during stress and has been found to contain cargo reflective of conditions of the cell they are derived from (Kumar et al, 2024). It has been previously shown that ER stress increased the release of EVs but α-synuclein reduced the release of exosomes (Jahangiri et al, 2022) showing that EV dynamics is impacted by cellular stress.

To explore the effects of cellular stress and sEVs, stress-inducing compounds and α-synuclein aggregates shown to activate the ISR was used to determine how stress alters the sEV proteome.

It was found that sEVs derived from cells treated with oligomers and PFFs were positive for α-synuclein (**Figure 6.19, 6.21**) which functions as an indicator that EVs are a medium for cell-to-cell transmission of α-synuclein. It is important to note that the oligomers and PFFs used on the treatment of cells could contribute to the increased expression detected in sEV samples.

It was also found that sEVs derived from cells treated with SA, oligomers and PFFs carried proteins associated with oxidative stress and cell death such as SELENBP1 and PSME1. Which supports the idea that sEVs will carry cargo indicatory of cell stress which links to the presented ROS and cytotoxicity data (**Figure 5.3, 6.4**).

sEVs derived from SA-treated undifferentiated cells were shown to have increased expression of SG-associated proteins such as FXR1 and RPS6KA3 which shows a novel link between sEVs and SGs.

There was increased expression of mitochondrial subunits (NDUFB9 and NDUFS7) in sEVs derived from differentiated SH-SY5Y cells treated with oligomers and PFFs (**Figure 6.27, 6.30**). The presence of mitochondrial subunits in EVs has been reported as a way to modulate metabolism and inflammation in recipient cells (Mambro et al, 2023). PARK7 was identified to have increased expression in sEVs isolated from oligomer treated differentiated SH-SY5Y (**Figure 6.27**). LC-MS proteomic analysis of PD patient sEVs showed presence of PARK7/DJ-1 also (Zhao et al, 2019; Anastasi et al, 2021; Dutta et al, 2023). Potentially indicating that sEVs will carry proteins involved in stress modulation, as PARK7 is involved in alleviating oxidative stress (Zhang et al, 2021).

It can be concluded that sEVs will carry proteins associated with cellular stress as shown with sEVs derived from SA, oligomers and PFFs. All stress conditions explored in the study of the sEV proteome were also shown to activate the ISR. Which suggests there could be a link between the ISR and sEVs. It would be of interest to explore how ISR activation directly impacts sEVs as well as the ability for stress-derived sEVs to activate the ISR in recipient cells.

7.3 Concluding Remarks

This thesis aimed to investigate the implications of oligomer and PFF-induced stress with primary focus on oligomers and PFFs ability to activate the ISR. The secondary aim explored the effects of oligomer and PFF-induced stress on the proteome of isolated sEVs.

It has been shown that synthesis of oligomers and PFFs was able to induce intracellular aggregation that was synonymous with oxidative stress and cellular toxicity. The sustained/chronic exposure to oligomers and PFFs moderately altered ISR activation as demonstrated by increased ATF4 and GADD34 expression, inhibition of protein synthesis and induced SG formation. Which has not been explored in wider literature.

When comparing the α-synuclein aggregates discussed in chapter five to the stress inducing compounds in chapter three, it can be determined that ISR activation and SG dynamics vary depending on stress conditions. We show that MPP+ at 10 mM activates the ISR independent of ATF4 and CHOP. Furthermore, oligomers and PFFs results in a comparatively moderate gene expression of specific ISR markers (e.g. ATF4 and GADD34) which could be due to the α-synuclein aggregates requiring a longer time or more cell loading (higher concentration of oligomers and PFFs added to cell medium) to induce substantial ISR activation. An alternative explanation is oligomers and PFFs interacts with various cell organelles resulting in different stresses and stress pathways being activated causing variable data.

The alteration of the ISR upon α-synuclein aggregation suggests that exploration of the ISR in PD therapeutics may be of some benefit. Moreover, further exploration into the extent and specific role of the ISR in α-synuclein stress is required.

With the newly revealed understanding of components of the eIF2α/ATF4 pathway being altered along with SG formation upon oligomer and PFF treatment, LC-MS analysis of sEV proteins derived from cells treated with oligomers and PFFs was investigated. sEV data supports the ability for oligomers and PFFs to induce oxidative stress/toxicity due to the expression of sEV proteins (derived from oligomer and PFF treated cells) associated with

oxidative stress and senescence (**Figure 7.1**). Altogether, data opens a door of potential studies into link between the ISR and sEVs.

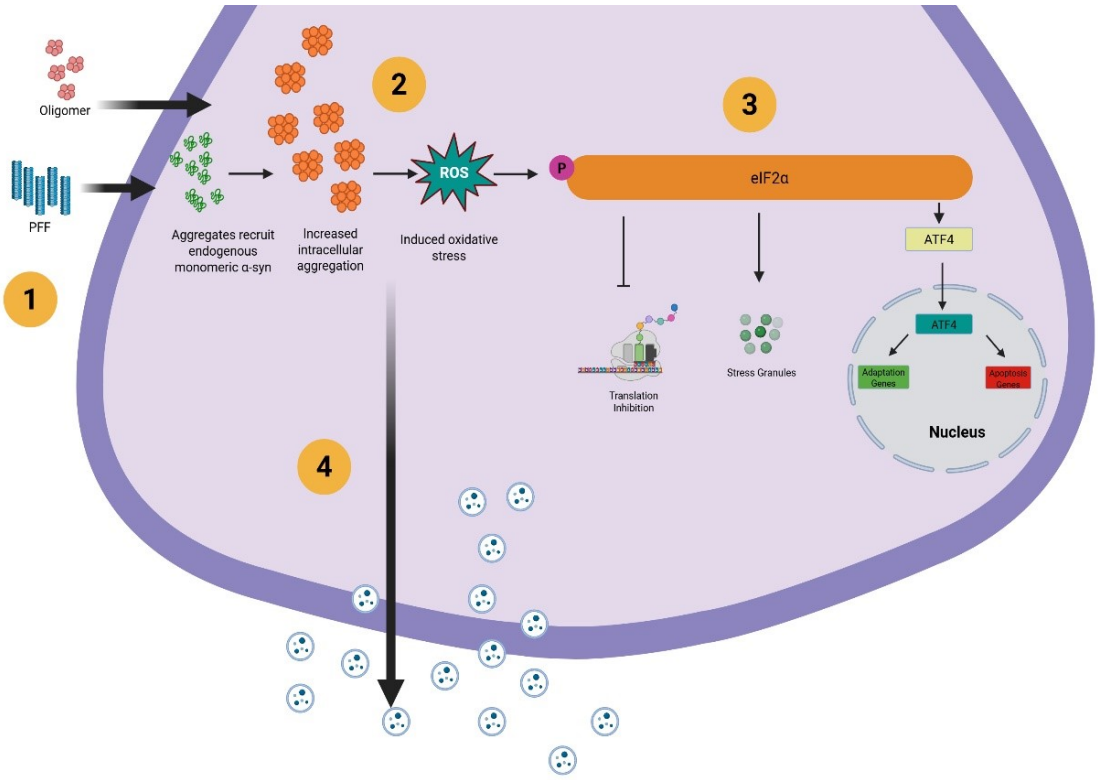

Figure 7.1 A summary of the proposed sequence of events during stress caused by oligomers and PFFs. (1) The synthesised α-synuclein aggregates (oligomers and PFFs) induce intracellular aggregation through the recruitment of endogenous α-synuclein which results in **(2)** oxidative stress. **(3)** This stress activates the ISR. The oxidative stress induces is linked to the **(4)** release of sEVs containing proteins positive for α-synuclein and associated with oxidative stress. The connection between the ISR and release of these sEVs has not yet been elucidated.

7.4 Future work

The data presented in chapters: three, five and six explored various the consequences of stress to understand how α-synuclein aggregate associated stress activates the ISR and alters sEV cargo. The aims of the study were met as it was proven that oligomers and PFFs induces expression of certain ISR markers plus reduces protein synthesis and alters the proteins present with sEVs coinciding with intracellular aggregation and stress induction. Moreover, there are experimental improvements that can be made to strengthen the hypothesis that oligomers and PFFs activate the ISR which underpins PD-associated neurodegeneration.

Alternative cell models should be used in the exploration of α-synuclein, cell stress and the ISR.

Human dopaminergic neurons which are the primary cell population affected by PD are often hard to isolate (Xicoy et al, 2017). Therefore, alternative cell models are used to study PD. The SH-SY5Y neuroblastoma cell line exhibits catecholaminergic phenotypes with the ability to release dopamine and noradrenaline (Xicoy et al, 2017). The cells can also be differentiated into post mitotic neurons using 5 – 100 μM ATRA enabling the presentation of further dopaminergic neuron-like features/markers (Xicoy et al, 2017). The Lund human mesencephalic (LUHMES) neuronal cell line isolated from human mesencephalon (Lauter et al, 2020) can be differentiated to exhibit dopaminergic neuron-like features with increases in markers such as TH and Tuj1 (Zhang et al, 2014). LUHMEs are known to release, and uptake dopamine plus develop extensive neurites (Zhang et al, 2014). iPSCs or neural stem cells (NSCs) are also used to model neurodegenerative disorders such as PD. NSCs can be differentiated into DA neurons that can mirror early and later stages of neuronal development (Xu et al, 2016). Altogether, 2D cell cultures are advantageous for experimentation due to their cost-effectiveness, batch consistency and are overall easier to use (Solana-Manrigue et al, 2025).

However, 2D models may neglect aspects of true physiological environments such as glial cell interactions (Smits et al, 2019). Therefore, the utilisation of 3D models in research has been explored as an alternative model in

understanding neurodegenerative diseases. An example is the differentiation of SH-SY5Y cells grown in differentiation medium (containing foetal bovine medium and retinoic acid) and Matrigel (Li et al, 2022). 3D models have been considered advantageous due to closely mimicking DA neurons. There is evidence of increased expression of neuronal-associated genes in 3D models such as TH compared to RA and RA/BDNF differentiated 2D SH-SY5Y cultures (Li et al, 2022). 3D models have also been used as a model of α-synuclein phosphorylation upon MPP+ treatment along with observations of increased aggregation into oligomers (Li et al, 2022). Yet, 3D models can still lack the complexity of the brain's physiological environment (Solana-Manrigue et al, 2025).

Organoids comprising of iPSCs or human embryonic stem cells (hESCs) have now been adopted to model areas of the brain such as the midbrain as it contains DA neurons. Additionally, implementation of co-culture systems of neurons with astrocytes in these organoids are also being explored (Kwak et al, 2020; Solana-Manrigue et al, 2025) as well as personalised organoids using patient cells (Solana-Manrigue et al, 2025). The primary limitation of organoids is the very short period in which they can be cultured before necrosis occurs (Zagare et al, 2021; Solana-Manrigue et al, 2025).

There is a progression in the availability in the cell models that can be used to study PD-associated neurodegeneration, but considerations around selection of cell models used should be based on the facilities available as well as the research question presented.

Exploration of the ISR upon oligomer and PFF treatment in cell models such as iPSCs would be beneficial. iPSCs are derived from human cells reprogrammed and the lacks the tumour background of SH-SY5Y cells (Aboul-Soud et al, 2021; Wang et al, 2024) which may have an impact on the manner in which SH-SY5Y responds to stress.

Investigating other gene and protein markers associated with the ISR is important in providing a more robust link between α-synuclein aggregates and the ISR.

Oligomers and PFFs treatment were found to induce ATF4 expression (**Figure 5.6**) but it was found that gene expression of both ATF5 and CHOP was not enhanced in response to oligomers and PFFs (**Figure 5.7, 5.8**). Therefore, as ATF4 has many proteins in which it interacts with (Pakos-Zebrucka et al, 2016), it would be of importance to this investigation to explore more genes and proteins associated with ATF4. Some of these proteins include: ATF3 (cell death), FAM175B/Abro1 (involved in oxidative stress responses), mTORC1 (autophagy inhibition), TRIB3 (repression of ATF4-CHOP), XIAP (inhibitor of apoptosis), as well as others (Pakos-Zebrucka et al, 2016).

To truly stipulate if EVs are a medium for cell-to-cell transmission and transmission of cell stress, EV-recipient cell experiments should be carried out.

The research explored in Chapter Six provides proteomic analysis of sEVs in response to cell stress imposed by SA as well as α-synuclein aggregates. sEVs has been implicated in modulation (Kumar et al, 2024), cell stress and dysfunction (O'Neill et al, 2019) and prion transmission (Khadka et al, 2023; Zhang et al, 2018). Administering sEVs from stressed cells to treatment-naïve/control SH-SY5Y recipient cells, with subsequent gene expression and proteomic analysis of the recipient cells would be important in understanding pathological transmission between cells mediated by sEVs. Additionally, assessing intracellular aggregation of α-synuclein in recipient cells in response to exposure to sEVs derived from oligomer and PFFs treated cells would provide proof of cell-to-cell transmission of α-synuclein.

8 Chapter Eight: References

Abeliovich, A., Schmitz, Y., Fariñas, I., Choi-Lundberg, D., Ho, W. H., Castillo, P. E., Shinsky, N., Verdugo, J. M., Armanini, M., Ryan, A., Hynes, M., Phillips, H., Sulzer, D., & Rosenthal, A. (2000). Mice lacking alpha-synuclein display functional deficits in the nigrostriatal dopamine system. *Neuron, 25*(1), 239–252. 10.1016/s0896-6273(00)80886-7

Abels, E. R., & Breakefield, X. O. (2016). Introduction to Extracellular Vesicles: Biogenesis, RNA Cargo Selection, Content, Release, and Uptake. *Cellular and Molecular Neurobiology, 36*(3), 301–312. 10.1007/s10571-016-0366-z

Abhange, K., Makler, A., Wen, Y., Ramnauth, N., Mao, W., Asghar, W., & Wan, Y. (2021). Small extracellular vesicles in cancer. *Bioactive Materials, 6*(11), 3705–3743. 10.1016/j.bioactmat.2021.03.015

Aboul-Soud, M. A. M., Alzahrani, A. J., & Mahmoud, A. (2021). Induced Pluripotent Stem Cells (iPSCs)—Roles in Regenerative Therapies, Disease Modelling and Drug Screening. *Cells, 10*(9), 2319. 10.3390/cells10092319

Adachi, Y., Williams, A. M., Masuda, M., Taketani, Y., Anderson, P. J., & Ivanov, P. (2024). Chronic stress antagonizes formation of Stress Granules. *bioRxiv: The Preprint Server for Biology,* , 2024.10.29.620814. 10.1101/2024.10.29.620814

Adams, C. J., Kopp, M. C., Larburu, N., Nowak, P. R., & Ali, M. M. U. (2019). Structure and Molecular Mechanism of ER Stress Signaling by the Unfolded Protein Response Signal Activator IRE1. *Frontiers in Molecular Biosciences, 6*10.3389/fmolb.2019.00011

Advani, V. M., & Ivanov, P. (2020). Stress granule subtypes: an emerging link to neurodegeneration. *Cellular and Molecular Life Sciences : CMLS, 77*(23), 4827–4845. 10.1007/s00018-020-03565-0

Akyüz, N., Rost, S., Mehanna, A., Bian, S., Loers, G., Oezen, I., Mishra, B., Hoffmann, K., Guseva, D., Laczynska, E., Irintchev, A., Jakovcevski, I., & Schachner, M. (2013). Dermatan 4-O-sulfotransferase1 ablation accelerates

peripheral nerve regeneration. *Experimental Neurology, 247*, 517–530. 10.1016/j.expneurol.2013.01.025

Al Ojaimi, M., Banimortada, B. J., Alragheb, A., Hajir, R. S., Alves, C., Walid, D., Raza, A., & El-Hattab, A. W. (2025). Molecular and clinical aspects of histone-related disorders. *Human Genomics, 19*, 47. 10.1186/s40246-025-00734-9

Alam, M. M., De, Y., Li, X., Liu, J., Back, T. C., Trivett, A., Karim, B., Barbut, D., Zasloff, M., & Oppenheim, J. J. (2022). Alpha synuclein, the culprit in Parkinson disease, is required for normal immune function. *Cell Reports, 38*(2), 110090. 10.1016/j.celrep.2021.110090

Alam, P., Bousset, L., Melki, R., & Otzen, D. E. (2019). α-synuclein oligomers and fibrils: a spectrum of species, a spectrum of toxicities. *Journal of Neurochemistry, 150*(5), 522–534. 10.1111/jnc.14808

Alausa, A., Victor, U. C., Fadahunsi, O. S., Owolabi, N., Adeniji, A., Olatinwo, M., Ogunlana, A. T., Olaleke, B., Balogun, T. A., Ogundepo, S., & Adegbola, P. I. (2022). Checkpoints and immunity in cancers: Role of GNG12. *Pharmacological Research, 180*, 106242. 10.1016/j.phrs.2022.106242

Albert, M., Brinkmann, K., & Kashkar, H. (2014). Noxa and cancer therapy. *Molecular & Cellular Oncology, 1*(1), e29906. 10.4161/mco.29906

Alexander, M. S., Rozkalne, A., Colletta, A., Spinazzola, J. M., Johnson, S., Rahimov, F., Meng, H., Lawlor, M. W., Estrella, E., Kunkel, L. M., & Gussoni, E. (2016). CD82 is a marker for prospective isolation of human muscle satellite cells and is linked to muscular dystrophies. *Cell Stem Cell, 19*(6), 800–807. 10.1016/j.stem.2016.08.006

Amodio, G., Moltedo, O., Fasano, D., Zerillo, L., Oliveti, M., Di Pietro, P., Faraonio, R., Barone, P., Pellecchia, M. T., De Rosa, A., De Michele, G., Polishchuk, E., Polishchuk, R., Bonifati, V., Nitsch, L., Pierantoni, G. M., Renna, M., Criscuolo, C., Paladino, S., & Remondelli, P. (2019). PERK-Mediated Unfolded Protein Response Activation and Oxidative Stress in

PARK20 Fibroblasts. *Frontiers in Neuroscience, 13*, 673. 10.3389/fnins.2019.00673

Ananbeh, H., Vodicka, P., & Kupcova Skalnikova, H. (2021). Emerging Roles of Exosomes in Huntington's Disease. *International Journal of Molecular Sciences, 22*(8), 4085. 10.3390/ijms22084085

Anantharam, V., Kaul, S., Song, C., Kanthasamy, A., & Kanthasamy, A. G. (2007). Pharmacological Inhibition of Neuronal NADPH Oxidase Protects against 1-Methyl-4-Phenylpyridinium (MPP+)-Induced Oxidative Stress and Apoptosis in Mesencephalic Dopaminergic Neuronal Cells. *Neurotoxicology, 28*(5), 988–997. 10.1016/j.neuro.2007.08.008

Anastasi, F., Masciandaro, S. M., Carratore, R. D., Dell'Anno, M. T., Signore, G., Falleni, A., McDonnell, L. A., & Bongioanni, P. (2021). Proteomics Profiling of Neuron-Derived Small Extracellular Vesicles from Human Plasma: Enabling Single-Subject Analysis. *International Journal of Molecular Sciences, 22*(6), 2951. 10.3390/ijms22062951

Anderson, E. N., Hirpa, D., Zheng, K. H., Banerjee, R., & Gunawardena, S. (2019). The Non-amyloidal Component Region of α-Synuclein Is Important for α-Synuclein Transport Within Axons. *Frontiers in Cellular Neuroscience, 13*, 540. 10.3389/fncel.2019.00540

Apostolova, D., Apostolov, G., Moten, D., Batsalova, T., & Dzhambazov, B. (2024). Claudin-12: guardian of the tissue barrier or friend of tumor cells. *Tissue Barriers,* , 2387408. 10.1080/21688370.2024.2387408

Arif, A., Alameri, A. A., Tariq, U. B., Ansari, S. A., Sakr, H. I., Qasim, M. T., Aljoborae, F. F. M., Ramírez-Coronel, A. A., Jabbar, H. S., Gabr, G. A., Mirzaei, R., & Karampoor, S. (2023). The functions and molecular mechanisms of Tribbles homolog 3 (TRIB3) implicated in the pathophysiology of cancer. *International Immunopharmacology, 114*, 109581. 10.1016/j.intimp.2022.109581

Armstrong, M. J., & Okun, M. S. (2020). Diagnosis and Treatment of Parkinson Disease: A Review. *JAMA, 323*(6), 548–560. 10.1001/jama.2019.22360

Asadi, M. R., Sadat Moslehian, M., Sabaie, H., Jalaiei, A., Ghafouri-Fard, S., Taheri, M., & Rezazadeh, M. (2021). Stress Granules and Neurodegenerative Disorders: A Scoping Review. *Frontiers in Aging Neuroscience, 13*, 650740. 10.3389/fnagi.2021.650740

Ascherio, A., Chen, H., Weisskopf, M. G., O'Reilly, E., McCullough, M. L., Calle, E. E., Schwarzschild, M. A., & Thun, M. J. (2006). Pesticide exposure and risk for Parkinson's disease. *Annals of Neurology, 60*(2), 197–203. 10.1002/ana.20904

Ashe, K. H. (2020). The biogenesis and biology of amyloid β oligomers in the brain. *Alzheimer's & Dementia, 16*(11), 1561. 10.1002/alz.12084

Ashraf, D., Khan, M. R., Dawson, T. M., & Dawson, V. L. (2024). Protein Translation in the Pathogenesis of Parkinson’s Disease. *International Journal of Molecular Sciences, 25*(4), 2393. 10.3390/ijms25042393

Avelar, R. A., Gupta, R., Carvette, G., da Veiga Leprevost, F., Colina, J., Teitel, J., Nesvizhskii, A. I., O'Connor, C. M., Hatzoglou, M., Shenolikar, S., Arvan, P., Narla, G., & DiFeo, A. (2024). Integrated stress response plasticity governs normal cell adaptation to chronic stress via the PP2A-TFE3-ATF4 pathway. *Research Square,* , rs.3.rs–4013396. 10.21203/rs.3.rs-4013396/v1

Aviner, R. (2020). The science of puromycin: From studies of ribosome function to applications in biotechnology. *Computational and Structural Biotechnology Journal, 18*, 1074–1083. 10.1016/j.csbj.2020.04.014

Avola, R., Graziano, A. C. E., Pannuzzo, G., Albouchi, F., & Cardile, V. (2018). New insights on Parkinson's disease from differentiation of SH-SY5Y into dopaminergic neurons: An involvement of aquaporin4 and 9. *Molecular and Cellular Neurosciences, 88*, 212–221. 10.1016/j.mcn.2018.02.006

B’chir, W., Maurin, A., Carraro, V., Averous, J., Jousse, C., Muranishi, Y., Parry, L., Stepien, G., Fafournoux, P., & Bruhat, A. (2013). The eIF2α/ATF4 pathway is essential for stress-induced autophagy gene expression. *Nucleic Acids Research, 41*(16), 7683–7699. 10.1093/nar/gkt563

Baltussen, L. L., Rosianu, F., & Ultanir, S. K. (2018). Kinases in synaptic development and neurological diseases. *Progress in Neuro-Psychopharmacology & Biological Psychiatry, 84*(Pt B), 343–352. 10.1016/j.pnpbp.2017.12.006

Baradaran-Heravi, Y., Van Broeckhoven, C., & van der Zee, J. (2020). Stress granule mediated protein aggregation and underlying gene defects in the FTD-ALS spectrum. *Neurobiology of Disease, 134*, 104639. 10.1016/j.nbd.2019.104639

Bayati, A., & McPherson, P. S. (2024). Alpha-synuclein, autophagy-lysosomal pathway, and Lewy bodies: Mutations, propagation, aggregation, and the formation of inclusions. *The Journal of Biological Chemistry, 300*(10), 107742. 10.1016/j.jbc.2024.107742

Bayer, T. A. (2015). Proteinopathies, a core concept for understanding and ultimately treating degenerative disorders? *European Neuropsychopharmacology, 25*(5), 713–724. 10.1016/j.euroneuro.2013.03.007

B'chir, W., Maurin, A., Carraro, V., Averous, J., Jousse, C., Muranishi, Y., Parry, L., Stepien, G., Fafournoux, P., & Bruhat, A. (2013). The eIF2α/ATF4 pathway is essential for stress-induced autophagy gene expression. *Nucleic Acids Research, 41*(16), 7683–7699. 10.1093/nar/gkt563

Beatriz, M., Rodrigues, R. J., Vilaça, R., Egas, C., Pinheiro, P. S., Daley, G. Q., Schlaeger, T. M., Raimundo, N., Rego, A. C., & Lopes, C. (2023). Extracellular vesicles improve GABAergic transmission in Huntington's disease iPSC-derived neurons. *Theranostics, 13*(11), 3707–3724. 10.7150/thno.81981

Behrends, M., & Engmann, O. (2020). Linker histone H1.5 is an underestimated factor in differentiation and carcinogenesis. *Environmental Epigenetics, 6*(1), dvaa013. 10.1093/eep/dvaa013

Bellucci, A., Navarria, L., Zaltieri, M., Falarti, E., Bodei, S., Sigala, S., Battistin, L., Spillantini, M., Missale, C., & Spano, P. (2011). Induction of the unfolded protein response by α-synuclein in experimental models of Parkinson's

disease. *Journal of Neurochemistry, 116*(4), 588–605. 10.1111/j.1471-4159.2010.07143.

Bendor, J., Logan, T., & Edwards, R. H. (2013). The Function of α-Synuclein. *Neuron, 79*(6), 10.1016/j.neuron.2013.09.004. 10.1016/j.neuron.2013.09.004

Bernal-Conde, L. D., Ramos-Acevedo, R., Reyes-Hernández, M. A., Balbuena-Olvera, A. J., Morales-Moreno, I. D., Argüero-Sánchez, R., Schüle, B., & Guerra-Crespo, M. (2019). Alpha-Synuclein Physiology and Pathology: A Perspective on Cellular Structures and Organelles. *Frontiers in Neuroscience, 13*, 1399. 10.3389/fnins.2019.01399

Bharathi, n., Indi, S. S., & Rao, K. S. J. (2007). Copper- and iron-induced differential fibril formation in alpha-synuclein: TEM study. *Neuroscience Letters, 424*(2), 78–82. 10.1016/j.neulet.2007.06.052

Bhusal, A., Kim, J., Kim, S., Hwang, E. M., Ryu, H., Ali, M. S., Park, S., Lee, W., & Suk, K. (2024). The microglial innate immune protein PGLYRP1 mediates neuroinflammation and consequent behavioral changes. *Cell Reports, 43*(3), 113813. 10.1016/j.celrep.2024.113813

Bo, R., Li, Y., Zhou, T., Chen, N., & Yuan, Y. (2022). The neuroinflammatory role of glucocerebrosidase in Parkinson's disease. *Neuropharmacology, 207*, 108964. 10.1016/j.neuropharm.2022.108964

Boer, D. E. C., van Smeden, J., Bouwstra, J. A., & Aerts, J. M. F. G. (2020). Glucocerebrosidase: Functions in and Beyond the Lysosome. *Journal of Clinical Medicine, 9*(3), 736. 10.3390/jcm9030736

Bogorad, A. M., Lin, K. Y., & Marintchev, A. (2018). eIF2B Mechanisms of Action and Regulation: A Thermodynamic View. *Biochemistry, 57*(9), 1426–1435. 10.1021/acs.biochem.7b00957

Bond, S., Lopez-Lloreda, C., Gannon, P. J., Akay-Espinoza, C., & Jordan-Sciutto, K. L. (2020). The Integrated Stress Response and Phosphorylated Eukaryotic Initiation Factor 2α in Neurodegeneration. *Journal of*

Neuropathology and Experimental Neurology, 79(2), 123–143. 10.1093/jnen/nlz129

Bordeleau, M., Cencic, R., Lindqvist, L., Oberer, M., Northcote, P., Wagner, G., & Pelletier, J. (2006). RNA-mediated sequestration of the RNA helicase eIF4A by Pateamine A inhibits translation initiation. *Chemistry & Biology, 13*(12), 1287–1295. 10.1016/j.chembiol.2006.10.005

Bové, J., Prou, D., Perier, C., & Przedborski, S. (2005). Toxin-Induced Models of Parkinson's Disease. *NeuroRx, 2*(3), 484–494.

Bressler, K. R., Ross, J. A., Ilnytskyy, S., Vanden Dungen, K., Taylor, K., Patel, K., Zovoilis, A., Kovalchuk, I., & Thakor, N. (2021). Depletion of eukaryotic initiation factor 5B (eIF5B) reprograms the cellular transcriptome and leads to activation of endoplasmic reticulum (ER) stress and c-Jun N-terminal kinase (JNK). *Cell Stress & Chaperones, 26*(1), 253–264. 10.1007/s12192-020-01174-1

Brion, J. P., Anderton, B. H., Authelet, M., Dayanandan, R., Leroy, K., Lovestone, S., Octave, J. N., Pradier, L., Touchet, N., & Tremp, G. (2001). Neurofibrillary tangles and tau phosphorylation. *Biochemical Society Symposium,* (67), 81–88. 10.1042/bss0670081

Brooker, S. M., & Krainc, D. (2021). Glucocerebrosidase dysfunction in neurodegenerative disease. *Essays in Biochemistry, 65*(7), 873–883. 10.1042/EBC20210018

Brush, M. H., & Shenolikar, S. (2008). Control of Cellular GADD34 Levels by the 26S Proteasome. *Molecular and Cellular Biology, 28*(23), 6989–7000. 10.1128/MCB.00724-08

Buée, L., Bussière, T., Buée-Scherrer, V., Delacourte, A., & Hof, P. R. (2000). Tau protein isoforms, phosphorylation and role in neurodegenerative disorders. *Brain Research. Brain Research Reviews, 33*(1), 95–130. 10.1016/s0165-0173(00)00019-9

Bui, T. M., Wiesolek, H. L., & Sumagin, R. (2020). ICAM-1: A master regulator of cellular responses in inflammation, injury resolution, and

tumorigenesis. *Journal of Leukocyte Biology, 108*(3), 787–799. 10.1002/JLB.2MR0220-549R

Bui, T. M., Wiesolek, H. L., & Sumagin, R. (2020b). ICAM-1: A master regulator of cellular responses in inflammation, injury resolution, and tumorigenesis. *Journal of Leukocyte Biology, 108*(3), 787–799. 10.1002/JLB.2MR0220-549R

Burré, J., Sharma, M., Tsetsenis, T., Buchman, V., Etherton, M., & Südhof, T. C. (2010). α-Synuclein Promotes SNARE-Complex Assembly in vivo and in vitro. *Science (New York, N.Y.), 329*(5999), 1663–1667. 10.1126/science.1195227

Cadena Sandoval, M., Heberle, A. M., Rehbein, U., Barile, C., Ramos Pittol, J. M., & Thedieck, K. (2021). mTORC1 Crosstalk With Stress Granules in Aging and Age-Related Diseases. *Frontiers in Aging, 2*, 761333. 10.3389/fragi.2021.761333

Cai, Q., Pan, P., & Sheng, Z. (2007). Syntabulin–Kinesin-1 Family Member 5B-Mediated Axonal Transport Contributes to Activity-Dependent Presynaptic Assembly. *The Journal of Neuroscience, 27*(27), 7284–7296. 10.1523/JNEUROSCI.0731-07.2007

Calabresi, P., Mechelli, A., Natale, G., Volpicelli-Daley, L., Di Lazzaro, G., & Ghiglieri, V. (2023). Alpha-synuclein in Parkinson's disease and other synucleinopathies: from overt neurodegeneration back to early synaptic dysfunction. *Cell Death & Disease, 14*(3), 176. 10.1038/s41419-023-05672-9

Campos-Melo, D., Hawley, Z. C. E., Droppelmann, C. A., & Strong, M. J. (2021). The Integral Role of RNA in Stress Granule Formation and Function. *Frontiers in Cell and Developmental Biology, 9*, 621779. 10.3389/fcell.2021.621779

Canham, L., Sendac, S., Diagbouga, M. R., Wolodimeroff, E., Pirri, D., Tardajos Ayllon, B., Feng, S., Souilhol, C., Chico, T. J. A., Evans, P. C., & Serbanovic-Canic, J. (2023). EVA1A (Eva-1 Homolog A) Promotes Endothelial Apoptosis and Inflammatory Activation Under Disturbed Flow Via Regulation

of Autophagy. *Arteriosclerosis, Thrombosis, and Vascular Biology, 43*(4), 547–561. 10.1161/ATVBAHA.122.318110

Cascella, R., Chen, S. W., Bigi, A., Camino, J. D., Xu, C. K., Dobson, C. M., Chiti, F., Cremades, N., & Cecchi, C. (2021). The release of toxic oligomers from α-synuclein fibrils induces dysfunction in neuronal cells. *Nature Communications, 12*, 1814. 10.1038/s41467-021-21937-3

Cerri, S., Mus, L., & Blandini, F. (2019). Parkinson's Disease in Women and Men: What's the Difference? - PubMed. *J Parkinson Dis., 9*(3), 501–515. 10.3233/JPD-191683

Chakrabarty, Y., Yang, Z., Chen, H., & Chan, D. C. (2024). The HRI branch of the integrated stress response selectively triggers mitophagy. *Molecular Cell, 84*(6), 1090–1100.e6. 10.1016/j.molcel.2024.01.016

Chang, W., Cerione, R. A., & Antonyak, M. A. (2021). Extracellular Vesicles and Their Roles in Cancer Progression. *Methods in Molecular Biology (Clifton, N.J.), 2174*, 143–170. 10.1007/978-1-0716-0759-6_10

Chaudhuri, K. R., Healy, D. G., & Schapira, A. H. V. (2006). Non-motor symptoms of Parkinson's disease: diagnosis and management. *The Lancet. Neurology, 5*(3), 235–245. 10.1016/S1474-4422(06)70373-8

Chen, G., Xu, T., Yan, Y., Zhou, Y., Jiang, Y., Melcher, K., & Xu, H. E. (2017). Amyloid beta: structure, biology and structure-based therapeutic development. *Acta Pharmacologica Sinica, 38*(9), 1205–1235. 10.1038/aps.2017.28

Chen, K., Martens, Y. A., Meneses, A., Ryu, D. H., Lu, W., Raulin, A. C., Li, F., Zhao, J., Chen, Y., Jin, Y., Linares, C., Goodwin, M., Li, Y., Liu, C., Kanekiyo, T., Holtzman, D. M., Golde, T. E., Bu, G., & Zhao, N. (2022). LRP1 is a neuronal receptor for α-synuclein uptake and spread. *Molecular Neurodegeneration, 17*(1), 57. 10.1186/s13024-022-00560-w

Chen, X., Guo, C., & Kong, J. (2012). Oxidative stress in neurodegenerative diseases. *Neural Regeneration Research, 7*(5), 376–385. 10.3969/j.issn.1673-5374.2012.05.009

Chen, X., Shi, C., He, M., Xiong, S., & Xia, X. (2023). Endoplasmic reticulum stress: molecular mechanism and therapeutic targets. *Signal Transduction and Targeted Therapy, 8*(1), 1–40. 10.1038/s41392-023-01570-w

Chen, Y., Podojil, J. R., Kunjamma, R. B., Jones, J., Weiner, M., Lin, W., Miller, S. D., & Popko, B. (2019). Sephin1, which prolongs the integrated stress response, is a promising therapeutic for multiple sclerosis. *Brain: A Journal of Neurology, 142*(2), 344–361. 10.1093/brain/awy322

Chen, Y., Zhang, H., & Zhang, Y. (2019). Targeting receptor tyrosine kinase EphB4 in cancer therapy. *Seminars in Cancer Biology, 56*, 37–46. 10.1016/j.semcancer.2017.10.002

Chiaradia, E., Tancini, B., Emiliani, C., Delo, F., Pellegrino, R. M., Tognoloni, A., Urbanelli, L., & Buratta, S. (2021). Extracellular Vesicles under Oxidative Stress Conditions: Biological Properties and Physiological Roles. *Cells, 10*(7), 1763. 10.3390/cells10071763

Chin, K. S., Yassi, N., Churilov, L., Masters, C. L., & Watson, R. (2020). Prevalence and clinical associations of tau in Lewy body dementias: A systematic review and meta-analysis. *Parkinsonism & Related Disorders, 80*, 184–193. 10.1016/j.parkreldis.2020.09.030

Cho, Y., Kim, G., & Park, J. (2021). Mitochondrial aconitase 1 regulates age-related memory impairment via autophagy/mitophagy-mediated neural plasticity in middle-aged flies. *Aging Cell, 20*(12), e13520. 10.1111/acel.13520

Chun, H. S., Gibson, G. E., DeGiorgio, L. A., Zhang, H., Kidd, V. J., & Son, J. H. (2001). Dopaminergic cell death induced by MPP(+), oxidant and specific neurotoxicants shares the common molecular mechanism. *Journal of Neurochemistry, 76*(4), 1010–1021. 10.1046/j.1471-4159.2001.00096.

Chung, Y., Yim, C., Pereira, G. P., Son, S., Kjølbye, L. R., Mazurkiewicz, L. E., Weeks, A. M., Förster, F., von Heijne, G., Souza, P. C. T., & Kim, H. (2024). Spc2 modulates substrate- and cleavage site-selection in the yeast signal peptidase complex. *The Journal of Cell Biology, 223*(12), e202211035. 10.1083/jcb.202211035

Cochran, B. J., Ong, K., Manandhar, B., & Rye, K. (2021). APOA1: a Protein with Multiple Therapeutic Functions. *Current Atherosclerosis Reports, 23*(3), 11. 10.1007/s11883-021-00906-7

Cömert, C., Brick, L., Ang, D., Palmfeldt, J., Meaney, B. F., Kozenko, M., Georgopoulos, C., Fernandez-Guerra, P., & Bross, P. (2020). A recurrent de novo HSPD1 variant is associated with hypomyelinating leukodystrophy. *Cold Spring Harbor Molecular Case Studies, 6*(3), a004879. 10.1101/mcs.a004879

Comfort, N., Cai, K., Bloomquist, T. R., Strait, M. D., Ferrante, A. W., & Baccarelli, A. A. (2021). Nanoparticle Tracking Analysis for the Quantification and Size Determination of Extracellular Vesicles. *Journal of Visualized Experiments : JoVE,* (169), 10.3791/62447. 10.3791/62447

Costa-Mattioli, M., & Walter, P. (2020). The integrated stress response: From mechanism to disease. *Science (New York, N.Y.), 368*(6489), eaat5314. 10.1126/science.aat5314

Costanzi, C., & Pehrson, J. R. (2001). MACROH2A2, a New Member of the MACROH2A Core Histone Family*. *Journal of Biological Chemistry, 276*(24), 21776–21784. 10.1074/jbc.M010919200

Coyne, A. N., & Rothstein, J. D. (2021). The ESCRT-III protein VPS4, but not CHMP4B or CHMP2B, is pathologically increased in familial and sporadic ALS neuronal nuclei. *Acta Neuropathologica Communications, 9*(1), 127. 10.1186/s40478-021-01228-0

Cuende, J., Moreno, S., Bolaños, J. P., & Almeida, A. (2008). Retinoic acid downregulates Rae1 leading to APCCdh1 activation and neuroblastoma SH-SY5Y differentiation. *Oncogene, 27*(23), 3339–3344. 10.1038/sj.onc.1210987

Cui, J., Chen, W., Sun, J., Guo, H., Madley, R., Xiong, Y., Pan, X., Wang, H., Tai, A. W., Weiss, M. A., Arvan, P., & Liu, M. (2015). Competitive Inhibition of the Endoplasmic Reticulum Signal Peptidase by Non-cleavable Mutant Preprotein Cargos. *The Journal of Biological Chemistry, 290*(47), 28131–28140. 10.1074/jbc.M115.692350

da Costa, C. A., Manaa, W. E., Duplan, E., & Checler, F. (2020). The Endoplasmic Reticulum Stress/Unfolded Protein Response and Their Contributions to Parkinson's Disease Physiopathology. *Cells, 9*(11), 2495. 10.3390/cells9112495

Danzer, K. M., Haasen, D., Karow, A. R., Moussaud, S., Habeck, M., Giese, A., Kretzschmar, H., Hengerer, B., & Kostka, M. (2007). Different species of alpha-synuclein oligomers induce calcium influx and seeding. *The Journal of Neuroscience: The Official Journal of the Society for Neuroscience, 27*(34), 9220–9232. 10.1523/JNEUROSCI.2617-07.2007

D'Arcy, M. S. (2019). Cell death: a review of the major forms of apoptosis, necrosis and autophagy. *Cell Biology International, 43*(6), 582–592. 10.1002/cbin.11137

Darvishi, B., Boroumandieh, S., Majidzadeh-A, K., Salehi, M., Jafari, F., & Farahmand, L. (2020). The role of activated leukocyte cell adhesion molecule (ALCAM) in cancer progression, invasion, metastasis and recurrence: A novel cancer stem cell marker and tumor-specific prognostic marker. *Experimental and Molecular Pathology, 115*, 104443. 10.1016/j.yexmp.2020.104443

Das, N., Schmidt, T. A., Krawetz, R. J., & Dufour, A. (2019). Proteoglycan 4: From Mere Lubricant to Regulator of Tissue Homeostasis and Inflammation: Does proteoglycan 4 have the ability to buffer the inflammatory response? *BioEssays: News and Reviews in Molecular, Cellular and Developmental Biology, 41*(1), e1800166. 10.1002/bies.201800166

Daubner, S. C., Le, T., & Wang, S. (2011). Tyrosine Hydroxylase and Regulation of Dopamine Synthesis. *Archives of Biochemistry and Biophysics, 508*(1), 1–12. 10.1016/j.abb.2010.12.017

de Hoop, M. J., Huber, L. A., Stenmark, H., Williamson, E., Zerial, M., Parton, R. G., & Dotti, C. G. (1994). The involvement of the small GTP-binding protein Rab5a in neuronal endocytosis. *Neuron, 13*(1), 11–22. 10.1016/0896-6273(94)90456-1

Deas, E., Cremades, N., Angelova, P. R., Ludtmann, M. H. R., Yao, Z., Chen, S., Horrocks, M. H., Banushi, B., Little, D., Devine, M. J., Gissen, P.,

Klenerman, D., Dobson, C. M., Wood, N. W., Gandhi, S., & Abramov, A. Y. (2016). Alpha-Synuclein Oligomers Interact with Metal Ions to Induce Oxidative Stress and Neuronal Death in Parkinson's Disease. *Antioxidants & Redox Signaling, 24*(7), 376–391. 10.1089/ars.2015.6343

Deas, E., Plun-Favteau, & Wood, N. W. (2009). PINK1 function in health and disease - PMC. *EMBO Mol Med., 1*(3), 152–165. 10.1002/emmm.200900024

Demmings, M. D., Tennyson, E. C., Petroff, G. N., Tarnowski-Garner, H. E., & Cregan, S. P. (2021). Activating transcription factor-4 promotes neuronal death induced by Parkinson's disease neurotoxins and α-synuclein aggregates. *Cell Death and Differentiation, 28*(5), 1627–1643. 10.1038/s41418-020-00688-6

Deng, G., Luo, Y., Zhang, Y., Zhang, J., & He, Z. (2022) Enabled homolog (ENAH) regulated by RNA binding protein splicing factor 3b subunit 4 (SF3B4) exacerbates the proliferation, invasion and migration of hepatocellular carcinoma cells via Notch signaling pathway. *Bioengineered, 13*(2), 2194–2206. 10.1080/21655979.2021.2023983

Derisbourg, M. J., Hartman, M. D., & Denzel, M. S. (2021). Perspective: Modulating the integrated stress response to slow aging and ameliorate age-related pathology. *Nature Aging, 1*(9), 760–768. 10.1038/s43587-021-00112-9

Devi, L., Raghavendran, V., Prabhu, B. M., Avadhani, N. G., & Anandatheerthavarada, H. K. (2008). Mitochondrial Import and Accumulation ofα-Synuclein Impair Complex I in Human Dopaminergic Neuronal Cultures and Parkinson Disease Brain. *The Journal of Biological Chemistry, 283*(14), 9089–9100. 10.1074/jbc.M710012200

Dey, S., Baird, T. D., Zhou, D., Palam, L. R., Spandau, D. F., & Wek, R. C. (2010). Both Transcriptional Regulation and Translational Control of ATF4 Are Central to the Integrated Stress Response. *The Journal of Biological Chemistry, 285*(43), 33165–33174. 10.1074/jbc.M110.167213

Dhakal, S., Wyant, C. E., George, H. E., Morgan, S. E., & Rangachari, V. (2021). Prion-like C-terminal domain of TDP-43 and α-Synuclein interact

synergistically to generate neurotoxic hybrid fibrils. *Journal of Molecular Biology, 433*(10), 166953. 10.1016/j.jmb.2021.166953

Di Liegro, C. M., Schiera, G., & Di Liegro, I. (2018). H1.0 Linker Histone as an Epigenetic Regulator of Cell Proliferation and Differentiation. *Genes, 9*(6), 310. 10.3390/genes9060310

Di Mambro, T., Pellielo, G., Agyapong, E. D., Carinci, M., Chianese, D., Giorgi, C., Morciano, G., Patergnani, S., Pinton, P., & Rimessi, A. (2023). The Tricky Connection between Extracellular Vesicles and Mitochondria in Inflammatory-Related Diseases. *International Journal of Molecular Sciences, 24*(9), 8181. 10.3390/ijms24098181

Dias, V., Junn, E., & Mouradian, M. M. (2013). The Role of Oxidative Stress in Parkinson's Disease. *Journal of Parkinson's Disease, 3*(4), 461–491. 10.3233/JPD-130230

Dilsiz, N. (2024). A comprehensive review on recent advances in exosome isolation and characterization: Toward clinical applications. *Translational Oncology, 50*, 102121. 10.1016/j.tranon.2024.102121

Dimasi, P., Quintiero, A., Shelkovnikova, T. A., & Buchman, V. L. (2017). Modulation of p-eIF2α cellular levels and stress granule assembly/disassembly by trehalose. *Scientific Reports, 7*(1), 44088. 10.1038/srep44088

Doherty, C. P. A., Ulamec, S. M., Maya-Martinez, R., Good, S. C., Makepeace, J., Khan, G. N., van Oosten-Hawle, P., Radford, S. E., & Brockwell, D. J. (2020). A short motif in the N-terminal region of α-synuclein is critical for both aggregation and function. *Nature Structural & Molecular Biology, 27*(3), 249–259. 10.1038/s41594-020-0384-x

Domingues, R., Sant'Anna, R., da Fonseca, A. C. C., Robbs, B. K., Foguel, D., & Outeiro, T. F. (2022). Extracellular alpha-synuclein: Sensors, receptors, and responses. *Neurobiology of Disease, 168*, 105696. 10.1016/j.nbd.2022.105696

Dommett, R. M., Klein, N., & Turner, M. W. (2006). Mannose-binding lectin in innate immunity: past, present and future. *Tissue Antigens, 68*(3), 193–209. 10.1111/j.1399-0039.2006.00649.

Dong-Chen, X., Yong, C., Yang, X., Chen-Yu, S., & Li-Hua, P. (2023). Signaling pathways in Parkinson's disease: molecular mechanisms and therapeutic interventions. *Signal Transduction and Targeted Therapy, 8*(1), 1–18. 10.1038/s41392-023-01353-3

Dorszewska, J., Kowalska, M., Prendecki, M., Piekut, T., Kozłowska, J., & Kozubski, W. (2021). Oxidative stress factors in Parkinson's disease. *Neural Regeneration Research, 16*(7), 1383–1391. 10.4103/1673-5374.300980

Du, X., Xie, X., & Liu, R. (2020). The Role of α-Synuclein Oligomers in Parkinson's Disease. *International Journal of Molecular Sciences, 21*(22), 8645. 10.3390/ijms21228645

Dudman, J., & Qi, X. (2020). Stress Granule Dysregulation in Amyotrophic Lateral Sclerosis. *Frontiers in Cellular Neuroscience, 14*, 598517. 10.3389/fncel.2020.598517

Dumitriu, D., Rodriguez, A., & Harrison, J. H. (2011). High-throughput, detailed, cell-specific neuroanatomy of dendritic spines using microinjection and confocal microscopy - PubMed. *Nat Protoc., 6*(9), 1391–1411. 10.1038/nprot.2011.389

Dunn, K. W., Kamocka, M. M., & McDonald, J. H. (2011). A practical guide to evaluating colocalization in biological microscopy. *American Journal of Physiology - Cell Physiology, 300*(4), C723–C742. 10.1152/ajpcell.00462.2010

Durham, P. L., & Snyder, J. M. (1995). Characterization of alpha 1, beta 1, and gamma 1 laminin subunits during rabbit fetal lung development. *Developmental Dynamics: An Official Publication of the American Association of Anatomists, 203*(4), 408–421. 10.1002/aja.1002030404

Dutta, S., Hornung, S., Taha, H. B., & Bitan, G. (2023). Biomarkers for parkinsonian disorders in CNS-originating EVs: promise and challenges. *Acta Neuropathologica, 145*(5), 515–540. 10.1007/s00401-023-02557-1

Eckenstaler, R., Hauke, M., & Benndorf, R. A. (2022). A current overview of RhoA, RhoB, and RhoC functions in vascular biology and pathology. *Biochemical Pharmacology, 206*, 115321. 10.1016/j.bcp.2022.115321

Elbitar, S., Renard, M., Arnaud, P., Hanna, N., Jacob, M., Guo, D., Tsutsui, K., Gross, M., Kessler, K., Tosolini, L., Dattilo, V., Dupont, S., Jonquet, J., Langeois, M., Benarroch, L., Aubart, M., Ghaleb, Y., Abou Khalil, Y., Varret, M., . . . Abifadel, M. (2021). Pathogenic variants in THSD4, encoding the ADAMTS-like 6 protein, predispose to inherited thoracic aortic aneurysm. *Genetics in Medicine: Official Journal of the American College of Medical Genetics, 23*(1), 111–122. 10.1038/s41436-020-00947-4

Elhodaky, M., & Diamond, A. M.Selenium-Binding Protein 1 in Human Health and Disease - PMC. *Int J Mol Sci., 19*(11), 3437. 10.3390/ijms19113437

Enam, S. U., Zinshteyn, B., Goldman, D. H., Cassani, M., Livingston, N. M., Seydoux, G., & Green, R. (2020). Puromycin reactivity does not accurately localize translation at the subcellular level. *eLife, 9*, e60303. 10.7554/eLife.60303

English, B. C., Van Prooyen, N., Örd, T., Örd, T., & Sil, A. (2017). The transcription factor CHOP, an effector of the integrated stress response, is required for host sensitivity to the fungal intracellular pathogen Histoplasma capsulatum. *PLoS Pathogens, 13*(9), e1006589. 10.1371/journal.ppat.1006589

Esteves, A. R., Swerdlow, R. H., & Cardoso, S. M. (2014). LRRK2, a puzzling protein: insights into Parkinson's disease pathogenesis. *Experimental Neurology, 0*, 206–216. 10.1016/j.expneurol.2014.05.025

Fang, L., Che, Y., Zhang, C., Huang, J., Lei, Y., Lu, Z., Sun, N., & He, J. (2021). LAMC1 upregulation via TGFβ induces inflammatory cancer-associated

fibroblasts in esophageal squamous cell carcinoma via NF-κB–CXCL1–STAT3. *Molecular Oncology, 15*(11), 3125–3146. 10.1002/1878-0261.13053

Farrar, C. A., Tran, D., Li, K., Wu, W., Peng, Q., Schwaeble, W., Zhou, W., & Sacks, S. H. (2016). Collectin-11 detects stress-induced L-fucose pattern to trigger renal epithelial injury. *The Journal of Clinical Investigation, 126*(5), 1911–1925. 10.1172/JCI83000

Farzadfard, A., Pedersen, J. N., Meisl, G., Somavarapu, A. K., Alam, P., Goksøyr, L., Nielsen, M. A., Sander, A. F., Knowles, T. P. J., Pedersen, J. S., & Otzen, D. E. (2022). The C-terminal tail of α-synuclein protects against aggregate replication but is critical for oligomerization. *Communications Biology, 5*(1), 123. 10.1038/s42003-022-03059-8

Feng, C., Flores, M., Dhoj, C., Garcia, A., Belleca, S., Abbas, D. A., Parres-Gold, J., Anguiano, A., Porter, E., & Wang, Y. (2022). Observation of α-Synuclein Preformed Fibrils Interacting with SH-SY5Y Neuroblastoma Cell Membranes Using Scanning Ion Conductance Microscopy. *ACS Chemical Neuroscience, 13*(24), 3547–3553. 10.1021/acschemneuro.2c00478

Feng, W., Wang, X., Wu, Y., Li, X., Chen, S., Wang, X., Wang, Z., Fang, F., & Chen, C. (2024). Clinical analysis of PAFAH1B1 gene variants in pediatric patients with epilepsy. *Seizure, 117*, 98–104. 10.1016/j.seizure.2024.01.020

Ferrari, E., Salvadè, M., Zianni, E., Brumana, M., DiLuca, M., & Gardoni, F. (2023). Detrimental effects of soluble α-synuclein oligomers at excitatory glutamatergic synapses. *Frontiers in Aging Neuroscience, 15*, 1152065. 10.3389/fnagi.2023.1152065

Fiorese, C. J., Schulz, A. M., Lin, Y., Rosin, N., Pellegrino, M. W., & Haynes, C. M. (2016). The transcription factor ATF5 mediates a mammalian mitochondrial UPR. *Current Biology : CB, 26*(15), 2037–2043. 10.1016/j.cub.2016.06.002

Flagmeier, P., Meisl, G., Vendruscolo, M., Knowles, T. P. J., Dobson, C. M., Buell, A. K., & Galvagnion, C. (2016). Mutations associated with familial Parkinson's disease alter the initiation and amplification steps of α-synuclein

aggregation. *Proceedings of the National Academy of Sciences of the United States of America, 113*(37), 10328–10333. 10.1073/pnas.1604645113

Flury, A., Aljayousi, L., Park, H., Khakpour, M., Mechler, J., Aziz, S., McGrath, J. D., Deme, P., Sandberg, C., Ibáñez, F. G., Braniff, O., Ngo, T., Smith, S., Velez, M., Ramirez, D. M., Avnon-Klein, D., Murray, J. W., Liu, J., Parent, M., Ayata, P. (2025). A neurodegenerative cellular stress response linked to dark microglia and toxic lipid secretion. *Neuron, 113*(4), 554–571.e14. 10.1016/j.neuron.2024.11.018

Fonseka, P., & Mathivanan, S. (2023). Extracellular Vesicles Biogenesis, Cargo Sorting and Implications in Disease Conditions. *Cells, 12*(2), 280. 10.3390/cells12020280

Freibaum, B. D., Messing, J., Nakamura, H., Yurtsever, U., Wu, J., Kim, H. J., Hixon, J., Lemieux, R., Duffner, J., Huynh, W., Wong, K., White, M., Lee, C., Meyers, R., Parker, R., & Taylor, J. P. (2023). Identification of small molecule inhibitors of G3BP-driven stress granule formation. *bioRxiv,* , 2023.06.27.546770. 10.1101/2023.06.27.546770

Fu, S., Zhang, Y., Li, Y., Luo, L., Zhao, Y., & Yao, Y. (2020). Extracellular vesicles in cardiovascular diseases. *Cell Death Discovery, 6*, 68. 10.1038/s41420-020-00305-y

Fujimura, K., Sasaki, A. T., & Anderson, P. (2012). Selenite targets eIF4E-binding protein-1 to inhibit translation initiation and induce the assembly of non-canonical stress granules. *Nucleic Acids Research, 40*(16), 8099–8110. 10.1093/nar/gks566

Fujita, K. A., Ostaszewski, M., Matsuoka, Y., Ghosh, S., Glaab, E., Trefois, C., Crespo, I., Perumal, T. M., Jurkowski, W., Antony, P. M. A., Diederich, N., Buttini, M., Kodama, A., Satagopam, V. P., Eifes, S., del Sol, A., Schneider, R., Kitano, H., & Balling, R. (2014). Integrating Pathways of Parkinson's Disease in a Molecular Interaction Map. *Molecular Neurobiology, 49*(1), 88–102. 10.1007/s12035-013-8489-4

Gallop, A., Weagley, J., Paracha, S., & Grossberg, G. (2021). The Role of The Gut Microbiome in Parkinson's Disease. *Journal of Geriatric Psychiatry and Neurology, 34*(4), 253–262. 10.1177/08919887211018268

Ganguly, G., Chakrabarti, S., Chatterjee, U., & Saso, L. (2017). Proteinopathy, oxidative stress and mitochondrial dysfunction: cross talk in Alzheimer's disease and Parkinson's disease. *Drug Design, Development and Therapy, 11*, 797–810. 10.2147/DDDT.S130514

Garcia-Contreras, M., & Thakor, A. S. (2022). Extracellular vesicles in Alzheimer's disease: from pathology to therapeutic approaches. *Neural Regeneration Research, 18*(1), 18–22. 10.4103/1673-5374.343882

Gasperini, L., Rossi, A., Cornella, N., Peroni, D., Zuccotti, P., Potrich, V., Quattrone, A., & Macchi, P. (2018). The hnRNP RALY regulates PRMT1 expression and interacts with the ALS-linked protein FUS: implication for reciprocal cellular localization. *Molecular Biology of the Cell, 29*(26), 3067–3081. 10.1091/mbc.E18-02-0108

Gavin, R. L., Koo, C. Z., & Tomlinson, M. G. (2020). Tspan18 is a novel regulator of thrombo-inflammation. *Medical Microbiology and Immunology, 209*(4), 553–564. 10.1007/s00430-020-00678-y

Ge, P., Dawson, V. L., & Dawson, T. M. (2020). PINK1 and Parkin mitochondrial quality control: a source of regional vulnerability in Parkinson's disease. *Molecular Neurodegeneration, 15*(1), 20. 10.1186/s13024-020-00367-7

Ghadami, S., & Dellinger, K. (2023). The lipid composition of extracellular vesicles: applications in diagnostics and therapeutic delivery. *Frontiers in Molecular Biosciences, 10*, 1198044. 10.3389/fmolb.2023.1198044

Ghosh, D., Singh, P. K., Sahay, S., Jha, N. N., Jacob, R. S., Sen, S., Kumar, A., Riek, R., & Maji, S. K. (2015). Structure based aggregation studies reveal the presence of helix-rich intermediate during α-Synuclein aggregation. *Scientific Reports, 5*, 9228. 10.1038/srep09228

Girardin, S. E., Cuziol, C., Philpott, D. J., & Arnoult, D. (2021). The eIF2α kinase HRI in innate immunity, proteostasis, and mitochondrial stress. *The FEBS Journal, 288*(10), 3094–3107. 10.1111/febs.15553

Glineburg, M. R., Yildirim, E., Gomez, N., Li, X., Pak, J., Altheim, C., Waksmacki, J., McInerney, G., Barmada, S. J., & Todd, P. K. (2023). Stress granule formation helps to mitigate neurodegeneration. *bioRxiv: The Preprint Server for Biology,* , 2023.11.07.566060. 10.1101/2023.11.07.566060

Goh, C. W., Lee, I. C., Sundaram, J. R., George, S. E., Yusoff, P., Brush, M. H., Sze, N. S. K., & Shenolikar, S. (2018). Chronic oxidative stress promotes GADD34-mediated phosphorylation of the TAR DNA-binding protein TDP-43, a modification linked to neurodegeneration. *The Journal of Biological Chemistry, 293*(1), 163–176. 10.1074/jbc.M117.814111

Goleva, E., Berdyshev, E., Kreimer, S., Reisz, J. A., D'Alessandro, A., Bronova, I., Lyubchenko, T., Richers, B. N., Hall, C. F., Xiao, O., Bronoff, A., Bafna, S., Agueusop, I., Gloaguen, E., Zahn, J., Bissonnette, R., Zhang, A., & Leung, D. Y. M. (2025). Longitudinal integrated proteomic and metabolomic skin changes in patients with atopic dermatitis treated with dupilumab. *Journal of Allergy and Clinical Immunology, 155*(5), 1536–1546. 10.1016/j.jaci.2025.01.020

Gomes, P. A., Bodo, C., Nogueras-Ortiz, C., Samiotaki, M., Chen, M., Soares-Cunha, C., Silva, J. M., Coimbra, B., Stamatakis, G., Santos, L., Panayotou, G., Tzouanou, F., Waites, C. L., Gatsogiannis, C., Sousa, N., Kapogiannis, D., Costa-Silva, B., & Sotiropoulos, I. (2023). A novel isolation method for spontaneously released extracellular vesicles from brain tissue and its implications for stress-driven brain pathology. *Cell Communication and Signaling : CCS, 21*, 35. 10.1186/s12964-023-01045-z

Greenwald, J., & Riek, R. (2010). Biology of amyloid: structure, function, and regulation. *Structure (London, England: 1993), 18*(10), 1244–1260. 10.1016/j.str.2010.08.009

Gregory, L. C., Ferreira, C. B., Young-Baird, S. K., Williams, H. J., Harakalova, M., van Haaften, G., Rahman, S. A., Gaston-Massuet, C., Kelberman, D.,

Qasim, W., Camper, S. A., Dever, T. E., Shah, P., Robinson, I. C. A. F., & Dattani, M. T. (2019). Impaired EIF2S3 function associated with a novel phenotype of X-linked hypopituitarism with glucose dysregulation. *EBioMedicine, 42*, 470–480. 10.1016/j.ebiom.2019.03.013

Gremlich, S., Roth-Kleiner, M., Equey, L., Fytianos, K., Schittny, J. C., & Cremona, T. P. (2020). Tenascin-C inactivation impacts lung structure and function beyond lung development. *Scientific Reports, 10*(1), 5118. 10.1038/s41598-020-61919-x

Grmai, L., Michaca, M., Lackner, E., Narayanan, N. V. P., & Vasudevan, D. (2024). Integrated stress response signaling acts as a metabolic sensor in fat tissues to regulate oocyte maturation and ovulation. *Cell Reports, 43*(3), 113863. 10.1016/j.celrep.2024.113863

Gu, Q., Mi, L., Lai, C., Guan, X., Lu, N., Zhan, T., Wang, G., Lu, C., Xu, L., Gao, X., & Zhang, J. (2024). CPXM1 correlates to poor prognosis and immune cell infiltration in gastric cancer. *Heliyon, 10*(3), e21909. 10.1016/j.heliyon.2023.e21909

Guan, B., van Hoef, V., Jobava, R., Elroy-Stein, O., Valasek, L. S., Cargnello, M., Gao, X., Krokowski, D., Merrick, W. C., Kimball, S. R., Komar, A. A., Koromilas, A. E., Wynshaw-Boris, A., Topisirovic, I., Larsson, O., & Hatzoglou, M. (2017). A Unique ISR Program Determines Cellular Responses to Chronic Stress. *Molecular Cell, 68*(5), 885–900.e6. 10.1016/j.molcel.2017.11.007

Guerrero-Ferreira, R., Taylor, N. M., Mona, D., Ringler, P., Lauer, M. E., Riek, R., Britschgi, M., & Stahlberg, H. (2018). Cryo-EM structure of alpha-synuclein fibrils. *eLife, 7*, e36402. 10.7554/eLife.36402

Guo, E., Ishii, Y., Mueller, J., Srivatsan, A., Gahman, T., Putnam, C. D., Wang, J. Y. J., & Kolodner, R. D. (2020). FEN1 endonuclease as a therapeutic target for human cancers with defects in homologous recombination. *Proceedings of the National Academy of Sciences of the United States of America, 117*(32), 19415–19424. 10.1073/pnas.2009237117

Guo, T., Noble, W., & Hanger, D. P. (2017). Roles of tau protein in health and disease. *Acta Neuropathologica, 133*(5), 665–704. 10.1007/s00401-017-1707-9

Gussakovsky, D., Black, N. A., Booy, E. P., & McKenna, S. A. (2024). The role of SRP9/SRP14 in regulating Alu RNA. *RNA Biology, 21*(1), 1–12. 10.1080/15476286.2024.2430817

Gustafsson, G., Lööv, C., Persson, E., Lázaro, D. F., Takeda, S., Bergström, J., Erlandsson, A., Sehlin, D., Balaj, L., György, B., Hallbeck, M., Outeiro, T. F., Breakefield, X. O., Hyman, B. T., & Ingelsson, M. (2018). Secretion and Uptake of α-Synuclein Via Extracellular Vesicles in Cultured Cells. *Cellular and Molecular Neurobiology, 38*(8), 1539–1550. 10.1007/s10571-018-0622-5

Haaxma, C. A., Bloem, B. R., Borm, G. F., Oyen, W. J. G., Leenders, K. L., Eshuis, S., Booij, J., Dluzen, D. E., & Horstink, M. W. I. M. (2007). Gender differences in Parkinson's disease. *Journal of Neurology, Neurosurgery, and Psychiatry, 78*(8), 819–824. 10.1136/jnnp.2006.103788

Hadizadeh, N., Bagheri, D., Shamsara, M., Hamblin, M. R., Farmany, A., Xu, M., Liang, Z., Razi, F., & Hashemi, E. (2022). Extracellular vesicles biogenesis, isolation, manipulation and genetic engineering for potential in vitro and in vivo therapeutics: An overview. *Frontiers in Bioengineering and Biotechnology, 10*, 1019821. 10.3389/fbioe.2022.1019821

Hai, T., Wolford, C. C., & Chang, Y. (2018). ATF3, a Hub of the Cellular Adaptive-Response Network, in the Pathogenesis of Diseases: Is Modulation of Inflammation a Unifying Component? *Gene Expression, 15*(1), 1–11.

Ham, S. J., Lee, D., Xu, W. J., Cho, E., Choi, S., Min, S., Park, S., & Chung, J. (2021). Loss of UCHL1 rescues the defects related to Parkinson’s disease by suppressing glycolysis. *Science Advances, 7*(28), eabg4574. 10.1126/sciadv.abg4574

Henneke, G., Friedrich-Heineken, E., & Hübscher, U. (2003). Flap endonuclease 1: a novel tumour suppresser protein. *Trends in Biochemical Sciences, 28*(7), 384–390. 10.1016/S0968-0004(03)00138-5

Hetz, C., Zhang, K., & Kaufman, R. J. (2020). Mechanisms, regulation and functions of the unfolded protein response. *Nature Reviews Molecular Cell Biology, 21*(8), 421–438. 10.1038/s41580-020-0250-z

Hijaz, B. A., & Volpicelli-Daley, L. A. (2020). Initiation and propagation of α-synuclein aggregation in the nervous system. *Molecular Neurodegeneration, 15*(1), 19. 10.1186/s13024-020-00368-6

HIZ, S., KILIÇ, S., BADEMCİ, G., KARAKULAK, T., ERDOĞAN, A., ÖZDEN, B., ERESEN, Ç, ERDAL, E., YİŞ, U., TEKİN, M., KARAKÜLAH, G., KARACA, E., & ÖZTÜRK, M.VARS1 mutations associated with neurodevelopmental disorder are located on a short amino acid stretch of the anticodon-binding domain. *Turkish Journal of Biology, 46*(6), 458–464. 10.55730/1300-0152.2631

Hoeffer, C. A., & Klann, E. (2010). mTOR Signaling: At the Crossroads of Plasticity, Memory, and Disease. *Trends in Neurosciences, 33*(2), 67. 10.1016/j.tins.2009.11.003

Hofmann, S., Kedersha, N., Anderson, P., & Ivanov, P. (2021). Molecular mechanisms of stress granule assembly and disassembly. *Biochimica Et Biophysica Acta. Molecular Cell Research, 1868*(1), 118876. 10.1016/j.bbamcr.2020.118876

Homann, N., König, I. R., Marks, M., Benesova, M., Stickel, F., Millonig, G., Mueller, S., & Seitz, H. K. (2009). Alcohol and colorectal cancer: the role of alcohol dehydrogenase 1C polymorphism. *Alcoholism, Clinical and Experimental Research, 33*(3), 551–556. 10.1111/j.1530-0277.2008.00868.

Homann, N., Stickel, F., König, I. R., Jacobs, A., Junghanns, K., Benesova, M., Schuppan, D., Himsel, S., Zuber-Jerger, I., Hellerbrand, C., Ludwig, D., Caselmann, W. H., & Seitz, H. K. (2006). Alcohol dehydrogenase 1C*1 allele is a genetic marker for alcohol-associated cancer in heavy drinkers. *International Journal of Cancer, 118*(8), 1998–2002. 10.1002/ijc.21583

Hong, D., Fink, A. L., & Uversky, V. N. (2008). Structural Characteristics of the α-Synuclein Oligomers Stabilized by the Flavonoid Baicalein. *Journal of Molecular Biology, 383*(1), 214–223. 10.1016/j.jmb.2008.08.039

Hong, J., Kim, B., Choo, H., Park, J., Yi, J., Yu, D., Lee, H., Yoon, G., Lee, J., & Ko, Y. (2014). Mitochondrial Complex I Deficiency Enhances Skeletal Myogenesis but Impairs Insulin Signaling through SIRT1 Inactivation. *The Journal of Biological Chemistry, 289*(29), 20012–20025. 10.1074/jbc.M114.560078

Howe, J. W., Sortwell, C. E., Duffy, M. F., Kemp, C. J., Russell, C. P., Kubik, M., Patel, P., Luk, K. C., El-Agnaf, O. M. A., & Patterson, J. R. (2021). Preformed fibrils generated from mouse alpha-synuclein produce more inclusion pathology in rats than fibrils generated from rat alpha-synuclein. *Parkinsonism & Related Disorders, 89*, 41–47. 10.1016/j.parkreldis.2021.06.010

Hsu, L. J., Sagara, Y., Arroyo, A., Rockenstein, E., Sisk, A., Mallory, M., Wong, J., Takenouchi, T., Hashimoto, M., & Masliah, E. (2000). alpha-synuclein promotes mitochondrial deficit and oxidative stress. *The American Journal of Pathology, 157*(2), 401–410. 10.1016/s0002-9440(10)64553-1

Hu, C., Fan, J., He, G., Dong, C., Zhou, S., & Zheng, Y. (2022). Signal peptidase complex catalytic subunit SEC11A upregulation is a biomarker of poor prognosis in patients with head and neck squamous cell carcinoma. *PLoS ONE, 17*(6), e0269166. 10.1371/journal.pone.0269166

Hu, H., Tian, M., Ding, C., & Yu, S. (2019). The C/EBP Homologous Protein (CHOP) Transcription Factor Functions in Endoplasmic Reticulum Stress-Induced Apoptosis and Microbial Infection. *Frontiers in Immunology, 9*, 3083. 10.3389/fimmu.2018.03083

Hu, H., Yin, S., Ma, R., Chen, R., Li, S., Chen, Y., Fei, H., & Yang, L. (2021). CREBBP knockdown suppressed proliferation and promoted chemo-sensitivity via PERK-mediated unfolded protein response in ovarian cancer. *Journal of Cancer, 12*(15), 4595–4603. 10.7150/jca.56135

Hu, W., Lei, L., Xie, X., Huang, L., Cui, Q., Dang, T., Liu, G. L., Li, Y., Sun, X., & Zhou, Z. (2019). Heterogeneous nuclear ribonucleoprotein L facilitates recruitment of 53BP1 and BRCA1 at the DNA break sites induced by oxaliplatin in colorectal cancer. *Cell Death & Disease, 10*(8), 550. 10.1038/s41419-019-1784-x

Huang, Y., & Mahley, R. W. (2014). Apolipoprotein E: structure and function in lipid metabolism, neurobiology, and Alzheimer's diseases. *Neurobiology of Disease, 72 Pt A*, 3–12. 10.1016/j.nbd.2014.08.025

Huang, Y., Chen, L., Deng, Q., Zhao, X., Guo, Z., Song, L., & Li, J. (2023). P1.13-01 A Proteomics-Annotated Risk Model to Predict Recurrence in Stage I Non-Small Cell Lung Cancer. *Journal of Thoracic Oncology, 18*(11, Supplement), S211–S212. 10.1016/j.jtho.2023.09.340

Huang, Y., Krein, P. M., Muruve, D. A., & Winston, B. W. (2002). Complement factor B gene regulation: synergistic effects of TNF-alpha and IFN-gamma in macrophages. *Journal of Immunology (Baltimore, Md.: 1950), 169*(5), 2627–2635. 10.4049/jimmunol.169.5.2627

Humeau, J., Leduc, M., Cerrato, G., Loos, F., Kepp, O., & Kroemer, G. (2020). Phosphorylation of eukaryotic initiation factor-2α (eIF2α) in autophagy. *Cell Death & Disease, 11*(6), 1–12. 10.1038/s41419-020-2642-6

Igarashi, K., & Kashiwagi, K. (2010). Modulation of cellular function by polyamines. *The International Journal of Biochemistry & Cell Biology, 42*(1), 39–51. 10.1016/j.biocel.2009.07.009

Ishiguro, Y., Tsunemi, T., Shimada, T., Yoroisaka, A., Ueno, S., Takeshige-Amano, H., Hatano, T., Inoue, Y., Saiki, S., & Hattori, N. (2024). Extracellular vesicles contain filamentous alpha-synuclein and facilitate the propagation of Parkinson's pathology. *Biochemical and Biophysical Research Communications, 703*, 149620. 10.1016/j.bbrc.2024.149620

Ito, T., Wuerth, J. D., & Weber, F. (2023). Protection of eIF2B from inhibitory phosphorylated eIF2: A viral strategy to maintain mRNA translation during the PKR-triggered integrated stress response. *The Journal of Biological Chemistry, 299*(11), 105287. 10.1016/j.jbc.2023.105287

Ivanov, P., Kedersha, N., & Anderson, P. (2019). Stress Granules and Processing Bodies in Translational Control. *Cold Spring Harbor Perspectives in Biology, 11*(5), a032813. 10.1101/cshperspect.a032813

Iyer, A., & Claessens, M. M. A. E. (2019). Disruptive membrane interactions of alpha-synuclein aggregates. *Biochimica Et Biophysica Acta (BBA) - Proteins and Proteomics, 1867*(5), 468–482. 10.1016/j.bbapap.2018.10.006

Izzo, A., Kamieniarz-Gdula, K., Ramírez, F., Noureen, N., Kind, J., Manke, T., van Steensel, B., & Schneider, R. (2013). The genomic landscape of the somatic linker histone subtypes H1.1 to H1.5 in human cells. *Cell Reports, 3*(6), 2142–2154. 10.1016/j.celrep.2013.05.003

Izzo, A., Ziegler-Birling, C., Hill, P. W. S., Brondani, L., Hajkova, P., Torres-Padilla, M., & Schneider, R. (2017). Dynamic changes in H1 subtype composition during epigenetic reprogramming. *The Journal of Cell Biology, 216*(10), 3017–3028. 10.1083/jcb.201611012

Jahangiri, B., Saei, A. K., Obi, P. O., Asghari, N., Lorzadeh, S., Hekmatirad, S., Rahmati, M., Velayatipour, F., Asghari, M. H., Saleem, A., & Moosavi, M. A. (2022). Exosomes, autophagy and ER stress pathways in human diseases: Cross-regulation and therapeutic approaches. *Biochimica Et Biophysica Acta (BBA) - Molecular Basis of Disease, 1868*(10), 166484. 10.1016/j.bbadis.2022.166484

Jauhiainen, A., Thomsen, C., Strömbom, L., Grundevik, P., Andersson, C., Danielsson, A., Andersson, M. K., Nerman, O., Rörkvist, L., Ståhlberg, A., & Åman, P. (2012). Distinct cytoplasmic and nuclear functions of the stress induced protein DDIT3/CHOP/GADD153. *PloS One, 7*(4), e33208. 10.1371/journal.pone.0033208

Jia, J., Han, Z., Wang, X., Zheng, X., Wang, S., & Cui, Y. (2022). H2B gene family: A prognostic biomarker and correlates with immune infiltration in glioma. *Frontiers in Oncology, 12*, 966817. 10.3389/fonc.2022.966817

Jia, Y., Yu, L., Ma, T., Xu, W., Qian, H., Sun, Y., & Shi, H. (2022). Small extracellular vesicles isolation and separation: Current techniques, pending

questions and clinical applications. *Theranostics, 12*(15), 6548–6575. 10.7150/thno.74305

Jiang, D., Borg, M., Lorković, Z. J., Montgomery, S. A., Osakabe, A., Yelagandula, R., Axelsson, E., & Berger, F. (2020). The evolution and functional divergence of the histone H2B family in plants. *PLoS Genetics, 16*(7), e1008964. 10.1371/journal.pgen.1008964

Jiang, P., Gan, M., Ebrahim, A. S., Lin, W., Melrose, H. L., & Yen, S. C. (2010). ER stress response plays an important role in aggregation of α-synuclein. *Molecular Neurodegeneration, 5*, 56. 10.1186/1750-1326-5-56

Jing, Y., Luo, Y., Li, L., Liu, M., & Liu, J. (2024a). Deficiency of copper responsive gene stmn4 induces retinal developmental defects. *Cell Biology and Toxicology, 40*(1), 2. 10.1007/s10565-024-09847-8

Jos, S., Gogoi, H., Prasad, T. K., Hurakadli, M. A., Kamariah, N., Padmanabhan, B., & Padavattan, S. (2021). Molecular insights into α-synuclein interaction with individual human core histones, linker histone, and dsDNA. *Protein Science : A Publication of the Protein Society, 30*(10), 2121–2131. 10.1002/pro.4167

Kalivendi, S. V., Kotamraju, S., Cunningham, S., Shang, T., Hillard, C. J., & Kalyanaraman, B. (2003). 1-Methyl-4-phenylpyridinium (MPP+)-induced apoptosis and mitochondrial oxidant generation: role of transferrin-receptor-dependent iron and hydrogen peroxide. *Biochemical Journal, 371*(Pt 1), 151–164. 10.1042/BJ20021525

Kaul, S., Kanthasamy, A., Kitazawa, M., Anantharam, V., & Kanthasamy, A. G. (2003). Caspase-3 dependent proteolytic activation of protein kinase C delta mediates and regulates 1-methyl-4-phenylpyridinium (MPP+)-induced apoptotic cell death in dopaminergic cells: relevance to oxidative stress in dopaminergic degeneration. *The European Journal of Neuroscience, 18*(6), 1387–1401. 10.1046/j.1460-9568.2003.02864.

Khadka, A., Spiers, J. G., Cheng, L., & Hill, A. F. (2023). Extracellular vesicles with diagnostic and therapeutic potential for prion diseases. *Cell and Tissue Research, 392*(1), 247–267. 10.1007/s00441-022-03621-0

Khayami, R., Hashemi, S. R., & Kerachian, M. A. (2020). Role of aldo-keto reductase family 1 member B1 (AKR1B1) in the cancer process and its therapeutic potential. *Journal of Cellular and Molecular Medicine, 24*(16), 8890–8902. 10.1111/jcmm.15581

Kikuchi, J., Kinoshita, I., Shimizu, Y., Kikuchi, E., Takeda, K., Aburatani, H., Oizumi, S., Konishi, J., Kaga, K., Matsuno, Y., Birrer, M. J., Nishimura, M., & Dosaka-Akita, H. (2011). Minichromosome maintenance (MCM) protein 4 as a marker for proliferation and its clinical and clinicopathological significance in non-small cell lung cancer. *Lung Cancer (Amsterdam, Netherlands), 72*(2), 229–237. 10.1016/j.lungcan.2010.08.020

Kim, J., Kwon, Y., & Kim, Y. (2023). The stress-responsive protein REDD1 and its pathophysiological functions. *Experimental & Molecular Medicine, 55*(9), 1933–1944. 10.1038/s12276-023-01056-3

Kim, J., Yoon, H., Basak, J., & Kim, J. (2014). Apolipoprotein E in synaptic plasticity and Alzheimer's disease: potential cellular and molecular mechanisms. *Molecules and Cells, 37*(11), 767–776. 10.14348/molcells.2014.0248

Kim-Han, J. S., Antenor-Dorsey, J. A., & O'Malley, K. L. (2011). The parkinsonian mimetic, MPP+, specifically impairs mitochondrial transport in dopamine axons. *The Journal of Neuroscience: The Official Journal of the Society for Neuroscience, 31*(19), 7212–7221. 10.1523/JNEUROSCI.0711-11.2011

Kini, H. K., Kong, J., & Liebhaber, S. A. (2014). Cytoplasmic Poly(A) Binding Protein C4 Serves a Critical Role in Erythroid Differentiation. *Molecular and Cellular Biology, 34*(7), 1300–1309. 10.1128/MCB.01683-13

Klein, P., Kallenberger, S. M., Roth, H., Roth, K., Ly-Hartig, T. B. N., Magg, V., Aleš, J., Talemi, S. R., Qiang, Y., Wolf, S., Oleksiuk, O., Kurilov, R., Di Ventura, B., Bartenschlager, R., Eils, R., Rohr, K., Hamprecht, F. A., Höfer, T., Fackler, O. T., Ruggieri, A. (2022). Temporal control of the integrated stress response by a stochastic molecular switch. *Science Advances, 8*(12), eabk2022. 10.1126/sciadv.abk2022

Komatsu, M., & Ruoslahti, E. (2005). R-Ras is a global regulator of vascular regeneration that suppresses intimal hyperplasia and tumor angiogenesis. *Nature Medicine, 11*(12), 1346–1350. 10.1038/nm1324

Kon, T., Mori, F., Tanji, K., Miki, Y., Nishijima, H., Nakamura, T., Kinoshita, I., Suzuki, C., Kurotaki, H., Tomiyama, M., & Wakabayashi, K. (2022). Accumulation of Nonfibrillar TDP-43 in the Rough Endoplasmic Reticulum Is the Early-Stage Pathology in Amyotrophic Lateral Sclerosis. *Journal of Neuropathology and Experimental Neurology, 81*(4), 271–281. 10.1093/jnen/nlac015

Kong, L., Zhang, D., Huang, S., Lai, J., Lu, L., Zhang, J., & Hu, S. (2023). Extracellular Vesicles in Mental Disorders: A State-of-art Review. *International Journal of Biological Sciences, 19*(4), 1094–1109. 10.7150/ijbs.79666

Konno, T., Parutto, P., Crapart, C. C., Davì, V., Bailey, D. M. D., Awadelkareem, M. A., Hockings, C., Brown, A. I., Xiang, K. M., Agrawal, A., Chambers, J. E., Vander Werp, M. J., Koning, K. M., Elfari, L. M., Steen, S., Metzakopian, E., Westrate, L. M., Koslover, E. F., & Avezov, E. (2024). Endoplasmic reticulum morphology regulation by RTN4 modulates neuronal regeneration by curbing luminal transport. *Cell Reports, 43*(7), 114357. 10.1016/j.celrep.2024.114357

Kosho, T. (2016). CHST14/D4ST1 deficiency: New form of Ehlers-Danlos syndrome. *Pediatrics International: Official Journal of the Japan Pediatric Society, 58*(2), 88–99. 10.1111/ped.12878

Krokowski, D., Jobava, R., Guan, B., Farabaugh, K., Wu, J., Majumder, M., Bianchi, M. G., Snider, M. D., Bussolati, O., & Hatzoglou, M. (2015). Coordinated Regulation of the Neutral Amino Acid Transporter SNAT2 and the Protein Phosphatase Subunit GADD34 Promotes Adaptation to Increased Extracellular Osmolarity. *The Journal of Biological Chemistry, 290*(29), 17822–17837. 10.1074/jbc.M114.636217

Kulow, V. A., Roegner, K., Labes, R., Kasim, M., Mathia, S., Czopek, C. S., Berndt, N., Becker, P. N., Ter-Avetisyan, G., Luft, F. C., Enghard, P., Hinze, C., Klocke, J., Eckardt, K., Schmidt-Ott, K. M., Persson, P. B., Rosenberger, C., & Fähling, M. (2025). Beyond hemoglobin: Critical role of 2,3-

bisphosphoglycerate mutase in kidney function and injury. *Acta Physiologica (Oxford, England), 241*(1), e14242. 10.1111/apha.14242

Kumar, M. A., Baba, S. K., Sadida, H. Q., Marzooqi, S. A., Jerobin, J., Altemani, F. H., Algehainy, N., Alanazi, M. A., Abou-Samra, A., Kumar, R., Al-Shabeeb Akil, A. S., Macha, M. A., Mir, R., & Bhat, A. A. (2024). Extracellular vesicles as tools and targets in therapy for diseases. *Signal Transduction and Targeted Therapy, 9*(1), 27. 10.1038/s41392-024-01735-1

Kumar, V., Singh, D., Singh, B. K., Singh, S., Mittra, N., Jha, R. R., Patel, D. K., & Singh, C. (2018). Alpha-synuclein aggregation, Ubiquitin proteasome system impairment, and L-Dopa response in zinc-induced Parkinsonism: resemblance to sporadic Parkinson's disease. *Molecular and Cellular Biochemistry, 444*(1-2), 149–160. 10.1007/s11010-017-3239-y

Kuwahara, T., Yamayoshi, S., Noda, T., & Kawaoka, Y. (2019). G Protein Pathway Suppressor 1 Promotes Influenza Virus Polymerase Activity by Activating the NF-κB Signaling Pathway. *mBio, 10*(6), 2867. 10.1128/mBio.02867-19

Kwak, T. H., Kang, J. H., Hali, S., Kim, J., Kim, K., Park, C., Lee, J., Ryu, H. K., Na, J. E., Jo, J., Je, H. S., Ng, H., Kwon, J., Kim, N., Hong, K. H., Sun, W., Chung, C. H., Rhyu, I. J., & Han, D. W. (2020). Generation of homogeneous midbrain organoids with in vivo-like cellular composition facilitates neurotoxin-based Parkinson's disease modeling. *Stem Cells (Dayton, Ohio), 38*(6), 727–740. 10.1002/stem.3163

Lam, H. T., Graber, M. C., Gentry, K. A., & Bieschke, J. (2016). Stabilization of α-Synuclein Fibril Clusters Prevents Fragmentation and Reduces Seeding Activity and Toxicity. *Biochemistry, 55*(4), 675–685. 10.1021/acs.biochem.5b01168

Laplante, M., & Sabatini, D. M. (2009). mTOR signaling at a glance. *Journal of Cell Science, 122*(20), 3589–3594. 10.1242/jcs.051011

Lashuel, H. A. (2020). Do Lewy bodies contain alpha-synuclein fibrils? and Does it matter? A brief history and critical analysis of recent reports. *Neurobiology of Disease, 141*, 104876. 10.1016/j.nbd.2020.104876

Lashuel, H. A., Overk, C. R., Oueslati, A., & Masliah, E. (2013). The many faces of α-synuclein: from structure and toxicity to therapeutic target. *Nature Reviews. Neuroscience, 14*(1), 38–48. 10.1038/nrn3406

Lauter, G., Coschiera, A., Yoshihara, M., Sugiaman-Trapman, D., Ezer, S., Sethurathinam, S., Katayama, S., Kere, J., & Swoboda, P. (2020). Differentiation of ciliated human midbrain-derived LUHMES neurons. *Journal of Cell Science, 133*(21), jcs249789. 10.1242/jcs.249789

Leak, R. K., Frosch, M. P., Beach, T. G., & Halliday, G. M. (2019). α-Synuclein: Prion or Prion-like? *Acta Neuropathologica, 138*(4), 509–514. 10.1007/s00401-019-02057-1

Lechuga, S., Marino-Melendez, A., Davis, A., Zalavadia, A., Khan, A., Longworth, M. S., & Ivanov, A. I. (2024). Coactosin-like protein 1 regulates integrity and repair of model intestinal epithelial barriers via actin binding dependent and independent mechanisms. *Frontiers in Cell and Developmental Biology, 12*, 1405454. 10.3389/fcell.2024.1405454

Lee, H., Kim, W., Kang, H., Jang, J., Choi, I. J., Chun, K., & Kim, S. (2021). Upregulation of LAMB1 via ERK/c-Jun Axis Promotes Gastric Cancer Growth and Motility. *International Journal of Molecular Sciences, 22*(2), 626. 10.3390/ijms22020626

Lee, H., Suk, J., Patrick, C., Bae, E., Cho, J., Rho, S., Hwang, D., Masliah, E., & Lee, S. (2010). Direct Transfer of α-Synuclein from Neuron to Astroglia Causes Inflammatory Responses in Synucleinopathies. *The Journal of Biological Chemistry, 285*(12), 9262–9272. 10.1074/jbc.M109.081125

Lee, S., Desplats, P., Lee, H., Spencer, B., & Masliah, E. (2012). Cell-to-Cell Transmission of α-Synuclein Aggregates. *Methods in Molecular Biology (Clifton, N.J.), 849*, 347–359. 10.1007/978-1-61779-551-0_23

Lemarchant, S., Wojciechowski, S., Vivien, D., & Koistinaho, J. (2017). ADAMTS-4 in central nervous system pathologies. *Journal of Neuroscience Research, 95*(9), 1703–1711. 10.1002/jnr.24021

Li, J., Jin, C., Zou, C., Qiao, X., Ma, P., Hu, D., Li, W., Jin, J., Jin, X., & Fan, P. (2020). GNG12 regulates PD-L1 expression by activating NF-κB signaling in pancreatic ductal adenocarcinoma. *FEBS Open Bio, 10*(2), 278–287. 10.1002/2211-5463.12784

Li, J., Luo, J., Liu, L., Fu, H., & Tang, L. (2018). The genetic association between apolipoprotein E gene polymorphism and Parkinson disease. *Medicine, 97*(43), e12884. 10.1097/MD.0000000000012884

Li, L., Sun, H., Liu, X., Gao, S., Jiang, H., Hu, X., & Jin, W. (2015). Down-Regulation of NDUFB9 Promotes Breast Cancer Cell Proliferation, Metastasis by Mediating Mitochondrial Metabolism. *PLoS ONE, 10*(12), e0144441. 10.1371/journal.pone.0144441

Li, Y., Zhao, C., Luo, F., Liu, Z., Gui, X., Luo, Z., Zhang, X., Li, D., Liu, C., & Li, X. (2018). Amyloid fibril structure of α-synuclein determined by cryo-electron microscopy. *Cell Research, 28*(9), 897–903. 10.1038/s41422-018-0075-x

Li, Z., Cui, L., Jin, M., Hu, D., Hou, X., Liu, S., Zhang, X., & Zhu, J. (2022). A Matrigel-based 3D construct of SH-SY5Y cells models the α-synuclein pathologies of Parkinson's disease. *Disease Models & Mechanisms, 15*(3), dmm049125. 10.1242/dmm.049125

Liao, F., Yoon, H., & Kim, J. (2017). Apolipoprotein E metabolism and functions in brain and its role in Alzheimer's disease. *Current Opinion in Lipidology, 28*(1), 60–67. 10.1097/MOL.0000000000000383

Licari, E., Sánchez-Del-Campo, L., & Falletta, P. (2021). The two faces of the Integrated Stress Response in cancer progression and therapeutic strategies. *The International Journal of Biochemistry & Cell Biology, 139*, 106059. 10.1016/j.biocel.2021.106059

Lindner, P., Christensen, S. B., Nissen, P., Møller, J. V., & Engedal, N. (2020). Cell death induced by the ER stressor thapsigargin involves death receptor 5, a non-autophagic function of MAP1LC3B, and distinct contributions from unfolded protein response components. *Cell Communication and Signaling: CCS, 18*(1), 12. 10.1186/s12964-019-0499-z

Liu, B., Fang, L., Mo, P., Chen, C., Ji, Y., Pang, L., Chen, H., Deng, Y., Ou, W., & Liu, S. (2023). Apoe-knockout induces strong vascular oxidative stress and significant changes in the gene expression profile related to the pathways implicated in redox, inflammation, and endothelial function. *Cellular Signalling, 108*, 110696. 10.1016/j.cellsig.2023.110696

Liu, D., Yin, B., Wang, Q., Ju, W., Chen, Y., Qiu, H., Li, J., Peng, X., & Lu, C. (2012). Cytoplasmic poly(A) binding protein 4 is highly expressed in human colorectal cancer and correlates with better prognosis. *Journal of Genetics and Genomics = Yi Chuan Xue Bao, 39*(8), 369–374. 10.1016/j.jgg.2012.05.007

Liu, K., Zhao, C., Adajar, R. C., DeZwaan-McCabe, D., & Rutkowski, D. T. (2024). A beneficial adaptive role for CHOP in driving cell fate selection during ER stress. *EMBO Reports, 25*(1), 228–253. 10.1038/s44319-023-00026-0

Liu, P., Wu, A., Li, H., Zhang, J., Ni, J., Quan, Z., & Qing, H. (2022). Rab21 Protein Is Degraded by Both the Ubiquitin-Proteasome Pathway and the Autophagy-Lysosome Pathway. *International Journal of Molecular Sciences, 23*(3), 1131. 10.3390/ijms23031131

Liu, W. N., Yan, M., & Chan, A. M. (2017). A thirty-year quest for a role of R-Ras in cancer: from an oncogene to a multitasking GTPase. *Cancer Letters, 403*, 59–65. 10.1016/j.canlet.2017.06.003

Liu, Y., Wang, M., Cheng, A., Yang, Q., Wu, Y., Jia, R., Liu, M., Zhu, D., Chen, S., Zhang, S., Zhao, X., Huang, J., Mao, S., Ou, X., Gao, Q., Wang, Y., Xu, Z., Chen, Z., Zhu, L., . . . Chen, X. (2020). The role of host eIF2α in viral infection. *Virology Journal, 17*(1), 112. 10.1186/s12985-020-01362-6

Liu, Y., Yang, J., Wang, Y., Zeng, Q., Fan, Y., Huang, A., & Fan, H. (2024). The proteasome activator subunit PSME1 promotes HBV replication by inhibiting the degradation of HBV core protein. *Genes & Diseases, 11*(6), 101142. 10.1016/j.gendis.2023.101142

Liu, Y., Zhang, Y., Li, T., Han, J., & Wang, Y. (2020). The tight junction protein TJP1 regulates the feeding-modulated hepatic circadian clock. *Nature Communications, 11*, 589. 10.1038/s41467-020-14470-2

Lockshin, E. R., & Calakos, N. (2024). The integrated stress response in brain diseases: A double-edged sword for proteostasis and synapses. *Current Opinion in Neurobiology, 87*, 102886. 10.1016/j.conb.2024.102886

López-Gil, J. C., García-Silva, S., Ruiz-Cañas, L., Navarro, D., Palencia-Campos, A., Giráldez-Trujillo, A., Earl, J., Dorado, J., Gómez-López, G., Monfort-Vengut, A., Alcalá, S., Gaida, M. M., García-Mulero, S., Cabezas-Sáinz, P., Batres-Ramos, S., Barreto, E., Sánchez-Tomero, P., Vallespinós, M., Ambler, L., . . . Sainz, B. (2024). The Peptidoglycan Recognition Protein 1 confers immune evasive properties on pancreatic cancer stem cells. *Gut, 73*(9), 1489–1508. 10.1136/gutjnl-2023-330995

Lu, A., Disoma, C., Zhou, Y., Chen, Z., Zhang, L., Shen, Y., Zhou, M., Du, A., Zheng, R., Li, S., Alsaadawe, M., Li, S., Li, J., Wang, W., Jiang, T., Peng, J., & Xia, Z. (2019). Protein interactome of the deamidase phosphoribosylformylglycinamidine synthetase (PFAS) by LC-MS/MS. *Biochemical and Biophysical Research Communications, 513*(3), 746–752. 10.1016/j.bbrc.2019.04.039

Lu, D., Wolfgang, C. D., & Hai, T. (2006). Activating transcription factor 3, a stress-inducible gene, suppresses Ras-stimulated tumorigenesis. *The Journal of Biological Chemistry, 281*(15), 10473–10481. 10.1074/jbc.M509278200

Lu, W., Wilczynska, A., Smith, E., & Bushell, M. (2014). The diverse roles of the eIF4A family: you are the company you keep. *Biochemical Society Transactions, 42*(1), 166–172. 10.1042/BST20130161

Ludtmann, M. H. R., Angelova, P. R., Horrocks, M. H., Choi, M. L., Rodrigues, M., Baev, A. Y., Berezhnov, A. V., Yao, Z., Little, D., Banushi, B., Al-Menhali, A. S., Ranasinghe, R. T., Whiten, D. R., Yapom, R., Dolt, K. S., Devine, M. J., Gissen, P., Kunath, T., Jaganjac, M., . . . Gandhi, S. (2018). α-synuclein oligomers interact with ATP synthase and open the permeability transition pore in Parkinson's disease. *Nature Communications, 9*(1), 1–16. 10.1038/s41467-018-04422-2

Ma, J., Liu, Y., Valladolid-Acebes, I., Recio-López, P., Peng, G., Li, J., Berggren, P., Juntti-Berggren, L., & Tong, N. (2023). ATF5 is a regulator of ER

stress and β-cell apoptosis in different mouse models of genetic- and diet-induced obesity and diabetes mellitus. *Cellular Signalling, 102*, 110535. 10.1016/j.cellsig.2022.110535

Ma, M., Hu, Z., Zhao, Y., Chen, Y., & Li, Y. (2016). Phosphorylation induces distinct alpha-synuclein strain formation. *Scientific Reports, 6*(1), 37130. 10.1038/srep37130

Mackenzie, I. R., Nicholson, A. M., Sarkar, M., Messing, J., Purice, M. D., Pottier, C., Annu, K., Baker, M., Perkerson, R. B., Kurti, A., Matchett, B. J., Mittag, T., Temirov, J., Hsiung, G. R., Krieger, C., Murray, M. E., Kato, M., Fryer, J. D., Petrucelli, L., . . . Rademakers, R. (2017). TIA1 mutations in amyotrophic lateral sclerosis and frontotemporal dementia promote phase separation and alter stress granule dynamics. *Neuron, 95*(4), 808–816.e9. 10.1016/j.neuron.2017.07.025

Magnuson, B., Ekim, B., & Fingar, D. C. (2012). Regulation and function of ribosomal protein S6 kinase (S6K) within mTOR signalling networks. *The Biochemical Journal, 441*(1), 1–21. 10.1042/BJ20110892

Mapa, M. S. T., Le, V. Q., & Wimalasena, K. (2018). Characteristics of the mitochondrial and cellular uptake of MPP+, as probed by the fluorescent mimic, 4'I-MPP. *PloS One, 13*(8), e0197946. 10.1371/journal.pone.0197946

Mappin-Kasirer, B., Pan, H., Lewington, S., Kizza, J., Gray, R., Clarke, R., & Peto, R. (2020). Tobacco smoking and the risk of Parkinson disease: A 65-year follow-up of 30,000 male British doctors. *Neurology, 94*(20), e2132–e2138. 10.1212/WNL.0000000000009437

Margolis, D. J., Gupta, J., Apter, A. J., Ganguly, T., Hoffstad, O., Papadopoulos, M., Rebbeck, T. R., & Mitra, N. (2014). Filaggrin-2 variation is associated with more persistent atopic dermatitis in African American subjects. *The Journal of Allergy and Clinical Immunology, 133*(3), 784–789. 10.1016/j.jaci.2013.09.015

Markmiller, S., Soltanieh, S., Server, K. L., Mak, R., Jin, W., Fang, M. Y., Luo, E., Krach, F., Yang, D., Sen, A., Fulzele, A., Wozniak, J. M., Gonzalez, D. J., Kankel, M. W., Gao, F., Bennett, E. J., Lécuyer, E., & Yeo, G. W. (2018a).

Context-Dependent and Disease-Specific Diversity in Protein Interactions within Stress Granules. *Cell, 172*(3), 590–604.e13. 10.1016/j.cell.2017.12.032

Marques, O., & Outeiro, T. F. (2012). Alpha-synuclein: from secretion to dysfunction and death. *Cell Death & Disease, 3*(7), e350. 10.1038/cddis.2012.94

Martí, Y., Matthaeus, F., Lau, T., & Schloss, P. (2017). Methyl-4-phenylpyridinium (MPP+) differentially affects monoamine release and re-uptake in murine embryonic stem cell-derived dopaminergic and serotonergic neurons. *Molecular and Cellular Neurosciences, 83*, 37–45. 10.1016/j.mcn.2017.06.009

Martin, J. L., Dawson, S. J., & Gale, J. E. (2022). An emerging role for stress granules in neurodegenerative disease and hearing loss. *Hearing Research, 426*, 108634. 10.1016/j.heares.2022.108634

Martire, S., & Banaszynski, L. A. (2020). The roles of histone variants in fine-tuning chromatin organization and function. *Nature Reviews. Molecular Cell Biology, 21*(9), 522–541. 10.1038/s41580-020-0262-8

Márton, M., Bánhegyi, G., Gyöngyösi, N., Kálmán, E. É, Pettkó-Szandtner, A., Káldi, K., & Kapuy, O. (2022). A systems biological analysis of the ATF4-GADD34-CHOP regulatory triangle upon endoplasmic reticulum stress. *FEBS Open Bio, 12*(11), 2065–2082. 10.1002/2211-5463.13484

Mathieu, C., Dupret, J., & Rodrigues-Lima, F. (2019). The Structure and the Regulation of Glycogen Phosphorylases in Brain. *Advances in Neurobiology, 23*, 125–145. 10.1007/978-3-030-27480-1_4

Mazzio, E. A., Soliman, Y. I., & Soliman, K. F. A. (2010). Variable toxicological response to the loss of OXPHOS through 1-methyl-4-phenylpyridinium-induced mitochondrial damage and anoxia in diverse neural immortal cell lines. *Cell Biology and Toxicology, 26*(6), 527–539. 10.1007/s10565-010-9161-7

McEwen, E., Kedersha, N., Song, B., Scheuner, D., Gilks, N., Han, A., Chen, J., Anderson, P., & Kaufman, R. J. (2005). Heme-regulated inhibitor kinase-

mediated phosphorylation of eukaryotic translation initiation factor 2 inhibits translation, induces stress granule formation, and mediates survival upon arsenite exposure. *The Journal of Biological Chemistry, 280*(17), 16925–16933. 10.1074/jbc.M412882200

McGlinchey, R. P., Ni, X., Shadish, J. A., Jiang, J., & Lee, J. C. (2021). The N terminus of α-synuclein dictates fibril formation. *Proceedings of the National Academy of Sciences of the United States of America, 118*(35), e2023487118. 10.1073/pnas.2023487118

McInerney, G. M., Kedersha, N. L., Kaufman, R. J., Anderson, P., & Liljeström, P. (2005). Importance of eIF2α Phosphorylation and Stress Granule Assembly in Alphavirus Translation Regulation. *Molecular Biology of the Cell, 16*(8), 3753–3763. 10.1091/mbc.E05-02-0124

McNeill, A., Iovino, E., Mansard, L., Vache, C., Baux, D., Bedoukian, E., Cox, H., Dean, J., Goudie, D., Kumar, A., Newbury-Ecob, R., Fallerini, C., Renieri, A., Lopergolo, D., Mari, F., Blanchet, C., Willems, M., Roux, A., Pippucci, T., & Delpire, E. (2020). SLC12A2 variants cause a neurodevelopmental disorder or cochleovestibular defect. *Brain, 143*(8), 2380–2387. 10.1093/brain/awaa176

McRae, S. A., Richards, C. M., Da Silva, D. E., Riar, I., Yang, S., Zurfluh, N. E., Gibon, J., & Klegeris, A. (2024). Pro-neuroinflammatory and neurotoxic potential of extracellular histones H1 and H3. *Neuroscience Research, 204*, 34–45. 10.1016/j.neures.2024.01.004

Mencke, P., Boussaad, I., Romano, C. D., Kitami, T., Linster, C. L., & Krüger, R. (2021). The Role of DJ-1 in Cellular Metabolism and Pathophysiological Implications for Parkinson's Disease. *Cells, 10*(2), 347. 10.3390/cells10020347

Méndez-Albelo, N. M., Sandoval, S. O., Xu, Z., & Zhao, X. (2024). An in-depth review of the function of RNA-binding protein FXR1 in neurodevelopment. *Cell and Tissue Research, 398*(2), 63–77. 10.1007/s00441-024-03912-8

Menšíková, K., Matěj, R., Colosimo, C., Rosales, R., Tučková, L., Ehrmann, J., Hraboš, D., Kolaříková, K., Vodička, R., Vrtěl, R., Procházka, M., Nevrlý,

M., Kaiserová, M., Kurčová, S., Otruba, P., & Kaňovský, P. (2022). Lewy body disease or diseases with Lewy bodies? *NPJ Parkinson's Disease, 8*, 3. 10.1038/s41531-021-00273-9

Milburn, J. V., Hoog, A. M., Winkler, S., van Dongen, K. A., Leitner, J., Patzl, M., Saalmüller, A., de Luca, K., Steinberger, P., Mair, K. H., & Gerner, W. (2021). Expression of CD9 on porcine lymphocytes and its relation to T cell differentiation and cytokine production. *Developmental and Comparative Immunology, 121*, 104080. 10.1016/j.dci.2021.104080

Mills, A. A. (2017). The Chromodomain Helicase DNA-Binding Chromatin Remodelers: Family Traits that Protect from and Promote Cancer. *Cold Spring Harbor Perspectives in Medicine, 7*(4), a026450. 10.1101/cshperspect.a026450

Minakaki, G., Menges, S., Kittel, A., Emmanouilidou, E., Schaeffner, I., Barkovits, K., Bergmann, A., Rockenstein, E., Adame, A., Marxreiter, F., Mollenhauer, B., Galasko, D., Buzás, E. I., Schlötzer-Schrehardt, U., Marcus, K., Xiang, W., Lie, D. C., Vekrellis, K., Masliah, E., . . . Klucken, J. (2018). Autophagy inhibition promotes SNCA/alpha-synuclein release and transfer via extracellular vesicles with a hybrid autophagosome-exosome-like phenotype. *Autophagy, 14*(1), 98–119. 10.1080/15548627.2017.1395992

Mingot, J., Bohnsack, M. T., Jäkle, U., & Görlich, D. (2004). Exportin 7 defines a novel general nuclear export pathway. *The EMBO Journal, 23*(16), 3227–3236. 10.1038/sj.emboj.7600338

Mizuno, Y., Hattori, N., Mori, H., Suzuki, T., & Tanaka, K. (2001). Parkin and Parkinson's disease. *Current Opinion in Neurology, 14*(4), 477–482. 10.1097/00019052-200108000-00008

Moreno, M. R., Boswell, K., Casbolt, H. L., & Bulgakova, N. A. (2022). Multifaceted control of E-cadherin dynamics by Adaptor Protein Complex 1 during epithelial morphogenesis. *Molecular Biology of the Cell, 33*(9), ar80. 10.1091/mbc.E21-12-0598

Mori, F., Yasui, H., Miki, Y., Kon, T., Arai, A., Kurotaki, H., Tomiyama, M., & Wakabayashi, K. (2023). Colocalization of TDP-43 and stress granules at the

early stage of TDP-43 aggregation in amyotrophic lateral sclerosis. *Brain Pathology, 34*(2), e13215. 10.1111/bpa.13215

Moriarity, J. L., Hurt, K. J., Resnick, A. C., Storm, P. B., Laroy, W., Schnaar, R. L., & Snyder, S. H. (2002). UDP-glucuronate decarboxylase, a key enzyme in proteoglycan synthesis: cloning, characterization, and localization. *The Journal of Biological Chemistry, 277*(19), 16968–16975. 10.1074/jbc.M109316200

Mou, Z., Yuan, Y., Zhang, Z., Song, L., & Chen, N. (2020). Endoplasmic reticulum stress, an important factor in the development of Parkinson's disease. *Toxicology Letters, 324*, 20–29. 10.1016/j.toxlet.2020.01.019

Moustafa, A. A., Chakravarthy, S., Phillips, J. R., Gupta, A., Keri, S., Polner, B., Frank, M. J., & Jahanshahi, M. (2016). Motor symptoms in Parkinson's disease: A unified framework. *Neuroscience and Biobehavioral Reviews, 68*, 727–740. 10.1016/j.neubiorev.2016.07.010

Mulcahy, L. A., Pink, R. C., & Carter, D. R. F. (2014). Routes and mechanisms of extracellular vesicle uptake. *Journal of Extracellular Vesicles, 3*, 10.3402/jev.v3.24641. 10.3402/jev.v3.24641

Naganuma, F., Murata, D., Inoue, M., Maehori, Y., Harada, R., Furumoto, S., Kudo, Y., Nakamura, T., & Okamura, N. (2023). A Novel Near-Infrared Fluorescence Probe THK-565 Enables In Vivo Detection of Amyloid Deposits in Alzheimer’s Disease Mouse Model. *Molecular Imaging and Biology, 25*(6), 1115–1124. 10.1007/s11307-023-01843-4

Nagao, Y., Kitada, S., Kojima, K., Toh, H., Kuhara, S., Ogishima, T., & Ito, A. (2000). Glycine-rich region of mitochondrial processing peptidase alpha-subunit is essential for binding and cleavage of the precursor proteins. *The Journal of Biological Chemistry, 275*(44), 34552–34556. 10.1074/jbc.M003110200

Nakamura, Y., Kita, S., Tanaka, Y., Fukuda, S., Obata, Y., Okita, T., Nishida, H., Takahashi, Y., Kawachi, Y., Tsugawa-Shimizu, Y., Fujishima, Y., Nishizawa, H., Takakura, Y., Miyagawa, S., Sawa, Y., Maeda, N., & Shimomura, I. (2020). Adiponectin Stimulates Exosome Release to Enhance Mesenchymal Stem-

Cell-Driven Therapy of Heart Failure in Mice. *Molecular Therapy, 28*(10), 2203–2219. 10.1016/j.ymthe.2020.06.026

Neill, G., & Masson, G. R. (2023). A stay of execution: ATF4 regulation and potential outcomes for the integrated stress response. *Frontiers in Molecular Neuroscience, 16*, 1112253. 10.3389/fnmol.2023.1112253

Neumann, J., Bras, J., Deas, E., O'Sullivan, S. S., Parkkinen, L., Lachmann, R. H., Li, A., Holton, J., Guerreiro, R., Paudel, R., Segarane, B., Singleton, A., Lees, A., Hardy, J., Houlden, H., Revesz, T., & Wood, N. W. (2009). Glucocerebrosidase mutations in clinical and pathologically proven Parkinson's disease. *Brain: A Journal of Neurology, 132*(Pt 7), 1783–1794. 10.1093/brain/awp044

Neupane, S., De Cecco, E., & Aguzzi, A. (2023). The Hidden Cell-to-Cell Trail of α-Synuclein Aggregates. *Journal of Molecular Biology, 435*(12), 167930. 10.1016/j.jmb.2022.167930

Niehaus, J. Z., Good, M., Jackson, L. E., Ozolek, J. A., Silverman, G. A., & Luke, C. J. (2015). Human SERPINB12 Is an Abundant Intracellular Serpin Expressed in Most Surface and Glandular Epithelia. *Journal of Histochemistry and Cytochemistry, 63*(11), 854–865. 10.1369/0022155415600498

Niehaus, J. Z., Good, M., Jackson, L. E., Ozolek, J. A., Silverman, G. A., & Luke, C. J. (2015). Human SERPINB12 Is an Abundant Intracellular Serpin Expressed in Most Surface and Glandular Epithelia. *Journal of Histochemistry and Cytochemistry, 63*(11), 854–865. 10.1369/0022155415600498

Nigri, J., Leca, J., Tubiana, S., Finetti, P., Guillaumond, F., Martinez, S., Lac, S., Iovanna, J. L., Audebert, S., Camoin, L., Vasseur, S., Bertucci, F., & Tomasini, R. (2022). CD9 mediates the uptake of extracellular vesicles from cancer-associated fibroblasts that promote pancreatic cancer cell aggressiveness. *Science Signaling, 15*(745), eabg8191. 10.1126/scisignal.abg8191

Nikolic, A., Maule, F., Bobyn, A., Ellestad, K., Paik, S., Marhon, S. A., Mehdipour, P., Lun, X., Chen, H., Mallard, C., Hay, A. J., Johnston, M. J., Gafuik, C. J., Zemp, F. J., Shen, Y., Ninkovic, N., Osz, K., Labit, E., Berger, N.

D., . . . Gallo, M. (2023). macroH2A2 antagonizes epigenetic programs of stemness in glioblastoma. *Nature Communications, 14*(1), 3062. 10.1038/s41467-023-38919-2

Niskanen, J., Peltonen, S., Ohtonen, S., Fazaludeen, M. F., Luk, K. C., Giudice, L., Koistinaho, J., Malm, T., Goldsteins, G., Albert, K., & Lehtonen, Š. (2025). Uptake of alpha-synuclein preformed fibrils is suppressed by inflammation and induces an aberrant phenotype in human microglia. *Glia, 73*(1), 159–174. 10.1002/glia.24626

Novak, R., Hrkac, S., Salai, G., Bilandzic, J., Mitar, L., & Grgurevic, L. (2022). The Role of ADAMTS-4 in Atherosclerosis and Vessel Wall Abnormalities. *Journal of Vascular Research, 59*(2), 69–77. 10.1159/000521498

Nuytemans, K., Theuns, J., Cruts, M., & Van Broeckhoven, C. (2010). Genetic Etiology of Parkinson Disease Associated with Mutations in the SNCA, PARK2, PINK1, PARK7, and LRRK2 Genes: A Mutation Update. *Human Mutation, 31*(7), 763–780. 10.1002/humu.21277

O'Neill, C. P., Gilligan, K. E., & Dwyer, R. M. (2019). Role of Extracellular Vesicles (EVs) in Cell Stress Response and Resistance to Cancer Therapy. *Cancers, 11*(2), 136. 10.3390/cancers11020136

Ohgita, T., Namba, N., Kono, H., Shimanouchi, T., & Saito, H. (2022). Mechanisms of enhanced aggregation and fibril formation of Parkinson's disease-related variants of α-synuclein. *Scientific Reports, 12*(1), 6770. 10.1038/s41598-022-10789-6

Oikonomakos, N. G., Skamnaki, V. T., Tsitsanou, K. E., Gavalas, N. G., & Johnson, L. N. (2000). A new allosteric site in glycogen phosphorylase b as a target for drug interactions. *Structure (London, England: 1993), 8*(6), 575–584. 10.1016/s0969-2126(00)00144-1

Ok, S., Park, J., Byun, S., Kang, K., Son, J., & Kang, M. (2023). ATF4 Responds to Metabolic Stress in Drosophila. *Frontiers in Bioscience (Landmark Edition), 28*(12), 344. 10.31083/j.fbl2812344

Okur, V., Chen, Z., Vossaert, L., Peacock, S., Rosenfeld, J., Zhao, L., Du, H., Calamaro, E., Gerard, A., Zhao, S., Kelsay, J., Lahr, A., Mighton, C., Porter, H. M., Siemon, A., Silver, J., Svihovec, S., Fong, C., Grant, C. L., . . . Yuan, B. (2021). De novo variants in H3-3A and H3-3B are associated with neurodevelopmental delay, dysmorphic features, and structural brain abnormalities. *Npj Genomic Medicine, 6*(1), 1–10. 10.1038/s41525-021-00268-8

Oliveira, M. M., Mohamed, M., Elder, M. K., Banegas-Morales, K., Mamcarz, M., Lu, E. H., Golhan, E. A. N., Navrange, N., Chatterjee, S., Abel, T., & Klann, E. (2024). The integrated stress response effector GADD34 is repurposed by neurons to promote stimulus-induced translation. *Cell Reports, 43*(2), 113670. 10.1016/j.celrep.2023.113670

Ou, M., Ju, X., Cai, Y., Sun, X., Wang, J., Fu, X., Sun, Q., & Luo, Z. (2020). Heterogeneous nuclear ribonucleoprotein A3 controls mitotic progression of neural progenitors via interaction with cohesin. *Development (Cambridge, England), 147*(10), dev185132. 10.1242/dev.185132

Ou, Z., Pan, J., Tang, S., Duan, D., Yu, D., Nong, H., & Wang, Z. (2021). Global Trends in the Incidence, Prevalence, and Years Lived With Disability of Parkinson's Disease in 204 Countries/Territories From 1990 to 2019. *Frontiers in Public Health, 9*, 776847. 10.3389/fpubh.2021.776847

Owyong, T. C., Shippey, L. E., Ding, S., Owen, D. S., Zhang, S., White, J. M., Wong, W. W. H., Smith, D. P., & Hong, Y. (2025). Development of NIAD-4 derivatives for fluorescence-based detection of protein aggregates. *Sensors & Diagnostics, 4*(1), 55–62. 10.1039/D4SD00182F

Pajares, M., I. Rojo, A., Manda, G., Boscá, L., & Cuadrado, A. (2020). Inflammation in Parkinson’s Disease: Mechanisms and Therapeutic Implications. *Cells, 9*(7), 1687. 10.3390/cells9071687

Pakos-Zebrucka, K., Koryga, I., Mnich, K., Ljujic, M., Samali, A., & Gorman, A. M. (2016). The integrated stress response. *EMBO Reports, 17*(10), 1374–1395. 10.15252/embr.201642195

Pan, J., Liu, M., Duan, X., & Wang, D. (2023). A short peptide LINC00665_18aa encoded by lncRNA LINC00665 suppresses the proliferation and migration of osteosarcoma cells through the regulation of the CREB1/RPS6KA3 interaction. *PloS One, 18*(6), e0286422. 10.1371/journal.pone.0286422

Pan, Y., You, B., Zhao, X., Zhang, S., & Li, W. (2024). CHOP regulated by METTL14-m6A affects cell cycle arrest and regorafenib sensitivity in HCC cells. *BMC Cancer, 24*, 525. 10.1186/s12885-024-12275-w

Parhamifar, L., Andersen, H., & Moghimi, S. M. (2013). Lactate dehydrogenase assay for assessment of polycation cytotoxicity. *Methods in Molecular Biology (Clifton, N.J.), 948*, 13–22. 10.1007/978-1-62703-140-0_2

Parkkinen, L., O'Sullivan, S. S., Collins, C., Petrie, A., Holton, J. L., Revesz, T., & Lees, A. J. (2011). Disentangling the Relationship between Lewy Bodies and Nigral Neuronal Loss in Parkinson's Disease. *Journal of Parkinson's Disease, 1*(3), 277–286. 10.3233/JPD-2011-11046

Parra-Rivas, L. A., Madhivanan, K., Aulston, B. D., Wang, L., Prakashchand, D. D., Boyer, N. P., Saia-Cereda, V. M., Branes-Guerrero, K., Pizzo, D. P., Bagchi, P., Sundar, V. S., Tang, Y., Das, U., Scott, D. A., Rangamani, P., Ogawa, Y., & Subhojit Roy, n. (2023). Serine-129 phosphorylation of α-synuclein is an activity-dependent trigger for physiologic protein-protein interactions and synaptic function. *Neuron, 111*(24), 4006–4023.e10. 10.1016/j.neuron.2023.11.020

Pasquini, J., Brooks, D. J., & Pavese, N. (2021). The Cholinergic Brain in Parkinson's Disease. *Movement Disorders Clinical Practice, 8*(7), 1012–1026. 10.1002/mdc3.13319

Patterson, J. R., Polinski, N. K., Duffy, M. F., Kemp, C. J., Luk, K. C., Volpicelli-Daley, L. A., Kanaan, N. M., & Sortwell, C. E. (2019). Generation of Alpha-Synuclein Preformed Fibrils from Monomers and use In Vivo. *Journal of Visualized Experiments : JoVE,* (148), 10.3791/59758. 10.3791/59758

Patzke, C., Max, K. E. A., Behlke, J., Schreiber, J., Schmidt, H., Dorner, A. A., Kröger, S., Henning, M., Otto, A., Heinemann, U., & Rathjen, F. G. (2010). The

coxsackievirus-adenovirus receptor reveals complex homophilic and heterophilic interactions on neural cells. *The Journal of Neuroscience: The Official Journal of the Society for Neuroscience, 30*(8), 2897–2910. 10.1523/JNEUROSCI.5725-09.2010

Pauwels, E. K. J., & Boer, G. J. (2023). Parkinson's Disease: A Tale of Many Players. *Medical Principles and Practice: International Journal of the Kuwait University, Health Science Centre, 32*(3), 155–165. 10.1159/000531422

Pavon, J. M., Whitson, H. E., & Okun, M. S. (2010). Parkinson's disease in women: A call for improved clinical studies and for comparative effectiveness research. *Maturitas, 65*(4), 352–358. 10.1016/j.maturitas.2010.01.001

Peccati, F., Hernando, J., Blancafort, L., Solans-Monfort, X., & Sodupe, M. (2015). Disaggregation-induced fluorescence enhancement of NIAD-4 for the optical imaging of amyloid-β fibrils. *Physical Chemistry Chemical Physics: PCCP, 17*(30), 19718–19725. 10.1039/c5cp02728d

Pettifer, K. M., Jiang, S., Bau, C., Ballerini, P., D'Alimonte, I., Werstiuk, E. S., & Rathbone, M. P. (2007). MPP+-induced cytotoxicity in neuroblastoma cells: Antagonism and reversal by guanosine. *Purinergic Signalling, 3*(4), 399–409. 10.1007/s11302-007-9073-z

Pilch, J., Mizera, J., Tota, M., & Donizy, P. (2024). GNAQ/GNA11-Related Benign and Malignant Entities—A Common Histoembriologic Origin or a Tissue-Dependent Coincidence. *Cancers, 16*(21), 3672. 10.3390/cancers16213672

Ping, Z., Xiaomu, W., Xufang, X., Wenfeng, C., Liang, S., & Tao, W. (2018). GAPDH rs1136666 SNP indicates a high risk of Parkinson's disease. *Neuroscience Letters, 685*, 55–62. 10.1016/j.neulet.2018.06.011

Pires, G., McElligott, S., Drusinsky, S., Halliday, G., Potier, M., Wisniewski, T., & Drummond, E. (2019). Secernin-1 is a novel phosphorylated tau binding protein that accumulates in Alzheimer's disease and not in other tauopathies. *Acta Neuropathologica Communications, 7*(1), 195. 10.1186/s40478-019-0848-6

Pitale, P. M., Gorbatyuk, O., & Gorbatyuk, M. (2017). Neurodegeneration: Keeping ATF4 on a Tight Leash. *Frontiers in Cellular Neuroscience, 11*, 410. 10.3389/fncel.2017.00410

Politis, M., & Niccolini, F. (2015). Serotonin in Parkinson's disease. *Behavioural Brain Research, 277*, 136–145. 10.1016/j.bbr.2014.07.037

Protter, D. S. W., & Parker, R. (2016). Principles and Properties of Stress granules. *Trends in Cell Biology, 26*(9), 668–679. 10.1016/j.tcb.2016.05.004

Prusty, B. K., Chowdhury, S. R., Gulve, N., & Rudel, T. (2018). Peptidase Inhibitor 15 (PI15) Regulates Chlamydial CPAF Activity. *Frontiers in Cellular and Infection Microbiology, 8*, 183. 10.3389/fcimb.2018.00183

Qin, Y., Capaldo, C., Gumbiner, B. M., & Macara, I. G. (2005). The mammalian Scribble polarity protein regulates epithelial cell adhesion and migration through E-cadherin. *The Journal of Cell Biology, 171*(6), 1061–1071. 10.1083/jcb.200506094

Qiu, T., Tan, L., Yan, J., & Luo, Q. (2024). Erbin: an important therapeutic target for blocking tumor metastasis. *Frontiers in Pharmacology, 15*, 1474798. 10.3389/fphar.2024.1474798

Qiu, X., Campos, Y., van de Vlekkert, D., Gomero, E., Tanwar, A. C., Kalathur, R., Weesner, J. A., Bongiovanni, A., Demmers, J., & d'Azzo, A. (2022). Distinct functions of dimeric and monomeric scaffold protein Alix in regulating F-actin assembly and loading of exosomal cargo. *The Journal of Biological Chemistry, 298*(10), 102425. 10.1016/j.jbc.2022.102425

Querfurth, H., & Lee, H. (2021). Mammalian/mechanistic target of rapamycin (mTOR) complexes in neurodegeneration. *Molecular Neurodegeneration, 16*(1), 44. 10.1186/s13024-021-00428-5

Quiroz-Baez, R., Hernández-Ortega, K., & Martínez-Martínez, E. (2020). Insights Into the Proteomic Profiling of Extracellular Vesicles for the Identification of Early Biomarkers of Neurodegeneration. *Frontiers in Neurology, 11*, 580030. 10.3389/fneur.2020.580030

Rabouw, H. H., Langereis, M. A., Anand, A. A., Visser, L. J., de Groot, R. J., Walter, P., & van Kuppeveld, F. J. M. (2019). Small molecule ISRIB suppresses the integrated stress response within a defined window of activation. *Proceedings of the National Academy of Sciences of the United States of America, 116*(6), 2097–2102. 10.1073/pnas.1815767116

Raghav, A., Singh, M., Jeong, G., Giri, R., Agarwal, S., Kala, S., & Gautam, K. A. (2022). Extracellular vesicles in neurodegenerative diseases: A systematic review. *Frontiers in Molecular Neuroscience, 15*, 1061076. 10.3389/fnmol.2022.1061076

Rainey, N. E., Armand, A., & Petit, P. X. (2024). Sodium arsenite and arsenic trioxide differently affect the oxidative stress of lymphoblastoid cells: An intricate crosstalk between mitochondria, autophagy and cell death. *PloS One, 19*(5), e0302701. 10.1371/journal.pone.0302701

Rana, A. K., & Singh, D. (2018). Targeting glycogen synthase kinase-3 for oxidative stress and neuroinflammation: Opportunities, challenges and future directions for cerebral stroke management. *Neuropharmacology, 139*, 124–136. 10.1016/j.neuropharm.2018.07.006

Rashid, M., Lorzadeh, S., Gao, A., Ghavami, S., & Coombs, K. M. (2023). PSMA2 knockdown impacts expression of proteins involved in immune and cellular stress responses in human lung cells. *Biochimica Et Biophysica Acta. Molecular Basis of Disease, 1869*(2), 166617. 10.1016/j.bbadis.2022.166617

Redding, A., & Grabocka, E. (2023). Stress granules and hormetic adaptation of cancer. *Trends in Cancer, 9*(12), 995–1005. 10.1016/j.trecan.2023.08.005

References

References

Reineke, L. C., & Neilson, J. R. (2019). Differences between acute and chronic stress granules, and how these differences may impact function in human disease. *Biochemical Pharmacology, 162*, 123–131. 10.1016/j.bcp.2018.10.009

Repici, M., Hassanjani, M., Maddison, D. C., Garção, P., Cimini, S., Patel, B., Szegö, É M., Straatman, K. R., Lilley, K. S., Borsello, T., Outeiro, T. F., Panman, L., & Giorgini, F. (2019). The Parkinson's Disease-Linked Protein DJ-1 Associates with Cytoplasmic mRNP Granules During Stress and Neurodegeneration. *Molecular Neurobiology, 56*(1), 61–77. 10.1007/s12035-018-1084-y

Reyes, R., Cardeñes, B., Machado-Pineda, Y., & Cabañas, C. (2018). Tetraspanin CD9: A Key Regulator of Cell Adhesion in the Immune System. *Frontiers in Immunology, 9*, 863. 10.3389/fimmu.2018.00863

Richards, C. M., McRae, S. A., Ranger, A. L., & Klegeris, A. (2023). Extracellular histones as damage-associated molecular patterns in neuroinflammatory responses. *Reviews in the Neurosciences, 34*(5), 533–558. 10.1515/revneuro-2022-0091

Riggs, C. L., Kedersha, N., Ivanov, P., & Anderson, P. (2020). Mammalian stress granules and P bodies at a glance. *Journal of Cell Science, 133*(16), jcs242487. 10.1242/jcs.242487

Riise, R., Odqvist, L., Mattsson, J., Monkley, S., Abdillahi, S. M., Tyrchan, C., Muthas, D., & Yrlid, L. F. (2019). Bleomycin hydrolase regulates the release of chemokines important for inflammation and wound healing by keratinocytes. *Scientific Reports, 9*(1), 20407. 10.1038/s41598-019-56667-6

Risiglione, P., Leggio, L., Cubisino, S. A. M., Reina, S., Paternò, G., Marchetti, B., Magrì, A., Iraci, N., & Messina, A. (2020). High-Resolution Respirometry Reveals MPP+ Mitochondrial Toxicity Mechanism in a Cellular Model of Parkinson's Disease. *International Journal of Molecular Sciences, 21*(21), 7809. 10.3390/ijms21217809

Rizzo, J., Taheraly, A., & Janbon, G. (2021). Structure, composition and biological properties of fungal extracellular vesicles. *microLife, 2*, uqab009. 10.1093/femsml/uqab009

Rosa-Mercado, N. A., Buskirk, A. R., & Green, R. (2024). Translation elongation inhibitors stabilize select short-lived transcripts. *RNA, 30*(12), 1572–1585. 10.1261/rna.080138.124

Rozpedek, W., Pytel, D., Mucha, B., Leszczynska, H., Diehl, J. A., & Majsterek, I. (2016). The Role of the PERK/eIF2α/ATF4/CHOP Signaling Pathway in Tumor Progression During Endoplasmic Reticulum Stress. *Current Molecular Medicine, 16*(6), 533–544. 10.2174/1566524016666160523143937

Rubin, C. I., & Atweh, G. F. (2004). The role of stathmin in the regulation of the cell cycle. *Journal of Cellular Biochemistry, 93*(2), 242–250. 10.1002/jcb.20187

Ruggieri, A., Dazert, E., Metz, P., Hofmann, S., Bergeest, J., Mazur, J., Bankhead, P., Hiet, M., Kallis, S., Alvisi, G., Samuel, C. E., Lohmann, V., Kaderali, L., Rohr, K., Frese, M., Stoecklin, G., & Bartenschlager, R. (2012). Dynamic Oscillation of Translation and Stress Granule Formation Mark the Cellular Response to Virus Infection. *Cell Host & Microbe, 12*(1), 10.1016/j.chom.2012.05.013. 10.1016/j.chom.2012.05.013

Rui, Q., Ni, H., Li, D., Gao, R., & Chen, G. (2018). The Role of LRRK2 in Neurodegeneration of Parkinson Disease. *Current Neuropharmacology, 16*(9), 1348–1357. 10.2174/1570159X16666180222165418

Ruiz-Ramos, R., Lopez-Carrillo, L., Rios-Perez, A. D., De Vizcaya-Ruíz, A., & Cebrian, M. E. (2009). Sodium arsenite induces ROS generation, DNA oxidative damage, HO-1 and c-Myc proteins, NF-kappaB activation and cell proliferation in human breast cancer MCF-7 cells. *Mutation Research, 674*(1-2), 109–115. 10.1016/j.mrgentox.2008.09.021

Russo, I., Kaganovich, A., Ding, J., Landeck, N., Mamais, A., Varanita, T., Biosa, A., Tessari, I., Bubacco, L., Greggio, E., & Cookson, M. R. (2019). Transcriptome analysis of LRRK2 knock-out microglia cells reveals alterations of inflammatory- and oxidative stress-related pathways upon treatment with α-synuclein fibrils. *Neurobiology of Disease, 129*, 67–78. 10.1016/j.nbd.2019.05.012

Ryoo, H. D. (2024). The integrated stress response in metabolic adaptation. *The Journal of Biological Chemistry, 300*(4), 107151. 10.1016/j.jbc.2024.107151

Ryoo, H. D., & Vasudevan, D. (2017). Two distinct nodes of translational inhibition in the Integrated Stress Response. *BMB Reports, 50*(11), 539–545. 10.5483/BMBRep.2017.50.11.157

Saito, Y. (2017). DJ-1 as a Biomarker of Parkinson's Disease. *Advances in Experimental Medicine and Biology, 1037*, 149–171. 10.1007/978-981-10-6583-5_10

Sakamoto, S., Miyara, M., Sanoh, S., Ohta, S., & Kotake, Y. (2017). Mild MPP+ exposure-induced glucose starvation enhances autophagosome synthesis and impairs its degradation. *Scientific Reports, 7*, 46668. 10.1038/srep46668

Salat, D., & Tolosa, E. (2013). Levodopa in the treatment of Parkinson's disease: current status and new developments. *Journal of Parkinson's Disease, 3*(3), 255–269. 10.3233/JPD-130186

Sallinen, V., Torkko, V., Sundvik, M., Reenilä, I., Khrustalyov, D., Kaslin, J., & Panula, P. (2009). MPTP and MPP+ target specific aminergic cell populations in larval zebrafish. *Journal of Neurochemistry, 108*(3), 719–731. 10.1111/j.1471-4159.2008.05793.

Samuel, F., Flavin, W. P., Iqbal, S., Pacelli, C., Sri Renganathan, S. D., Trudeau, L., Campbell, E. M., Fraser, P. E., & Tandon, A. (2016). Effects of Serine 129 Phosphorylation on α-Synuclein Aggregation, Membrane Association, and Internalization. *The Journal of Biological Chemistry, 291*(9), 4374–4385. 10.1074/jbc.M115.705095

Samuelov, L., Sarig, O., Harmon, R. M., Rapaport, D., Ishida-Yamamoto, A., Isakov, O., Koetsier, J. L., Gat, A., Goldberg, I., Bergman, R., Spiegel, R., Eytan, O., Geller, S., Peleg, S., Shomron, N., Goh, C. S. M., Wilson, N. J., Smith, F. J. D., Pohler, E., . . . Sprecher, E. (2013). Desmoglein 1 deficiency results in severe dermatitis, multiple allergies and metabolic wasting. *Nature Genetics, 45*(10), 1244–1248. 10.1038/ng.2739

Sanchez, I. I., Nguyen, T. B., England, W. E., Lim, R. G., Vu, A. Q., Miramontes, R., Byrne, L. M., Markmiller, S., Lau, A. L., Orellana, I., Curtis, M. A., Faull, R. L. M., Yeo, G. W., Fowler, C. D., Reidling, J. C., Wild, E. J., Spitale, R. C., & Thompson, L. M. (2021). Huntington's disease mice and human brain tissue

exhibit increased G3BP1 granules and TDP43 mislocalization. *The Journal of Clinical Investigation, 131*(12), e140723, 140723. 10.1172/JCI140723

Sandor, C., Honti, F., Haerty, W., Szewczyk-Krolikowski, K., Tomlinson, P., Evetts, S., Millin, S., Keane, T., McCarthy, S. A., Durbin, R., Talbot, K., Hu, M., Webber, C., Ponting, C. P., & Wade-Martins, R. (2017). Whole-exome sequencing of 228 patients with sporadic Parkinson's disease. *Scientific Reports, 7*, 41188. 10.1038/srep41188

Santos-Ribeiro, D., Godinas, L., Pilette, C., & Perros, F. (2018). The integrated stress response system in cardiovascular disease. *Drug Discovery Today, 23*(4), 920–929. 10.1016/j.drudis.2018.02.008

Sayyah, J., Bartakova, A., Nogal, N., Quilliam, L. A., Stupack, D. G., & Brown, J. H. (2014). The Ras-related protein, Rap1A, mediates thrombin-stimulated, integrin-dependent glioblastoma cell proliferation and tumor growth. *The Journal of Biological Chemistry, 289*(25), 17689–17698. 10.1074/jbc.M113.536227

Schoof, M., Boone, M., Wang, L., Lawrence, R., Frost, A., & Walter, P. (2024). eIF2B conformation and assembly state regulate the integrated stress response. *eLife, 10*, e65703. 10.7554/eLife.65703

Schulze, M., Sommer, A., Plötz, S., Farrell, M., Winner, B., Grosch, J., Winkler, J., & Riemenschneider, M. J. (2018). Sporadic Parkinson's disease derived neuronal cells show disease-specific mRNA and small RNA signatures with abundant deregulation of piRNAs. *Acta Neuropathologica Communications, 6*(1), 58. 10.1186/s40478-018-0561-x

Scotter, E. L., Chen, H., & Shaw, C. E. (2015). TDP-43 Proteinopathy and ALS: Insights into Disease Mechanisms and Therapeutic Targets. *Neurotherapeutics: The Journal of the American Society for Experimental NeuroTherapeutics, 12*(2), 352–363. 10.1007/s13311-015-0338

Scudamore, O., & Ciossek, T. (2018). Increased Oxidative Stress Exacerbates α-Synuclein Aggregation In Vivo. *Journal of Neuropathology & Experimental Neurology, 77*(6), 443–453. 10.1093/jnen/nly024

Sfakianos, A. P., Mellor, L. E., Pang, Y. F., Kritsiligkou, P., Needs, H., Abou-Hamdan, H., Désaubry, L., Poulin, G. B., Ashe, M. P., & Whitmarsh, A. J. (2018). The mTOR-S6 kinase pathway promotes stress granule assembly. *Cell Death & Differentiation, 25*(10), 1766–1780. 10.1038/s41418-018-0076-9

Sharma, A., Liu, H., Tobar-Tosse, F., Chand Dakal, T., Ludwig, M., Holz, F. G., Loeffler, K. U., Wüllner, U., & Herwig-Carl, M. C. (2020). Ubiquitin Carboxyl-Terminal Hydrolases (UCHs): Potential Mediators for Cancer and Neurodegeneration. *International Journal of Molecular Sciences, 21*(11), 3910. 10.3390/ijms21113910

Sharma, M., Naslavsky, N., & Caplan, S. (2008). A role for EHD4 in the regulation of early endosomal transport. *Traffic (Copenhagen, Denmark), 9*(6), 995–1018. 10.1111/j.1600-0854.2008.00732.x

Shelkovnikova, T. A., Dimasi, P., Kukharsky, M. S., An, H., Quintiero, A., Schirmer, C., Buée, L., Galas, M., & Buchman, V. L. (2017). Chronically stressed or stress-preconditioned neurons fail to maintain stress granule assembly. *Cell Death & Disease, 8*(5), e2788. 10.1038/cddis.2017.199

Shibagaki, N., Hanada, K., Yamaguchi, S., Yamashita, H., Shimada, S., & Hamada, H. (1998). Functional analysis of CD82 in the early phase of T cell activation: roles in cell adhesion and signal transduction. *European Journal of Immunology, 28*(4), 1125–1133. 10.1002/(SICI)1521-4141(199804)28:04<1125::AID-IMMU1125>3.0.CO;2-C

Shin, W., Park, M., Kim, J. H., Oh, S. W., Jang, J., Lee, H., & Lee, S. (2022). PTK7, a Catalytically Inactive Receptor Tyrosine Kinase, Increases Oncogenic Phenotypes in Xenograft Tumors of Esophageal Squamous Cell Carcinoma KYSE-30 Cells. *International Journal of Molecular Sciences, 23*(4), 2391. 10.3390/ijms23042391

Shippey, L. E., Campbell, S. G., Hill, A. F., & Smith, D. P. (2022). Propagation of Parkinson's disease by extracellular vesicle production and secretion. *Biochemical Society Transactions, 50*(5), 1303–1314. 10.1042/BST20220204

Si, J., Van den Haute, C., Lobbestael, E., Martin, S., van Veen, S., Vangheluwe, P., & Baekelandt, V. (2021a). ATP13A2 Regulates Cellular α-Synuclein Multimerization, Membrane Association, and Externalization. *International Journal of Molecular Sciences, 22*(5), 2689. 10.3390/ijms22052689

Siddiqui, I. J., Pervaiz, N., & Abbasi, A. A. (2016b). The Parkinson Disease gene SNCA: Evolutionary and structural insights with pathological implication. *Scientific Reports, 6*, 24475. 10.1038/srep24475

Sieurin, J., Andel, R., Tillander, A., Valdes, E. G., Pedersen, N. L., & Wirdefeldt, K. (2018). Occupational stress and risk for Parkinson's disease: A nationwide cohort study. *Movement Disorders: Official Journal of the Movement Disorder Society, 33*(9), 1456–1464. 10.1002/mds.27439

Silvestro, S., Chiricosta, L., Gugliandolo, A., Iori, R., Rollin, P., Perenzoni, D., Mattivi, F., Bramanti, P., & Mazzon, E. (2021). The Moringin/α-CD Pretreatment Induces Neuroprotection in an In Vitro Model of Alzheimer's Disease: A Transcriptomic Study. *Current Issues in Molecular Biology, 43*(1), 197–214. 10.3390/cimb43010017

Skou, L. D., Johansen, S. K., Okarmus, J., & Meyer, M. (2024). Pathogenesis of DJ-1/PARK7-Mediated Parkinson's Disease. *Cells, 13*(4), 296. 10.3390/cells13040296

Smith, D. P., Tew, D. J., Hill, A. F., Bottomley, S. P., Masters, C. L., Barnham, K. J., & Cappai, R. (2008). Formation of a High Affinity Lipid-Binding Intermediate during the Early Aggregation Phase of α-Synuclein. *Biochemistry, 47*(5), 1425–1434. 10.1021/bi701522m

Smith, J. K., Mellick, G. D., & Sykes, A. M. (2023). The role of the endolysosomal pathway in α-synuclein pathogenesis in Parkinson's disease. *Frontiers in Cellular Neuroscience, 16*10.3389/fncel.2022.1081426

Smits, L. M., Reinhardt, L., Reinhardt, P., Glatza, M., Monzel, A. S., Stanslowsky, N., Rosato-Siri, M. D., Zanon, A., Antony, P. M., Bellmann, J., Nicklas, S. M., Hemmer, K., Qing, X., Berger, E., Kalmbach, N., Ehrlich, M., Bolognin, S., Hicks, A. A., Wegner, F., . . . Schwamborn, J. C. (2019). Modeling

Parkinson’s disease in midbrain-like organoids. *Npj Parkinson's Disease, 5*(1), 1–8. 10.1038/s41531-019-0078-4

Solana-Manrique, C., Sánchez-Pérez, A. M., Paricio, N., & Muñoz-Descalzo, S. (2025). Two- and Three-Dimensional In Vitro Models of Parkinson's and Alzheimer's Diseases: State-of-the-Art and Applications. *International Journal of Molecular Sciences, 26*(2), 620. 10.3390/ijms26020620

Sproviero, D., La Salvia, S., Giannini, M., Crippa, V., Gagliardi, S., Bernuzzi, S., Diamanti, L., Ceroni, M., Pansarasa, O., Poletti, A., & Cereda, C. (2018). Pathological Proteins Are Transported by Extracellular Vesicles of Sporadic Amyotrophic Lateral Sclerosis Patients. *Frontiers in Neuroscience, 12*10.3389/fnins.2018.00487

Srinivasan, E., Chandrasekhar, G., Chandrasekar, P., Anbarasu, K., Vickram, A. S., Karunakaran, R., Rajasekaran, R., & Srikumar, P. S. (2021b). Alpha-Synuclein Aggregation in Parkinson's Disease. *Frontiers in Medicine, 8*, 736978. 10.3389/fmed.2021.736978

Stuendl, A., Kraus, T., Chatterjee, M., Zapke, B., Sadowski, B., Moebius, W., Hobert, M. A., Deuschle, C., Brockmann, K., Maetzler, W., Mollenhauer, B., & Schneider, A. (2021). α-Synuclein in Plasma-Derived Extracellular Vesicles Is a Potential Biomarker of Parkinson's Disease. *Movement Disorders: Official Journal of the Movement Disorder Society, 36*(11), 2508–2518. 10.1002/mds.28639

Stukalov, A., Girault, V., Grass, V., Karayel, O., Bergant, V., Urban, C., Haas, D. A., Huang, Y., Oubraham, L., Wang, A., Hamad, M. S., Piras, A., Hansen, F. M., Tanzer, M. C., Paron, I., Zinzula, L., Enghleitner, T., Reinecke, M., Lavacca, T. M., . . . Pichlmair, A. (2021). Multilevel proteomics reveals host perturbations by SARS-CoV-2 and SARS-CoV. *bioRxiv,* 10.1038/s41586-021-03493-4

Su, W., Mruk, D. D., Wong, E. W. P., Lui, W., & Cheng, C. Y. (2012). Polarity Protein Complex Scribble/Lgl/Dlg and Epithelial Cell Barriers. *Advances in Experimental Medicine and Biology, 763*, 149–170. 10.1007/978-1-4614-4711-5_7.

Sulatskaya, A. I., Rodina, N. P., Sulatsky, M. I., Povarova, O. I., Antifeeva, I. A., Kuznetsova, I. M., & Turoverov, K. K. (2018). Investigation of α-Synuclein Amyloid Fibrils Using the Fluorescent Probe Thioflavin T. *International Journal of Molecular Sciences, 19*(9), 2486. 10.3390/ijms19092486

Sulzer, D., & Edwards, R. H. (2019). The Physiological Role of α-Synuclein and Its Relationship to Parkinson's Disease. *Journal of Neurochemistry, 150*(5), 475–486. 10.1111/jnc.14810

Sun, Y., Han, L., & Sun, D. (2024). Comprehensive analysis of EML2 as a prognostic biomarker in colon cancer. *International Journal of Clinical and Experimental Pathology, 17*(1), 1–12. 10.62347/PALH4103

Sun, Y., Sukumaran, P., Selvaraj, S., Cilz, N. I., Schaar, A., Lei, S., & Singh, B. B. (2018). TRPM2 promotes neurotoxin MPP+/MPTP-induced cell death. *Molecular Neurobiology, 55*(1), 409–420. 10.1007/s12035-016-0338-9

Suragani, R. N. V. S., Zachariah, R. S., Velazquez, J. G., Liu, S., Sun, C., Townes, T. M., & Chen, J. (2012). Heme-regulated eIF2α kinase activated Atf4 signaling pathway in oxidative stress and erythropoiesis. *Blood, 119*(22), 5276–5284. 10.1182/blood-2011-10-388132

Sveinbjornsdottir, S. (2016). The clinical symptoms of Parkinson's disease. *Journal of Neurochemistry, 139 Suppl 1*, 318–324. 10.1111/jnc.13691

Sztal, T., Berger, S., Currie, P. D., & Hall, T. E. (2011). Characterization of the laminin gene family and evolution in zebrafish. *Developmental Dynamics: An Official Publication of the American Association of Anatomists, 240*(2), 422–431. 10.1002/dvdy.22537

Szwedo, A. A., Dalen, I., Pedersen, K. F., Camacho, M., Bäckström, D., Forsgren, L., Tzoulis, C., Winder-Rhodes, S., Hudson, G., Liu, G., Scherzer, C. R., Lawson, R. A., Yarnall, A. J., Williams-Gray, C. H., Macleod, A. D., Counsell, C. E., Tysnes, O., Alves, G., & Maple-Grødem, J. (2022a). GBA and APOE Impact Cognitive Decline in Parkinson's Disease: A 10-Year Population-Based Study. *Movement Disorders : Official Journal of the Movement Disorder Society, 37*(5), 1016–1027. 10.1002/mds.28932

Tai, L. M., Thomas, R., Marottoli, F. M., Koster, K. P., Kanekiyo, T., Morris, A. W. J., & Bu, G. (2016). The role of APOE in cerebrovascular dysfunction. *Acta Neuropathologica, 131*(5), 709–723. 10.1007/s00401-016-1547-z

Tao, S., Cui, D., Cheng, H., Liu, X., Jiang, Z., Chen, H., & Gao, Y. (2024). High expression of TBRG4 in relation to unfavorable outcome and cell ferroptosis in hepatocellular carcinoma. *BMC Cancer, 24*, 194. 10.1186/s12885-024-11943-1

Tapias, V., Hu, X., Luk, K. C., Sanders, L. H., Lee, V. M., & Greenamyre, J. T. (2017). Synthetic alpha-synuclein fibrils cause mitochondrial impairment and selective dopamine neurodegeneration in part via iNOS-mediated nitric oxide production. *Cellular and Molecular Life Sciences: CMLS, 74*(15), 2851–2874. 10.1007/s00018-017-2541-x

Teske, B. F., Fusakio, M. E., Zhou, D., Shan, J., McClintick, J. N., Kilberg, M. S., & Wek, R. C. (2013). CHOP induces activating transcription factor 5 (ATF5) to trigger apoptosis in response to perturbations in protein homeostasis. *Molecular Biology of the Cell, 24*(15), 2477–2490. 10.1091/mbc.E13-01-0067

Thomas, Y., Bui, N., & Strub, K. (1997). A truncation in the 14 kDa protein of the signal recognition particle leads to tertiary structure changes in the RNA and abolishes the elongation arrest activity of the particle. *Nucleic Acids Research, 25*(10), 1920–1929. 10.1093/nar/25.10.1920

Thorne, N. J., & Tumbarello, D. A. (2022). The relationship of alpha-synuclein to mitochondrial dynamics and quality control. *Frontiers in Molecular Neuroscience, 15*, 947191. 10.3389/fnmol.2022.947191

Tognoli, M. L., Dancourt, J., Bonsergent, E., Palmulli, R., de Jong, O. G., Van Niel, G., Rubinstein, E., Vader, P., & Lavieu, G. (2023). Lack of involvement of CD63 and CD9 tetraspanins in the extracellular vesicle content delivery process. *Communications Biology, 6*(1), 532. 10.1038/s42003-023-04911-1

Tolosa, E., Garrido, A., Scholz, S. W., & Poewe, W. (2021). Challenges in the diagnosis of Parkinson's disease. *The Lancet. Neurology, 20*(5), 385–397. 10.1016/S1474-4422(21)00030-2

Tong, Y., Zhang, P., Yang, X., Liu, X., Zhang, J., Grudniewska, M., Jung, I., Abegg, D., Liu, J., Childs-Disney, J. L., Gibaut, Q. M. R., Haniff, H. S., Adibekian, A., Mouradian, M. M., & Disney, M. D. (2024). Decreasing the intrinsically disordered protein α-synuclein levels by targeting its structured mRNA with a ribonuclease-targeting chimera. *Proceedings of the National Academy of Sciences of the United States of America, 121*(2), e2306682120. 10.1073/pnas.2306682120

Toomey, C. E., Heywood, W. E., Evans, J. R., Lachica, J., Pressey, S. N., Foti, S. C., Al Shahrani, M., D'Sa, K., Hargreaves, I. P., Heales, S., Orford, M., Troakes, C., Attems, J., Gelpi, E., Palkovits, M., Lashley, T., Gentleman, S. M., Revesz, T., Mills, K., & Gandhi, S. (2022). Mitochondrial dysfunction is a key pathological driver of early stage Parkinson's. *Acta Neuropathologica Communications, 10*, 134. 10.1186/s40478-022-01424-6

Tricarico, C., Clancy, J., & D'Souza-Schorey, C. (2016). Biology and biogenesis of shed microvesicles. *Small GTPases, 8*(4), 220–232. 10.1080/21541248.2016.1215283

Trivedi, R., & Nagarajaram, H. A. (2022). Intrinsically Disordered Proteins: An Overview. *International Journal of Molecular Sciences, 23*(22), 14050. 10.3390/ijms232214050

Tu, Y., Chen, C., & Fan, G. (2019). Association between the expression of secreted phosphoprotein - related genes and prognosis of human cancer. *BMC Cancer, 19*(1), 1230. 10.1186/s12885-019-6441-3

Upadhya, R., & Shetty, A. K. (2021). Extracellular Vesicles for the Diagnosis and Treatment of Parkinson's Disease. *Aging and Disease, 12*(6), 1438–1450. 10.14336/AD.2021.0516

Valencia, J., Ferreira, M., Merino-Torres, J. F., Marcilla, A., & Soriano, J. M. (2022). The Potential Roles of Extracellular Vesicles as Biomarkers for Parkinson's Disease: A Systematic Review. *International Journal of Molecular Sciences, 23*(19), 11508. 10.3390/ijms231911508

van Veen, S., Martin, S., Van den Haute, C., Benoy, V., Lyons, J., Vanhoutte, R., Kahler, J. P., Decuypere, J., Gelders, G., Lambie, E., Zielich, J., Swinnen,

J. V., Annaert, W., Agostinis, P., Ghesquière, B., Verhelst, S., Baekelandt, V., Eggermont, J., & Vangheluwe, P. (2020a). ATP13A2 deficiency disrupts lysosomal polyamine export. *Nature, 578*(7795), 419–424. 10.1038/s41586-020-1968-7

Vanderweyde, T., Yu, H., Varnum, M., Liu-Yesucevitz, L., Citro, A., Ikezu, T., Duff, K., & Wolozin, B. (2012). Contrasting Pathology of the Stress Granule Proteins TIA-1 and G3BP in Tauopathies. *The Journal of Neuroscience, 32*(24), 8270–8283. 10.1523/JNEUROSCI.1592-12.2012

Vellingiri, B., Chandrasekhar, M., Sabari, S. S., Gopalakrishnan, A. V., Narayanasamy, A., Venkatesan, D., Iyer, M., Kesari, K., & Dey, A. (2022). Neurotoxicity of pesticides - A link to neurodegeneration - PubMed. *Ecotoxicol Environ Saf., 15*(243), 113972. 10.1016/j.ecoenv.2022.113972

Verma, D. K., Seo, B. A., Ghosh, A., Ma, S., Hernandez-Quijada, K., Andersen, J. K., Ko, H. S., & Kim, Y. (2021). Alpha-Synuclein Preformed Fibrils Induce Cellular Senescence in Parkinson's Disease Models. *Cells, 10*(7), 1694. 10.3390/cells10071694

Volpicelli-Daley, L. A., Luk, K. C., & Lee, V. M. -. (2014). Addition of exogenous α-Synuclein Pre-formed fibrils to Primary Neuronal Cultures to seed recruitment of endogenous α-Synuclein to Lewy body and Lewy Neurite-like aggregates. *Nature Protocols, 9*(9), 2135–2146. 10.1038/nprot.2014.143

Volpicelli-Daley, L. A., Luk, K. C., Patel, T. P., Tanik, S. A., Riddle, D. M., Stieber, A., Meany, D. F., Trojanowski, J. Q., & Lee, V. M. -. (2011). Exogenous α-Synuclein Fibrils Induce Lewy Body Pathology Leading to Synaptic Dysfunction and Neuron Death. *Neuron, 72*(1), 57–71. 10.1016/j.neuron.2011.08.033

von Coelln, R., Dawson, V. L., & Dawson, T. M. (2004). Parkin-associated Parkinson's disease. *Cell and Tissue Research, 318*(1), 175–184. 10.1007/s00441-004-0924-4

Wang, C., Zhou, C., Guo, T., Huang, P., Xu, X., & Zhang, M. (2022). Association between cigarette smoking and Parkinson's disease: a

neuroimaging study. *Therapeutic Advances in Neurological Disorders, 15*, 17562864221092566. 10.1177/17562864221092566

Wang, D., Qu, S., Zhang, Z., Tan, L., Chen, X., Zhong, H., & Chong, C. (2023). Strategies targeting endoplasmic reticulum stress to improve Parkinson's disease. *Frontiers in Pharmacology, 14*, 1288894. 10.3389/fphar.2023.1288894

Wang, H., Pommerenke, C., Hauer, V., Rand, U., Eberth, S., Nagel, S., Dirks, W., Werr, L., Fischer, M., & Steenpaß, L. (2024). 269P Human neuroblastoma cell-derived neurons and iPSC-derived neurons as models for neuromuscular disorders. *Neuromuscular Disorders, 43*, 104441.78. 10.1016/j.nmd.2024.07.087

Wang, J. Y., Roehrl, M. W., Roehrl, V. B., & Roehrl, M. H. (2022). A master autoantigen-ome links alternative splicing, female predilection, and COVID-19 to autoimmune diseases. *Journal of Translational Autoimmunity, 5*, 100147. 10.1016/j.jtauto.2022.100147

Wang, J., Cao, B., Ma, N., Wu, K., Chen, W., Wu, W., Dong, X., Liu, C., Gao, Y., Diao, T., Min, X., Yong, Q., Li, Z., Zhou, W., & Li, K. (2023). Collectin-11 promotes cancer cell proliferation and tumor growth. *JCI Insight, 8*(5), e159452. 10.1172/jci.insight.159452

Wang, J., Gan, Y., Cao, J., Dong, X., & Ouyang, W. (2022). Pathophysiology of stress granules: An emerging link to diseases (Review). *International Journal of Molecular Medicine, 49*(4), 44. 10.3892/ijmm.2022.5099

Wang, L., Yu, Y., Wang, L., Wang, Q., Zhang, Y., Gao, P., Ma, J., Chen, G., & Kong, X. (2023). The collectin subfamily member 11 (Ca-Colec11) from Qihe crucian carp (Carassius auratus) agglutinates and inhibits Aeromonas hydrophila and Staphylococcus aureus. *Fish & Shellfish Immunology, 133*, 108543. 10.1016/j.fsi.2023.108543

Wang, P., Lan, G., Xu, B., Yu, Z., Tian, C., Lei, X., Meissner, W. G., Feng, T., Yang, Y., & Zhang, J. (2023). α-Synuclein-carrying astrocytic extracellular vesicles in Parkinson pathogenesis and diagnosis. *Translational Neurodegeneration, 12*(1), 40. 10.1186/s40035-023-00372-y

Wang, R., Jiang, X., Bao, P., Qin, M., & Xu, J. (2019). Circadian control of stress granules by oscillating EIF2α. *Cell Death & Disease, 10*(3), 215. 10.1038/s41419-019-1471-y

Wang, S., He, H., Chen, L., Zhang, W., Zhang, X., & Chen, J. (2015). Protective Effects of Salidroside in the MPTP/MPP+-Induced Model of Parkinson's Disease through ROS–NO-Related Mitochondrion Pathway. *Molecular Neurobiology, 51*(2), 718–728. 10.1007/s12035-014-8755-0

Wang, X., Chemmama, I. E., Yu, C., Huszagh, A., Xu, Y., Viner, R., Block, S. A., Cimermancic, P., Rychnovsky, S. D., Ye, Y., Sali, A., & Huang, L. (2017). The proteasome-interacting Ecm29 protein disassembles the 26S proteasome in response to oxidative stress. *The Journal of Biological Chemistry, 292*(39), 16310–16320. 10.1074/jbc.M117.803619

Wek, R. C., Anthony, T. G., & Staschke, K. A. (2023). Surviving and Adapting to Stress: Translational Control and the Integrated Stress Response. *Antioxidants & Redox Signaling, 39*(4-6), 351–373. 10.1089/ars.2022.0123

Wheeler, J. R., Matheny, T., Jain, S., Abrisch, R., & Parker, R. (2016). Distinct stages in stress granule assembly and disassembly. *eLife, 5*, e18413. 10.7554/eLife.18413

Wilkaniec, A., Lenkiewicz, A. M., Czapski, G. A., Jęśko, H. M., Hilgier, W., Brodzik, R., Gąssowska-Dobrowolska, M., Culmsee, C., & Adamczyk, A. (2019). Extracellular Alpha-Synuclein Oligomers Induce Parkin S-Nitrosylation: Relevance to Sporadic Parkinson’s Disease Etiopathology. *Molecular Neurobiology, 56*(1), 125–140. 10.1007/s12035-018-1082-0

Woerman, A. L., & Luk, K. C. (2024). Are Preformed Fibrils a Model of Parkinson’s Disease? *Journal of Parkinson's Disease, 14*(6), 1095–1103. 10.3233/JPD-240228

Wohlschlegel, J., Argentini, M., Michiels, C., Letellier, C., Forster, V., Condroyer, C., He, Z., Thuret, G., Zeitz, C., Léger, T., & Audo, I. (2021). First

identification of ITM2B interactome in the human retina. *Scientific Reports, 11*, 17210. 10.1038/s41598-021-96571-6

Wolozin, B., & Ivanov, P. (2019). Stress granules and neurodegeneration. *Nature Reviews. Neuroscience, 20*(11), 649–666. 10.1038/s41583-019-0222-5

Wortel, I. M. N., van der Meer, L. T., Kilberg, M. S., & van Leeuwen, F. N. (2017). Surviving Stress: Modulation of ATF4-Mediated Stress Responses in Normal and Malignant Cells. *Trends in Endocrinology and Metabolism: TEM, 28*(11), 794–806. 10.1016/j.tem.2017.07.003

Wu, Q., Takano, H., Riddle, D. M., Trojanowski, J. Q., Coulter, D. A., & Lee, V. M. -. (2019). α-Synuclein (αSyn) Preformed Fibrils Induce Endogenous αSyn Aggregation, Compromise Synaptic Activity and Enhance Synapse Loss in Cultured Excitatory Hippocampal Neurons. *The Journal of Neuroscience: The Official Journal of the Society for Neuroscience, 39*(26), 5080–5094. 10.1523/JNEUROSCI.0060-19.2019

Xia, Q., Liao, L., Cheng, D., Duong, D. M., Gearing, M., Lah, J. J., Levey, A. I., & Peng, J. (2008). Proteomic identification of novel proteins associated with Lewy bodies. *Frontiers in Bioscience : A Journal and Virtual Library, 13*, 3850. 10.2741/2973

Xicoy, H., Wieringa, B., & Martens, G. J. M. (2017). The SH-SY5Y cell line in Parkinson's disease research: a systematic review. *Molecular Neurodegeneration, 12*(1), 10. 10.1186/s13024-017-0149-0

Xu, C., Kang, W., Chen, Y., Jiang, T., Zhang, J., Zhang, L., Ding, J., Liu, J., & Chen, S. (2017). DJ-1 Inhibits α-Synuclein Aggregation by Regulating Chaperone-Mediated Autophagy. *Frontiers in Aging Neuroscience, 9*, 308. 10.3389/fnagi.2017.00308

Xu, S., Liu, H., Wang, C., Deng, Y., Xu, B., Yang, T., & Liu, W. (2023). Dual roles of UPRer and UPRmt in neurodegenerative diseases. *Journal of Molecular Medicine (Berlin, Germany), 101*(12), 1499–1512. 10.1007/s00109-023-02382-9

Xu, X., Huang, J., Li, J., Liu, L., Han, C., Shen, Y., Zhang, G., Jiang, H., Lin, Z., Xiong, N., & Wang, T. (2016). Induced pluripotent stem cells and Parkinson's disease: modelling and treatment. *Cell Proliferation, 49*(1), 14–26. 10.1111/cpr.12229

Xue, C., Lin, T. Y., Chang, D., & Guo, Z. (2017). Thioflavin T as an amyloid dye: fibril quantification, optimal concentration and effect on aggregation. *Royal Society Open Science, 4*(1), 160696. 10.1098/rsos.160696

Xue, W., Hellewell, A. L., Gosal, W. S., Homans, S. W., Hewitt, E. W., & Radford, S. E. (2009). Fibril Fragmentation Enhances Amyloid Cytotoxicity♦. *The Journal of Biological Chemistry, 284*(49), 34272–34282. 10.1074/jbc.M109.049809

Xue, W., Zhu, H., Liu, H., & He, H. (2022). DIRAS2 Is a Prognostic Biomarker and Linked With Immune Infiltrates in Melanoma. *Frontiers in Oncology, 12*, 799185. 10.3389/fonc.2022.799185

Xun, Z., Lee, D., Lim, J., Canaria, C. A., Barnebey, A., Yanonne, S. M., & McMurray, C. T. (2012). Retinoic acid-induced differentiation increases the rate of oxygen consumption and enhances the spare respiratory capacity of mitochondria in SH-SY5Y cells. *Mechanisms of Ageing and Development, 133*(4), 176–185. 10.1016/j.mad.2012.01.008

Xylaki, M., Chopra, A., Weber, S., Bartl, M., Outeiro, T. F., & Mollenhauer, B. (2023). Extracellular Vesicles for the Diagnosis of Parkinson's Disease: Systematic Review and Meta-Analysis. *Movement Disorders: Official Journal of the Movement Disorder Society, 38*(9), 1585–1597. 10.1002/mds.29497

Yang, C., Xu, X., Dong, X., Yang, B., Dong, W., Luo, Y., Liu, X., Wu, Y., & Wang, J. (2021). DDIT3/CHOP promotes autophagy in chondrocytes via SIRT1-AKT pathway. *Biochimica Et Biophysica Acta. Molecular Cell Research, 1868*(9), 119074. 10.1016/j.bbamcr.2021.119074

Yang, C., Yang, X., Liu, C., Hou, J., Chen, X., Wang, L., & Wu, X. (2023). EPRS1 correlates with malignant progression in hepatocellular

carcinoma. *Infectious Agents and Cancer, 18*, 27. 10.1186/s13027-023-00503-0

Yang, J., Zhang, Y., Gao, X., Yuan, Y., Zhao, J., Zhou, S., Wang, H., Wang, L., Xu, G., Li, X., Wang, P., Zou, X., Zhu, D., Lv, Y., & Zhang, S. (2021). Plasma-Derived Exosomal ALIX as a Novel Biomarker for Diagnosis and Classification of Pancreatic Cancer. *Frontiers in Oncology, 11*, 628346. 10.3389/fonc.2021.628346

Yao, W., Yin, T., Tambini, M. D., & D'Adamio, L. (2019). The Familial dementia gene ITM2b/BRI2 facilitates glutamate transmission via both presynaptic and postsynaptic mechanisms. *Scientific Reports, 9*(1), 4862. 10.1038/s41598-019-41340-9

Ye, M., Huang, J., Mou, Q., Luo, J., Hu, Y., Lou, X., Yao, K., Zhao, B., Duan, Q., Li, X., Zhang, H., & Zhao, Y. (2021). CD82 protects against glaucomatous axonal transport deficits via mTORC1 activation in mice. *Cell Death & Disease, 12*(12), 1149. 10.1038/s41419-021-04445-6

Yee, A. G., Lee, S., Hunter, M. R., Glass, M., Freestone, P. S., & Lipski, J. (2014). Effects of the Parkinsonian toxin MPP+ on electrophysiological properties of nigral dopaminergic neurons. *Neurotoxicology, 45*, 1–11. 10.1016/j.neuro.2014.08.009

Yilmaz, A., Loustau, T., Salomé, N., Poilil Surendran, S., Li, C., Tucker, R. P., Izzi, V., Lamba, R., Koch, M., & Orend, G. (2022). Advances on the roles of tenascin-C in cancer. *Journal of Cell Science, 135*(18), jcs260244. 10.1242/jcs.260244

Yoon, S., Choi, J., Shah, M., Kwon, S. M., Yang, J., Park, Y. N., Wang, H., & Woo, H. G. (2021). USO1 isoforms differentially promote liver cancer progression by dysregulating the ER-Golgi network. *Carcinogenesis, 42*(9), 1208–1220. 10.1093/carcin/bgab067

Yu, J., Sane, S., Kim, J., Yun, S., Kim, H., Jo, K. B., Wright, J. P., Khoshdoozmasouleh, N., Lee, K., Oh, H. T., Thiel, K., Parvin, A., Williams, X., Hannon, C., Lee, H., & Kim, D. (2024). Biogenesis and delivery of extracellular vesicles: harnessing the power of EVs for diagnostics and

therapeutics. *Frontiers in Molecular Biosciences, 10*, 1330400. 10.3389/fmolb.2023.1330400

Zagare, A., Gobin, M., Monzel, A. S., & Schwamborn, J. C. (2021). A robust protocol for the generation of human midbrain organoids. *STAR Protocols, 2*(2), 100524. 10.1016/j.xpro.2021.100524

Zappa, F., Muniozguren, N. L., Conrad, J. E., & Acosta-Alvear, D. (2025). The integrated stress response engages a cell-autonomous, ligand-independent, DR5-driven apoptosis switch. *Cell Death & Disease, 16*(1), 101. 10.1038/s41419-025-07403-8

Zeng, H., Liu, Y., Liu, X., Li, J., Lu, L., Xue, C., Wu, X., Zhang, X., Zheng, Z., & Lu, G. (2024). Interplay of α-Synuclein Oligomers and Endoplasmic Reticulum Stress in Parkinson's Disease: Insights into Cellular Dysfunctions. *Inflammation,* 10.1007/s10753-024-02156-6

Zeng, Q., Zhang, F., Zhang, J., Hei, Z., Li, Z., Huang, M., Fang, P., Wang, E., Sun, X., & Zhou, X. (2023). Loss of threonyl-tRNA synthetase-like protein Tarsl2 has little impact on protein synthesis but affects mouse development. *The Journal of Biological Chemistry, 299*(5), 104704. 10.1016/j.jbc.2023.104704

Zeng, Y., Qiu, Y., Jiang, W., Shen, J., Yao, X., He, X., Li, L., Fu, B., & Liu, X. (2022). Biological Features of Extracellular Vesicles and Challenges. *Frontiers in Cell and Developmental Biology, 10*10.3389/fcell.2022.816698

Zhang, G., Wang, X., Li, C., Li, Q., An, Y. A., Luo, X., Deng, Y., Gillette, T. G., Scherer, P. E., & Wang, Z. V. (2021). Integrated Stress Response Couples Mitochondrial Protein Translation with Oxidative Stress Control. *Circulation, 144*(18), 1500–1515. 10.1161/CIRCULATIONAHA.120.053125

Zhang, J., Xie, S., Zhu, J., & Gong, Z. (2016). Requirement for flap endonuclease 1 (FEN1) to maintain genomic stability and transcriptional gene silencing in Arabidopsis. *The Plant Journal: For Cell and Molecular Biology, 87*(6), 629–640. 10.1111/tpj.13224

Zhang, S., Eitan, E., Wu, T., & Mattson, M. P. (2018). Intercellular transfer of pathogenic α-synuclein by extracellular vesicles is induced by the lipid peroxidation product 4-hydroxynonenal. *Neurobiology of Aging, 61*, 52–65. 10.1016/j.neurobiolaging.2017.09.016

Zhang, S., Yi, S., Wang, L., Li, S., Wang, H., Song, L., Ou, J., Zhang, M., Wang, R., Wang, M., Zheng, Y., Yang, K., Liu, T., & Ho, M. S. (2023). Cyclin-G-associated kinase GAK/dAux regulates autophagy initiation via ULK1/Atg1 in glia. *Proceedings of the National Academy of Sciences of the United States of America, 120*(29), e2301002120. 10.1073/pnas.2301002120

Zhang, W., Gong, P., Tian, Q., Han, S., Wang, J., He, P., Guo, Y., Wang, G., Chen, Q., Huang, J., & Li, M. (2022). The eIF4A Inhibitor Silvestrol Blocks the Growth of Human Glioblastoma Cells by Inhibiting AKT/mTOR and ERK1/2 Signaling Pathway. *Journal of Oncology, 2022*, 4396316. 10.1155/2022/4396316

Zhang, X., Gao, F., Wang, D., Li, C., Fu, Y., He, W., & Zhang, J. (2018). Tau Pathology in Parkinson's Disease. *Frontiers in Neurology, 9*, 809. 10.3389/fneur.2018.00809

Zhang, X., Smits, A. H., van Tilburg, G. B., Ovaa, H., Huber, W., & Vermeulen, M. (2018). Proteome-wide identification of ubiquitin interactions using UbIA-MS. *Nature Protocols, 13*(3), 530–550. 10.1038/nprot.2017.147

Zhang, X., Smits, A. H., van Tilburg, G. B., Ovaa, H., Huber, W., & Vermeulen, M. (2018). Proteome-wide identification of ubiquitin interactions using UbIA-MS. *Nature Protocols, 13*(3), 530–550. 10.1038/nprot.2017.147

Zhang, X., Yin, M., & Zhang, M. (2014). Cell-based assays for Parkinson's disease using differentiated human LUHMES cells. *Acta Pharmacologica Sinica, 35*(7), 945–956. 10.1038/aps.2014.36

Zhang, Y., Liu, Y., Liu, H., & Tang, W. H. (2019). Exosomes: biogenesis, biologic function and clinical potential. *Cell & Bioscience, 9*, 19. 10.1186/s13578-019-0282-2

Zhang, Z., Xu, X., Zhang, D., Zhao, S., Wang, C., Zhang, G., Chen, W., Liu, J., Gong, H., Rixiati, Y., Li, S., Shen, T., & Li, J. (2024). Targeting Erbin-mitochondria axis in platelets/megakaryocytes promotes B cell-mediated antitumor immunity. *Cell Metabolism, 36*(3), 541–556.e9. 10.1016/j.cmet.2023.12.020

Zhao, Y., & Lin, Y. (2010). Whole-Cell Protein Identification Using the Concept of Unique Peptides. *Genomics, Proteomics & Bioinformatics, 8*(1), 33–41. 10.1016/S1672-0229(10)60004-6

Zhao, Z., Chen, Z., Zhou, R., Zhang, X., Ye, Q., & Wang, Y. (2019). Increased DJ-1 and α-Synuclein in Plasma Neural-Derived Exosomes as Potential Markers for Parkinson's Disease. *Frontiers in Aging Neuroscience, 10*, 438. 10.3389/fnagi.2018.00438

Zheng, L., Zhang, Y., Chen, X., Chen, D., Dai, Y., & Tang, Z. (2019). Astragalus Polysaccharides Protects Thapsigargin-induced Endoplasmic Reticulum Stress in HT29 Cells. *Open Life Sciences, 14*, 494–501. 10.1515/biol-2019-0055

Zhou, X., Jia, Y., Mao, C., & Liu, S. (2024). Small extracellular vesicles: Non-negligible vesicles in tumor progression, diagnosis, and therapy. *Cancer Letters, 580*, 216481. 10.1016/j.canlet.2023.216481

Zhu, H., Lemos, H., Bhatt, B., Islam, B. N., Singh, A., Gurav, A., Huang, L., Browning, D. D., Mellor, A., Fulzele, S., & Singh, N. (2017b). Carbidopa, a drug in use for management of Parkinson disease inhibits T cell activation and autoimmunity. *PLoS ONE, 12*(9), e0183484. 10.1371/journal.pone.0183484

Zou, Z., Tao, T., Li, H., & Zhu, X. (2020). mTOR signaling pathway and mTOR inhibitors in cancer: progress and challenges. *Cell & Bioscience, 10*, 31. 10.1186/s13578-020-00396-1

9 Chapter Nine: Ethics approval

Uncovering the fundamental links between cellular stress and neurodegeneration in a Parkinson's disease model

Ethics Review ID: ER42036559

Workflow Status: Application Approved

Type of Ethics Review Template: Very low risk human participants studies

Primary Researcher / Principal Investigator

Laura Shippey
(Health and Wellbeing)

Converis Project Application:

Q1. Is this project ii) Doctoral research

Director of Studies

David Smith
(Health and Wellbeing)

Supervisory Team

Susan Campbell
(Biomolecular Sciences Research Centre)